Propagation et diffusion des ondes au niveau macroscopique des métamatériaux limites via le modèle micromorphique relaxé

Alexios Aivaliotis

N° d'ordre NNT : 2019LYSEI073

Année 2019

Thèse de doctorat de l'université de Lyon

opérée au sein de
INSA–Lyon

Ecole Doctorale Mécanique, Energétique, Génie Civil, Acoustique (MEGA)

Spécialité: Mécanique des solides, des matériaux des structures et des surfaces

Soutenue publiquement le 20/09/2019 par

Alexios Aivaliotis

Wave propagation and scattering at metamaterials' macroscopic boundaries via the relaxed micromorphic model

---

Devant le jury composé de :

COLLET Manuel	Directeur de Recherche, HDR	LTDS, École Centrale–Lyon	Examinateur
DAOUADJI Ali	Professeur des Universités	GEOMAS, INSA–Lyon	Co-Directeur de thèse
LOMBARD Bruno	Directeur de Recherche, HDR	LMA, Aix-Marseille Univ, CNRS	Rapporteur
MADEO Angela	Professeur des Universités	GEOMAS, INSA–Lyon	Directrice de thèse
NEFF Patrizio	Professeur des Universités	Universität Duisburg-Essen	Examinateur
SEPPECHER Pierre	Professeur des Universités	IMATH, Université de Toulon	Rapporteur

GEOMAS, INSA–Lyon 34 avenue des Arts, F–69621, Villeurbanne CEDEX – France

Département FEDORA – INSA Lyon - Ecoles Doctorales – Quinquennal 2016-2020

SIGLE	ECOLE DOCTORALE	NOM ET COORDONNEES DU RESPONSABLE
CHIMIE	**CHIMIE DE LYON** **http://www.edchimie-lyon.fr** Sec. : Renée EL MELHEM Bât. Blaise PASCAL, 3e étage **secretariat@edchimie-lyon.fr** INSA : R. GOURDON	M. Stéphane DANIELE Institut de recherches sur la catalyse et l'environnement de Lyon IRCELYON-UMR 5256 Équipe CDFA 2 Avenue Albert EINSTEIN 69 626 Villeurbanne CEDEX **directeur@edchimie-lyon.fr**
E.E.A.	**ÉLECTRONIQUE, ÉLECTROTECHNIQUE, AUTOMATIQUE** **http://edeea.ec-lyon.fr** Sec. : M.C. HAVGOUDOUKIAN **ecole-doctorale.eea@ec-lyon.fr**	M. Gérard SCORLETTI École Centrale de Lyon 36 Avenue Guy DE COLLONGUE 69 134 Écully Tél : 04.72.18.60.97 Fax 04.78.43.37.17 **gerard.scorletti@ec-lyon.fr**
E2M2	**ÉVOLUTION, ÉCOSYSTÈME, MICROBIOLOGIE, MODÉLISATION** **http://e2m2.universite-lyon.fr** Sec. : Sylvie ROBERJOT Bât. Atrium, UCB Lyon 1 Tél : 04.72.44.83.62 INSA : H. CHARLES **secretariat.e2m2@univ-lyon1.fr**	M. Philippe NORMAND UMR 5557 Lab. d'Ecologie Microbienne Université Claude Bernard Lyon 1 Bâtiment Mendel 43, boulevard du 11 Novembre 1918 69 622 Villeurbanne CEDEX **philippe.normand@univ-lyon1.fr**
EDISS	**INTERDISCIPLINAIRE SCIENCES-SANTÉ** **http://www.ediss-lyon.fr** Sec. : Sylvie ROBERJOT Bât. Atrium, UCB Lyon 1 Tél : 04.72.44.83.62 INSA : M. LAGARDE **secretariat.ediss@univ-lyon1.fr**	Mme Emmanuelle CANET-SOULAS INSERM U1060, CarMeN lab, Univ. Lyon 1 Bâtiment IMBL 11 Avenue Jean CAPELLE INSA de Lyon 69 621 Villeurbanne Tél : 04.72.68.49.09 Fax : 04.72.68.49.16 **emmanuelle.canet@univ-lyon1.fr**
INFOMATHS	**INFORMATIQUE ET MATHÉMATIQUES** **http://edinfomaths.universite-lyon.fr** Sec. : Renée EL MELHEM Bât. Blaise PASCAL, 3e étage Tél : 04.72.43.80.46 **infomaths@univ-lyon1.fr**	M. Luca ZAMBONI Bât. Braconnier 43 Boulevard du 11 novembre 1918 69 622 Villeurbanne CEDEX Tél : 04.26.23.45.52 **zamboni@maths.univ-lyon1.fr**
Matériaux	**MATÉRIAUX DE LYON** **http://ed34.universite-lyon.fr** Sec. : Stéphanie CAUVIN Tél : 04.72.43.71.70 Bât. Direction **ed.materiaux@insa-lyon.fr**	M. Jean-Yves BUFFIÈRE INSA de Lyon MATEIS - Bât. Saint-Exupéry 7 Avenue Jean CAPELLE 69 621 Villeurbanne CEDEX Tél : 04.72.43.71.70 Fax : 04.72.43.85.28 **jean-yves.buffiere@insa-lyon.fr**
MEGA	**MÉCANIQUE, ÉNERGÉTIQUE, GÉNIE CIVIL, ACOUSTIQUE** **http://edmega.universite-lyon.fr** Sec. : Stéphanie CAUVIN Tél : 04.72.43.71.70 Bât. Direction **mega@insa-lyon.fr**	M. Jocelyn BONJOUR INSA de Lyon Laboratoire CETHIL Bâtiment Sadi-Carnot 9, rue de la Physique 69 621 Villeurbanne CEDEX **jocelyn.bonjour@insa-lyon.fr**
ScSo	**ScSo*** **http://ed483.univ-lyon2.fr** Sec. : Véronique GUICHARD INSA : J.Y. TOUSSAINT Tél : 04.78.69.72.76 **veronique.cervantes@univ-lyon2.fr**	M. Christian MONTES Université Lyon 2 86 Rue Pasteur 69 365 Lyon CEDEX 07 **christian.montes@univ-lyon2.fr**

*ScSo : Histoire, Géographie, Aménagement, Urbanisme, Archéologie, Science politique, Sociologie, Anthropologie

To my beloved parents, Iraklis and Marianna.

"All that is gold does not glitter,
not all those who wander are lost."
-J.R.R. Tolkien

Acknowledgments

I wish to begin first by thanking my supervisors, Prof. Angela Madeo and Prof. Ali Daouadji, for their support and their insight. In particular, Angela guided me through this journey that was my Ph.D. with her abundant patience, knowledge and most importantly, her humane kindness. Thanks for this great experience!

Furthermore, I wish to thank Prof. Patrizio Neff for the interesting talks, his kind hospitality in Essen but also for the sharing of his deep understanding of mathematics and mechanics. Further thanks must go to the two reviewers of this manuscript, Prof. Pierre Seppecher and Dr. Bruno Lombard, who kindly and graciously accepted to review this thesis, as well as to Prof. Manuel Collet for being part of the jury of my public defense.

This thesis is the result of publications, for which many people are owed my gratitude. Dr. Gabriele Barbagallo, the Mathematica wizard and fellow believer, thanks for the help during some frustrating times; Dr. Domenico Tallarico, thanks for the very fun times we had in the office but also abroad and for your extremely knowledgeable insights; Prof. Marco d'Agostino, thanks for discussing mathematics and mechanics with me and for helping me understand what is happening! But the office life did not include only collaborators; indeed, I am grateful for making friends here, with whom we had so many fun lunches and outings together. In no particular order, José, Danai, Nicole, Rosy, Adnan, Thomas - thanks for everything guys and girls! A special thanks must go to Dr. François Nader, not only for his kind and valuable friendship and the always appropriate and politically correct humor, but also for proof-reading this thesis and correcting all the typos and errors he could find. The result would not have been the same without his contribution, plus I can take off some of the blame for the typos which were never found.

During the time spent in Lyon I changed, evolved and matured. A lot of people were responsible for this, friends old and new who, fortunately, are too many to mention here. The comfort of knowing there is always a person willing to talk at the other end of the line is the greatest blessing in my life. None of the end results of this process would have been the same if even one of you were not here and for that I thank you all from the bottom of my heart!

Lastly, I wish to thank my parents, Iraklis and Marianna. You have supported me in so many ways and phases of my life, which is difficult to put into words. Your love has always been the pillar which supports my life and for that, I thank you. This thesis is, thus, dedicated to you!

Abstract

Mechanical microstructured metamaterials are increasingly gaining attention from the scientific and engineering community. The exotic properties provided by these man-made artifacts could possibly revolutionize our everyday lives. However, the question of modeling the behavior of metamaterials is still a debate and the answer to it is of extreme scientific importance. Some renowned scientists choose to try and model the microstructure of a metamaterial at the molecular level, by using techniques such as high-frequency homogenization. Others choose an approach, which is reminiscent of the classical theory of elasticity: the one of **enriched continuum mechanics**. As the name suggests, the models which stem from this approach have enriched kinematics, in the sense that one adds extra degrees of freedom which account for the vibrations taking place in the microstructure. The goal of this thesis is to employ the novel enriched continuum model named **relaxed micromorphic model** in order to study wave propagation and, mainly, reflection and transmission phenomena at interfaces between classical materials and metamaterials.

The conception of new metamaterials showing unorthodox behaviors with respect to elastic wave propagation has become possible in recent years thanks to powerful dynamical homogenization techniques. Such methods effectively allow to describe the behavior of an infinite medium generated by periodically architectured base materials. Nevertheless, when it comes to the study of the scattering properties of finite-sized structures, dealing with the correct boundary conditions at the macroscopic scale becomes challenging. In this thesis, we show how finite-domain boundary value problems can be set-up in the framework of the relaxed micromorphic model by imposing continuity of macroscopic displacement and of generalized traction when non-local effects are neglected. The advantage of this approach is that these boundary conditions stem from a variational principle, which renders our problem mathematically well-posed.

First, we set up the full two-dimensional plane wave solution of the scattering from an interface separating a classical Cauchy medium from a relaxed micromorphic medium. Both media are assumed to be isotropic and semi-infinite to ease the semi-analytical implementation of the associated boundary value problem.

Generalized macroscopic boundary conditions are presented (continuity of macroscopic displacement, continuity of generalized tractions and, eventually, additional conditions involving purely microstructural constraints), which allow for the effective description of the scattering properties of an interface between a homogeneous solid and a mechanical metamaterial. The associated "generalized energy flux" is introduced in order to quantify the energy which is transmitted at the interface via a simple scalar, macroscopic quantity.

Two cases are considered in which the left homogeneous medium is "stiffer" and "softer" than the right metamaterial and the transmission coefficient is obtained as a function of the frequency and of the direction of propagation of the incident wave. We show that the contrast of the macroscopic stiffnesses of the two media, together with the type of boundary conditions, strongly influence the onset of Stoneley (or evanescent) waves at the interface. This allows for the

tailoring of the scattering properties of the interface at both low and high frequencies, ranging from zones of complete transmission to zones of zero transmission well beyond the band-gap region.

We then consider a bulk wave propagation problem and show that the transient waveforms arising from several localised pulses in a micro-structured material can be reproduced by a corresponding generalised continuum of the relaxed micromorphic type. Specifically, we compare the dynamic response of a bounded micro-structured material to that of bounded continua with special kinematic properties: (i) the relaxed micromorphic continuum and (ii) an equivalent Cauchy linear elastic continuum. We show that, while the Cauchy theory is able to describe the overall behavior of the metastructure only at low frequencies, the relaxed micromorphic model goes far beyond by giving a correct description of the pulse propagation in the frequency band-gap and at frequencies intersecting the optical branches. In addition, we observe a computational time reduction associated with the use of the relaxed micromorphic continuum, compared to the sensible computational time needed to perform a transient computation in a micro-structured domain.

Finally, we present the case of a metamaterial slab of finite width. Its scattering properties are studied via a semi-analytical solution of the relaxed micromorphic model and compared to numerical simulations encoding all details of the selected microstructure. The reflection coefficient obtained via the two methods is presented as a function of the frequency and of the direction of propagation of the incident wave. We find excellent agreement for a large range of frequencies going from the long-wave limit to frequencies beyond the first band-gap and for angles of incidence ranging from normal to near parallel incidence. The case of a semi-infinite metamaterial is also presented and is seen to be a reliable measure of the average behavior of the finite metastructure. A tremendous gain in terms of computational time is obtained when using the relaxed micromorphic model for the study of the considered metastructure.

Keywords: enriched continua, metamaterials, anisotropic metamaterials, band-gaps, wave-propagation, Stoneley waves, relaxed micromorphic model, interface, total reflection and transmission, transient dynamic response, scattering, finite-sized metastructures

Resumé

Les métamatériaux mécaniques microstructurés attirent de plus en plus l'attention de la communauté scientifique et technique. Les propriétés exotiques de ces matériaux artificiels pourraient révolutionner notre vie quotidienne. Cependant, la question de la modélisation du comportement des métamatériaux reste un débat et la réponse à cette question est d'extrême importance scientifique. Certains scientifiques renommés choisissent d'essayer de modéliser la microstructure des métamatériaux au niveau moléculaire, en utilisant des techniques comme l'homogénéisation haute fréquence. D'autres choisissent une approche qui évoque la théorie classique de l'élasticité : celle de la **mécanique des milieux continus enrichie**. Comme leur nom l'indique, les modèles issus de cette approche ont enrichi la cinématique, dans le sens où on y ajoute des degrés de liberté supplémentaires qui tiennent compte des vibrations qui se produisent dans la microstructure. Le but de cette thèse est d'utiliser le nouveau modèle de continuité enrichie appelé **modèle micromorphique relaxé** détendu afin d'étudier la propagation des ondes et, principalement, les phénomènes de réflexion et de transmission aux interfaces entre matériaux classiques et métamatériaux.

La conception de nouveaux métamatériaux présentant des comportements peu orthodoxes par rapport à la propagation des ondes élastiques est devenue possible ces dernières années grâce à de puissantes techniques d'homogénéisation dynamique. Ces méthodes permettent de décrire efficacement le comportement d'un milieu infini généré par des matériaux de base périodiquement architecturés. Néanmoins, lorsqu'il s'agît d'étudier les propriétés de diffusion de structures de taille finie, il devient difficile de traiter les conditions limites correctes à l'échelle macroscopique. Dans cette thèse, nous montrons comment les problèmes aux valeurs limites de domaines finis peuvent être mis en place dans le cadre du modèle micromorphique relâché en imposant la continuité du déplacement macroscopique et dans le cadre des contraintes généralisées lorsque les effets non locaux sont négligés. L'avantage de cette approche est que ces conditions aux limites découlent d'un principe variationnel, ce qui rend notre problème mathématiquement bien posé.

Tout d'abord, nous mettons en place la solution d'onde plane bidimensionnelle complète de la diffusion à partir d'une interface séparant un milieu de Cauchy classique d'un milieu micromorphique relaxé. Les deux milieux sont supposés isotropes et semi-infinis pour faciliter la mise en œuvre semi-analytique du problème de valeur limite associé.

Les conditions aux limites macroscopiques généralisées sont présentées (continuité du déplacement macroscopique, continuité des tractions généralisées et, éventuellement, conditions additionnelles impliquant des contraintes purement microstructurales). Ils permettent de bien décrire les propriétés de diffusion d'une interface qui sépare un solide homogène d'un métamatériau mécanique. Le "flux d'énergie généralisé" associé est introduit afin de quantifier l'énergie qui est transmise à l'interface à travers une simple quantité scalaire et macroscopique.

On considère deux cas différents dans lesquels le milieu homogène gauche est soit plus rigide soit plus flexible que le métamatériau droit et le coefficient de transmission est obtenu en fonction

de la fréquence et de la direction de propagation de l'onde incidente. On montre que le contraste des raideurs macroscopiques des deux milieux, ainsi que le type de conditions limites, influencent fortement l'apparition des ondes Stoneley (ou évanescentes) à l'interface. Cela permet d'adapter les propriétés de diffusion de l'interface pour de basses et hautes fréquences, allant des zones de transmission complète à des zones de transmission nulle bien au-delà de la zone de bande passante. On considère par la suite un problème de propagation des ondes de volume et on démontre que les formes d'ondes transitoires résultant de plusieurs impulsions localisées dans un matériau microstructuré peuvent être reproduite par un milieu généralisé correspondant au type micromorphe relaxé. Plus précisément, nous comparons la réponse dynamique d'un matériau microstructuré et lié à celle d'un milieu lié avec des propriétés cinématiques particulières : (i) le milieu micromorphique relaxé et (ii) un équivalent milieu élastique linéaire de Cauchy. On démontre que, bien que la théorie de Cauchy soit capable de décrire le comportement global de la métastructure à de basses fréquences, le modèle micromorphique détendu va bien au-delà en donnant une description correcte de la propagation de l'impulsion dans la bande de fréquence et à des fréquences qui croisent les branches optiques. De plus, on observe une réduction vis-à-vis le temps de calcul en comparant avec le temps de calcul pour effectuer un calcul transitoire dans un milieu micro-structuré, et ceci est due à l'utilisation du milieu micromorphique détendu.

Enfin, on présente le cas d'une dalle de métamatériau de largeur finie. Ses propriétés de diffusion sont étudiées en utilisant une solution semi-analytique du modèle micromorphique relaxé et comparées à des simulations numériques codant tous les détails de la microstructure sélectionnée. Le coefficient de réflexion obtenu par les deux méthodes est présenté en fonction de la fréquence et la direction de propagation de l'onde incidente. On trouve un excellent accord pour une large gamme de fréquences, allant de la limite des ondes longues aux fréquences au-delà de la première limite de la bande, et pour des angles d'incidence allant d'une incidence normale à une incidence presque parallèle. Le cas d'un métamatériau semi-infinie est également présenté et est considéré comme une mesure fiable du comportement moyen de la métastructure finie. Un gain considérable en termes de temps de calcul est obtenu en utilisant le modèle micromorphique relaxé pour l'étude de la métastructure considérée.

Mots-Clés: millieux continus enrichis, métamatériaux, matériaux anisotropes, band-gaps, propagation des ondes, ondes Stoneley, modèle micromorphe relaxé, interface, réflexion et transmission totale, réponse dynamique transitoire, diffusion, metastructures de taille finie

Contents

List of Figures

List of Tables

Chapter 1

General introduction

The word **metamaterial** is widely used today in specific scientific communities to indicate materials that go beyond ("meta" means beyond in Greek) the usual notion of materials, i.e. those produced by nature, or those more classical man-made materials, which are today part of our everyday life. They are in fact architectured materials with exotic properties, which cannot be found in natural or more classical man-made materials. This concept was first established for optical metamaterials that exhibit a negative refraction index (as shown by Victor Veselago in 1968 [98]) and was subsequently extended to mechanical metamaterials, which are engineered in such a way which provide, for instance, negative effective bulk modulus [52], negative effective mass density [51], negative longitudinal and volume compressibility [80], etc. There are even Mesoscopic Theories of Complex Continua (metamaterials of the a priori solid type that behave like fluids [84]), as they have a finite bulk modulus but a vanishing shear modulus. They are called metafluids and are illustrated by so-called "pentamode structures" [69]. General introductory references are Engheta and Ziolkowski [33] and Zoudhi et al. (2008)[111].

The basic idea underlying the design of these metamaterials is that of suitably engineering the architecture of their microstructure in such a way that the resulting macroscopic (homogenized) properties can exhibit the desired exotic characteristics. The most widespread class of metamaterials consists of those which are obtained by a periodic repetition in space of a specific unit cell and which are known as periodic metamaterials. One of the most appealing mechanical features is the possibility to filter waves in specific ranges of frequencies, referred to as frequency "stop-bands" or "**band-gaps**", i.e. frequency ranges for which elastic wave propagation is inhibited.

Nowadays, metamaterials hold a central role in engineering research thanks to their exotic mechanical and electromagnetic behavior. By exploiting these unorthodox properties, the conception of morphologically complex finite structures in many fields of engineering could be revolutionized. For instance, a finite ordered set of a metamaterial's unit-cell, that throughout this thesis we will call **metastructure**, would inherit the filtering properties of the periodic counterpart, leading to application ranging from seismic protection to stealth.

Recent years have seen the rapid development of acoustic metamaterials and phononic crystals whose mechanical properties allow exotic material behaviors such as the aforementioned band-gaps [56, 102, 108] but also cloaking [15, 20, 21, 26, 46, 73, 81, 97], focusing [28, 45, 93], wave-guiding [47, 94] etc. For such metamaterials, renowned scientists have provided analytical [103, 104, 105, 106] or numerical [40] homogenization techniques (in the spirit of the seminal works of Bloch [13] and Floquet [39]), thus obtaining a homogenized model which suitably describes, to a good extent, the dynamical behavior of the bulk periodic metamaterial at the

macroscopic scale. Rigorous models for studying the macroscopic mechanical behavior of non-periodic structures become rarer and usually rely on the use of detailed finite element modeling of the considered microstructures (see e.g. [48]), thus rendering the implementation of large structures computationally demanding and impractical. Theoretical models which account for every single element of such metastructures, however, are rapidly showing their limits both in terms of complexity and computational performance.

If the bulk behavior of these metamaterials has gathered the attention of the scientific community via the application of discrete modeling (such as Bloch-Floquet analysis or homogenization techniques [27, 55, 90, 103]) or, more recently, of enriched continuum models [9, 29, 57, 58, 59, 60, 62, 63, 64, 77, 78, 79], the study of the reflective/refractive properties at the boundary of such metamaterials is far from being well understood. Rare examples of the study of scattering phenomena at metamaterials boundaries in the framework of classical homogenization approaches can be found in [12, 19, 91, 103, 104]. The idea of using enriched continuum theories to describe microstructured materials needs to be fully developed in order to achieve a simplified modeling and more effective conception of large-sale engineering metastructures made up of metamaterials as building blocks. This would allow for the design of real, large-scale engineering structures which are able to resist vibrations and shocks in a large range of frequencies.

It is clear that having a good knowledge of the reflective and transmittive properties of metamaterial interfaces is a key point for the conception of metamaterial systems, which would completely transform the idea we currently have about reflection and transmission of elastic waves at the interface between two solids. It is for this reason that many authors convey their research towards what they call "metasurfaces" [53, 54, 109], i.e. relatively thin layers of metamaterials whose microstructure is able to interact with the incident wave-front in such a way that the resulting reflection/transmission patterns exhibit exotic properties, such as total reflection or total transmission, conversion of a bulk incident wave in interface waves, etc. At the current state of knowledge, little effort is made in trying to model metastructures, due to the difficulty of imposing suitable boundary conditions in the framework of homogenization theories (see [91]).

Notwithstanding the paramount importance these metasurfaces may have for technological advancements in the field of noise absorption or stealth, they show limitations in the sense that they work for relatively small frequency ranges, for which the wavelength of the incident wave is comparable to the thickness of the metasurface itself. This restricts the range of applicability of such devices, above all for what concerns low frequencies which would result in very thick metasurfaces.

We propose to shed new light in this direction by the introduction of an enriched continuum model of the micromorphic type, equipped with the proper boundary conditions for the effective description of finite sized band-gap metastructures. The **relaxed micromorphic model** (see [2, 3, 9, 10, 29, 57, 58, 59, 60, 61, 62, 63, 64, 65, 77, 78, 79] for preliminary results) has a simplified structure which allows to describe the homogenized properties of (periodic or even non-periodic) anisotropic metamaterials with a limited number of constant, frequency independent material parameters and for an extended frequency range going from the long-wave limit to frequencies which are beyond the first band-gap. The rigorous development of the relaxed micromorphic model for anisotropic metamaterials has been given in [29], where applications to different classes of symmetry and the particular case of tetragonal periodic metamaterials are also discussed. In the latter paper, a procedure to univocally determine some of the material parameters for periodic metamaterials with static tests is also provided. It is important to point out that

the relaxed micromorphic model is not obtained via a formal homogenization procedure, but is developed generalizing the framework of macroscopic continuum elasticity by introducing enriched kinematics and enhanced constitutive laws for the strain energy density. In this way, extra degrees of freedom are added to the classical macroscopic displacement via the introduction of the micro-distortion tensor and the chosen constitutive form for the anisotropic strain energy density. This allows to introduce a limited number of elastic parameters through fourth-order macro and micro elasticity tensors working on the sym/skew orthogonal decomposition of the introduced deformation measures (see [29] for details).

The need of using an enriched continuum model of the micromorphic type for describing the broadband macroscopic behavior of acoustic metamaterials as emerging from a numerical homogenization technique was recently proven in [90]. Nevertheless, the authors of the latter paper showed that a huge number of elastic parameters (up to 600 for the studied tetragonal two-dimensional metamaterials) is indeed needed to perform an accurate fitting of the dispersion curves issued by the Bloch-Floquet analysis. This extensive number of parameters can also be found in other micromorphic models of the Eringen [36] and Mindlin [71] type. The need of this vast number of parameters is related to the fact that the macroscopic class of symmetry of the metamaterial and the suitable (i.e. sym/skew-decomposed) deformation measures are usually not accounted for. As a matter of fact, the relaxed micromorphic model, as proposed in [29], is able to minimize the number of parameters (15 for the tetragonal 2D-case) thanks to the introduction of "generalized classes of symmetry" for metamaterials and to the sym/skew-decomposition choice of the introduced deformation measures. The fitting of the dispersion curves, which can be obtained by the inverse fitting procedure proposed in [29], cannot reproduce point-by-point the dispersion curves issued via Bloch-Floquet analysis (which is not the aim of our work), but is general enough to capture the main features of the studied metamaterials' behavior including dispersion, anisotropy, band-gaps for a wide range of frequencies and for wavelengths which can become very small and even comparable to the size of the unit cell.

Last, but most importantly, since it is issued by a variational procedure, the relaxed micromorphic model is naturally equipped with the correct macroscopic boundary conditions which have to be applied on the boundaries of the considered metamaterials. This implies that the global refractive properties of metamaterials' boundaries can be described in the simplified framework of enriched continuum mechanics, thus providing important information while keeping simple enough to allow important computational time-saving.

We want to stress here the fact that, when a new theory is being constructed, partial superposition with previous works is unavoidable. It is exactly such incessant progress that will ultimately allow to proceed towards the ambitious result of establishing a generalized version of the theory of elasticity for the study of microstructured metamaterials. In fact, as the theory of elasticity allows the averaged description of the mechanical behavior of classical materials without accounting for the complexity of all the atoms and molecules that constitute them, our long term goal is to build up a generalized theory of elasticity enclosing the dynamic response of metamaterials but without accounting for the detailed microstructure. Given the ambition of this final goal, it is clear that a series of papers is needed, with the aim to set up the model, to encompass its generalization to general anisotropy, to establish a simplified fitting procedure on real metamaterials, and to provide evidence that the obtained material parameters identification is able to reproduce real behaviors at large scales. Further research will be needed to prove the effectiveness of the established procedures to other metamaterials with different classes of symmetry and also independent tests of the effectiveness of the model (for example studying the reflective properties of interfaces embedded in anisotropic metamaterials) will be needed to

valorize the results obtained up to now.

This thesis contains six main chapters. Chapter 1 consists of a general introduction and also sets the notation used throughout the thesis. In chapter 2 discuss some main concepts of continuum mechanics and introduce the reader to the theory of enriched continuum modeling. Furthermore, we give some basic definitions and properties of periodic lattices, which we will need later on. Chapter 3 is devoted to introducing the relaxed micromorphic model. We will see how we can derive it from a variational principle and state the governing equations in the cases of anisotropic and isotropic media. We will also discuss how we can represent classes of symmetry, by making a recapitulation of the Mandel-Voigt vector notation.

After these preliminary chapters, we begin the presentation of the main results of this thesis. Chapter 4 is dedicated to the study of interface problems in the case of isotropy. We will consider an interface between two isotropic media, one described by the classical Cauchy equations of elasticity and one by the isotropic relaxed micromorphic model. We will show in full detail how we can study this problem and discuss the results obtained for two cases, one where the left Cauchy material is "stiffer" and one where it is "softer" than the metamaterial on the right side of the interface. We will then move on to discuss an application of the anisotropic relaxed micromorphic model in chapter 5. Imposing a pulse signal in a 2D metamaterial's plate we will see how to describe bulk wave propagation via the relaxed micromorphic model and compare the obtained results to in-silico experiments performed by direct numerical simulations in the commercial Finite Element solver *Comsol Multiphysics*^{TM}. Chapter 6 is dedicated to the study of reflection and transmission problems in the case of anisotropy, assuming metamaterials with tetragonal symmetry. Comparisons between the results issued by the relaxed micromorphic model and those obtained via direct numerical simulations are again provided Finally, chapter 7 discusses the conclusions of this thesis and further research perspectives.

1.1 Notation

Let $\mathbb{R}^{3\times3}$ be the set of all real 3×3 second order tensors (matrices) which we denote by capital letters. A simple and a double contraction between tensors of any suitable order is denoted by $\cdot$ and $:$ respectively, while the scalar product of such tensors by $\langle\cdot,\cdot\rangle$.[1] The Einstein sum convention is implied throughout this text unless otherwise specified. The standard Euclidean scalar product on $\mathbb{R}^{3\times3}$ is given by $\langle X,Y\rangle_{\mathbb{R}^{3\times3}} = \mathrm{tr}(X\cdot Y^{\mathrm{T}})$ and consequently the Frobenius tensor norm is $\|X\|^2 = \langle X,X\rangle_{\mathbb{R}^{3\times3}}$. From now on, for the sake of notational brevity, we omit the scalar product indices $\mathbb{R}^3, \mathbb{R}^{3\times3}$ when no confusion arises. The identity tensor on $\mathbb{R}^{3\times3}$ will be denoted by $\mathbb{1}$; then, $\mathrm{tr}(X) = \langle X,\mathbb{1}\rangle$. The following standard Lie-algebra theory abbreviations are used:

- $\mathrm{Sym}(3) := \{X\in\mathbb{R}^{3\times3} | X^{\mathrm{T}} = X\}$ is the vector space of all symmetric tensors.
- $\mathfrak{so}(3) := \{X\in\mathbb{R}^{3\times3} | X^{\mathrm{T}} = -X$ is the Lie-algebra of all skew-symmetric tensors.
- $\mathfrak{sl}(3) := \{X\in\mathbb{R}^{3\times3} |\, \mathrm{tr}(X) = 0\}$ is the Lie-algebra of all traceless tensors.
- $\mathbb{R}^{3\times3} \cong \mathfrak{gl}(3) = \{\mathfrak{sl}(3)\cap\mathrm{Sym}(3)\}\oplus\mathfrak{so}(3)\oplus\mathbb{R}\cdot\mathbb{1}$ is the orthogonal Cartan decomposition of the Lie algebra $\mathfrak{gl}(3)$.

Furthermore, for all $X\in\mathbb{R}^{3\times3}$, we set:

[1] For example, $(A\cdot v)_i = A_{ij}v_j, (A\cdot B)_{ik} = A_{ij}B_{jk}, A:B = A_{ij}B_{ji}, (C\cdot B)_{ijk} = C_{ijp}B_{pk}, (C:B)_i = C_{ijp}B_{pj}, \langle v,w\rangle = v\cdot w = v_iw_i, \langle A,B\rangle = A_{ij}B_{ij}$, etc.

- $\operatorname{sym} X = \frac{1}{2}(X + X^{\mathrm{T}}) \in \mathrm{Sym}(3)$, the symmetric part of the tensor X.
- $\operatorname{skew} X = \frac{1}{2}(X - X^{\mathrm{T}}) \in \mathfrak{so}(3)$, the skew-symmetric part of the tensor X.
- $\operatorname{dev} X = X - \frac{1}{3}\operatorname{tr} X \cdot \mathbb{1} \in \mathfrak{sl}(3)$, the deviatoric part of the tensor X.

Finally, the *Cartan-Lie decomposition* of a tensor $X \in \mathbb{R}^{3\times 3}$ is:

$$X = \operatorname{dev}\operatorname{sym} X + \operatorname{skew} X + \frac{1}{3}\operatorname{tr}(X) \cdot \mathbb{1}. \tag{1.1}$$

Consider a body which occupies a bounded open set $B_L \subset \mathbb{R}^3$ and assume that the boundary ∂B_L is a smooth surface of class C^2. An elastic material fills the domain B_L and we denote by Σ any material surface embedded in B_L. The outward unit normal to ∂B_L will be denoted by ν as will the outward unit normal to a surface Σ embedded in B_L (see Fig. 1.1). Given a field

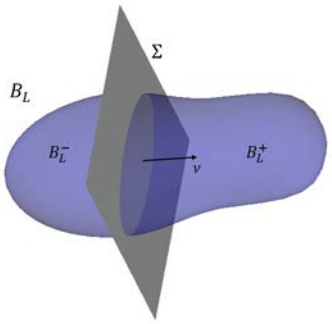

Figure 1.1: Schematic representation of the body B_L, the surface Σ and the sub-bodies B_L^- and B_L^+.

a defined on the surface Σ, we set

$$[[a]] = a^+ - a^-, \tag{1.2}$$

which defines a measure of the jump of a through the material surface Σ, where

$$[\cdot]^- := \lim_{\substack{x\in B_L^-\setminus\Sigma \\ x\to\Sigma}} [\cdot], \quad [\cdot]^+ := \lim_{\substack{x\in B_L^+\setminus\Sigma \\ x\to\Sigma}} [\cdot], \tag{1.3}$$

with B_L^-, B_L^+ being the two subdomains which result from splitting B_L by the surface Σ (see again Fig. 1.1).

The Lebesgue spaces of square integrable functions, vectors or tensors fields on B_L with values on $\mathbb{R}, \mathbb{R}^3, \mathbb{R}^{3\times 3}$ respectively, are denoted by $L^2(B_L)$. Moreover we introduce the standard Sobolev spaces[2]

$$\begin{aligned}
H^1(B_L) &= \left\{ u \in L^2(B_L) |\, \nabla u \in L^2(B_L), \|u\|^2_{H^1(B_L)} := \|u\|^2_{L^2(B_L)} + \|\nabla u\|^2_{L^2(B_L)} \right\}, \\
H(\operatorname{curl}; B_L) &= \left\{ v \in L^2(B_L) |\, \operatorname{curl} v \in L^2(B_L), \|v\|^2_{H(\operatorname{curl};B_L)} := \|v\|^2_{L^2(B_L)} + \|\operatorname{curl} v\|^2_{L^2(B_L)} \right\}, \\
H(\operatorname{div}; B_L) &= \left\{ v \in L^2(B_L) |\, \operatorname{div} v \in L^2(B_L), \|v\|^2_{H(\operatorname{div};B_L)} := \|v\|^2_{L^2(B_L)} + \|\operatorname{div} v\|^2_{L^2(B_L)} \right\},
\end{aligned} \tag{1.4}$$

of functions u and vector fields v respectively.

[2]The operators ∇, curl and div are the classical gradient, curl and divergence operators. In symbols, for a field u of any order, $(\nabla u)_i = u_{,i}$, for a vector field v, $(\operatorname{curl} v)_i = \varepsilon_{ijk} v_{k,j}$ and for a field w of order greater than 1, $\operatorname{div} w = w_{i,i}$.

For vector fields v with components in $H^1(B_L)$ and for tensor fields P with rows in $H(\mathrm{curl}; B_L)$ (resp. $H(\mathrm{div}; B_L)$), i.e.

$$v = (v_1, v_2, v_3)^{\mathrm{T}},\ v_i \in H^1(B_L), \quad P = (P_1^{\mathrm{T}}, P_2^{\mathrm{T}}, P_3^{\mathrm{T}})^{\mathrm{T}},\ P_i \in H(\mathrm{curl}; B_L) \text{ resp. } P_i \in H(\mathrm{div}; B_L), \tag{1.5}$$

where $i = 1, 2, 3$, we define

$$\begin{aligned} \nabla v &= \left((\nabla v_1)^{\mathrm{T}}, (\nabla v_2)^{\mathrm{T}}, (\nabla v_3)^{\mathrm{T}}\right)^{\mathrm{T}}, \\ \mathrm{Curl}\, P &= \left((\mathrm{curl}\, P_1)^{\mathrm{T}}, (\mathrm{curl}\, P_2)^{\mathrm{T}}, (\mathrm{curl}\, P_3)^{\mathrm{T}}\right)^{\mathrm{T}}, \\ \mathrm{Div}\, P &= (\mathrm{div} P_1, \mathrm{div} P_2, \mathrm{div} P_3)^{\mathrm{T}}. \end{aligned} \tag{1.6}$$

The corresponding Sobolev spaces are denoted by $H^1(B_L)$, $H(\mathrm{Div}; B_L)$, $H(\mathrm{Curl}; B_L)$.

Chapter 2

Classical and enriched continuum mechanics

2.1 Classical continuum mechanics

Continuum theories are successfully used for the description of the mechanical behavior of materials at the macroscopic scale. The main idea of continuum mechanics lies in the assumption that a solid can be treated as a *continuum*, rather than a discrete set of molecules. This simplifies the study of solids, since one does not have to take into account each separate interaction taking place at the molecular level. This fundamental idea has been used consistently since the 19th century, when Cauchy managed to prove that the use of such "averaged" theories was a powerful tool for determining the mechanical behavior of large-scale engineering structures. Indeed, one can immediately see the advantage of considering, say, a bridge as a large-scale object as opposed to viewing each of its atoms separately.

Classical continuum mechanics started with the ground-braking works of G. Piola ([85]) and was then extended by A. L. Cauchy ([17]). The main result of Cauchy's work was that the interactions between parts of a solid can be described via a symmetric tensor, called the *symmetric Cauchy force-stress tensor*, classically denoted by $\sigma : \Omega \subset \mathbb{R}^3 \to \mathrm{Sym}(3)$, where Ω is some domain occupied by the solid. This claim was proven via the classical tetrahedron argument (see, for example [22] for a demonstration). Following this, Cauchy derived the equations of motion that balance inertiae, external forces and stresses.

The main assumptions of Cauchy's theory are that:

(a). the displacement $u : \Omega \subset \mathbb{R}^3 \to \mathbb{R}^3$ is the only kinematic field,[1]

(b). the stress σ in each material point x is a symmetric tensor (Bolzmann's axiom of symmetry) and depends only on the gradient of the displacement ∇u evaluated in the same material point x.

The resulting model can then be derived from a variational principle, via a strain energy density and a kinetic energy density.[2] These energy densities are given by:

$$W = \frac{1}{2}\langle \mathbb{C}_{\mathrm{M}} \,\mathrm{sym}(\nabla u), \mathrm{sym}(\nabla u)\rangle_{\mathbb{R}^{3\times 3}}, \tag{2.1}$$

$$J = \frac{1}{2}\rho \left\| u_{,t} \right\|^2, \tag{2.2}$$

[1] This is equivalent to saying that the only possible motion of each point of the body is a translation.

[2] We will describe the procedure of how to derive these equations of motions from these energy densities later on in chapter 3.3.

where $\mathbb{C}_{\mathrm{M}} : \mathrm{Sym}(3) \to \mathrm{Sym}(3)$ is a symmetric fourth-order tensor with at most 21 independent coefficients and ρ is a scalar mass density.

The classical Cauchy elasticity equations, as derived from the above strain and kinetic energy densities, are then given by:

$$\rho\, u_{,tt} = \mathrm{Div}(\mathbb{C}_{\mathrm{M}}\, \mathrm{sym}\, \nabla u), \quad \text{in } \Omega, \tag{2.3}$$

where $\Omega \subset \mathbb{R}^3$ is a bounded domain (the solid we are considering).

In this thesis, whenever we talk about a Cauchy medium, we will always assume it to be isotropic, i.e. its material properties do not depend on the direction from which we examine them. In this case the elasticity tensor $\mathbb{C}_{\mathrm{M}}$ has only 3 non-zero components and the only two independent coefficients are the well-known Lamé parameters μ and λ. Then, the classical equations of motion take the form:

$$\rho\, u_{,tt} = \mathrm{Div}\, \sigma, \quad \rho\, u_{i,tt} = \sigma_{ij,j}, \tag{2.4}$$

where

$$\sigma = 2\mu\, \mathrm{sym}\, \nabla u + \lambda\, \mathrm{tr}(\mathrm{sym}\, \nabla u)\mathbb{1}, \quad \sigma_{ij} = \mu(u_{i,j} + u_{j,i}) + \lambda\, u_{k,k}\delta_{ij}. \tag{2.5}$$

Equation (2.4) can be rewritten in the following way:

$$\rho\, u_{,tt} = (\lambda + \mu)\nabla(\mathrm{Div}\, u) + \mu\nabla^2 u. \tag{2.6}$$

The displacement u can be rewritten in its *Helmholtz decomposition*, according to which u can be written as the sum of an irrotational (curl-free) scalar potential and a solenoidal (divergence-free) vector potential. We have:

$$u = \nabla\phi + \mathrm{curl}\, A, \tag{2.7}$$

where $\phi : \mathbb{R}^3 \to \mathbb{R}$ is the scalar potential and $A : \mathbb{R}^3 \to \mathbb{R}^3$ is the vector potential. Since $\mathrm{div} A = 0$ (gauge-invariance), we can show that equation (2.6) can be decomposed into two wave equations for the two potentials:

$$\textit{“longitudinal”}: \quad (2\mu + \lambda)\nabla^2\phi = \rho\, \phi_{,tt}, \tag{2.8}$$

$$\textit{“shear”}: \quad \mu\, \nabla^2 A = \rho\, A_{,tt}. \tag{2.9}$$

These equations govern the propagation of longitudinal and shear waves respectively. More details on this topic will be given in chapter 6.

Although this classical theory is indeed a very good approximation for many applications, modern day microstructured materials require a more refined theory to better capture their behavior [57, 58, 59]. This novel theory will be introduced in the following chapter and applied in chapters 4, 5 and 6.

2.2 Conservation of energy and energy flux for the classical Cauchy model

In this section we discuss energy conservation and derive the expression of the energy flux for the classical isotropic Cauchy model.

The mechanical system we are considering is conservative and, therefore, energy must be conserved in the sense that the following differential form of a continuity equation must hold:

$$E_{,t} + \mathrm{div} H = 0, \tag{2.10}$$

where $E = J + W$ is the total energy of the system and H is the energy flux vector, whose explicit expression we now compute.

We begin by differentiating expressions (2.1) and (2.2) with respect to time and using definition (2.5). We have:

$$E_{,t} = J_{,t} + W_{,t} = \rho \langle u_{,t}, u_{,tt} \rangle + \langle (2\mu \operatorname{sym} \nabla u + \lambda \operatorname{tr}(\operatorname{sym} \nabla u) \mathbb{1}), \operatorname{sym} \nabla(u_{,t}) \rangle = \rho \langle u_{,t}, u_{,tt} \rangle + \langle \sigma, \operatorname{sym} \nabla(u_{,t}) \rangle .$$

We now replace $\rho\, u_{,tt}$ from the equations of motion (2.4) and we use the fact that $\langle \sigma, \operatorname{sym} \nabla(u_{,t}) \rangle = \langle \sigma, \nabla(u_{,t}) \rangle = \operatorname{Div}(\sigma \cdot u_{,t}) - \operatorname{Div} \sigma \cdot u_{,t}$ (which is due to the symmetry of the Cauchy stress tensor σ,) to get

$$E_{,t} = \operatorname{Div} \sigma \cdot u_{,t} + \operatorname{Div}(\sigma \cdot u_{,t}) - \operatorname{Div} \sigma \cdot u_{,t} = \operatorname{Div}(\sigma \cdot u_{,t}). \tag{2.11}$$

Thus, by comparing (2.11) to the conservation of energy (2.10), we can deduce that the energy flux in a Cauchy continuum is given by (see e.g. [1])

$$H = -\sigma \cdot u_{,t}, \qquad H_k = -\sigma_{ik} u_{k,t}. \tag{2.12}$$

2.3 Enriched continuum theories

In the framework of continuum theories, the systematic use of Cauchy theories may sometimes represent too drastic a simplification of reality, especially when dealing with metamaterials, since some essential characteristics related to the heterogeneity of their microstructure are implicitly neglected. Indeed, every material is actually heterogeneous when one goes down to the molecular or atomic level. Nevertheless, as already pointed out, the effect of the microstructure is often not evident in the engineering scale. In such cases, a continuum Cauchy theory is a suitable choice for modeling the macroscopic mechanical behavior of the considered materials in the simplest and most effective way. On the other hand, there are cases in which the considered materials are heterogeneous even at relatively large scales and, as a consequence, the effect of their microstructure on the overall mechanical behavior of the medium cannot be neglected. In such cases, a continuum Cauchy theory may not be sufficient to fully describe the mechanical behavior of the considered material, especially when considering particular loading and/or boundary conditions.

Enriched continuum theories are an advanced tool at the frontier of which many disciplines meet: mathematics, theoretical and applied mechanics and engineering. For this reason, in order to surely advance towards the desired engineering applications passing through the intricate and nearly unexplored field of the continuum mechanics of metamaterials, we need to be guided by secure mathematical principles. In the meanwhile, we need to take care of introducing the minimal level of complexity in order to efficiently describe the targeted phenomena. To come to the point, we need to reach a reasonable compromise between the complexity of the model that we want to use and the detail at which microstructures can be described. And this is what we do thereupon. The general ideas may be traced back to Duhem (1893) [32] and Voigt (1887) [99].

An *enriched continuum model* is, as the name suggests, a continuum model where we enrich the kinematics by adding additional degrees of freedom. This means, that we no longer assume the displacement to be the only kinematical field.

Indeed, the kinematics are enriched by introducing an additional field of micro-distortions in the form of a second order tensor, which we denote by P. This new set of degrees of freedom accounts for microstructure related phenomena attached to each macroscopic material point $x \in \Omega$.

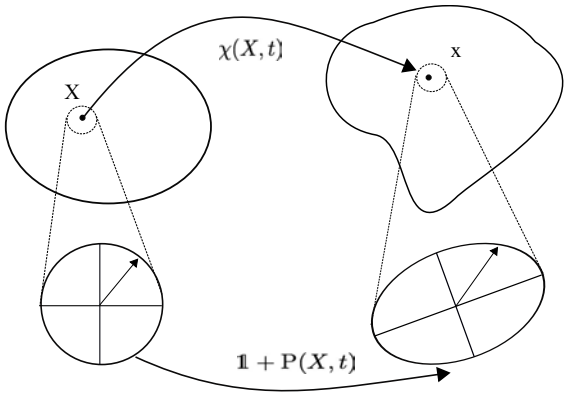

Figure 2.1: Enriched kinematics for a micromorphic continuum.

The introduction of additional kinematical fields was first proposed by the Cosserat brothers [25]. In their model, the added micromorphic displacements were meant to describe rigid rotations at the microscopic level and so, the newly introduced degrees of freedom are in the form of a skew-symmetric tensor $A \in \mathfrak{so}(3)$. However, as it often happens, the work of the Cosserat brothers was not appreciated and expanded until the second half of the 20th century. Mindlin [71, 72], Green and Rivlin [44], Toupin [95, 96], Eringen [34, 36, 37, 38] and Germain [41] all developed the brothers' work and gave it credibility. In Mindlin and Erigen's work, the kinematics was enriched introducing an additional non-symmetric field of micro-distortions $P \in \mathbb{R}^{3\times3}$. In this way, in each macroscopic material point $x \in \Omega$ there is a substructure attached. This micro-deformation was generalized to include micro-stretches, micro-strains, micro-shear, micro-distortions and micro-rotations and it was described by an affine mapping $\mathbb{1} + P$ (Fig. 2.1). For an extensive historic perspective see [78].

We now give a very short review of the classical enriched continuum models before moving on to discuss the novel enriched continuum model, which is the topic of this thesis.

The Mindlin-Eringen model

Maybe the best known and celebrated enriched continuum model is the Mindlin-Eringen model introduced in the early 1960's [23, 34, 35, 37, 38, 70, 71]. The additional degrees of freedom are represented by the second-order tensor $P \in \mathbb{R}^{3\times3}$, so there are 9 additional degrees of freedom. The elastic energy of the general anisotropic centro-symmetric micromorphic model of Mindlin and Eringen ([72] and [36]) is given by:

$$\begin{aligned} W =& \frac{1}{2}\langle \overline{\mathbb{C}_e}(\nabla u - P), (\nabla u - P)\rangle_{\mathbb{R}^{3\times3}} + \frac{1}{2}\langle \mathbb{C}_m \operatorname{sym} P, \operatorname{sym} P\rangle_{\mathbb{R}^{3\times3}} \\ &+ \frac{1}{2}\langle \overline{\mathbb{E}}_{\text{cross}}(\nabla u - P), \operatorname{sym} P\rangle_{\mathbb{R}^{3\times3}} + \frac{\mu L_c^2}{2}\langle \widehat{\mathbb{L}}\nabla P, \nabla P\rangle_{\mathbb{R}^{3\times3}}, \end{aligned} \tag{2.13}$$

where $\overline{\mathbb{C}_e} : \mathbb{R}^{3\times3} \to \mathbb{R}^{3\times3}$ is a 4^{th} order micromorphic elasticity tensors with at most 45 independent coefficients and acts on the *non-symmetric elastic distortion* $e = \nabla u - P$. $\overline{\mathbb{E}}_{\text{cross}} : \mathbb{R}^3 \times \mathbb{R}^3 \to \mathbb{R}^3 \times \mathbb{R}^3$ is a 4^{th} order cross-coupling tensor with the symmetry $(\overline{\mathbb{E}}_{\text{cross}})_{ijkl} = (\overline{\mathbb{E}}_{\text{cross}})_{jikl}$ and has at most 54 independent coefficients, $\mathbb{C}_m : \operatorname{Sym}(3) \to \operatorname{Sym}(3)$ has the 21 independent coefficients of classical elasticity and finally, $\widehat{\mathbb{L}} : \mathbb{R}^{3\times3\times3} \to \mathbb{R}^{3\times3\times3}$ is a 6^{th} order tensor containing 378 independent coefficients. The parameter $\mu > 0$ is a typical shear modulus and $L_c > 0$ is a

characteristic length.[3] We see then that we have a total of 498 independent coefficients.

The Cosserat micropolar model

The second famous micromorphic model is Cossreat's micropolar model [25]. "Micropolar continua" is the denomination given by A.C. Eringen to a subclass of "micromorphic" bodies, in which the additionally introduced internal deformation at each material point reduces to a pure rotation. Here, the microstructure is assumed to have three orthogonal rigid directions and, therefore, the micro-deformation field can only describe micro-rotations. Under this assumption, it suffices to consider a skew-symmetric micromorphic distortion field $A \in \mathfrak{so}(3)$, thus introducing only 3 additional degrees of freedom instead of 9 as in the Mindlin-Eringen model. The strain energy of the Cosserat model is:

$$\begin{aligned} W =& \frac{1}{2}\langle \mathbb{C}_e \operatorname{sym} \nabla u, \operatorname{sym} \nabla u \rangle_{\mathbb{R}^{3\times 3}} + \frac{1}{2}\langle \mathbb{C}_c(\operatorname{skew} \nabla u - A), (\operatorname{skew} \nabla u - A) \rangle_{\mathbb{R}^{3\times 3}} \\ &+ \frac{\mu L_c^2}{2}\langle \overline{\mathbb{L}} \nabla \operatorname{axl} A, \nabla \operatorname{axl} A \rangle_{\mathbb{R}^{3\times 3}}, \end{aligned} \tag{2.14}$$

where $\mathbb{C}_e : \operatorname{Sym}(3) \to \operatorname{Sym}(3)$ is the classical 4^{th} order elasticity tensor acting on the symmetric strain $\operatorname{sym} \nabla u$, $\mathbb{C}_c : \mathfrak{so}(3) \to \mathfrak{so}(3)$ is a 4^{th} order tensor acting on the 2^{nd} order skew-symmetric strain $\operatorname{skew}(\nabla u - A)$ and $\overline{\mathbb{L}} : \mathbb{R}^{3\times 3} \to \mathbb{R}^{3\times 3}$ is a 4^{th} order constitutive tensor acting on the 2^{nd} order tensor $\nabla \operatorname{axl} A$.

Although a wide set of materials seem to fit the hypothesis that the mircrostructure can only rotate, it is still difficult to fit additional parameters in a reliable manner ([68]).

[3] Here we have assumed just a decoupled format of the energy. Mixed terms of strain and curvature have been discarded by assuming centro-symmetry.

Chapter 3

The relaxed micromorphic model

The **relaxed micromorphic model**, introduced and described in [9, 42, 77, 78, 79], is an enriched continuum model. It differs from the Mindlin-Eringen representation in that it is endowed with more geometric structure (by introducing the sym/skew decomposition of the chosen deformation measures). In order to formally derive the governing equations for the model, we introduce a strain and a kinetic energy density. Following standard variational techniques, we demonstrate in this chapter how we can derive both the bulk governing equations as well as the boundary conditions for the relaxed micromorphic model but also of the classical Cauchy model. This is achieved by setting the first variation of the action functional to be equal to zero.

The relaxed micromorphic model is not obtained via a direct upscaling approach based, for example, on classical or numerical dynamical homogenization [26, 90, 103]. The theoretical framework is set up directly at the macroscopic scale and the homogenized behavior can be mapped back onto specific metamaterials' microstructures via an inverse fitting procedure of the dispersion curves, e.g. on Bloch-Floquet diagrams. If it cannot be expected that the relaxed micromorphic model reproduces point by point the dispersive behavior of real metamaterials, it can, to a very good extent, qualitatively and quantitatively reproduce the averaged properties of such materials, including the metamaterial's dispersion, band-gap and macroscopic scattering.

Previous studies have provided the foundation of the theoretical basis for the definition of isotropic and anisotropic relaxed micromorphic media, including well-posedness results [42, 77, 78, 83]. They have also explored the bulk behavior of such media, starting a comparison with real metamaterials [58, 59, 64] and have attempted some academic studies of 1D refractive problems at relaxed micromorphic interfaces [58, 65]. In this thesis, for the first time, we propose a complete 2D framework for the study of the refractive properties of relaxed micromorphic interfaces. Potentially, this provides powerful tools for advancing towards the validation of the model on real metastructures, where it is certain that the scattering properties do not only depend on the frequency, but also on the angle of incidence. Although we could target specific microstructures (as we will do, for example in chapters 5 and 6), the true efficacy of the model lies in its ability of providing boundary conditions (continuity of macroscopic displacement and of "generalized" tractions), which are pertinent at the macroscopic scale.

The rigorous development of the relaxed micromorphic model for anisotropic metamaterials has been given in [29], where applications to different classes of symmetry and the particular case of tetragonal periodic metamaterials are also discussed. In the latter paper, a procedure to univocally determine some of the material parameters for periodic metamaterials with static tests is also provided.

None of the other generalized continuum models (as second gradient models or Mindlin-

Eringen model) have been able to well describe band-gaps in metamaterials to the same extent as the relaxed micromorphic model ([60, 62]). Indeed, second gradient models cannot grasp complex dispersion due to their simplified kinematics, allowing only acoustic branches to be accounted for. On the other hand, the Mindlin-Eringen model, although it considers an appropriate kinematical framework, relies on a large number of constitutive parameters, thus making any physical interpretation very tricky. Due to its simplified constitutive relations for the strain energy density, the relaxed micromorphic model allows to account for the main overall dispersion properties of band-gap metastructures, via a relatively contained number of elastic parameters. Such parameters simplification relies on the "sym-skew-trace" orthogonal decomposition adopted for the micro and macro deformation measures of the relaxed micromorphic model.

3.1 Energy formulation of the relaxed micromorphic model

We begin with the most general case possible, which is the fully anisotropic case but we do not assume any specific symmetry class or under any other assumption, as will be done in the latter chapters of this thesis, in order to make our results as general as possible.[1]

Let Ω be an open bounded domain in $\mathbb{R}^3$ with piecewise smooth boundary $\partial\Omega$ and closure $\overline{\Omega}$ and $[0,T] \subset \mathbb{R}$ the time interval. Furthermore, we set $\Omega_0 = \Omega \times \{0\}$. The kinematical fields of the relaxed micromorphic model are the *macro-displacement* u and the *micro-distortion tensor* P, where:

$$u : \overline{\Omega} \times [0,T] \to \mathbb{R}^3, \qquad P : \overline{\Omega} \times [0,T] \to \mathbb{R}^{3\times 3}. \tag{3.1}$$

We now need an appropriate space of functions, the so-called *space of configurations*, in order to perform the variation of the action functional. This space is given by:

$$\mathcal{Q} := \left\{ (u,P) \in \mathcal{C}^1\left(\overline{\Omega}\times[0,T],\mathbb{R}^3\right) \times \mathcal{C}^1\left(\overline{\Omega}\times[0,T],\mathbb{R}^{3\times 3}\right) : (u,P) \text{ verify } (\mathrm{C}_1) \text{ and } (\mathrm{C}_2) \right\}, \tag{3.2}$$

where,

- (C_1) is the following set of boundary conditions to our problem:

$$\left.\begin{aligned} u(x,t) &= \phi(x,t) \\ P_i(x,t)\times\nu &= p_i(x,t) \end{aligned}\right\} \text{ on } \partial\Omega\times[0,T], \tag{3.3}$$

  where $i = 1,2,3$, ν is the unit normal vector to $\partial\Omega \times [0,T]$ and P_i are the rows of P. Finally, ϕ and p_i are prescribed functions.

- (C_2) is the following set of initial conditions:

$$\left.\begin{aligned} u|_{\Omega_0} &= u_0, & u_{,t}|_{\Omega_0} &= \underline{u}_0 \\ P|_{\Omega_0} &= P_0, & P_{,t}|_{\Omega_0} &= \underline{P}_0 \end{aligned}\right\} \text{ in } \Omega_0, \tag{3.4}$$

  where $u_0(x)$, $\underline{u}_0(x)$, $P_0(x)$, $\underline{P}_0(x)$ are prescribed functions.

We remark here that the boundary condition $P_i(x,t)\times\nu = 0$, $i = 1,2,3$ is equivalent to $P_i(x,t)\cdot n = 0$, $i = 1,2,3$ for all tangential vectors n on $\partial\Omega$. This is due to the fact that the problem is posed for $P \in H(\mathrm{Curl};\Omega)$ and so the variational setting allows only to prescribe tangential boundary condition, see [78] for more details.

[1] In the forthcoming chapters, we will mainly work in the tetragonal symmetry case and under the plane-strain assumption.

3.1.1 Strain energy density

The strain energy for an anisotropic relaxed micromorphic medium is given by [3, 4, 29]:

$$\begin{aligned} W(\nabla u, P, \operatorname{Curl} P) = &\underbrace{\frac{1}{2}\langle \mathbb{C}_e \operatorname{sym}(\nabla u - P), \operatorname{sym}(\nabla u - P)\rangle}_{\text{anisotropic elastic-energy}} + \underbrace{\frac{1}{2}\langle \mathbb{C}_{\text{micro}} \operatorname{sym} P, \operatorname{sym} P\rangle}_{\text{micro-self-energy}} \\ &+ \underbrace{\frac{1}{2}\langle \mathbb{C}_c \operatorname{skew}(\nabla u - P), \operatorname{skew}(\nabla u - P)\rangle}_{\text{local anisotropic rotational elastic coupling}} \\ &+ \underbrace{\frac{L_c^2}{2}\left(\langle \mathbb{L}_e \operatorname{sym}\operatorname{Curl} P, \operatorname{sym}\operatorname{Curl} P\rangle + \langle \mathbb{L}_c \operatorname{skew}\operatorname{Curl} P, \operatorname{skew}\operatorname{Curl} P\rangle\right)}_{\text{curvature}}. \end{aligned} \tag{3.5}$$

Here, $\mathbb{C}_e, \mathbb{C}_{\text{micro}} : \operatorname{Sym}(3) \to \operatorname{Sym}(3)$ are classical 4^{th} order elasticity tensors, with at most 21 independent components, acting on symmetric second order tensors only. This is seen by the fact that $\mathbb{C}_e$ acts on the symmetric elastic strain $\varepsilon_{\text{e}} := \operatorname{sym}(\nabla u - P)$ and $\mathbb{C}_{\text{micro}}$ acts on the symmetric micro-strain $\operatorname{sym} P$ and both map to symmetric tensors. The tensor $\mathbb{C}_c : \mathfrak{so}(3) \to \mathfrak{so}(3)$ is a 4^{th} order tensor, with 6 independent components, acting only on skew-symmetric tensors and this action gives skew-symmetric tensors. Finally, $\mathbb{L}_e : \operatorname{Sym}(3) \to \operatorname{Sym}(3)$ is a classical, positive-definite tensor with at most 21 independent parameters acting on the symmetric part of the curvature $\operatorname{sym}\operatorname{Curl} P$, and $\mathbb{L}_c : \mathfrak{so}(3) \to \mathfrak{so}(3)$ is a positive definite tensor with at most 6 independent components acting on the skew-symmetric part of the curvature.

The relaxed micromorphic curvature can be written as

$$\operatorname{Curl} P = -\operatorname{Curl}(\nabla u - P), \tag{3.6}$$

since Curl is gauge-invariant (the curl of the divergence of a vector field is always zero), see [77]. Furthermore, $\operatorname{Curl} P$ supports a completely invariant setting, as seen in [75, 76]. The algebraic advantage of using the curl of P (instead of the gradient) in the strain energy density is that the Curl operator acting on a second order tensor is again a second order tensor and so, we no longer need Mindlin-Eringen's 6^{th} order tensors but a 4^{th} order tensor, which acts on $\operatorname{Curl} P$. This is crucial, because the anisotropy classification of such tensors is easier and well-known [18].

This constitutive expression for the strain energy density of the relaxed micromorphic model is the most general one we can provide in the anisotropic and centrosymmetric setting. Counting coefficients, we see that this representation has maximally 75 $(21+21+6+21+6)$ independent coefficients. This number is reduced according to the symmetry class and state of the system (plane-strain/stress) one considers. For example, in the tetragonal symmetry case with the plane-strain assumption, this number reduces to 11 $(3+3+1+3+1)$ independent coefficients (see chapters 5 and 6).

An important feature which we must point out is that the relaxed micromorphic model can be used with $\mathbb{C}_c$ positive semi-definite or even zero. On the other hand, we assume that the constitutive tensors $\mathbb{C}_e$ and $\mathbb{C}_{\text{micro}}$ are strictly positive definite. Furthermore, the tensors $\mathbb{L}_e$ and $\mathbb{L}_c$ are positive definite and the characteristic length L_c is non-negative. Positive definiteness means that:

$$\begin{aligned}
\exists c_e^+ > 0 : \forall S \in \mathrm{Sym}(3) : \quad & \langle \mathbb{C}_e S, S\rangle_{\mathbb{R}^{3\times 3}} \geq c_e^+ ||S||^2_{\mathbb{R}^{3\times 3}}, \\
\exists c_m^+ > 0 : \forall S \in \mathrm{Sym}(3) : \quad & \langle \mathbb{C}_{\mathrm{micro}} S, S\rangle_{\mathbb{R}^{3\times 3}} \geq c_m^+ ||S||^2_{\mathbb{R}^{3\times 3}}, \\
\exists c_l^+ > 0 : \forall S \in \mathbb{R}^{3\times 3} : \quad & \langle \mathbb{L}_e S, S\rangle_{\mathbb{R}^{3\times 3}} \geq c_l^+ ||S||^2_{\mathbb{R}^{3\times 3}}.
\end{aligned} \tag{3.7}$$

As for the tensors $\mathbb{C}_c$ and $\mathbb{L}_c$ acting only on skew-symmetric second order tensors, we require them to be only positive semi-definite, i.e:

$$\begin{aligned}
&\forall \overline{A} \in \mathfrak{so}(3) : \langle \mathbb{C}_c \overline{A}, \overline{A}\rangle_{\mathbb{R}^{3\times 3}} \geq 0, \\
&\forall \overline{A} \in \mathfrak{so}(3) : \langle \mathbb{L}_c \overline{A}, \overline{A}\rangle_{\mathbb{R}^{3\times 3}} \geq 0.
\end{aligned} \tag{3.8}$$

The above definition implies that the rotational coupling tensor $\mathbb{C}_c$ could vanish, in which case the relaxed micromorphic model is rendered *non-redundant* [88]. This means that, although $\mathbb{C}_c$ could be identically equal to zero, the skew-symmetric part of P is not controlled locally but as a result of a boundary value problem and boundary conditions. In this sense, allowing $\mathbb{C}_c \equiv 0$ is one of the decisive possibilities offered by the relaxed micromorphic model.

The isotropic case

In the case of isotropy, the strain energy (3.5) simplifies to [2, 3, 58, 62, 63, 64, 78, 79]

$$\begin{aligned}
W = & \underbrace{\mu_e \left\|\mathrm{sym}(\nabla u - P)\right\|^2 + \frac{\lambda_e}{2}(\mathrm{tr}(\nabla u - P))^2}_{\text{isotropic elastic-energy}} + \underbrace{\mu_c \left\|\mathrm{skew}(\nabla u - P)\right\|^2}_{\substack{\text{invariant local isotropic} \\ \text{rotational elastic coupling}}} \\
& + \underbrace{\mu_{\mathrm{micro}} \left\|\mathrm{sym}\, P\right\|^2 + \frac{\lambda_{\mathrm{micro}}}{2}(\mathrm{tr}\, P)^2}_{\text{micro-self-energy}} + \underbrace{\frac{\mu_e L_c^2}{2} \left\|\mathrm{Curl}\, P\right\|^2}_{\text{isotropic curvature}}.
\end{aligned} \tag{3.9}$$

Strict positive definiteness of the strain energy in the isotropic case implies the following simple relations for the introduced parameters ([78])

$$\mu_e > 0, \quad 2\,\mu_e + 3\,\lambda_e > 0, \quad \mu_{\mathrm{micro}} > 0, \quad 2\,\mu_{\mathrm{micro}} + 3\,\lambda_{\mathrm{micro}} > 0, \quad \mu_c \geq 0, \quad L_c \geq 0. \tag{3.10}$$

Observe here that μ_c can be equal to zero, which is the equivalent to $\mathbb{C}_c \equiv 0$ in the anisotropic case.

Finally, we must remark that in the isotropic case, the relaxed micromorphic model admits linear elasticity as an upper energetic limit for any characteristic length scale $L_c > 0$ (see [9, 29]).

3.1.2 Kinetic energy density

The kinetic energy of the fully anisotropic relaxed micromorphic model is given by [4, 29]:

$$\begin{aligned}
J(u_{,t}, \nabla u_{,t}, P_{,t}) = & \frac{1}{2}\rho \left\|u_{,t}\right\|^2 + \frac{1}{2}\langle \mathbb{J}_{\mathrm{micro}}\, \mathrm{sym}\, P_{,t}, \mathrm{sym}\, P_{,t}\rangle + \frac{1}{2}\langle \mathbb{J}_c\, \mathrm{skew}\, P_{,t}, \mathrm{skew}\, P_{,t}\rangle \\
& + \frac{1}{2}\langle \mathbb{T}_e\, \mathrm{sym}\, \nabla u_{,t}, \mathrm{sym}\, \nabla u_{,t}\rangle + \frac{1}{2}\langle \mathbb{T}_c\, \mathrm{skew}\, \nabla u_{,t}, \mathrm{skew}\, \nabla u_{,t}\rangle,
\end{aligned} \tag{3.11}$$

Here, $\mathbb{J}_{\mathrm{micro}} : \mathrm{Sym}(3) \to \mathrm{Sym}(3)$ is the classical 4^{th} order free micro-inertia density tensor, $\mathbb{T}_e : \mathrm{Sym}(3) \to \mathrm{Sym}(3)$ is the classical 4^{th} order gradient micro-inertia density tensor with, in

general, 21 independent components each, $\mathbb{J}_c, \mathbb{T}_c : \mathfrak{so}(3) \to \mathfrak{so}(3)$ are 4^{th} order coupling tensors with 6 independent components and $\rho : \Omega \to \mathbb{R}^+$ is the macro-inertia mass density.

As for the positive definiteness and positive semi-definiteness of the constitutive tensors appearing in the kinetic energy density, we have:

$$\begin{aligned} &\exists c_j^+ > 0 : \forall S \in \mathrm{Sym}(3) : \qquad \langle \mathbb{J}_{\text{micro}} S, S \rangle_{\mathbb{R}^{3\times 3}} \geq c_j^+ ||S||^2_{\mathbb{R}^{3\times 3}}, \\ &\exists c_t^+ > 0 : \forall S \in \mathrm{Sym}(3) : \qquad \langle \mathbb{T}_e S, S \rangle_{\mathbb{R}^{3\times 3}} \geq c_t^+ ||S||^2_{\mathbb{R}^{3\times 3}}, \end{aligned} \tag{3.12}$$

and

$$\begin{aligned} &\forall \overline{A} \in \mathfrak{so}(3) : \langle \mathbb{J}_c \overline{A}, \overline{A} \rangle_{\mathbb{R}^{3\times 3}} \geq 0, \\ &\forall \overline{A} \in \mathfrak{so}(3) : \langle \mathbb{T}_c \overline{A}, \overline{A} \rangle_{\mathbb{R}^{3\times 3}} \geq 0. \end{aligned} \tag{3.13}$$

The isotropic case

In the isotropic case, the equivalent expression to (3.11) is given by ([57, 60])

$$\begin{aligned} J = &\frac{1}{2}\rho \langle u_{,t}, u_{,t} \rangle + \frac{1}{2}\eta_1 \|\mathrm{dev}\,\mathrm{sym}\, P_{,t}\|^2 + \frac{1}{2}\eta_2 \|\mathrm{skew}\, P_{,t}\|^2 + \frac{1}{6}\eta_3 \,\mathrm{tr}\,(P_{,t})^2 \\ &+ \frac{1}{2}\overline{\eta}_1 \|\mathrm{dev}\,\mathrm{sym}\,\nabla u_{,t}\|^2 + \frac{1}{2}\overline{\eta}_2 \|\mathrm{skew}\,\nabla u_{,t}\|^2 + \frac{1}{6}\overline{\eta}_3 \,\mathrm{tr}\,(\nabla u_{,t})^2 . \end{aligned} \tag{3.14}$$

Positive definiteness in the isotropic case implies:

$$\rho > 0, \quad \eta_1 > 0, \quad \eta_2 > 0, \quad \eta_3 > 0, \quad \overline{\eta}_1 > 0, \quad \overline{\eta}_2 > 0, \quad \overline{\eta}_3 > 0 \tag{3.15}$$

However, the most simplified form of the isotropic energy, which we will be considering in chapter 4, as discussed in [2, 3, 65], is given by

$$J = \frac{1}{2}\rho \|u_{,t}\|^2 + \frac{1}{2}\eta \|P_{,t}\|^2 , \tag{3.16}$$

where $\rho > 0$ is the apparent macroscopic density and $\eta > 0$ is the micro-inertia density. Comparing (3.16) to (3.14), we see that all the gradient micro-inertia terms vanish and that there is no Cartan-Lie splitting of the micro-distortion tensor P. This, however, will not be a particular issue, since the isotropic example we will be considering later on in chapter 4, is a purely "academic" experiment and not fitted on a specific real metamaterial (as done for example in [4, 57, 59]). Therefore, the need for a better fitting of dispersion curves (something which is achieved by introducing the gradient micro-inertia terms) will not be present when we discuss reflection and transmission problems in isotropic media and so, we will choose the simplest formulation possible for the kinetic energy as given by (3.16).

3.2 Variation of the action functional

Having introduced an appropriate space of configurations $\mathcal{Q}$ (given in (3.2)) and discussed the energy densities from which the relaxed micromorphic model stems, we are now ready to perform the variation of the action functional in order to derive the governing equations for the anisotropic and isotropic relaxed micromorphic model. This procedure is known and well-understood and for the sake of clarity we will not demonstrate each step here. The detailed computations are presented in Appendices A1 and A2.

The *action functional* $\mathcal{A} : \mathcal{Q} \to \mathbb{R}$ is the sum of the internal and external action functionals $\mathcal{A}^{\text{int}}, \mathcal{A}^{\text{ext}} : \mathcal{Q} \to \mathbb{R}$, (recall equation (3.2)) defined by

$$\mathcal{A}^{\text{int}}[(u,P)] := \int_0^T \int_\Omega \mathcal{L}(u_{,t}, \nabla u_{,t}, P_{,t}, \nabla u, P, \operatorname{Curl} P) dx\, dt, \tag{3.17}$$

$$\mathcal{A}^{\text{ext}}[(u,P)] := \int_0^T \int_\Omega \langle b^{\text{ext}}, u\rangle + \langle M^{\text{ext}}, P\rangle dx\, dt, \tag{3.18}$$

where $\mathcal{L}$ is the Lagrangian density of the system and b^{ext} and M^{ext} are the external body force and body double force (or, momentum), respectively. We assume throughout this computation that no external action affects the system, so we set $f^{\text{ext}} = M^{\text{ext}} = 0$. The derivatives appearing in (3.17) and (3.18) are to be understood in the sense of distributions.

The Lagrangian energy density is the standard split of kinetic minus strain energy, i.e.:

$$\mathcal{L}(u_{,t}, \nabla u_{,t}, P_{,t}, \nabla u, P, \operatorname{Curl} P) = J(u_{,t}, \nabla u_{,t}, P_{,t}) - W(\nabla u, P, \operatorname{Curl} P). \tag{3.19}$$

We are looking for stationary points of the action functional $\mathcal{A} = \mathcal{A}^{\text{int}} + \mathcal{A}^{\text{ext}} = \mathcal{A}^{\text{int}}$, since we assume no external forces. To that end, we have to calculate its first variation $\delta\mathcal{A}$ and solve:

$$\delta\mathcal{A} = \int_0^T \int_\Omega J(u_{,t}, \nabla u_{,t}, P_{,t}) - W(\nabla u, P, \operatorname{Curl} P)\, dx\, dt = 0. \tag{3.20}$$

In the following, we show how to solve this problem by considering the variations of the strain and kinetic energies separately.

Variation of the strain energy

We begin with the variation of the strain energy. Using expression (3.5), we have:

$$\begin{aligned}
\delta \int_0^T \int_\Omega W(\nabla u, P, \operatorname{Curl} P) dx\, dt = {} & \delta \int_0^T \int_\Omega \frac{1}{2} \langle \mathbb{C}_e \operatorname{sym}(\nabla u - P), \operatorname{sym}(\nabla u - P)\rangle\, dx\, dt \\
& + \delta \int_0^T \int_\Omega \frac{1}{2} \langle \mathbb{C}_{\text{micro}} \operatorname{sym} P, \operatorname{sym} P\rangle\, dx\, dt \\
& + \delta \int_0^T \int_\Omega \frac{1}{2} \langle \mathbb{C}_c \operatorname{skew}(\nabla u - P), \operatorname{skew}(\nabla u - P)\rangle\, dx\, dt \\
& + \delta \int_0^T \int_\Omega \frac{L_c^2}{2} \langle \mathbb{L}_e \operatorname{sym} \operatorname{Curl} P, \operatorname{sym} \operatorname{Curl} P\rangle\, dx\, dt \\
& + \delta \int_0^T \int_\Omega \langle \mathbb{L}_c \operatorname{skew} \operatorname{Curl} P, \operatorname{skew} \operatorname{Curl} P\rangle\, dx\, dt.
\end{aligned} \tag{3.21}$$

To compute these integrals, we apply integration by parts and make use of the symmetry of the constitutive tensors which appear in each term (see Appendix A1).

We can then collect the bulk and boundary terms. We find:

$$\begin{aligned}
\int_0^T \int_\Omega & -\langle \operatorname{Div}(\mathbb{C}_e \operatorname{sym}(\nabla u - P) + \mathbb{C}_c \operatorname{skew}(\nabla u - P)), \delta u\rangle\, dx\, dt \\
& + \int_0^T \int_\Omega \langle -\mathbb{C}_e \operatorname{sym}(\nabla u - P) - \mathbb{C}_c \operatorname{skew}(\nabla u - P) + \mathbb{C}_{\text{micro}} \operatorname{sym} P \\
& \qquad + L_c^2 \operatorname{Curl}\left(\mathbb{L}_e \operatorname{sym} \operatorname{Curl} P + \mathbb{L}_c \operatorname{skew} \operatorname{Curl} P\right), \delta P\rangle\, dx\, dt,
\end{aligned} \tag{3.22}$$

for the bulk term and

$$\int_0^T \int_{\partial\Omega} \langle (\mathbb{C}_e \operatorname{sym}(\nabla u - P) + \mathbb{C}_c \operatorname{skew}(\nabla u - P)) \cdot \nu, \delta u \rangle dS dt + L_c^2 \sum_{i=1}^{3} \int_0^T \int_{\partial\Omega} \langle ((\mathbb{L}_e \operatorname{sym} \operatorname{Curl} P + \mathbb{L}_c \operatorname{skew} \operatorname{Curl} P)_i \times \operatorname{curl}(\delta P)_i), \nu \rangle \, dS \, dt, \quad (3.23)$$

for the boundary term.

Variation of the kinetic energy

As for the kinetic energy, using expression (3.11), we have:

$$\begin{aligned} \delta \int_0^T \int_\Omega J(u_{,t}, \nabla u_{,t}, P_{,t}) dx \, dt = & \delta \int_0^T \int_\Omega \frac{1}{2} \rho \, \|u_{,t}\|^2 \, dx \, dt \\ & + \delta \int_0^T \int_\Omega \frac{1}{2} \langle \mathbb{J}_{\text{micro}} \operatorname{sym} P_{,t}, \operatorname{sym} P_{,t} \rangle \, dx \, dt \\ & + \delta \int_0^T \int_\Omega \frac{1}{2} \langle \mathbb{J}_c \operatorname{skew} P_{,t}, \operatorname{skew} P_{,t} \rangle \, dx \, dt \\ & + \delta \int_0^T \int_\Omega \frac{1}{2} \langle \mathbb{T}_e \operatorname{sym} \nabla u_{,t}, \operatorname{sym} \nabla u_{,t} \rangle \, dx \, dt \\ & + \delta \int_0^T \int_\Omega \frac{1}{2} \langle \mathbb{T}_c \operatorname{skew} \nabla u_{,t}, \operatorname{skew} \nabla u_{,t} \rangle \, dx \, dt. \end{aligned} \quad (3.24)$$

These integrals are computed again by applying integration by parts and using the symmetries of the constitutive tensors. The detailed computations are shown in Appendix A2.

Once again we collect the bulk and boundary terms which result from the first variation of the action functional. The bulk term is:

$$\int_0^T \int_\Omega \langle -\rho \, u_{,tt} + \operatorname{Div}(\mathbb{T}_e \operatorname{sym} \nabla u_{,tt} + \mathbb{T}_c \operatorname{skew} \nabla u_{,tt}), \delta u \rangle - \langle \mathbb{J}_{\text{micro}} \operatorname{sym} P_{,tt} + \mathbb{J}_c \operatorname{skew} P_{,tt}, \delta P \rangle \, dx \, dt, \quad (3.25)$$

while the boundary term is given by:

$$\int_0^T \int_{\partial\Omega} \langle (\mathbb{T}_e \operatorname{sym} \nabla u_{,tt} + \mathbb{T}_c \operatorname{skew} \nabla u_{,tt}) \cdot \nu, \delta u \rangle \, dS \, dt. \quad (3.26)$$

A remark on the boundary terms

In the above procedure, we did not consider any external boundary terms. Indeed, the external action was assumed to occur only by body forces (such as gravity). We can, of course, add external tractions to our variational problem if we wish. This would result to the boundary terms being equal to a known given function instead of zero. In that case, the external action would take to form

$$\mathcal{A}^{\text{ext}}[(u, P)] := \int_0^T \int_\Omega \langle b^{\text{ext}}, u \rangle + \langle M^{\text{ext}}, P \rangle dx \, dt + \int_0^T \int_{\partial\Omega} \langle t^{\text{ext}}, u \rangle + \langle \tau^{\text{ext}}, P \rangle dS \, dt, \quad (3.27)$$

where, as before, b^{ext} and M^{ext} are the external body force and body double force, respectively and t^{ext} and τ^{ext} are external tractions assigned on the boundary of the domain.

3.2.1 The governing equations of the anisotropic relaxed micromorphic model

We are now ready to write down the bulk governing equations of the anisotropic relaxed micromorphic model. This is done by imposing the first variation of the action functional to vanish, i.e. $\delta\mathcal{A} = 0$. This is now known and given as the sum of expressions (3.22) and (3.25). Since all these calculations were done for an arbitrary closed bounded domain Ω and for an arbitrary time T, we can drop the integrals and equate the terms which are coupled with the same variation (δu or δP). Finally, we are left with the following system of governing equations (presented here in the sym − skew split):

$$\left\{\begin{array}{rcl} \rho\, u_{tt} - \operatorname{Div}\widehat{\sigma}_{,tt} &=& \operatorname{Div}\widetilde{\sigma}, \\ \mathbb{J}_{\text{micro}}\operatorname{sym} P_{,tt} &=& \widetilde{\sigma}_e - s - \operatorname{sym}\operatorname{Curl} m, \\ \mathbb{J}_c \operatorname{skew} P_{,tt} &=& \widetilde{\sigma}_c - \operatorname{skew}\operatorname{Curl} m, \end{array}\right. \tag{3.28}$$

where we set

$$\begin{aligned} &\widetilde{\sigma}_e = \mathbb{C}_e \operatorname{sym}(\nabla u - P), \qquad \widetilde{\sigma}_c = \mathbb{C}_c \operatorname{skew}(\nabla u - P), \qquad \widetilde{\sigma} = \widetilde{\sigma}_e + \widetilde{\sigma}_c, \qquad \widehat{\sigma} = \mathbb{T}_e \operatorname{sym}\nabla u + \mathbb{T}_c \operatorname{skew}\nabla u, \\ &s = \mathbb{C}_{\text{micro}} \operatorname{sym} P, \qquad m := L_c^2\,(\mathbb{L}_e \operatorname{sym}\operatorname{Curl} P + \mathbb{L}_c \operatorname{skew}\operatorname{Curl} P). \end{aligned} \tag{3.29}$$

In the case where we impose some external action (see (3.27)), the boundary conditions which accompany these bulk equations are

$$f := (\widetilde{\sigma} + \widehat{\sigma})\cdot\nu = t^{\text{ext}}(x,t), \quad \text{or} \qquad u = \phi(x,t), \qquad \forall x \in \partial\Omega_0, \tag{3.30}$$

$$\tau\cdot n_i := -m\cdot\epsilon\cdot\nu = \tau^{\text{ext}}(x,t), \quad \text{or} \quad P\cdot n_i = p_i(x,t), \quad i = 2,3, \qquad \forall x \in \partial\Omega_0, \tag{3.31}$$

where ϵ is the Levi-Civita permutation symbol, ν is the normal to the boundary and n_1 and n_2 are orthogonal vectors tangent to the boundary $\partial\Omega_0$ (a contour where the external perturbation is applied). We will discuss the boundary conditions (3.30) and (3.31) in greater detail in the following chapters.

3.2.2 The isotropic governing equations

In the case of isotropy, we take the same steps, but we change the energy: instead of (3.5) we consider expression (3.9) for the strain energy and instead of (3.11) we consider (3.14) for the kinetic energy. The same considerations apply and the variation of the (new) action functional is done in a virtually identical way. For the sake of clarity and coherence, we skip the calculations for the case of isotropy and simply write down the resulting governing equations. These are:

$$\left\{\begin{array}{rcl} \rho\, u_{tt} - \operatorname{Div}\widehat{\sigma}_{,tt} &=& \operatorname{Div}\widetilde{\sigma} \\ \widetilde{\mathcal{I}}_{,tt} &=& \widetilde{\sigma} - s - \operatorname{Curl} m \end{array}\right., \tag{3.32}$$

where,

$$\begin{aligned} \widehat{\sigma} &= \overline{\eta}_1 \operatorname{dev}\operatorname{sym}\nabla u + \overline{\eta}_2 \operatorname{skew}\nabla u + \frac{\overline{\eta}_3}{3}\operatorname{tr}(\nabla u) \\ \widetilde{\sigma} &= 2\,\mu_e\ \operatorname{sym}(\nabla u - P) + 2\,\mu_c\ \operatorname{skew}(\nabla u - P) + \lambda_e\ \operatorname{tr}(\nabla u - P)\,\mathbb{1}, \\ \widetilde{\mathcal{I}} &= \eta_1 \operatorname{dev}\operatorname{sym} P + \eta_2 \operatorname{skew} P + \frac{\eta_3}{3}\operatorname{tr}(P)\mathbb{1} \\ s &= 2\mu_{\text{micro}} \operatorname{sym} P + \lambda_{\text{micro}} \operatorname{tr}(P)\mathbb{1} \\ m &= \mu_e L_c^2 \operatorname{Curl} P. \end{aligned} \tag{3.33}$$

As noted in section 3.1.2, we will be considering an even simpler kinetic energy for the isotropic case without the split on P and the micro-gradient inertia terms, which is given by (3.16). For this energy and again following the same steps in order to impose the first variation of the action functional to vanish, the governing equations are given by:

$$\begin{cases} \rho\, u_{tt} = & \operatorname{Div} \widetilde{\sigma} \\ \eta\, P_{tt} = & \widetilde{\sigma} - s - \operatorname{Curl} m, \end{cases} \tag{3.34}$$

where,

$$\begin{aligned} \widetilde{\sigma} &= 2\mu_e \operatorname{sym}(\nabla u - P) + \lambda_e \operatorname{tr}(\nabla u - P)\, \mathbb{1} + 2\mu_c \operatorname{skew}(\nabla u - P), \\ s &= 2\mu_{\text{micro}} \operatorname{sym} P + \lambda_{\text{micro}} (\operatorname{tr} P)\ \mathbb{1}, \\ m &= \mu_e L_c^2 \operatorname{Curl} P. \end{aligned} \tag{3.35}$$

3.3 Variation of the action functional and the governing equations of the classical Cauchy model

In this section we will present how to derive the classical Cauchy model from the strain and kinetic energies (2.1) and (2.2) by following the recipe presented in section 3.2. This is a simpler calculation and easier to follow than the case of the relaxed micromorphic model and is therefore presented in full detail. Once again, the main tool in the following computations is integration by parts.

We begin with the variation of the strain energy density (2.1). We have

$$\begin{aligned} \delta \int_0^T \int_\Omega W(\nabla u) dx\, dt &= \delta \int_0^T \int_\Omega \frac{1}{2} \langle \mathbb{C}_{\text{M}} \operatorname{sym}(\nabla u), \operatorname{sym}(\nabla u) \rangle dx\, dt \\ \left(_{\text{symmetry of } \mathbb{C}_{\text{M}}}\right) &= \int_0^T \int_\Omega \langle \mathbb{C}_{\text{M}} \operatorname{sym} \nabla u, \nabla \delta u \rangle dx\, dt \\ &= \int_0^T \int_\Omega \operatorname{div} \left(\mathbb{C}_{\text{M}} \operatorname{sym} \nabla u \cdot \delta u \right) dx\, dt - \int_0^T \int_\Omega \langle \operatorname{Div}(\mathbb{C}_{\text{M}} \operatorname{sym} \nabla u), \delta u \rangle dx\, dt \\ &= \int_0^T \int_{\partial\Omega} \langle \mathbb{C}_{\text{M}} \operatorname{sym} \nabla u \cdot \nu, \delta u \rangle dx\, dt - \int_0^T \int_\Omega \langle \operatorname{Div}(\mathbb{C}_{\text{M}} \nabla u), \delta u \rangle dx\, dt. \end{aligned} \tag{3.36}$$

The bulk term is given by

$$\int_0^T \int_\Omega \langle \operatorname{Div}(\mathbb{C}_{\text{M}} \nabla u), \delta u \rangle dx\, dt, \tag{3.37}$$

while the boundary term by

$$\int_0^T \int_{\partial\Omega} \langle \mathbb{C}_{\text{M}} \operatorname{sym} \nabla u \cdot \nu, \delta u \rangle dx\, dt \tag{3.38}$$

As for the variation of the kinetic energy density (2.2), we have:

$$\begin{aligned}
\delta \int_0^T \int_\Omega J(u_{,t}) dx\, dt &= \frac{1}{2}\,\delta \int_0^T \int_\Omega \rho\, \|u_{,t}\|^2\, dx\, dt \\
&= \rho \int_0^T \int_\Omega \langle u_{,t}, \delta u_{,t}\rangle dx\, dt \\
&= \rho \int_0^T \int_\Omega \frac{d}{dt}\langle u_{,t}, \delta u\rangle dx\, dt - \rho \int_0^T \int_\Omega \langle u_{,tt}, \delta u\rangle dx\, dt \\
&= \rho \int_0^T \frac{d}{dt}\left(\int_\Omega \langle u_{,t}, \delta u\rangle dx\right) dt - \rho \int_0^T \int_\Omega \langle u_{,tt}, \delta u\rangle dx\, dt \\
&= \rho \int_{0\times\{T\}} \langle u_{,t}(x,T), \delta u(x,T)\rangle dx - \rho \int_{\Omega\times\{0\}} \langle u_{,t}(x,0), \delta u(x,0)\rangle dx \\
&\quad - \rho \int_0^T \int_\Omega \langle u_{,tt}, \delta u\rangle dx\, dt.
\end{aligned} \tag{3.39}$$

The bulk term from the variation of the kinetic energy is given by

$$\rho \int_0^T \int_\Omega \langle u_{,tt}, \delta u\rangle dx\, dt. \tag{3.40}$$

The bulk terms (3.37) and (3.40) give the governing equations:

$$\rho\, u_{,tt} = \operatorname{Div}(\mathbb{C}_{\mathrm{M}} \operatorname{sym} \nabla u), \quad \text{in } \Omega, \tag{3.41}$$

while the (spatial) boundary term (3.38) gives the expression for the traction:

$$f := (\mathbb{C}_{\mathrm{M}} \operatorname{sym} \nabla u) \cdot \nu, \quad \text{on } \partial\Omega, \tag{3.42}$$

where, once again, we can assign it to a prescribed function or set it equal to zero.

3.4 The constitutive tensors in the Mandel-Voigt notation

We will now consider an equivalent formulation of the relaxed micromorphic model, which is obtained by using the Mandel-Voigt vector notation for the macro-strain $\operatorname{sym} \nabla u$ as well as for the micro-strain $\operatorname{sym} P$.

The idea is to replace these second order tensors with appropriate vectors, whose components are the column-wise sorted components of the tensors (a sorting which is done arbitrarily). In a similar fashion, the fourth-order constitutive tensors will be assigned to corresponding second order tensors. This representation is more suitable and easier to handle if one wants to specify the anisotropy classes of the constitutive tensors in a format easily found in the literature. This method was first put forth by Mandel [66] and Voigt [100, 101], hence the name. We mainly follow [9] in the following.

Consider the linear mapping $\mathfrak{M}_{\alpha ij} : \operatorname{Sym}(3) \to \mathbb{R}^6$, which isomorphically maps the independent components of $(\operatorname{sym} \nabla u)_{ij}$ and $(\operatorname{sym} \nabla u)_{ij}$ to corresponding vectors ε_α and β_α in the following way:

$$\varepsilon_\alpha = \mathfrak{M}_{\alpha ij} (\operatorname{sym} \nabla u)_{ij}, \tag{3.43}$$

and

$$\beta_\alpha = \mathfrak{M}_{\alpha ij} (\operatorname{sym} P)_{ij}. \tag{3.44}$$

Here, Latin subscripts can take the values $\{1,2,3\}$ while Greek subscripts range in $\{1,2,3,4,5,6\}$. We then have:

$$\varepsilon = \begin{pmatrix} (\operatorname{sym}\nabla u)_{11} \\ (\operatorname{sym}\nabla u)_{22} \\ (\operatorname{sym}\nabla u)_{33} \\ c\,(\operatorname{sym}\nabla u)_{23} \\ c\,(\operatorname{sym}\nabla u)_{13} \\ c\,(\operatorname{sym}\nabla u)_{12} \end{pmatrix}, \qquad \beta = \begin{pmatrix} (\operatorname{sym} P)_{11} \\ (\operatorname{sym} P)_{22} \\ (\operatorname{sym} P)_{33} \\ c\,(\operatorname{sym} P)_{23} \\ c\,(\operatorname{sym} P)_{13} \\ c\,(\operatorname{sym} P)_{12} \end{pmatrix}, \tag{3.45}$$

where the coefficient c is either 2 (for Voigt [100, 101]) or $\sqrt{2}$ (for Mandel [66]). Equation (3.45) defines the mapping $\mathfrak{M}$. The components of this mapping can be represented as 3×3 matrices. We fix the index α and we have:

$$\begin{gathered} \mathfrak{M}_{1ij} = \begin{pmatrix} 1 & 0 & 0 \\ 0 & 0 & 0 \\ 0 & 0 & 0 \end{pmatrix}, \qquad \mathfrak{M}_{2ij} = \begin{pmatrix} 0 & 0 & 0 \\ 0 & 1 & 0 \\ 0 & 0 & 0 \end{pmatrix}, \qquad \mathfrak{M}_{3ij} = \begin{pmatrix} 0 & 0 & 0 \\ 0 & 0 & 0 \\ 0 & 0 & 1 \end{pmatrix} \\ \mathfrak{M}_{4ij} = \begin{pmatrix} 0 & 0 & 0 \\ 0 & 0 & \frac{c}{2} \\ 0 & \frac{c}{2} & 0 \end{pmatrix}, \qquad \mathfrak{M}_{5ij} = \begin{pmatrix} 0 & 0 & \frac{c}{2} \\ 0 & 0 & 0 \\ \frac{c}{2} & 0 & 0 \end{pmatrix}, \qquad \mathfrak{M}_{6ij} = \begin{pmatrix} 0 & \frac{c}{2} & 0 \\ \frac{c}{2} & 0 & 0 \\ 0 & 0 & 0 \end{pmatrix} \end{gathered} \tag{3.46}$$

The inverse mapping $\mathfrak{M}^{-1}_{ij\alpha} : \mathbb{R}^6 \to \operatorname{Sym}(3)$ is defined as:

$$(\operatorname{sym}\nabla u)_{ij} = \mathfrak{M}^{-1}_{ij\alpha}\,\varepsilon_\alpha, \qquad (\operatorname{sym} P)_{ij} = \mathfrak{M}^{-1}_{ij\alpha}\,\beta_\alpha. \tag{3.47}$$

Furthermore, we require that

$$\mathfrak{M}_{\gamma ij}\,\mathfrak{M}^{-1}_{ij\gamma} = \widetilde{\delta}_{\alpha\gamma}, \tag{3.48}$$

where $\widetilde{\delta}$ is the Kronecker delta in $\mathbb{R}^6\times\mathbb{R}^6$. The components of this inverse mapping are given by:

$$\begin{gathered} \mathfrak{M}_{ij1} = \begin{pmatrix} 1 & 0 & 0 \\ 0 & 0 & 0 \\ 0 & 0 & 0 \end{pmatrix}, \qquad \mathfrak{M}^{-1}_{ij2} = \begin{pmatrix} 0 & 0 & 0 \\ 0 & 1 & 0 \\ 0 & 0 & 0 \end{pmatrix}, \qquad \mathfrak{M}^{-1}_{ij3} = \begin{pmatrix} 0 & 0 & 0 \\ 0 & 0 & 0 \\ 0 & 0 & 1 \end{pmatrix} \\ \mathfrak{M}^{-1}_{ij4} = \begin{pmatrix} 0 & 0 & 0 \\ 0 & 0 & \frac{1}{c} \\ 0 & \frac{1}{c} & 0 \end{pmatrix}, \qquad \mathfrak{M}^{-1}_{ij5} = \begin{pmatrix} 0 & 0 & \frac{1}{c} \\ 0 & 0 & 0 \\ \frac{1}{c} & 0 & 0 \end{pmatrix}, \qquad \mathfrak{M}^{-1}_{ij6} = \begin{pmatrix} 0 & \frac{1}{c} & 0 \\ \frac{1}{c} & 0 & 0 \\ 0 & 0 & 0 \end{pmatrix} \end{gathered} \tag{3.49}$$

The mapping $\mathfrak{M}$ has zeros everywhere, except in the $\{111, 222, 333, 423, 513, 612\}$ components. We can express it compactly as (see [9] for a proof):

$$\begin{aligned}\mathfrak{M}_{\alpha ij} =& \widetilde{\delta}_{\alpha 1}\delta_{i1}\delta_{j1} + \widetilde{\delta}_{\alpha 2}\delta_{i2}\delta_{j2} + \widetilde{\delta}_{\alpha 3}\delta_{i3}\delta_{j3} + \frac{c}{2}\left(\widetilde{\delta}_{\alpha 4}(\delta_{i2}\delta_{j3} + \delta_{i3}\delta_{j2}) + \widetilde{\delta}_{\alpha 5}(\delta_{i1}\delta_{j3} + \delta_{i3}\delta_{j1})\right) \\ &+ \frac{c}{2}\,\widetilde{\delta}_{\alpha 6}\,(\delta_{i1}\delta_{j2} + \delta_{i2}\delta_{j1})\end{aligned} \tag{3.50}$$

In the same fashion, we have for the inverse mapping $\mathfrak{M}^{-1}$:

$$\begin{aligned}\mathfrak{M}^{-1}_{ij\alpha} =& \widetilde{\delta}_{\alpha 1}\delta_{i1}\delta_{j1} + \widetilde{\delta}_{\alpha 2}\delta_{i2}\delta_{j2} + \widetilde{\delta}_{\alpha 3}\delta_{i3}\delta_{j3} + \frac{1}{c}\left(\widetilde{\delta}_{\alpha 4}(\delta_{i2}\delta_{j3} + \delta_{i3}\delta_{j2}) + \widetilde{\delta}_{\alpha 5}(\delta_{i1}\delta_{j3} + \delta_{i3}\delta_{j1})\right) \\ &+ \frac{1}{c}\,\widetilde{\delta}_{\alpha 6}\,(\delta_{i1}\delta_{j2} + \delta_{i2}\delta_{j1}).\end{aligned} \tag{3.51}$$

The anisotropic strain energy of the relaxed micromorphic model (3.5) can be written in index notation as:

$$\begin{aligned}W =& \frac{1}{2}(\mathbb{C}_e)_{ijkl}(\mathrm{sym}(\nabla u - P))_{ij}(\mathrm{sym}(\nabla u - P))_{kl} + \frac{1}{2}(\mathbb{C}_c)_{ijkl}(\mathrm{skew}(\nabla u - P))_{ij}(\mathrm{skew}(\nabla u - P))_{kl} \\ &+ \frac{1}{2}(\mathbb{C}_m)_{ijkl}(\mathrm{sym}\, P)_{ij}(\mathrm{sym}\, P)_{kl} + \frac{\mu_e L_c^2}{2}\left(P_{ia,b}\epsilon_{jab}\right)\left(P_{ic,d}\epsilon_{jcd}\right).\end{aligned} \tag{3.52}$$

The symmetric term in $\nabla u - P$ is:

$$\frac{1}{2}(\mathbb{C}_e)_{ijkl}(\mathrm{sym}(\nabla u - P))_{ij}(\mathrm{sym}(\nabla u - P))_{kl}. \tag{3.53}$$

We can now express this in terms of $\varepsilon - \beta$ as:

$$\frac{1}{2}\left(\widetilde{\mathbb{C}}_e\right)_{\alpha\gamma}(\varepsilon_\alpha - \beta_\alpha)(\varepsilon_\gamma - \beta_\gamma) = \frac{1}{2}\left(\widetilde{\mathbb{C}}_e\right)_{\alpha\gamma}\mathfrak{M}_{\alpha ij}(\mathrm{sym}(\nabla u - P))_{ij}\mathfrak{M}_{\gamma kl}(\mathrm{sym}(\nabla u - P))_{kl}, \tag{3.54}$$

where $\widetilde{\mathbb{C}}_e : \mathbb{R}^6 \to \mathbb{R}^6$ is a general second order symmetric tensor on $\mathbb{R}^{6\times 6}$ (matrix) with at most 21 independent components. It is the Mandel-Voigt equivalent to $\mathbb{C}_e$ and we can now define it using the mapping $\mathfrak{M}$. Comparing (3.54) to the corresponding part of (3.52), we find:

$$(\mathbb{C}_e)_{ijkl} = \mathfrak{M}_{\alpha ij}\left(\widetilde{\mathbb{C}}_e\right)_{\alpha\gamma}\mathfrak{M}_{\gamma kl}, \quad (\mathbb{C}_e)^{-1}_{ijkl} = \mathfrak{M}^{-1}_{ij\alpha}\left(\widetilde{\mathbb{C}}_e\right)^{-1}_{\alpha\gamma}\mathfrak{M}^{-1}_{kl\gamma}. \tag{3.55}$$

The second equation in (3.55) is proven in [9].

The converse relations to (3.55) are given by:

$$\left(\widetilde{\mathbb{C}}_e\right)_{\alpha\gamma} = \mathfrak{M}^{-1}_{ij\alpha}\,(\mathbb{C}_e)_{ijkl}\,\mathfrak{M}^{-1}_{kl\gamma}, \quad \left(\widetilde{\mathbb{C}}_e\right)^{-1}_{\alpha\gamma} = \mathfrak{M}_{\alpha ij}\,(\mathbb{C}_e)^{-1}_{ijkl}\,\mathfrak{M}_{\gamma kl}. \tag{3.56}$$

Following the same procedure we can obtain analogous equations for all the remaining symmetric constitutive tensors appearing in the energies (3.5) and (3.11). We have, thus found a way to formally represent fourth order symmetric tensors as second order symmetric tensors and conversely.

Using (3.56) and (3.51), we see that the second order tensor $\widetilde{\mathbb{C}}_e$ can now be written with respect to the fourth-order tensor $\mathbb{C}_e$, as:

$$\widetilde{\mathbb{C}}_e = \begin{pmatrix} (\mathbb{C}_e)_{1111} & (\mathbb{C}_e)_{1122} & (\mathbb{C}_e)_{1133} & \frac{2}{c}(\mathbb{C}_e)_{1123} & \frac{2}{c}(\mathbb{C}_e)_{1113} & \frac{2}{c}(\mathbb{C}_e)_{1112} \\ (\mathbb{C}_e)_{2211} & (\mathbb{C}_e)_{2222} & (\mathbb{C}_e)_{2233} & \frac{2}{c}(\mathbb{C}_e)_{2223} & \frac{2}{c}(\mathbb{C}_e)_{2213} & \frac{2}{c}(\mathbb{C}_e)_{2212} \\ (\mathbb{C}_e)_{3311} & (\mathbb{C}_e)_{3322} & (\mathbb{C}_e)_{3333} & \frac{2}{c}(\mathbb{C}_e)_{3323} & \frac{2}{c}(\mathbb{C}_e)_{3313} & \frac{2}{c}(\mathbb{C}_e)_{3312} \\ \frac{2}{c}(\mathbb{C}_e)_{2311} & \frac{2}{c}(\mathbb{C}_e)_{2322} & \frac{2}{c}(\mathbb{C}_e)_{2333} & \frac{4}{c^2}(\mathbb{C}_e)_{2323} & \frac{4}{c^2}(\mathbb{C}_e)_{2313} & \frac{4}{c^2}(\mathbb{C}_e)_{2312} \\ \frac{2}{c}(\mathbb{C}_e)_{1311} & \frac{2}{c}(\mathbb{C}_e)_{1322} & \frac{2}{c}(\mathbb{C}_e)_{1333} & \frac{4}{c^2}(\mathbb{C}_e)_{1323} & \frac{4}{c^2}(\mathbb{C}_e)_{1313} & \frac{4}{c^2}(\mathbb{C}_e)_{1312} \\ \frac{2}{c}(\mathbb{C}_e)_{1211} & \frac{2}{c}(\mathbb{C}_e)_{1222} & \frac{2}{c}(\mathbb{C}_e)_{1233} & \frac{4}{c^2}(\mathbb{C}_e)_{1223} & \frac{4}{c^2}(\mathbb{C}_e)_{1213} & \frac{4}{c^2}(\mathbb{C}_e)_{1212} \end{pmatrix}, \tag{3.57}$$

which is a symmetric 6×6 matrix. This last fact is due to the symmetry of $\mathbb{C}_e$, according to which $(\mathbb{C}_e)_{ijkl} = (\mathbb{C}_e)_{klij}$.

We now must find a way to suitably represent fourth order skew-symmetric tensors as second order tensors. This is done via the the axl mapping. Given a skew-symmetric matrix $\overline{A} \in \mathfrak{so}(3)$

$$\overline{A} = \begin{pmatrix} 0 & \overline{A}_{12} & \overline{A}_{13} \\ -\overline{A}_{12} & 0 & \overline{A}_{23} \\ -\overline{A}_{13} & -\overline{A}_{23} & 0 \end{pmatrix}, \tag{3.58}$$

we define:

$$\operatorname{axl}(\overline{A}) = \left(-\overline{A}_{23}, \overline{A}_{13}, -\overline{A}_{12}\right)^{\mathrm{T}}, \quad \left[\operatorname{axl}(\overline{A})\right]_k = -\frac{1}{2}\epsilon_{ijk}\overline{A}_{ij} = \frac{1}{2}\epsilon_{kij}\overline{A}_{ji}. \tag{3.59}$$

We can then always represent a fourth order tensor $\mathbb{C}_c : \mathfrak{so}(3) \to \mathfrak{so}(3)$ acting on skew-symmetric matrices by its version acting only on axial vectors [9]. We have:

$$\langle \mathbb{C}_c \operatorname{skew}(X), \operatorname{skew}(X) \rangle_{\mathbb{R}^{3\times 3}} = \langle \widetilde{\mathbb{C}}_c \operatorname{axl}(\operatorname{skew}(X)), \operatorname{axl}(\operatorname{skew}(X)) \rangle_{\mathbb{R}^3}, \tag{3.60}$$

where $\widetilde{\mathbb{C}}_c : \mathbb{R}^3 \to \mathbb{R}^3$ is a symmetric second order tensor. Therefore, $\widetilde{\mathbb{C}}_c$ has only 6 independent components and so does $\mathbb{C}_c$. Finally, given a second order tensor X, we have:

$$\|\operatorname{skew}(X)\|^2_{\mathbb{R}^{3\times 3}} = 2\,\|\operatorname{axl}(\operatorname{skew}(X))\|^2_{\mathbb{R}^3}\,. \tag{3.61}$$

3.4.1 Invariance conditions

In this section we will discuss how this reduced formulation provided by the Mandel-Voigt representation is able to be treated in an invariant setting.

Let $\mathcal{G}$ be the symmetry group of the material and $Q \in \mathcal{G}$ a coordinate transformation. The application of this transform (which generates the so-called Rayleigh action [5]) to the macro-displacement u and the micro-distortion tensor P ([9]) is:

$$\begin{aligned} x &= Q^{\mathrm{T}} \cdot \xi, & P^{\#}(\xi) &:= Q \cdot \left[P\left(Q^{\mathrm{T}} \cdot \xi\right)\right] \cdot Q^{\mathrm{T}}, \\ u^{\#}(\xi) &:= Q \cdot u(Q^{\mathrm{T}} \cdot \xi), & \nabla_\xi u^{\#}(\xi) &= Q \cdot \nabla_x u(Q^{\mathrm{T}} \cdot \xi) \cdot Q^{\mathrm{T}}. \end{aligned} \tag{3.62}$$

This means that we require that P transforms as ∇u under simultaneous rotations of the reference and spatial configurations. Using this definition, it can be shown ([75]) that:

$$\mathrm{Curl}_\xi\, P^\#(\xi) = Q \cdot \left[\mathrm{Curl}_x\, P\left(Q^{\mathrm{T}} \cdot \xi\right)\right] \cdot Q^{\mathrm{T}}. \tag{3.63}$$

In [75], the authors explain in detail that possessing a material symmetry is equivalent to requiring that, under the transformation (3.62) with any $Q \in \mathcal{G}-$symmetry group of the material, both the strain and the kinetic energy density are *form-invariant*. This means that we require ([9]):

$$\begin{aligned} W\left(\nabla_\xi u^\#(\xi), P^\#(\xi), \mathrm{Curl}_\xi\, P^\#(\xi)\right) &= W\left(\nabla_x u(x).P(x), \mathrm{Curl}_x\, P(x)\right), \\ J\left(u^\#(\xi), \nabla_\xi u^\#(\xi), P\right) &= J\left(u(x), \nabla_x u(x), P(x)\right). \end{aligned} \tag{3.64}$$

This is equivalent to saying that, for every $Q \in \mathcal{G}-$ symmetry group of the material, we have [9]:

$$\begin{aligned} W\left(\nabla u, P, \mathrm{Curl}\, P\right) &= W\left(Q \cdot \nabla u \cdot Q^{\mathrm{T}}, Q \cdot P \cdot Q^{\mathrm{T}}, Q \cdot (\mathrm{Curl}\, P) \cdot Q^{\mathrm{T}}\right), \\ J\left(u, \nabla u, P\right) &= J\left(Q \cdot u, Q \cdot \nabla u \cdot Q^{\mathrm{T}}, Q \cdot P \cdot Q^{\mathrm{T}}\right). \end{aligned} \tag{3.65}$$

This invariance condition is dependent on the set $\mathcal{G}$, which contains the transformation matrix Q. Depending on the symmetry properties of this group we can define different material classes [9, 29].[2]

3.4.2 Tetragonal symmetry and isotropy

In this thesis we will be considering two cases of material symmetries: tetragonal symmetry and isotropy. For this reason, we will see how the symmetric and skew-symmetric constitutive tensors can be considered in this section. From now on, we denote by $\widetilde{\mathbb{E}}$ a symmetric tensor and by $\widetilde{\mathbb{K}}$ a skew-symmetric tensor (both in Mandel-Voigt notation). So, the constitutive tensors $\widetilde{\mathbb{C}}_e, \widetilde{\mathbb{C}}_{\mathrm{micro}}, \widetilde{\mathbb{L}}_e, \widetilde{\mathbb{J}}_{\mathrm{micro}}, \widetilde{\mathbb{T}}_e$ acting on vectors in $\mathbb{R}^6$ (and are equivalent to symmetric matrices) must have the form of $\widetilde{\mathbb{E}}$, while the skew-symmetric tensors $\widetilde{\mathbb{C}}_c, \widetilde{\mathbb{L}}_c, \widetilde{\mathbb{T}}_c$ which act on vectors in $\mathbb{R}^3$ (and are equivalent to skew-symmetric matrices) must have the form of $\widetilde{\mathbb{K}}$.

Tetragonal symmetry

The tetragonal crystal lattice has a unit cell shaped like a rectangular prism with a square basis. Thus, the material symmetry has three mutually orthogonal planes of reflection, plus 90° rotation symmetry with respect to one of those planes. This means that a rotation of the unit cell through an angle of 90° brings the atoms in their initial position. The constitutive tensors in this case have the following structure:

$$\widetilde{\mathbb{E}}^{\mathrm{tetr}} = \begin{pmatrix} 2\mu_e + \lambda_e & \lambda_e & \lambda_e^* & 0 & 0 & 0 \\ & 2\mu_e + \lambda_e & \lambda_e^* & 0 & 0 & 0 \\ & & v_e & 0 & 0 & 0 \\ & & & \mu_e^* & 0 & 0 \\ & \mathrm{sym} & & & \mu_e^* & 0 \\ & & & & & \mu_e^{**} \end{pmatrix}, \quad \widetilde{\mathbb{K}}^{\mathrm{tetr}} = \frac{1}{2}\begin{pmatrix} \mu_c^* & 0 & 0 \\ 0 & \mu_c^* & 0 \\ 0 & 0 & \mu_c \end{pmatrix}, \tag{3.66}$$

[2] For example, the case of full anisotropy corresponds to $\mathcal{G} = \{-\mathbb{1}, \mathbb{1}\}$, while the case of isotropy to $\mathcal{G} = \mathrm{SO}(3)$.

where $\mu_e, \lambda_e, \lambda_e^*, \mu_e^*, v_e, , \mu_e^{**}, \mu_c^*, \mu_e$ are the $6+2$ independent coefficients of the tetragonal symmetry case.

Isotropy

Isotropy means that the properties of the crystal lattice are completely independent of the direction. If we want to visualize the unit cell in this case, one could imagine a sphere. The constitutive tensors in this case are given by:

$$\widetilde{\mathbb{E}}^{\text{iso}} = \begin{pmatrix} 2\mu_e+\lambda_e & \lambda_e & \lambda_e & 0 & 0 & 0 \\ & 2\mu_e+\lambda_e & \lambda_e & 0 & 0 & 0 \\ & & 2\mu_e+\lambda_e & 0 & 0 & 0 \\ & & & \mu_e & 0 & 0 \\ & \text{sym} & & & \mu_e & 0 \\ & & & & & \mu_e \end{pmatrix}, \quad \widetilde{\mathbb{K}}^{\text{iso}} = \frac{\mu_c}{2}\mathbb{1}, \tag{3.67}$$

3.5 Conservation of energy and energy flux for the relaxed micromorphic model

In this section we will discuss energy conservation and derive the expression for the energy flux for the relaxed micromorphic model, much as we did for the classical Cauchy model in chapter 2.2. We will demonstrate here how to compute the expression for the energy flux *in the case of isotropy*, which is the main focus of chapter 4. The detailed computation for the case of anisotropy, which is the point of interest of chapter 6 is merely stated here and presented in full detail in Appendix A3.1.

Energy conservation is once again given by equation (2.10):

$$E_{,t} + \text{div} H = 0,$$

where $E = J + W$ is the total energy of the system and H is the generalized energy flux vector. We remark here that the kinetic energy density is given by expression (3.16) and not by the more general (3.14).

In order to derive the expression for the flux, we first need to recall some facts from differential calculus.

Let ψ be a vector field and A a second order tensor field. Then

$$\langle \nabla\psi, A\rangle = \text{Div}(\psi \cdot A) - \langle \psi, \text{Div}\, A\rangle. \tag{3.68}$$

Taking $\psi = u_{,t}$ and $A = \widetilde{\sigma}$ we have

$$\langle \nabla u_{,t}, \widetilde{\sigma}\rangle = \text{Div}(u_{,t} \cdot \widetilde{\sigma}) - \langle u_{,t}, \text{Div}\, \widetilde{\sigma}\rangle\,. \tag{3.69}$$

Furthermore, we have the following identity:

$$\langle m, \text{Curl}\, P_{,t}\rangle = \text{Div}\left((m^{\text{T}} \cdot P_{,t}) : \varepsilon\right) + \langle \text{Curl}\, m, P_{,t}\rangle\,, \tag{3.70}$$

which follows from the identity $\text{div}(v \times w) = w \cdot \text{curl}\, v - v \cdot \text{curl}\, w$, where v, w are suitable vector fields, $\times$ is the usual vector product and : is the double contraction between tensors. Finally,

we recall that given a symmetric tensor S, a skew-symmetric tensor A and a generic tensor C, we have

$$\langle S, C\rangle = \langle S, \operatorname{sym} C\rangle\,, \quad \text{and} \quad \langle A, C\rangle = \langle A, \operatorname{skew} C\rangle\,. \tag{3.71}$$

We can now derive the energy flux of an isotropic relaxed micromorphic medium with no gradient micro-inertia. Differentiating equations (3.9) and (3.16) with respect to time, we have:

$$\begin{aligned} E_{,t} =& \rho\,\langle u_{,t}, u_{,tt}\rangle + \eta\,\langle P_{,t}, P_{,tt}\rangle + \langle 2\mu_e \operatorname{sym}(\nabla u - P), \operatorname{sym}(\nabla u_{,t} - P_{,t})\rangle + \langle \lambda_e \operatorname{tr}(\nabla u - P)\mathbb{1}, \nabla u_{,t} - P_{,t}\rangle \\ &+ \langle 2\mu_c \operatorname{skew}(\nabla u - P), \operatorname{skew}(\nabla u_{,t} - P_{,t})\rangle + \langle 2\mu_{\text{micro}} \operatorname{sym} P, \operatorname{sym} P_{,t}\rangle + \langle \lambda_{\text{micro}}(\operatorname{tr} P)\mathbb{1}, P_{,t}\rangle \\ &+ \left\langle \mu_e L_c^2 \operatorname{Curl} P, \operatorname{Curl} P_{,t}\right\rangle, \end{aligned} \tag{3.72}$$

or equivalently, suitably collecting terms and using definitions (3.29) for $\widetilde{\sigma}, s$ and m and the identities (3.71):

$$\begin{aligned} E_{,t} =& \rho\,\langle u_{,t}, u_{,tt}\rangle + \eta\,\langle P_{,t}, P_{,tt}\rangle + \langle 2\mu_e \operatorname{sym}(\nabla u - P) + \lambda_e \operatorname{tr}(\nabla u - P), \operatorname{sym}(\nabla u_{,t} - P_{,t})\rangle \\ &+ \langle 2\mu_c \operatorname{skew}(\nabla u - P), \operatorname{skew}(\nabla u_{,t} - P_{,t})\rangle + \langle 2\mu_{\text{micro}} \operatorname{sym} P + \lambda_{\text{micro}}(\operatorname{tr} P)\mathbb{1}, \operatorname{sym} P_{,t}\rangle \\ &+ \left\langle \mu_e L_c^2 \operatorname{Curl} P, \operatorname{Curl} P_{,t}\right\rangle \\ =& \rho\,\langle u_{,t}, u_{,tt}\rangle + \eta\,\langle P_{,t}, P_{,tt}\rangle + \langle \widetilde{\sigma}, \nabla u_{,t}\rangle - \langle \widetilde{\sigma} - s, P_{,t}\rangle + \langle m, \operatorname{Curl} P_{,t}\rangle\,. \end{aligned} \tag{3.73}$$

We can now replace $\rho\, u_{,tt}$ and $\eta\, P_{,tt}$ by the governing equations (3.34) and use (3.69) and (3.70) to finally get

$$\begin{aligned} E_{,t} &= \langle u_{,t}, \operatorname{Div}\widetilde{\sigma}\rangle + \langle P_{,t}, \widetilde{\sigma} - s - \operatorname{Curl} m\rangle + \operatorname{Div}(u_{,t}\cdot\widetilde{\sigma}) - \langle u_{,t}, \operatorname{Div}\widetilde{\sigma}\rangle - \langle \widetilde{\sigma} - s, P_{,t}\rangle + \langle m, \operatorname{Curl} P_{,t}\rangle \\ &= \operatorname{Div}(\widetilde{\sigma}^{\mathrm{T}}\cdot u_{,t}) - \langle \operatorname{Curl} m, P_{,t}\rangle + \operatorname{Div}\left(\left(m^{\mathrm{T}}\cdot P_{,t}\right) : \varepsilon\right) + \langle \operatorname{Curl} m, P_{,t}\rangle \\ &= \operatorname{Div}\left(\widetilde{\sigma}^{\mathrm{T}}\cdot u_{,t} + \left(m^{\mathrm{T}}\cdot P_{,t}\right) : \varepsilon\right). \end{aligned} \tag{3.74}$$

Energy conservation is once again expressed by the continuity equation

$$E_{,t} + \operatorname{div} H = 0,$$

where $E = J + W$ is the total energy and H the generalized energy flux vector. Thus, by comparison of (3.74) with the above equation, the energy flux for a relaxed micromorphic medium is given by:

$$H = -\widetilde{\sigma}^{\mathrm{T}}\cdot u_{,t} - \left(m^{\mathrm{T}}\cdot P_{,t}\right) : \epsilon, \qquad H_k = -u_{i,t}\widetilde{\sigma}_{ik} - m_{ih}P_{ij,t}\varepsilon_{jhk}. \tag{3.75}$$

Finally, the energy flux for an anisotropic relaxed micromorphic continuum is given by:

$$H = -\left(\widetilde{\sigma} + \widehat{\sigma}\right)^{\mathrm{T}}\cdot u_{,t} - \left(m^{\mathrm{T}}\cdot P_{,t}\right) : \epsilon, \quad H_k = -u_{i,t}\left(\widetilde{\sigma}_{ik} + \widehat{\sigma}_{ik}\right) - m_{ih}P_{ij,t}\epsilon_{jhk}. \tag{3.76}$$

This expression is derived in detail in Appendix A3.1.

3.6 An equivalent macroscopic Cauchy model

When considering wavelengths which are larger than the typical microstructure size, the influence of the microstructure itself becomes minimal and the relaxed micromorphic model is equivalent to a classical Cauchy continuum with elastic stiffness tensor $\mathbb{C}_{\text{macro}}$ (see [9, 29]). A clear identification of the equivalent macroscopic fourth order tensor $\mathbb{C}_{\text{macro}}$ via the constitutive tensors $\mathbb{C}_{\text{micro}}$ and $\mathbb{C}_e$ can also be derived as a harmonic tensor mean, i.e.

$$\mathbb{C}_{\text{macro}} := \mathbb{C}_{\text{micro}}\left(\mathbb{C}_{\text{micro}} + \mathbb{C}_e\right)^{-1}\mathbb{C}_e\,. \tag{3.77}$$

The homogenization formula (3.77) can be used to characterize the material with classical experimental (or numerical) procedures and to obtain a useful relation between the parameters of the relaxed micromorphic model and those of the equivalent Cauchy continuum which can be considered representative of the dynamic response of the metastructure at low frequencies. The equations of motion for the macroscopic Cauchy model are the ones of classical elasticity with constitutive tensor $\mathbb{C}_{\text{macro}}$:

$$\begin{aligned} \rho\, u_{,tt} &= \text{Div}\,[\mathbb{C}_{\text{macro}}\ \text{sym}\,\nabla u] && && \forall x \in \Omega, \\ f &:= (\mathbb{C}_{\text{macro}}\ \text{sym}\,\nabla u)\cdot\nu = t^{\text{ext}}(x,t) \qquad \text{or} \qquad u = \varphi(x,t), && && \forall x \in \partial\Omega_0, \end{aligned} \tag{3.78}$$

where ν is, as usual, the normal to the boundary of the domain Ω occupied by the solid.

Chapter 4

Low-and high-frequency Stoneley waves, reflection and transmission at a Cauchy/relaxed micromorphic interface

We begin the main part of this thesis with this chapter, which mainly focuses on the study of reflection and transmission problems on an interface separating a classical homogeneous medium and a mechanical metamaterial described by the relaxed micromorphic model. Here, both media under consideration (the classical Cauchy and the relaxed micromorphic) are assumed to be **isotropic**. We assume that the kinetic energy density of the relaxed micromorphic medium is given by (3.16) and, therefore, the continuum is governed by equations (3.34), which we restate here for clarity:

$$\begin{cases} \rho\, u_{tt} = & \operatorname{Div} \widetilde{\sigma} \\ \eta\, P_{tt} = & \widetilde{\sigma} - s - \operatorname{Curl} m, \end{cases}$$

where,

$$\begin{aligned} \widetilde{\sigma} &= 2\mu_e \operatorname{sym}(\nabla u - P) + \lambda_e \operatorname{tr}(\nabla u - P)\, \mathbb{1} + 2\mu_c \operatorname{skew}(\nabla u - P), \\ s &= 2\mu_{\text{micro}} \operatorname{sym} P + \lambda_{\text{micro}} (\operatorname{tr} P)\ \mathbb{1}, \\ m &= \mu_e L_c^2 \operatorname{Curl} P. \end{aligned}$$

In this chapter, we model the reflective and diffractive properties of an interface which separates a bulk homogeneous material from a bulk metamaterial. This interface does not itself contain any internal structure, but its refractive properties can be modulated by suitably tailoring the bulk properties of the two adjacent media and, in particular, their relative macroscopic stiffness. The homogeneous material is modeled via a classical linear-elastic Cauchy model, while the metamaterial is described by the linear relaxed micromorphic model.

Concerning the study of the metamaterial's boundaries, the relaxed micromorphic model is a powerful tool, which, as we saw in chapter 3, provides coherent macroscopic boundary conditions allowing the study of realistic interface problems.

As we saw in chapter 3.6, the relaxed micromorphic model can be assumed to be an equivalent Cauchy model for wavelengths large enough with constitutive tensor $\mathbb{C}_{\text{macro}}$ given by (3.77). We are able to clearly show that when the homogeneous material is "stiffer" than the considered metamaterial (in the sense of the equivalent Cauchy model), zones of very high (sometimes total) transmission can be found at both low and high frequencies. More precisely, we find that high-frequency total transmission is discriminated by a critical angle, beyond which total transmission gradually shifts towards total reflection. Engineering systems of this type could

be fruitfully exploited for the conception of wave filters, for non-destructive evaluation or for selective cloaking.

On the other hand, we show that when the homogeneous material is "softer" than the metamaterial (in the sense of the equivalent Cauchy model), zones of very high (sometimes total), broadband total reflection can be achieved for almost all frequencies and angles of incidence. This could be of paramount importance for the conception of wave screens that are able to isolate regions from noise and/or vibration. We are also able to show that such total reflection phenomena are related to the onset of classical Stoneley interface waves at low frequencies [92] and of new microstructure-related interface waves at higher frequencies. Interface waves propagating at the interface between an elastic solid and air are called Rayleigh waves, after Lord Rayleigh, who was the first to show their existence [87]. Interface waves propagating at the surface between two solids are called Stoneley waves after R. Stoneley who first showed their existence [92].

We underline again the fact that no precise microstructure is targeted in this chapter, since the presented results can be re-adjusted for any specific metamaterial without changing the overall results. This is due to the fact that the properties we unveil here only depend on the "relative stiffnesses" of the considered media and not on the absolute stiffness of the metamaterial itself.

We begin by discussing the types of boundary conditions, which have to be imposed in the interface problems we will discuss. We will then make a digression into classical wave propagation theory in elastic media, in order to set up notation and concepts. Following that, we will see how we can model interface problems in this setting. We will then generalize these ideas into generalized continua modeled via the relaxed micromorphic model, with our final goal being to study interfaces between classical homogeneous media and metamaterials. We will finally present results and findings.

4.1 Boundary conditions

4.1.1 Boundary conditions on an interface between two classical Cauchy media

As it is well known (see e.g. [1, 43, 65]), the boundary conditions which can be imposed at an interface between two Cauchy media are continuity of displacement or continuity of traction.[1] For the displacement, this means

$$[[u]] = 0 \Rightarrow u^- = u^+, \tag{4.1}$$

where u^- is the macroscopic displacement on the "minus" side (the $x_1 < 0$ half-plane) and u^+ is the macroscopic displacement on the "plus" side (the $x_1 > 0$ half-plane).

As for the jump of traction we have

$$[[t]] = 0 \Rightarrow t^- = t^+, \tag{4.2}$$

where t^- and t^+ are the surface traction vectors on the "minus" and on the "plus" side, respectively. We recall that in a Cauchy medium, $t = \sigma \cdot \nu$, ν being the outward unit normal to the surface and σ being the Cauchy stress tensor given by (2.5).

[1] It is also well known that if no surface tractions are present at the considered interface, imposing continuity of displacement implies continuity of tractions and vice versa. Both such continuity conditions must then be satisfied at the interface.

4.1.2 Boundary conditions on an interface between a classical Cauchy medium and a relaxed micromorphic medium

We will be imposing two kinds of boundary conditions between a Cauchy and a relaxed micromorphic medium (see [65] for a detailed discussion). The first kind is that of a free microstructure, i.e. we allow the microstructure to vibrate freely. The second kind is that of a fixed microstructure, i.e. we do not allow any movement of the microstructure at the interface.

Again, we impose continuity of displacement, i.e.

$$u^- = u^+, \tag{4.3}$$

where now the "plus" side is occupied by the relaxed micromorphic medium.[2] Imposing continuity of displacement also implies continuity of traction,[3] i.e.

$$t = \widetilde{t},$$

where $t = \sigma \cdot \nu$ is the surface traction calculated on the Cauchy side and the traction for the relaxed micromorphic model is given by

$$\widetilde{t}_i = \widetilde{\sigma}_{ij}\nu_j, \tag{4.4}$$

where ν is the outward unit normal vector to the interface and $\widetilde{\sigma}$ is given in (3.29).

The least action principle provides us with another jump duality condition for the case of the connection between a Cauchy and a relaxed micromorphic medium. This extra jump condition specifies what we call "free microstructure" or "fixed microstructure" (see chapter 3.2.1 and [65]).

In order to define the two types of boundary conditions we are interested in, we need the concept of double force τ which is the dual quantity of the micro-distortion tensor P and is defined as [65]

$$\tau = -m \cdot \varepsilon \cdot \nu, \quad \tau_{ij} = -m_{ik}\varepsilon_{kjh}\nu_h, \tag{4.5}$$

where the involved quantities have been defined in (3.29).

Free microstructure

In this case, the macroscopic displacement is continuous while the microstructure of the relaxed micromorphic medium is free to move at the interface ([57, 58, 65]). Leaving the interface free to move means that P is arbitrary, which, on the other hand, implies the double force τ must vanish. We have then

$$[[u_i]] = 0, \quad \widetilde{t}_i - t_i = 0, \quad \tau_{ij} = 0, \quad i = 1,2,3,\ j = 2,3. \tag{4.6}$$

Figure 4.1 gives a schematic representation of this boundary condition.

[2] In the following, it will be natural to collect variables of the relaxed medium in two vectors v_1 and v_2, so that the components of the displacement u^+ will be denoted by $u^+ = (v_1^1, v_2^1, v_1^1)^{\mathrm{T}}$, see equations (4.71), (4.72).

[3] This fact can be deduced from the minimization of the action functional. Indeed, imposing the variation to be zero, we find the boundary condition $[[\langle T, \delta u\rangle]] = 0 \Rightarrow t\,u^+ - \widetilde{t}\,u^- = 0$, which implies $t = \widetilde{t}$ since we impose continuity of displacement.

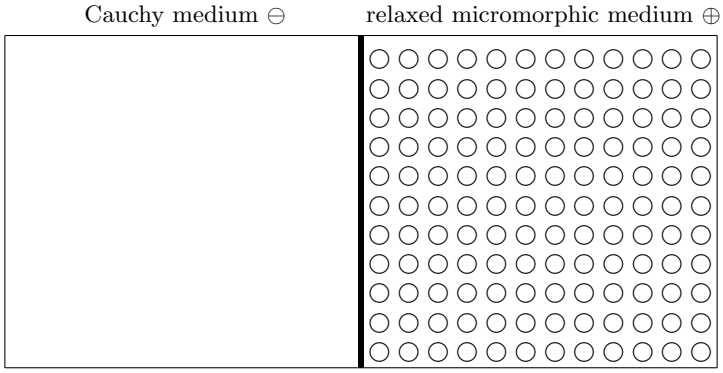

Figure 4.1: Schematic representation of a macro internal clamp with free microstructure at a Cauchy/relaxed-micromorphic interface [58, 65].

Fixed microstructure

This is the case in which we impose that the microstructure on the relaxed micromorphic side does not vibrate at the interface. The boundary conditions in this case are (see [65])[4]

$$[[u_i]] = 0, \quad \widetilde{t}_i - t_i = 0, \quad P_{ij} = 0, \quad i = 1,2,3,\ j = 2,3. \tag{4.7}$$

Observe that in equations (4.6) and (4.7) the components tangent to the interface do not have to be assigned when considering a relaxed micromorphic medium. This is explained in detail in [65, 77, 78], where the peculiarities of the relaxed micromorphic model are presented. In Figure 4.2 we give a schematic representation of the realization of this boundary condition between a homogeneous material and a metamaterial.

As we briefly mentioned in chapter 3.1 (and is explained in [77, 78] in greater detail), only the tangent part of the double force in (4.6) or of the micro-distortion tensor in (4.7) must be assigned. This is peculiar of the relaxed micromorphic model and is related to the fact that only $\operatorname{Curl} P$ appears in the energy. In a standard Mindlin-Eringen model, where the whole ∇P appears in the energy, the whole double force τ (or alternatively the whole micro-distortion tensor P) must be assigned at the interface. Finally, in an internal variable model (no derivatives of P in the energy), no conditions on P or τ must be assigned at the considered interface.

We explicitly remark (and we will show this fact in all detail in the remainder of this chapter) that the free microstructure boundary condition of Fig. 4.1 is the only one that permits one to obtain an equivalent Cauchy/Cauchy system when considering low frequencies. Indeed, in this case, since the tensor P is left free, it can adjust itself in order to recover a Cauchy medium in the homogenized limit. On the other hand, the fixed microstructure boundary condition of Fig. 4.2 imposes an artificial value on P along the interface, so that the effect of the microstructure is present in the system. It follows that a Cauchy/Cauchy interface cannot be recovered as a homogenized limit of the system shown in Fig. 4.2.

[4]Let us remark again that the first condition (continuity of displacement) implies the second one when no surface tractions are applied at the interface. On the other hand, imposing the tangent part of P to be equal to zero implies that the double force τ is left arbitrary.

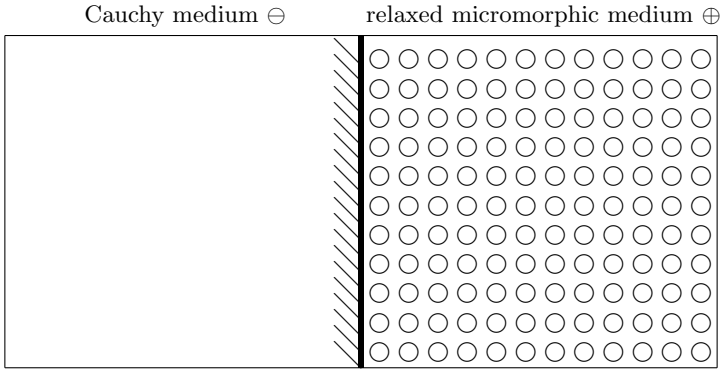

Figure 4.2: Schematic representation of a macro internal clamp with fixed microstructure at a Cauchy/relaxed-micromorphic interface [58, 65].

4.2 Wave propagation, reflection and transmission at an interface between two Cauchy media

We now want to study wave propagation, reflection and transmission at the interface between two Cauchy media in two space dimensions. All the results of this section are well established, but it is essential to repeat them in order to set up notation and to clearly present the conceptual steps which must be followed in order to solve the interface problem.

When we discuss reflection and transmission, we assume that the surface of discontinuity (the interface between the two media) from which the wave reflects and refracts is the x_2 axis ($x_1 = 0$), see Fig. 4.3.

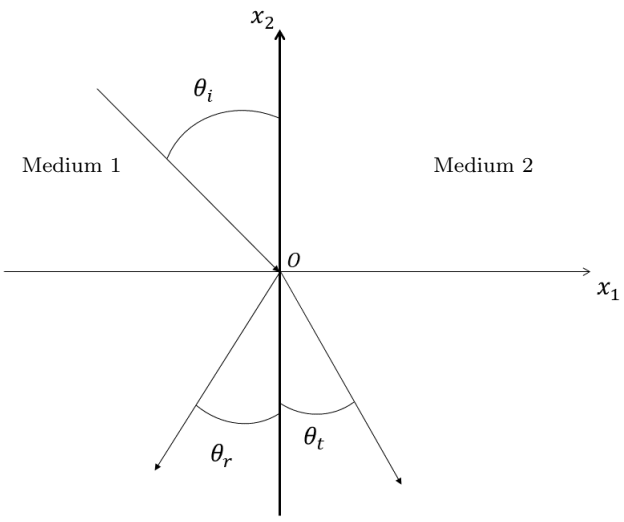

Figure 4.3: Generic representation of an interface separating two media at $x_1 = 0$. The figure also schematically represents the conventions used for incident, reflected and transmitted waves.

Incident waves propagate from $-\infty$ in the $x_1 < 0$ half-plane towards the interface, reflected waves propagate from the interface towards $-\infty$ in the $x_1 < 0$ half-plane and refracted (or, equivalently, transmitted) waves propagate from the interface towards $+\infty$ in the $x_1 > 0$ half-

plane. Remark that, since we consider 2D wave propagation, the incident wave can hit the interface at an arbitrary angle.

As is classical, we will consider both in-plane (in the $(x_1x_2)-$ plane) and out-of-plane (along the x_3 direction) motions. Nevertheless, all the considered components of the displacement, namely u_1, u_2 and u_3 will only depend on the x_1, x_2 space components (plane wave hypothesis). We hence write

$$u = (u_1(x_1, x_2, t), u_2(x_1, x_2, t), u_3(x_1, x_2, t))^{\mathrm{T}}. \tag{4.8}$$

As will be evident, depending on the type of wave (longitudinal, SV shear or SH shear)[5] some components of these fields will be equal to zero.

We now make a small digression on wave propagation in classical Cauchy media. These results are of course well known (see e.g. [1, 43]), however, we present them here in detail following our notation, so that we can carry all the results and considerations over to the relaxed micromorphic model as a natural extension.

4.2.1 Wave propagation in Cauchy media

We start by writing the governing equations (2.4) for the special case where the displacement only depends on the in-plane space variables x_1 and x_2. Plugging u as in (4.8) into (2.4) gives the following system of PDEs:

$$\left.\begin{aligned} \rho\, u_{1,tt} &= (2\mu+\lambda)u_{1,11} + (\mu+\lambda)u_{2,12} + \mu\, u_{1,22} \\ \rho\, u_{2,tt} &= (2\mu+\lambda)u_{2,22} + (\mu+\lambda)u_{1,12} + \mu\, u_{2,11} \end{aligned}\right\} \tag{4.9}$$

$$\rho\, u_{3,tt} = \mu(u_{3,11} + u_{3,22}). \tag{4.10}$$

We remark that the first two equations (4.9) are coupled, while the third (4.10) is uncoupled from the first two.

We now formulate the plane wave ansatz, according to which the displacement vector u takes the same value at all points lying on the same orthogonal line to the $(x_1x_2)-$plane (no dependence on x_3). Moreover, we also consider that the displacement field is periodic in space. In symbols, the plane-wave ansatz reads

$$u = \widehat{\psi}\, e^{i(\langle x,k\rangle - \omega t)} = \widehat{\psi}\, e^{i(x_1k_1+x_2k_2-\omega t)}, \tag{4.11}$$

$$u_3 = \widehat{\psi}_3\, e^{i(\langle x,k\rangle - \omega t)} = \widehat{\psi}_3\, e^{i(x_1k_1+x_2k_2-\omega t)}, \tag{4.12}$$

where $\widehat{\psi} = (\widehat{\psi}_1, \widehat{\psi}_2)^{\mathrm{T}}$ is the vector of amplitudes, $k = (k_1, k_2)^{\mathrm{T}}$ is the wave-vector, which fixes the direction of propagation of the considered wave and $x = (x_1, x_2)^{\mathrm{T}}$ is the position vector. Moreover, $\widehat{\psi}_3$ is a scalar amplitude for the third component of the displacement. We explicitly remark that in equation (4.11) we consider (with a slight abuse of notation) $u = (u_1, u_2)^{\mathrm{T}}$ to be the vector involving only the in-plane displacement components u_1 and u_2 which are coupled via equations (4.9). We start by considering the first system of coupled equations and we plug

[5] Following classical nomenclature ([1]) we call longitudinal (or L) waves the waves whose displacement vector is in the same direction of the wave vector. Moreover SV waves are shear waves whose displacement vectors is orthogonal to the wave vector and lies in the $(x_1x_2)-$plane. SH waves are shear waves whose displacement vector is orthogonal to the wave vector and lies in a plane orthogonal to the $(x_1x_2)-$plane.

the plane-wave ansatz (4.11) into (4.9), so obtaining

$$\begin{aligned}(\omega^2 - c_L^2 k_1^2 - c_S^2 k_2^2)\widehat{\psi}_1 - c_V^2 k_1 k_2 \widehat{\psi}_2 = 0,\\ -c_V^2 k_1 k_2 \widehat{\psi}_1 + (\omega^2 - c_L^2 k_2^2 - c_S^2 k_1^2)\widehat{\psi}_2 = 0,\end{aligned} \tag{4.13}$$

where we made the abbreviations

$$c_L^2 = \frac{2\mu + \lambda}{\rho}, \quad c_S^2 = \frac{\mu}{\rho}, \quad c_V^2 = c_L^2 - c_S^2 = \frac{\mu + \lambda}{\rho}, \tag{4.14}$$

where μ, λ are the Lamé parameters of the material and ρ is its apparent density. This system of algebraic equations can be written compactly as $A \cdot \widehat{\psi} = 0$, where A is the matrix of coefficients

$$A = \begin{pmatrix} \omega^2 - c_L^2 k_1^2 - c_S^2 k_2^2 & -c_V^2 k_1 k_2 \\ -c_V^2 k_1 k_2 & \omega^2 - c_L^2 k_2^2 - c_S^2 k_1^2 \end{pmatrix}. \tag{4.15}$$

For $A \cdot \widehat{\psi} = 0$ to have a solution other than the trivial one, we impose $\det A = 0$. We have (see Appendix B for a detailed calculation of this expression)

$$\det A = \frac{\left((2\mu + \lambda)\left(k_1^2 + k_2^2\right) - \rho\omega^2\right)\left(\mu\left(k_1^2 + k_2^2\right) - \rho\omega^2\right)}{\rho^2}. \tag{4.16}$$

We now solve the algebraic equation $\det A = 0$ with respect to the first component k_1 of the wave-vector k (as will be evident in section 4.2.2, the second component of the wave-vector k_2 is always known when imposing boundary conditions)

$$\begin{aligned}\left((2\mu + \lambda)\left(k_1^2 + k_2^2\right) - \rho\omega^2\right)\left(\mu\left(k_1^2 + k_2^2\right) - \rho\omega^2\right) = 0,\\ (2\mu + \lambda)\left(k_1^2 + k_2^2\right) - \rho\omega^2 = 0 \quad \text{or} \quad \mu\left(k_1^2 + k_2^2\right) - \rho\omega^2 = 0,\\ k_1^2 = \frac{\rho\,\omega^2}{2\mu + \lambda} - k_2^2 \quad \text{or} \quad k_1^2 = \frac{\rho}{\mu}\omega^2 - k_2^2,\end{aligned} \tag{4.17}$$

$$k_1 = \pm\sqrt{\frac{\omega^2}{c_L^2} - k_2^2} \quad \text{or} \quad k_1 = \pm\sqrt{\frac{\omega^2}{c_S^2} - k_2^2}, \tag{4.18}$$

As we will show in the remainder of this subsection, the first and second solution in (4.18) is associated to what we call a longitudinal and SV shear wave, respectively. The choice of sign for these solutions is related to the direction of propagation of the considered wave (positive for incident and transmitted waves, negative for reflected waves).[6]

We will show later on in detail, that once boundary conditions are imposed at a given interface between two Cauchy media, the value of the component k_2 of the wave-vector k can be considered to be known. We will see that k_2 is always real and positive, which means that, according to (4.18), the first component k_1 of the wave-vector can be either real or purely imaginary, depending on the values of the frequency and of the material parameters. Two scenarios are then possible:

[6] As a matter of fact, the sign + or − in expressions (4.18) is uniquely determined by imposing that the solution preserves the conservation of energy at the considered interface. For Cauchy media, as well as for isotropic relaxed micromorphic media, it turns out that one must choose positive k_1 for transmitted and incident waves and negative k_1 for reflected ones (according to our convention).

1. both k_1 and k_2 are real: This means that, according to the wave ansatz (4.11), we have a harmonic wave which propagates in the direction given by the wave-vector k lying in the $(x_1x_2)-$ plane. The wave-vector of the considered wave has two non-vanishing components in the $(x_1x_2)-$plane. A simplified illustration of this case is given in Fig. 4.4.

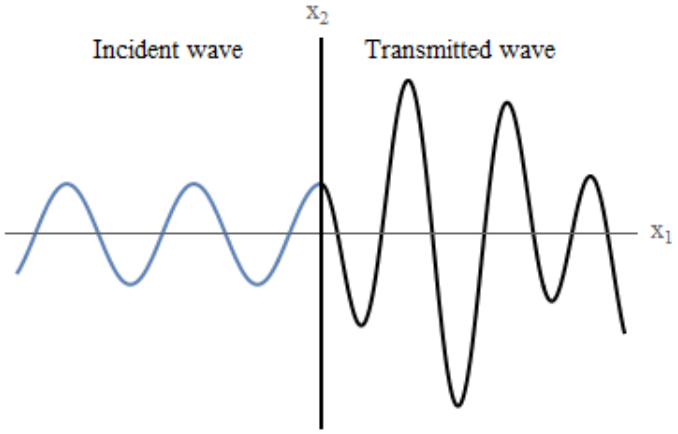

Figure 4.4: Schematic representation of an incident wave which propagates after hitting the interface. For graphical simplicity, only normal incidence and normal transmission are depicted.

2. k_2 is real and k_1 purely imaginary: In this case, according to equation (4.11), the wave continues to propagate in the x_2 direction (along the interface), but decays with a negative exponential in the x_1 direction (away from the interface). Such a wave propagating only along the interface is known as a Stoneley interface wave ([7, 92]). An illustration of this phenomenon is given in Fig. 4.5.

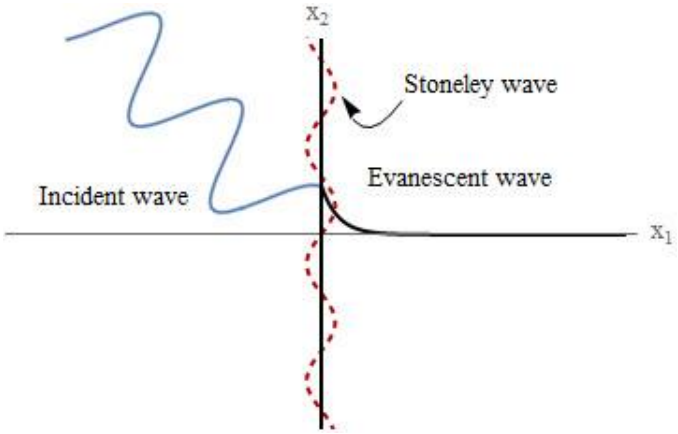

Figure 4.5: Schematic representation of an incident wave which is transformed into an interface wave along the interface and decays exponentially away from it (Stoneley wave).

In conclusion, we can say that when considering wave propagation in $2-$dimensional Cauchy media, it is possible that, given the material parameters, some frequencies exist for which all the energy of the incident wave can be redirected in Stoneley waves traveling along the interface, thus inhibiting transmission across the interface. Such waves are also possible at the interface between a Cauchy and a relaxed micromorphic medium, in a generalized setting.

Assuming the second component k_2 of the wave-vector to be known, we now calculate the solution $\widehat{\psi}$ to the algebraic equations $A \cdot \widehat{\psi} = 0$; these solutions make up the kernel (or nullspace) of the matrix A and are essentially eigenvectors to the eigenvalue 0. Hence, as is common nomenclature ([65]), we call them eigenvectors.

Using the first solution of (4.18), we see that it also implies

$$k_1^2 = \frac{\omega^2}{c_L^2} - k_2^2. \tag{4.19}$$

Using this relation between k_1 and k_2 in the first equation of (4.13), we obtain

$$\begin{aligned}
\left(\omega^2 - c_L^2\left(\frac{\omega^2}{c_L^2} - k_2^2\right) - c_S^2 k_2^2\right)\widehat{\psi}_1 - c_V^2\sqrt{\frac{\omega^2}{c_L^2} - k_2^2}\; k_2\widehat{\psi}_2 = 0,\\
(\omega^2 - \omega^2 + c_L^2 k_2^2 - c_S^2 k_2^2)\widehat{\psi}_1 - c_V^2\sqrt{\frac{\omega^2}{c_L^2} - k_2^2}\; k_2\widehat{\psi}_2 = 0,\\
(\underbrace{c_L^2 - c_S^2}_{=c_V^2})k_2^2\widehat{\psi}_1 - c_V^2\sqrt{\frac{\omega^2}{c_L^2} - k_2^2}\; k_2\widehat{\psi}_2 = 0,
\end{aligned} \tag{4.20}$$

this implies

$$\widehat{\psi}_2 = \frac{k_2}{\sqrt{\frac{\omega^2}{c_L^2} - k_2^2}}\;\widehat{\psi}_1 \Leftrightarrow \widehat{\psi}_2 = \frac{c_L k_2}{\sqrt{\omega^2 - c_L^2 k_2^2}}\;\widehat{\psi}_1. \tag{4.21}$$

So, the eigenvector of the matrix A in this case is given by

$$\widehat{\psi}^L := \begin{pmatrix} 1 \\ \frac{c_L k_2}{\sqrt{\omega^2 - c_L^2 k_2^2}} \end{pmatrix} = \begin{pmatrix} 1 \\ \frac{k_2}{k_1} \end{pmatrix}. \tag{4.22}$$

We explicitly remark that the definition of $\widehat{\psi}^L$ given by the first equality allows us to compute the vector $\widehat{\psi}^L$ once k_2 is known, i.e. when imposing boundary conditions. On the other hand, the equivalent definition $\widehat{\psi}^L = (1, k_2/k_1)^{\mathrm{T}}$ allows us to remark that $k_1\widehat{\psi}^L = (k_1, k_2)^{\mathrm{T}}$ is still a solution of the equation $A \cdot \widehat{\psi} = 0$. In this case, the vector of amplitudes is collinear with the wave-vector k. This allows us to talk about **longitudinal waves**, since the displacement vector $(u_1, u_2)^{\mathrm{T}}$ given by expression (4.11) (and hence the motion) is parallel to the direction of propagation of the traveling wave. We also notice that, given the eigenvector $\widehat{\psi}^L$, all vectors $a\,\widehat{\psi}^L$, with $a \in \mathbb{C}$, are solutions to the equation $A \cdot \widehat{\psi} = 0$. Analogous considerations can be carried out when considering the second solution of (4.18), which also implies

$$k_1^2 = \frac{\omega^2}{c_S^2} - k_2^2. \tag{4.23}$$

Using this relation between k_1 and k_2 in the second equality of (4.13) gives

$$\left(\omega^2 - c_L^2\left(\frac{\omega^2}{c_S^2} - k_2^2\right) - c_S^2 k_2\right)\widehat{\psi}_1 - c_V^2\sqrt{\frac{\omega^2}{c_S^2} - k_2^2}\; k_2\widehat{\psi}_2 = 0,$$

$$\left(\omega^2 - \frac{c_L^2}{c_S^2}\omega^2 + c_L^2 k_2^2 - c_S^2 k_2^2\right)\widehat{\psi}_1 - c_V^2\sqrt{\frac{\omega^2}{c_S^2} - k_2^2}\; k_2\widehat{\psi}_2 = 0,$$

$$\left(\omega^2\frac{c_S^2 - c_L^2}{c_S^2} + (c_L^2 - c_S^2)k_2^2\right)\widehat{\psi}_1 - c_V^2\sqrt{\frac{\omega^2}{c_S^2} - k_2^2}\; k_2\widehat{\psi}_2 = 0,$$

$$\left(-\omega^2\frac{c_V^2}{c_S^2} + c_V^2 k_2^2\right)\widehat{\psi}_1 - c_V^2\sqrt{\frac{\omega^2}{c_S^2} - k_2^2}\; k_2\widehat{\psi}_2 = 0, \tag{4.24}$$

$$\tag{4.25}$$

this implies

$$k_2\sqrt{\omega^2 - k_2^2 c_S^2}\;\widehat{\psi}_2 = \frac{k_2^2 c_S^2 - \omega^2}{c_S}\;\widehat{\psi}_1 \Leftrightarrow \widehat{\psi}_2 = \frac{k_2^2 c_S^2 - \omega^2}{k_2 c_S\sqrt{\omega^2 - k_2^2 c_S^2}}\;\widehat{\psi}_1. \tag{4.26}$$

Therefore, the eigenvector of the matrix A in this case is given by[7]

$$\widehat{\psi}^{SV} := \begin{pmatrix} 1 \\ \frac{k_2^2 c_S^2 - \omega^2}{k_2 c_S\sqrt{\omega^2 - k_2^2 c_S^2}} \end{pmatrix} = \begin{pmatrix} 1 \\ -\frac{k_1}{k_2} \end{pmatrix}. \tag{4.27}$$

Finally, replacing the plane-wave ansatz (4.12) for the third component u_3 of the displacement in equation (4.10) gives[8]

$$\begin{aligned} -\omega^2\rho\,\widehat{\psi}_3 e^{i(\langle x,k\rangle - \omega t)} &= \mu(-k_1^2 - k_2^2)\widehat{\psi}_3 e^{i(\langle x,k\rangle - \omega t)}, \\ \rho\,\omega^2 &= \mu(k_1^2 + k_2^2), \\ k_1 &= \pm\sqrt{\frac{\omega^2}{c_S^2} - k_2^2}. \end{aligned} \tag{4.28}$$

This relation, compared to the second of equations (4.18), tells us that the same relation between k_1 and k_2 exists when considering SV or SH waves.

Equations (4.18) and (4.28) give rise to the well-known dispersion curves for Cauchy continua for in-plane and out-of-plane waves (see Fig. 4.6).

[7] Analogously to the case of longitudinal waves, we can remark that the vector $(k_2, -k_1)^{\mathrm{T}}$ is still a solution of the equation $A\cdot\widehat{\psi} = 0$. This means that, in this case, the vector of amplitudes lies in the $(x_1x_2)-$plane and is orthogonal to the direction of propagation given by the wave-vector k. This allows us to introduce the concept of **transverse in-plane waves**, or "shear vertical" SV waves, since the displacement $(u_1, u_2)^{\mathrm{T}}$ given by (4.11) (and hence the motion) is orthogonal to the direction of propagation of the traveling wave, but lying in the $(x_1x_2)-$plane. We also remark that any vector $a\,\widehat{\psi}^{SV}$, with $a \in \mathbb{C}$, is solution to the equation $A\cdot\widehat{\psi} = 0$. The first equality defining $\widehat{\psi}$ in (4.27) allows to directly compute $\widehat{\psi}$ when k_2 is known, i.e. when imposing boundary conditions.

[8] The component u_3 of the displacement being orthogonal to the $(x_1x_2)-$plane and thus to the direction of propagation of the wave, allows us to talk about **transverse, out-of-plane waves** or, equivalently, "shear horizontal" SH waves. Such waves have the same speed c_S as the SV waves.

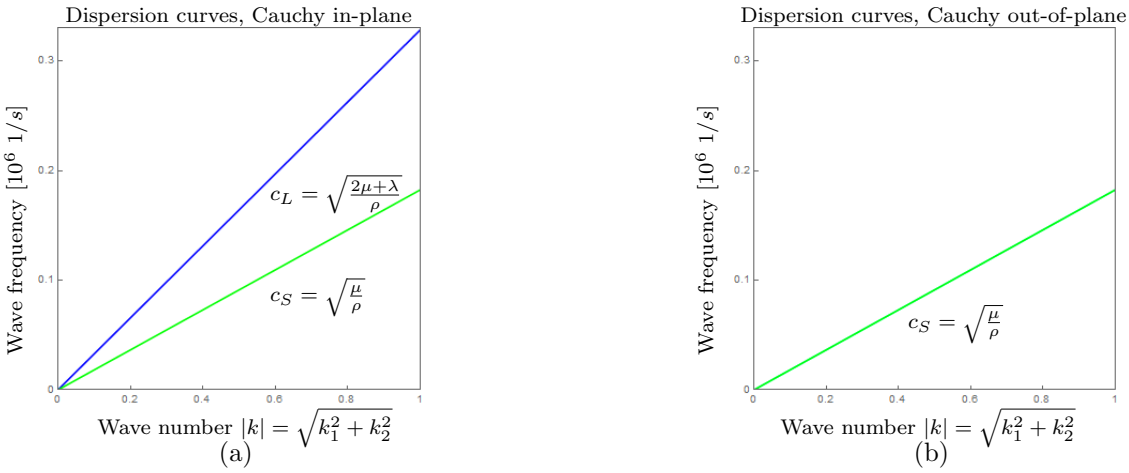

Figure 4.6: Dispersion diagrams for in-plane (a) and out-of-plane (b) modes in isotropic Cauchy continua. The material parameters used in these Figures are the ones given in Table 4.5.

Plane-wave ansatz: solution for the displacement field in a Cauchy medium

We have seen in section 4.2.1 how to write the displacement field making use of the concepts of longitudinal, SV and SH waves.

According to equations (4.11) and (4.12) and considering the 2D eigenvectors (4.22) and (4.27), we can finally write the solution for the displacement field $u = (u_1, u_2, u_3)^{\mathrm{T}}$ as

$$u = u^L + u^{SV} = a^L \psi^L e^{i\left(x_1 k_1^L + x_2 k_2^L - \omega t\right)} + a^{SV} \psi^{SV} e^{i\left(x_1 k_1^{SV} + x_2 k_2^{SV} - \omega t\right)}, \tag{4.29}$$

when we consider a longitudinal or an SV wave, or

$$u = u^{SH} = a^{SH} \psi^{SH} e^{i\left(x_1 k_1^{SH} + x_2 k_2^{SH} - \omega t\right)}, \tag{4.30}$$

when we consider an SH wave. In these formulas, starting from equations (4.22) and (4.27), we defined the unit vectors

$$\psi^L = \frac{1}{\left|\widehat{\psi}^L\right|} \begin{pmatrix} \widehat{\psi}_1^L \\ \widehat{\psi}_2^L \\ 0 \end{pmatrix}, \quad \psi^{SV} = \frac{1}{\left|\widehat{\psi}^{SV}\right|} \begin{pmatrix} \widehat{\psi}_1^{SV} \\ \widehat{\psi}_2^{SV} \\ 0 \end{pmatrix}, \quad \text{and} \quad \psi^{SH} = \begin{pmatrix} 0 \\ 0 \\ 1 \end{pmatrix}. \tag{4.31}$$

Finally, $a^L, a^{SV}, a^{SH} \in \mathbb{C}$ are arbitrary constants.

We also explicitly remark that in equations (4.29) and (4.30), k_1^L and k_2^L are related via the first equation of (4.18), k_1^{SV} and k_2^{SV} via the second equation of (4.18) and k_1^{SH} and k_2^{SH} via (4.28).

As we already mentioned, k_2 will be known when imposing boundary conditions, so the only unknowns in the solution (4.29) (resp (4.30)) remain the scalar amplitudes a^L, a^{SV} (resp. a^{SH}). We will show in the following subsection how, using the form (4.29) (resp. (4.30)) for the solution in the problem of reflection and transmission at an interface between Cauchy media, the unknown amplitudes can be computed by imposing boundary conditions.

4.2.2 Interface between two Cauchy media

We now turn to the problem of reflection and transmission of elastic waves at an interface between two Cauchy media (cf. Fig. 4.3). We assume that an incident longitudinal wave[9] propagates on the "minus" side, hits the interface (which is the x_2 axis) and is subsequently reflected into a longitudinal wave and an SV wave and is transmitted into the second medium on the "plus" side into a longitudinal wave and an SV wave as well, according to equations (4.29). If we send an incident SH wave, equation (4.30) tells us that it will reflect and transmit only into SH waves.

Incident longitudinal/SV-transverse wave

According to our previous considerations, and given the linearity of the considered problem, the solution of the dynamical problem (2.4) on the "minus" side can be written as[10]

$$u^-(x_1,x_2,t) = a^{L,\mathrm{i}}\psi^{L,\mathrm{i}}e^{i\left(\langle x,k^{L,\mathrm{i}}\rangle-\omega t\right)}+a^{L,\mathrm{r}}\psi^{L,\mathrm{r}}e^{i\left(\langle x,k^{L,\mathrm{r}}\rangle-\omega t\right)}+a^{SV,\mathrm{r}}\psi^{SV,\mathrm{r}}e^{i\left(\langle x,k^{SV,\mathrm{r}}\rangle-\omega t\right)} =: u^{L,\mathrm{i}}+u^{L,\mathrm{r}}+u^{SV,\mathrm{r}}. \tag{4.32}$$

As for the "plus" side, the solution is

$$u^+(x_1,x_2,t) = a^{L,\mathrm{t}}\psi^{L,\mathrm{t}}e^{i\left(\langle x,k^{L,\mathrm{t}}\rangle-\omega t\right)} + a^{SV,\mathrm{t}}\psi^{SV,\mathrm{t}}e^{i\left(\langle x,k^{SV,\mathrm{t}}\rangle-\omega t\right)} =: u^{L,\mathrm{t}} + u^{SV,\mathrm{t}}. \tag{4.33}$$

The vectors $\psi^{L,\mathrm{i}}, \psi^{SV,\mathrm{r}}$ and $\psi^{SV,\mathrm{t}}$ are as in (4.31).

Now the new task is given an incident wave, i.e. knowing $a^{L,\mathrm{i}}$ and $k^{L,\mathrm{i}}$, to calculate all the respective parameters of the "new" waves.

We see that the jump condition (4.1) can be further developed considering that $u^- = u^{L,\mathrm{i}} + u^{L,\mathrm{r}} + u^{SV,\mathrm{r}}$ and $u^+ = u^{L,\mathrm{t}} + u^{SV,\mathrm{t}}$. We equate the first components of (4.1)

$$u_1^{L,\mathrm{i}} + u_1^{L,\mathrm{r}} + u_1^{SV,\mathrm{r}} = u_1^{L,\mathrm{t}} + u_1^{SV,\mathrm{t}},$$

which, evaluating the involved expression at $x_1 = 0$ (the interface), implies

$$\begin{aligned} a^{L,\mathrm{i}}\psi_1^{L,\mathrm{i}}e^{i\left(x_2k_2^{L,\mathrm{i}}-\omega t\right)} + a^{L,\mathrm{r}}\psi_1^{L,\mathrm{r}}e^{i\left(x_2k_2^{L,\mathrm{r}}-\omega t\right)} + a^{SV,\mathrm{r}}\psi_1^{SV,\mathrm{r}}e^{i\left(x_2k_2^{SV,\mathrm{r}}-\omega t\right)} \\ = a^{L,\mathrm{t}}\psi_1^{L,\mathrm{t}}e^{i\left(x_2k_2^{L,\mathrm{t}}-\omega t\right)} + a^{SV,\mathrm{t}}\psi_1^{SV,\mathrm{t}}e^{i\left(x_2k_2^{SV,\mathrm{t}}-\omega t\right)}, \end{aligned}$$

or, simplifying everywhere the time exponential

$$a^{L,\mathrm{i}}\psi_1^{L,\mathrm{i}}e^{ix_2k_2^{L,\mathrm{i}}} + a^{L,\mathrm{r}}\psi_1^{L,\mathrm{r}}e^{ix_2k_2^{L,\mathrm{r}}} + a^{SV,\mathrm{r}}\psi_1^{SV,\mathrm{r}}e^{ix_2k_2^{SV,\mathrm{r}}} = a^{L,\mathrm{t}}\psi_1^{L,\mathrm{t}}e^{ix_2k_2^{L,\mathrm{t}}} + a^{SV,\mathrm{t}}\psi_1^{SV,\mathrm{t}}e^{ix_2k_2^{SV,\mathrm{t}}}. \tag{4.34}$$

This must hold for all $x_2 \in \mathbb{R}$. The exponentials in this expression form a family of linearly independent functions and, therefore, we can safely assume that the coefficients $a^{L,\mathrm{i}}, a^{L,\mathrm{r}}, a^{SV,\mathrm{r}}, a^{L,\mathrm{t}}, a^{SV,\mathrm{t}}$ are never all zero simultaneously. This means, than in order for (4.34) to hold, we must require that the exponents of the exponentials are all equal to one another. Canceling out the imaginary unit i and x_2, we deduce the fundamental relation[11]

[9] The exact same considerations can be carried over when the incident wave is SV transverse.

[10] With a clear extension of the previously introduced notation, we denote by $a^{L,\mathrm{i}}, a^{L,\mathrm{r}}, a^{L,\mathrm{t}}, a^{SV,\mathrm{r}}, a^{SV,\mathrm{t}}$ and $\psi^{L,\mathrm{i}}, \psi^{L,\mathrm{r}}, \psi^{L,\mathrm{t}}, \psi^{SV,\mathrm{r}}, \psi^{SV,\mathrm{t}}$ the amplitudes and eigenvectors of longitudinal incident, reflected, transmitted, in-plane transverse incident, reflected and transmitted waves respectively. Analogously, $a^{SV,\mathrm{i}}$ and $\psi^{SV,\mathrm{i}}$ will denote the amplitude and eigenvector related to in-plane transverse incident waves.

[11] It is now clear why we said previously that the second components of all wave-vectors are known, since they are all equal to the second component of the wave-vector of the prescribed incident wave, which is known by definition.

$$\boxed{k_2^{L,\mathrm{i}} = k_2^{L,\mathrm{r}} = k_2^{SV,\mathrm{r}} = k_2^{L,\mathrm{t}} = k_2^{SV,\mathrm{t}}}, \tag{4.35}$$

which is the well-known **Snell's law** for in-plane waves (see [1, 7, 43, 110]). Using (4.35) we see that the exponentials in (4.34) can be canceled out leaving only

$$a^{L,\mathrm{i}}\psi_1^{L,\mathrm{i}} + a^{L,\mathrm{r}}\psi_1^{L,\mathrm{r}} + a^{SV,\mathrm{r}}\psi_1^{SV,\mathrm{r}} = a^{L,\mathrm{t}}\psi_1^{L,\mathrm{t}} + a^{SV,\mathrm{t}}\psi_1^{SV,\mathrm{t}}. \tag{4.36}$$

Analogously, equating the second components of the displacements in the jump conditions (4.1), using (4.35) and the fact that this must hold for all $x_2 \in \mathbb{R}$, gives

$$a^{L,\mathrm{i}}\psi_2^{L,\mathrm{i}} + a^{L,\mathrm{r}}\psi_2^{L,\mathrm{r}} + a^{SV,\mathrm{r}}\psi_2^{SV,\mathrm{r}} = a^{L,\mathrm{t}}\psi_2^{L,\mathrm{t}} + a^{SV,\mathrm{t}}\psi_2^{SV,\mathrm{t}}. \tag{4.37}$$

As for the jump of traction, we remark that the total traction on both sides is

$$T^- = t^{L,\mathrm{i}} + t^{L,\mathrm{r}} + t^{SV,\mathrm{r}}, \quad T^+ = t^{L,\mathrm{t}} + t^{SV,\mathrm{t}},$$

with the t's being evaluated at $x_1 = 0$. The tractions are vectors of the form

$$t = (t_1, t_2, 0)^{\mathrm{T}}, \tag{4.38}$$

with

$$t_i = \sigma_{ij}\nu_j, \tag{4.39}$$

where $\nu = (\nu_1, \nu_2, \nu_3)^{\mathrm{T}} = (1, 0, 0)^{\mathrm{T}}$ is the normal vector to the interface, i.e. to the x_2 axis.[12]

The traction jump condition (4.2) can now be written component-wise as

$$\sigma_{11}^{L,\mathrm{i}} + \sigma_{11}^{L,\mathrm{r}} + \sigma_{11}^{SV,\mathrm{r}} = \sigma_{11}^{L,\mathrm{t}} + \sigma_{11}^{SV,\mathrm{t}}, \tag{4.40}$$

$$\sigma_{21}^{L,\mathrm{i}} + \sigma_{21}^{L,\mathrm{r}} + \sigma_{21}^{SV,\mathrm{r}} = \sigma_{21}^{L,\mathrm{t}} + \sigma_{21}^{SV,\mathrm{t}}. \tag{4.41}$$

Calculating the stresses according to eq. (2.5), where we use the solutions (4.32) and (4.33) for the displacement and again using (4.35) gives

$$\begin{aligned} &a^{L,\mathrm{i}}\left((2\mu+\lambda)\psi_1^{L,\mathrm{i}}k_1^{L,\mathrm{i}} + \lambda\psi_2^{L,\mathrm{i}}k_2^{L,\mathrm{i}}\right) + a^{L,\mathrm{r}}\left((2\mu+\lambda)\psi_1^{L,\mathrm{r}}k_1^{L,\mathrm{r}} + \lambda\psi_2^{L,\mathrm{r}}k_2^{L,\mathrm{r}}\right) \\ &\qquad + a^{SV,\mathrm{r}}\left((2\mu+\lambda)\psi_1^{SV,\mathrm{r}}k_1^{SV,\mathrm{r}} + \lambda\psi_2^{SV,\mathrm{r}}k_2^{SV,\mathrm{r}}\right) \\ &= a^{L,\mathrm{t}}\left((2\mu^+ + \lambda^+)\psi_1^{L,\mathrm{t}}k_1^{L,\mathrm{t}} + \lambda^+\psi_2^{L,\mathrm{t}}k_2^{L,\mathrm{t}}\right) + a^{SV,\mathrm{t}}\left((2\mu^+ + \lambda^+)\psi_1^{SV,\mathrm{t}}k_1^{SV,\mathrm{t}} + \lambda^+\psi_2^{SV,\mathrm{t}}k_2^{SV,\mathrm{t}}\right), \end{aligned} \tag{4.42}$$

and

$$\begin{aligned} &a^{L,\mathrm{i}}\mu\left(\psi_1^{L,\mathrm{i}}k_2^{L,\mathrm{i}} + \psi_2^{L,\mathrm{i}}k_1^{L,\mathrm{i}}\right) + a^{L,\mathrm{r}}\mu\left(\psi_1^{L,\mathrm{r}}k_2^{L,\mathrm{r}} + \psi_2^{L,\mathrm{r}}k_1^{L,\mathrm{r}}\right) + a^{SV,\mathrm{r}}\mu\left(\psi_1^{SV,\mathrm{r}}k_2^{SV,\mathrm{r}} + \psi_2^{SV,\mathrm{r}}k_1^{SV,\mathrm{r}}\right) \\ &\qquad = a^{L,\mathrm{t}}\mu^+\left(\psi_1^{L,\mathrm{t}}k_2^{L,\mathrm{t}} + \psi_2^{L,\mathrm{t}}k_1^{L,\mathrm{t}}\right) + a^{SV,\mathrm{t}}\mu^+\left(\psi_1^{SV,\mathrm{t}}k_2^{SV,\mathrm{t}} + \psi_2^{SV,\mathrm{t}}k_1^{SV,\mathrm{t}}\right). \end{aligned} \tag{4.43}$$

Thus, equations (4.36), (4.37), (4.42), (4.43) form an algebraic system for the unknown amplitudes $a^{L,\mathrm{r}}$, $a^{SV,\mathrm{r}}$, $a^{L,\mathrm{t}}$, $a^{SV,\mathrm{t}}$ from which we can fully calculate the solution.

[12] We immediately see that the only components of the stress tensor which have a contribution in the calculation of the traction jump are σ_{11} and σ_{21}.

Incident SH-transverse wave

In this case, the solution on the "minus" side of the interface is

$$u^-(x_1,x_2,t) = a^{SH,\mathrm{i}}\psi^{SH,\mathrm{i}}e^{i\left(\langle x,k^{SH,\mathrm{i}}\rangle-\omega t\right)} + a^{SH,\mathrm{r}}\psi^{SH,\mathrm{r}}e^{i\left(\langle x,k^{SH,\mathrm{r}}\rangle-\omega t\right)}, \tag{4.44}$$

and on the "plus" side

$$u^+(x_1,x_2,t) = a^{SH,\mathrm{t}}\psi^{SH,\mathrm{t}}e^{i\left(\langle x,k^{SH,\mathrm{t}}\rangle-\omega t\right)}, \tag{4.45}$$

where the vectors $\psi^{SH,\mathrm{i}}, \psi^{SH,\mathrm{r}}, \psi^{SH,\mathrm{t}}$ are all equal to $(0,0,1)^{\mathrm{T}}$, according to the third equation of (4.31). Following the same reasoning as in section 4.2.2, the continuity of displacement condition now only involves the u_3 component, which is the only non-zero one, and reads (evaluating again at $x_1 = 0$)

$$a^{SH,\mathrm{i}}e^{i\left(x_2k_2^{SH,\mathrm{i}}\right)} + a^{SH,\mathrm{r}}e^{i\left(x_2k_2^{SH,\mathrm{r}}\right)} = a^{SH,\mathrm{t}}e^{i\left(x_2k_2^{SH,\mathrm{t}}\right)}, \tag{4.46}$$

which, since the exponentials build a family of linearly independent functions and if we exclude the case where all amplitudes $a^{SH,\mathrm{i}}, a^{SH,\mathrm{r}}, a^{SH,\mathrm{t}}$ are identically equal to zero, becomes **Snell's law** for out-of-plane motions

$$\boxed{k_2^{SH,\mathrm{i}} = k_2^{SH,\mathrm{r}} = k_2^{SH,\mathrm{t}}}. \tag{4.47}$$

Using that, we see that the exponentials in (4.46) cancel out leaving only

$$a^{SH,\mathrm{i}} + a^{SH,\mathrm{r}} = a^{SH,\mathrm{t}}. \tag{4.48}$$

As for the jump in traction in the case of SH waves, the total traction on both sides is $T^- = t^{SH,\mathrm{i}} + t^{SH,\mathrm{r}}$, $T^+ = t^{SH,\mathrm{t}}$, with the t's being evaluated at $x_1 = 0$. Now the tractions are vectors of the form

$$t = (0,0,t_3)^{\mathrm{T}},$$

where, once again, $f_i = \sigma_{ij}\nu_j$, where $\nu = (1,0,0)^{\mathrm{T}}$ is the vector normal to the interface.[13] Condition (4.2) can now be written as

$$\sigma_{31}^{SH,\mathrm{i}} + \sigma_{31}^{SH,\mathrm{r}} = \sigma_{31}^{SH,\mathrm{t}} \tag{4.49}$$

The stresses are calculated again by (2.5) and using the solutions (4.44) and (4.45) for the displacement and using (4.47) gives

$$\mu\left(a^{SH,\mathrm{i}}k_1^{SH,\mathrm{i}} + a^{SH,\mathrm{r}}k_1^{SH,\mathrm{r}}\right) = \mu^+a^{SH,\mathrm{t}}k_1^{SH,\mathrm{t}}. \tag{4.50}$$

Equations (4.48) and (4.50) build a system for the unknown amplitudes $a^{SH,\mathrm{r}}, a^{SH,\mathrm{t}}$, which we can solve to fully determine the solution to the reflection-transmission problem.

A condition for the onset of Stoneley waves at a Cauchy/Cauchy interface

In this subsection we show how we can find explicit conditions for the onset of Stoneley waves at Cauchy/Cauchy interfaces. This can be done by simply requesting that the quantities under the square roots in equation (4.18) become negative.

[13] We now see that the component of the stress which has an influence in this boundary condition is σ_{31}.

Assume that the incident wave is longitudinal. This means that its speed is given by $c_L^- = \sqrt{(2\mu^- + \lambda^-)/\rho^-}$ and that the wave vector k can now be written as

$$k = (k_1, k_2) = |k|(\sin\theta_\mathrm{i}, -\cos\theta_\mathrm{i}),$$

where $|k| = \omega/c_L^-$ and θ_i is the angle of incidence. This incident longitudinal wave gives rise to a longitudinal and a transverse wave both on the "−" and on the "+" side. Setting the quantity under the square root in the first equation in (4.18) to be negative and using the fact that $k_2 = -|k|\cos\theta_\mathrm{i}$, gives a condition for the appearance of Stoneley waves in the case of an incident longitudinal wave:

$$\begin{aligned}
\frac{\omega^2}{(c_L^+)^2} - k_2^+ < 0 \Leftrightarrow \frac{\omega^2}{(c_L^+)^2} - k_2^2 < 0 &\Leftrightarrow \frac{\omega^2}{(c_L^+)^2} < |k|^2\cos^2\theta_\mathrm{i} \\
&\Leftrightarrow \frac{\omega^2}{(c_L^+)^2} < \frac{\omega^2}{(c_L^-)^2}\cos^2\theta_\mathrm{i} \\
&\Leftrightarrow \cos^2\theta_\mathrm{i} > \left(\frac{c_L^-}{c_L^+}\right)^2 \\
&\Leftrightarrow \cos^2\theta_\mathrm{i} > \frac{\rho^+(2\mu^- + \lambda^-)}{\rho^-(2\mu^+ + \lambda^+)}.
\end{aligned} \tag{4.51}$$

To establish the previous relation we also used the fact that $k_2^+ = k_2$, as established by **Snell's law** in (4.35).

Similar arguments can be carried out when considering all other possibilities for incident, transmitted and reflected waves, as detailed in Tables 4.1 and 4.2.

Incident Wave	Transmitted L	Transmitted SV	Transmitted SH
L	$\cos^2\theta_\mathrm{i} > \frac{\rho^+(2\mu^-+\lambda^-)}{\rho^-(2\mu^+ + \lambda^+)}$	$\cos^2\theta_\mathrm{i} > \frac{\rho^+(2\mu^-+\lambda^-)}{\rho^-\mu^+}$	–
SV	$\cos^2\theta_\mathrm{i} > \frac{\rho^+\mu^-}{\rho^-(2\mu^+ + \lambda^+)}$	$\cos^2\theta_\mathrm{i} > \frac{\rho^+\mu^-}{\rho^-\mu^+}$	–
SH	–	–	$\cos^2\theta_\mathrm{i} > \frac{\rho^+\mu^-}{\rho^-\mu^+}$

Table 4.1: Conditions for the appearance of transmitted Stoneley waves for all types of waves at a Cauchy/Cauchy interface.

Incident Wave	Reflected L	Reflected SV
L	–	–
SV	$\cos^2\theta_\mathrm{i} > \frac{\mu^-}{2\mu^- + \lambda^-}$	–
SH	–	–

Table 4.2: Conditions for the appearance of reflected Stoneley waves for all types of waves at a Cauchy/Cauchy interface.

The conditions in Tables 4.1 and 4.2 establish that the square of the cosine of the angle of incidence must be greater than a given quantity (this happens for smaller angles) for Stoneley

waves to appear. This means that it is most likely to observe Stoneley waves when the angle of incidence is smaller than the normal incidence angle, i.e. for incident waves which are inclined with respect to the surface upon which they hit. Moreover, if there exists a strong contrast in stiffness between the two sides and the "−" side is by far stiffer than the "+" side, then Stoneley waves could be observed for angles closer to normal incidence. On the other hand, if the "−" side is only slightly stiffer than the "+" side, then Stoneley waves will be observed only for smaller angles (far from normal incidence). We refer to Appendix B3 for an explicit calculation of all these conditions.

In order to fix ideas, assuming that both materials on the left and on the right have the same density, i.e. $\rho^- = \rho^+$ and examining Table 4.1, we can deduce that Stoneley waves appear only when the expressions on the right of each inequality are less than one, i.e:[14]

- For an incident L wave, the transmitted L mode becomes Stoneley only if the Lamé parameters of the material are chosen in such a way that $2\mu^+ + \lambda^+ > 2\mu^- + \lambda^-$.

- For an incident L wave, the transmitted SV mode becomes Stoneley only if the Lamé parameters of the material are chosen in such a way that $\mu^+ > 2\mu^- + \lambda^-$.

- For an incident SV wave, the transmitted L mode becomes Stoneley only if the Lamé parameters of the material are chosen in such a way that $2\mu^+ + \lambda^+ > \mu^-$.

- For an incident SV wave, the transmitted SV mode becomes Stoneley only if the Lamé parameters of the material are chosen in such a way that $\mu^+ > \mu^-$.

- For an incident SH wave, the transmitted SH mode (which is the only transmitted mode) becomes Stoneley only if the Lamé parameters of the material are chosen in such a way that $\mu^+ > \mu^-$.

- Reflected waves can become Stoneley waves only when the incident wave is SV. The only mode which can be converted into a Stoneley wave is the L mode when $\mu^- > -\lambda^-$.

All these cases are shown graphically in Figure 4.7. Figures 4.7(a) and 4.7(b) demonstrate the case of an incident L wave. From Table 4.1 we deduce that either only the L transmitted mode will be Stoneley or both L and SV (when $\rho^- = \rho^+$). The same is true for the case of an incident SV wave as shown in Figures 4.7(c) and 4.7(d). For incident SH waves, we only have one transmitted mode which can also be Stoneley as shown in Figure 4.7(e). Figure 4.7(f) shows the only possible manifestation of a reflected Stoneley wave, which is the L mode for the case of an incident SV wave.

[14] In order to respect positive definiteness of the strain energy density, we must require that $2\mu^+ + \lambda^+ > 0$ and $\mu^+ > 0$.

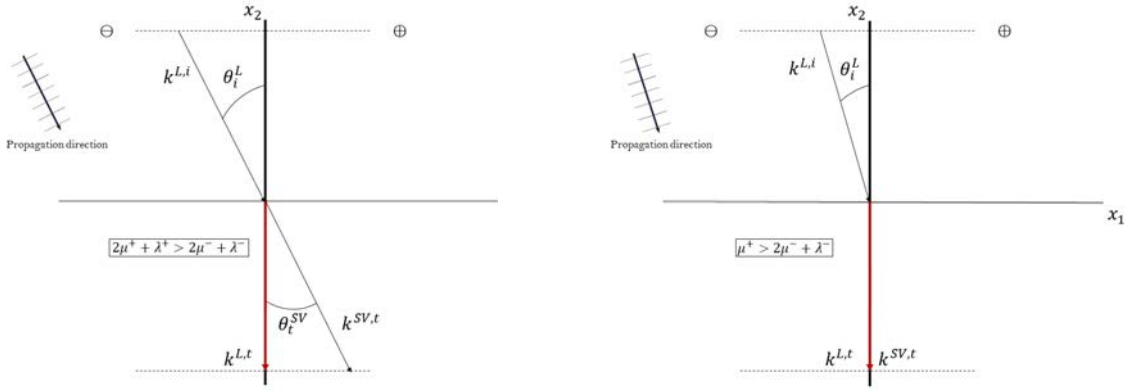

(a)

(b)

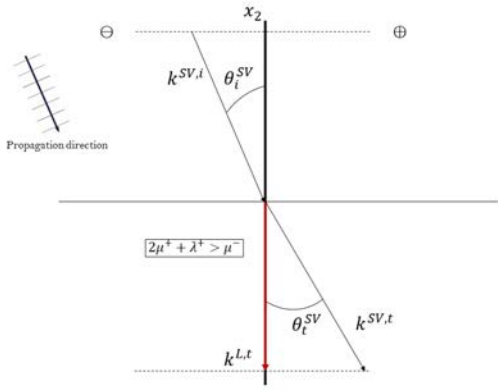

(c)

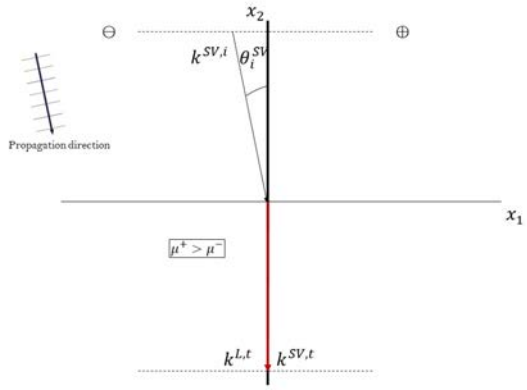

(d)

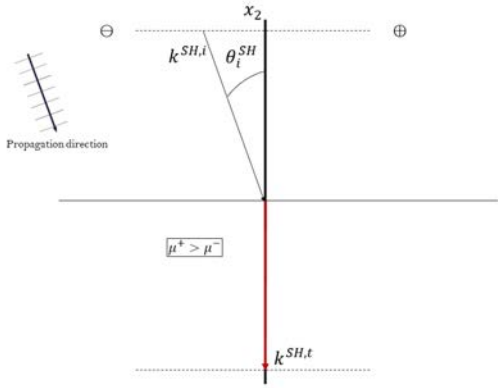

(e)

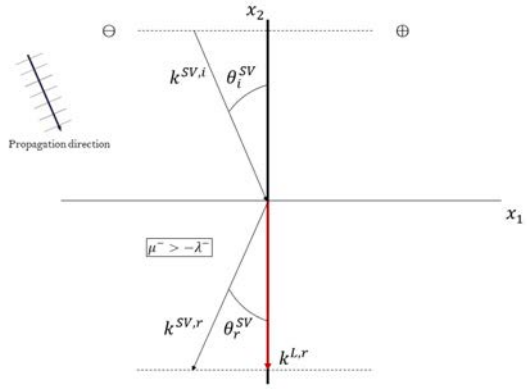

(f)

Figure 4.7: Possible manifestations of Stoneley waves at a Cauchy/Cauchy interface for L and SV transmitted modes for all possible incident waves. The vectors in black represent propagative modes, while the vectors in red represent modes which propagate along the surface only (Stoneley modes).

Determination of the reflection and transmission coefficients

We denote by H_1 the first (normal) component of the flux vector and we introduce the following quantities

$$J^{\mathrm{i}} = \frac{1}{T}\int_0^T H_1^{\mathrm{i}}(x,t)dt, \quad J^{\mathrm{r}} = \frac{1}{T}\int_0^T H_1^{\mathrm{r}}(x,t)dt, \quad J^{\mathrm{t}} = \frac{1}{T}\int_0^T H_1^{\mathrm{t}}(x,t)dt, \tag{4.52}$$

where $H_1^{\mathrm{i}} = H_1^{L,\mathrm{i}}$ (or, $H_1^{\mathrm{i}} = H_1^{SV,\mathrm{i}}$ if we consider an incident SV wave), $H_1^{\mathrm{r}} = H_1^{L,\mathrm{r}} + H_1^{SV,\mathrm{r}}$ and $H_1^{\mathrm{t}} = H_1^{L,\mathrm{t}} + H_1^{SV,\mathrm{t}}$, T being the period of the wave.[15] Then, the **reflection** and **transmission coefficients** are defined as

$$\mathcal{R} = \frac{J^{\mathrm{r}}}{J^{\mathrm{i}}}, \quad \mathcal{T} = \frac{J^{\mathrm{t}}}{J^{\mathrm{i}}}. \tag{4.53}$$

These coefficients tell us what part of the average normal flux of the incident wave is reflected and what part is transmitted; also, since the system is conservative, we must have $\mathcal{R} + \mathcal{T} = 1$.

The integrals involved in these expressions are the average normal fluxes of the respective waves (incident, reflected or transmitted). We use Lemma 1 (provided with proof in Appendix B) in the computations of these coefficients.

In order to have a physical meaning, the final solution for the displacement u must be real, so that we consider only the real parts of the displacements and stresses for the computation of the flux. For the first component of the flux vector for a longitudinal or SV wave, we have, according to equation (2.12) and using the plane-wave ansatz

$$\begin{aligned}
\frac{1}{T}\int_0^T H_1 dt &= \frac{1}{T}\int_0^T \mathrm{Re}\left(-u_{1,t}\right)\mathrm{Re}\left(\sigma_{11}\right) + \mathrm{Re}\left(-u_{2,t}\right)\mathrm{Re}\left(\sigma_{12}\right) dt \\
&= \frac{1}{T}\int_0^T \mathrm{Re}\left(i\,\omega\, a\,\psi_1 e^{i(\langle x,k\rangle-\omega t)}\right)\mathrm{Re}\left(\left[(2\mu+\lambda)\psi_1\, k_1 + \lambda\psi_2\, k_2\right] i\, a\, e^{i(\langle x,k\rangle-\omega t)}\right) \\
&\qquad + \mathrm{Re}\left(i\,\omega a\,\psi_2\, e^{i(\langle x,k\rangle-\omega t)}\right)\mathrm{Re}\left(\mu\left(\psi_1\, k_2 + \psi_2\, k_2\right) i\, a\, e^{i(\langle x,k\rangle-\omega t)}\right) dt \\
&\underset{\text{Lemma1}}{=} \frac{1}{2}\mathrm{Re}\left(\left[(2\mu+\lambda)|\psi_1|^2 k_1 + \lambda\psi_1^*\psi_2\, k_2 + \mu\left(\psi_1\,\psi_2^*\, k_2 + |\psi_2|^2 k_1\right)\right]|a|^2\omega\right).
\end{aligned} \tag{4.54}$$

As for the case of an SH wave, we have

$$\begin{aligned}
\frac{1}{T}\int_0^T H_1 dt &= \frac{1}{T}\int_0^T \mathrm{Re}\left(-u_{3,t}\right)\mathrm{Re}\left(\sigma_{13}\right) dt \qquad (4.55)\\
&= \frac{1}{T}\int_0^T \mathrm{Re}\left(i\,\omega\, a\, e^{i(\langle x,k\rangle-\omega t)}\right)\mathrm{Re}\left(i\, k_1\,\mu\, a\, e^{i(\langle x,k\rangle-\omega t)}\right) dt \\
&\underset{\text{Lemma1}}{=} \frac{1}{2}\mathrm{Re}\left(\mu\, k_1|a|^2\omega\right). \qquad (4.56)
\end{aligned}$$

These expressions for the fluxes, together with the linear decompositions given for H_1^{r} and H_1^{t}, allow us to explicitly compute the reflection and transmission coefficients.

4.2.3 The particular case of propagative waves

We have seen that, when considering two Cauchy media with an interface, two cases are possible, namely waves which propagate in the two considered half-planes and Stoneley waves, which only

[15] Or, in the case of an incident SH wave $H_1^{\mathrm{i}} = H_1^{SH,\mathrm{i}}$, $H_1^{\mathrm{r}} = H_1^{SH,\mathrm{r}}$ and $H_1^{\mathrm{t}} = H_1^{SH,\mathrm{t}}$.

propagate along the interface but decay away from it. Stoneley waves do not propagate in the considered media and are related to imaginary values of the first component of the wave number. When considering fully propagative waves (k_1 and k_2 both real) the results provided before can be interpreted on a more immediate physical basis, which we detail in the present section. The previous ansatz and calculations were performed without any hypothesis on the nature of the components of k: they were assumed to be either real or imaginary. However, when we consider a fully propagating wave we will demonstrate that we can recover some classical formulas and results which are usually found in the literature by considering the vector of direction of propagation of the wave, instead of the wave-vector k. For a fully propagative wave, the plane-wave ansazt can be written as

$$u = \widehat{\psi}\, e^{i(|k|\langle x,\xi\rangle - \omega t)} = \widehat{\psi}\, e^{i(|k|(x_1\xi_1 + x_2\xi_2) - \omega t)}, \tag{4.57}$$

where $|k|$ is now the wave-number, which is defined as the modulus of the wave-vector k and $\xi = (\xi_1, \xi_2)^{\mathrm{T}} := \frac{k}{|k|}$ is the so-called vector of propagation. This real vector ξ has unit length ($\xi_1^2 + \xi_2^2 = 1$).

By inserting $k_1 = |k|\,\xi_1$ and $k_2 = |k|\,\xi_2$ in (4.17) we find

$$|k|^2 = \frac{\omega^2}{c_L^2} \text{ or } |k|^2 = \frac{\omega^2}{c_S^2}, \tag{4.58}$$

or,

$$|k| = \pm\frac{\omega}{c_L} \text{ or } |k| = \pm\frac{\omega}{c_S}, \tag{4.59}$$

where, again, the signs in (4.59) must be chosen depending on what kind of wave we consider (positive for incident and transmitted waves, negative for reflected waves). Expressions (4.59) give the well-known linear dependence between the frequency ω and the wave-number $|k|$ through the speeds c_L and c_S for longitudinal and shear waves respectively. Such behavior is known as a "non-dispersive" behavior, which means that in a Cauchy medium longitudinal and shear waves propagate at a constant speed (c_L for longitudinal and c_S for shear waves).

Choosing the first solution in (4.59), so that $\omega = |k|c_L$ and inserting $k = |k|\xi$ into (4.22) we can can find the nullspace in the case of a propagative longitudinal wave

$$\widehat{\psi} = \begin{pmatrix} 1 \\ \frac{c_L|k|\xi_2}{\sqrt{|k|^2c_L^2 - c_L^2|k|\xi_2^2}} \end{pmatrix} = \begin{pmatrix} 1 \\ \frac{\xi_2}{\xi_1} \end{pmatrix} \tag{4.60}$$

Equivalently, choosing the second solution in (4.58) so that $\omega = |k|c_S$ and again inserting $k = |k|\xi$ into (4.27) we find for the second component of the eigenvector

$$\frac{k_2^2c_S^2 - \omega^2}{k_2c_S\sqrt{\omega^2 - k_2^2c_S^2}} = \frac{|k|^2\xi_2^2c_S^2 - |k|^2c_S^2}{|k|\xi_2c_S\sqrt{|k|^2c_S^2 - |k|^2\xi_2^2c_S^2}} = -\frac{\xi_1^2}{\xi_2\xi_1}, \tag{4.61}$$

so the eigenvector for a propagative shear wave is[16]

$$\widehat{\psi} = \begin{pmatrix} 1 \\ -\frac{\xi_1}{\xi_2} \end{pmatrix}. \tag{4.62}$$

[16]We neglected the sign of the $|k|$ in the above calculations. Fixing the direction of propagation will automatically impose the sign of both $|k|$ and ξ_1, which we then plug into equations (4.60) or (4.62).

The forms (4.60) and (4.62) for the eigenvectors of L and SV propagative waves are suggestive because they allow to immediately visualize the vector of propagation ξ and, thus, the eigenvectors ψ themselves in terms of the angles formed by the considered propagative wave and the interface (see Figure 4.8 and Table 4.3).

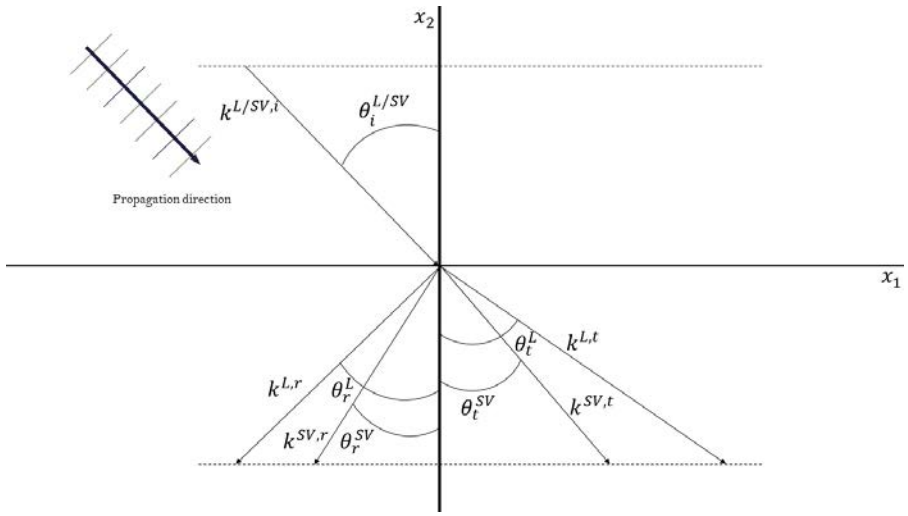

Figure 4.8: Illustration of reflection and transmission patterns for propagative waves and Snell's law at a Cauchy/Cauchy interface. The second components of all wave-vectors are equal to each other according to (4.35), forcing the reflected and transmitted wave-vectors to form angles with the interface as shown here according to (4.66).

In the propagative case, the solutions (4.32) and (4.33) particularize into

$$u^-(x_1,x_2,t) = a^{L,\mathrm{i}}\psi^{L,\mathrm{i}}e^{i\left(\langle x,|k|\xi^{L,\mathrm{i}}\rangle-\omega t\right)} + a^{L,\mathrm{r}}\psi^{L,\mathrm{r}}e^{i\left(\langle x,|k|\xi^{L,\mathrm{r}}\rangle-\omega t\right)} + a^{SV,\mathrm{r}}\psi^{SV,\mathrm{r}}e^{i\left(\langle x,|k|\xi^{SV,\mathrm{r}}\rangle-\omega t\right)}, \tag{4.63}$$

$$u^+(x_1,x_2,t) = a^{L,\mathrm{t}}\psi^{L,\mathrm{t}}e^{i\left(\langle x,|k|\xi^{L,\mathrm{t}}\rangle-\omega t\right)} + a^{SV,\mathrm{t}}\psi^{SV,\mathrm{t}}e^{i\left(\langle x,|k|\xi^{SV,\mathrm{t}}\rangle-\omega t\right)}. \tag{4.64}$$

Wave	ξ	ψ	Speed of propagation
L,i	$\left(\sin\theta_i^L, -\cos\theta_i^L, 0\right)^{\mathrm{T}}$	$\left(\sin\theta_i^L, -\cos\theta_i^L, 0\right)^{\mathrm{T}}$	c_L
SV,i	$\left(\sin\theta_i^{SV}, -\cos\theta_i^{SV}, 0\right)^{\mathrm{T}}$	$\left(\cos\theta_i^{SV}, \sin\theta_i^{SV}, 0\right)^{\mathrm{T}}$	c_S
L,r	$\left(-\sin\theta_r^L, -\cos\theta_r^L, 0\right)^{\mathrm{T}}$	$\left(-\sin\theta_r^L, -\cos\theta_r^L, 0\right)^{\mathrm{T}}$	c_L
SV,r	$\left(-\sin\theta_r^{SV}, -\cos\theta_r^{SV}, 0\right)^{\mathrm{T}}$	$\left(\cos\theta_r^{SV}, -\sin\theta_r^{SV}, 0\right)^{\mathrm{T}}$	c_S
L,t	$\left(\sin\theta_t^L, -\cos\theta_t^L, 0\right)^{\mathrm{T}}$	$\left(\sin\theta_t^L, -\cos\theta_t^L, 0\right)^{\mathrm{T}}$	c_L^+
SV,t	$\left(\sin\theta_t^{SV}, -\cos\theta_t^{SV}, 0\right)^{\mathrm{T}}$	$\left(\cos\theta_t^{SV}, \sin\theta_t^{SV}, 0\right)^{\mathrm{T}}$	c_S^+

Table 4.3: Summary of the vectors of direction of propagation and of vibration for all different waves produced at a Cauchy/Cauchy interface.

Using (4.63), (4.64) and the forms given in Table 4.3 for the propagation vectors ξ and the eigenvectors ψ as well as expressions (4.59) and (4.60), we can remark that the only unknowns

are the amplitudes a and the angles θ. The angles θ of the different waves can be computed in terms of the angle of the incident wave by using boundary conditions. Indeed, condition (4.35) can be rewritten in the propagative case as

$$|k^{L,\mathrm{i}}|\xi_2^{L,\mathrm{i}} = |k^{L,\mathrm{r}}|\xi_2^{L,\mathrm{r}} = |k^{SV,\mathrm{r}}|\xi_2^{SV,\mathrm{r}} = |k^{L,\mathrm{t}}|\xi_2^{L,\mathrm{t}} = |k^{SV,\mathrm{t}}|\xi_2^{SV,\mathrm{t}}, \tag{4.65}$$

which, using equations (4.59) and (4.60), as well as the ξ_2 given in Table 4.3 and simplifying the frequency, gives the well-known **Snell's law** (Fig. 4.8)[17]

$$\boxed{\frac{\cos\theta_i^L}{c_i} = \frac{\cos\theta_r^L}{c_L} = \frac{\cos\theta_r^{SV}}{c_S} = \frac{\cos\theta_t^L}{c_L^+} = \frac{\cos\theta_t^{SV}}{c_S^+}}, \tag{4.66}$$

where we have to choose the speed of the incident wave $c_i = c_L$ if it is longitudinal, or $c_i = c_S$ if it is shear.

As already remarked, once the angles of the different propagative waves are computed, the only unknowns in the solutions (4.63) and (4.64) are the scalar amplitudes a, which can be computed as done in subsections 4.2.2, by imposing boundary conditions. The treatise made in this section does not add new features to the previous considerations, but allows us to visualize the traveling waves according to the classical **Snell's law** and to recover classical results concerning the dispersion curves. Clearly, such reasoning cannot be repeated for Stoneley waves, for which the more general digression made in section 4.2.2 must be addressed.

4.3 Basics on dispersion curves analysis for bulk wave propagation in relaxed micromorphic media

Since it is useful for the comparison with the literature, we recall here the classical analysis of dispersion curves for the considered relaxed micromorphic medium (see [30, 62, 65]).

To that end, we make the hypothesis of propagative waves (see eq. (4.76)) and we show the plots of the frequency ω against the wave-number $|k|$ which are known as dispersion curves.

We will show that some frequency ranges, known as band-gaps, exist, such that for a given frequency in this range, no real value of the wave-number $|k|$ can be found. This basically means that the hypothesis of propagative wave is not satisfied in this range of frequencies and the solution must be more generally written as

$$e^{i(x_1 k_1 + x_2 k_2 - \omega t)}, \tag{4.67}$$

where k_1 and k_2 are both imaginary, giving rise to evanescent waves (i.e. waves decaying exponentially in both the x_1 and the x_2 direction).

We explicitly remark here, that this treatise on dispersion curves in the relaxed micromorphic model has already been performed in [30, 62, 65], but we recall it here for the 2D case in order to have a direct idea on the band-gap region of the considered medium.

From now on, we set the following parameter abbreviations for characteristic speeds and

[17] Equation (4.66) clarifies why the angles of the different reflected and transmitted waves are chosen to be as in Fig. 4.8, instead of choosing the opposite ones.

frequencies:

$$
\begin{aligned}
&c_m = \sqrt{\frac{\mu_e L_c^2}{\eta}}, \quad c_s = \sqrt{\frac{\mu_e + \mu_c}{\rho}}, \quad c_p = \sqrt{\frac{\lambda_e + 2\mu_e}{\rho}}, \quad c_l = \sqrt{\frac{\lambda_e + \mu_e - \mu_c}{\rho}}, \\
&\omega_s = \sqrt{\frac{2(\mu_e + \mu_{\text{micro}})}{\eta}}, \quad \omega_r = \sqrt{\frac{2\mu_c}{\eta}}, \quad \omega_t = \sqrt{\frac{\mu_{\text{micro}}}{\eta}}, \quad \omega_l = \sqrt{\frac{\lambda_{\text{micro}} + 2\mu_{\text{micro}}}{\eta}}, \\
&\omega_p = \sqrt{\frac{(3\lambda_e + 2\mu_e) + (3\lambda_{\text{micro}} + 2\mu_{\text{micro}})}{\eta}}.
\end{aligned}
\tag{4.68}
$$

As done for the Cauchy case, we suppose that the involved kinematic fields only depend on x_1 and x_2 (no dependence on the out-of-plane variable x_3), i.e.

$$
u = (u_1(x_1, x_2, t), u_2(x_1, x_2, t), u_3(x_1, x_2, t))^{\mathrm{T}}, \quad P = (P_1^{\mathrm{T}}(x_1, x_2, t), P_2^{\mathrm{T}}(x_1, x_2, t), P_3^{\mathrm{T}}(x_1, x_2, t))^{\mathrm{T}},
\tag{4.69}
$$

where we recall that, according to our notation, P_i^{T}, $i = 1, 2, 3$ are the rows of the micro-distortion tensor P.

We plug u and P from (4.69) into (3.34). The resulting system of equations is presented in Appendix B4.1 in component-wise notation. We proceed to make the following change of variables which are motivated by the Cartan-Lie decomposition of the tensor P:

$$
\begin{aligned}
&P^S = \frac{1}{3}(P_{11} + P_{22} + P_{33}), \quad P_1^D = P_{11} - P^S, \quad P_2^D = P_{22} - P^S, \quad P_{(1\gamma)} = \frac{1}{2}(P_{1\gamma} + P_{\gamma 1}), \\
&P_{[1\gamma]} = \frac{1}{2}(P_{1\gamma} - P_{\gamma 1}), \quad P_{(23)} = \frac{1}{2}(P_{23} + P_{32}), \quad P_{[23]} = \frac{1}{2}(P_{12} - P_{21}),
\end{aligned}
\tag{4.70}
$$

with $\gamma = 2, 3$. We can then collect the variables which are coupled (see the equations presented in Appendix B4.2) as

$$
v^1 = \left(u_1, u_2, P_1^D, P_2^D, P^S, P_{(12)}, P_{[12]}\right)^{\mathrm{T}}, \tag{4.71}
$$

$$
v^2 = \left(u_3, P_{(13)}, P_{[13]}, P_{(23)}, P_{[23]}\right)^{\mathrm{T}}. \tag{4.72}
$$

We make the following plane-wave ansatz:

$$
v^1 = \widehat{\phi}\, e^{i(\langle x,k\rangle - \omega t)} = \widehat{\phi}\, e^{i(x_1 k_1 + x_2 k_2 - \omega t)}, \tag{4.73}
$$

$$
v^2 = \widehat{\chi}\, e^{i(\langle x,\widetilde{k}\rangle - \omega t)} = \widehat{\chi}\, e^{i(x_1 \widetilde{k}_1 + x_2 \widetilde{k}_2 - \omega t)}, \tag{4.74}
$$

and end up with two mutually uncoupled systems of the form (see Appendix B4.3 for the explicit form of the matrices A_1 and A_2)

$$
A_1 \cdot \widehat{\phi} = 0, \quad A_2 \cdot \widehat{\chi} = 0, \tag{4.75}
$$

where $A_1 \in \mathbb{C}^{7\times 7}$, $A_2 \in \mathbb{C}^{5\times 5}$, $\widehat{\phi} \in \mathbb{C}^7$ and $\widehat{\chi} \in \mathbb{C}^5$. Closer examination of the first system reveals that the components of the kinematic fields involved in these equations are the first and second only, while in the second system only components involving the out-of-plane direction x_3 are always present in every equation. This means that, in analogy to the case of Cauchy media, we have the same kind of uncoupling between movement in the $(x_1x_2)-$ plane (in-plane) and in the $(x_2x_3)-$ plane (out-of-plane). There is, however, no immediate distinction of longitudinal and shear waves.

4.3.1 In-plane variables

We assume a propagating wave in which case the plane-wave ansatz is

$$v^1 = \widehat{\phi}\, e^{i(|k|(x_1\xi_1+x_2\xi_2)-\omega t)}, \tag{4.76}$$

where $\xi = (\xi_1, \xi_2)^{\mathrm{T}}$ is a real unit vector and $\widehat{\phi}$ is the vector defined of amplitudes.

The polynomial $\det A_1$ is of degree 14 in ω and of degree 10 in $|k|$. Solving the equation $\det A_1 = 0$ with respect to ω gives fourteen solutions of the form

$$\omega(|k|) = \pm\omega_1(|k|),\ \pm\omega_2(|k|),\ \pm\omega_3(|k|),\ \pm\omega_4(|k|),\ \pm\omega_5(|k|),\ \pm\omega_6(|k|),\ \pm\omega_7(|k|); \tag{4.77}$$

while solving $\det A_1 = 0$ with respect to $|k|$, gives ten solutions of the form

$$|k|(\omega) = \pm|k^{(1)}|(\omega),\ \pm|k^{(2)}|k(\omega),\ \pm|k^{(3)}|(\omega),\ \pm|k^{(4)}|(\omega),\ \pm|k^{(5)}|(\omega); \tag{4.78}$$

in both cases, we keep only the positive values because the wave is traveling in the $x_1 > 0$ direction.

Plotting the functions $\omega_i(|k|)$, $i = 1, \ldots, 7$ in the $(\omega, |k|)-$ plane gives us the dispersion curves for plane waves propagating in a relaxed micromorphic medium in two space dimensions (see Figure 4.10). The results concerning the dispersive behavior of relaxed micromorphic media are presented in [62, 65] and are recalled in Appendix B4.4 for the sake of completeness.

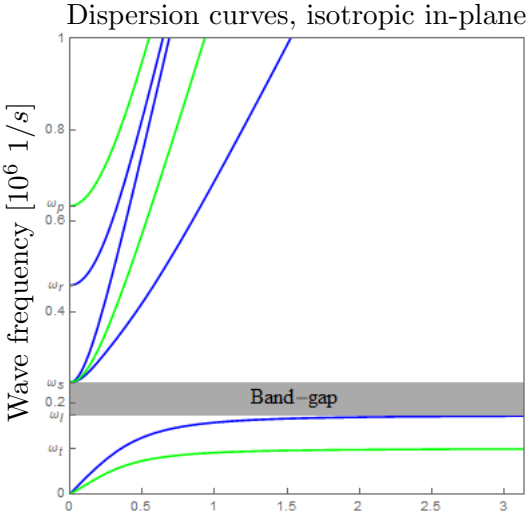

Figure 4.9

Figure 4.10: Dispersion diagrams for in-plane modes in the isotropic relaxed micromorphic continua. The material parameters used in these Figures are the ones given in Table 4.4.

4.3.2 Out-of-plane variables

Analogously to the case of in-plane variables, we assume a propagating wave in which case the plane-wave ansatz is

$$v^2 = \widehat{\chi}\, e^{i\left(|\widetilde{k}|(x_1\xi_1+x_2\xi_2)-\widetilde{\omega}t\right)}, \tag{4.79}$$

where $\xi = (\xi_1, \xi_2)^{\mathrm{T}}$ is a real unit vector and $\widehat{\chi}$ is the vector of amplitudes.

The polynomial $\det A_2$ is of degree 10 in $\widetilde{\omega}$ and of degree 8 in $|\widetilde{k}|$. Solving the equation $\det A_2 = 0$ with respect to $\widetilde{\omega}$ gives ten solutions of the form

$$\widetilde{\omega}(|\widetilde{k}|) = \pm\widetilde{\omega}_1(|\widetilde{k}|),\ \pm\widetilde{\omega}_2(|\widetilde{k}|),\ \pm\widetilde{\omega}_3(|\widetilde{k}|),\ \pm\widetilde{\omega}_4(|\widetilde{k}|),\ \pm\widetilde{\omega}_5(k); \tag{4.80}$$

while solving $\det A_2 = 0$ with respect to to $\widetilde{k}$, gives eight solutions

$$|\widetilde{k}|(\widetilde{\omega}) = \pm|\widetilde{k}^{(1)}|(\widetilde{\omega}),\ \pm|\widetilde{k}^{(2)}|(\widetilde{\omega}),\ \pm|\widetilde{k}^{(3)}|(\widetilde{\omega}),\ \pm|\widetilde{k}^{(4)}|(\widetilde{\omega}). \tag{4.81}$$

Once again, we only consider the positive values of the $\widetilde{\omega}$'s and $|\widetilde{k}|$'s since the waves are traveling in the $x_1 > 0$ direction. The dispersion curves for the out-of-plane variables are presented in Figure 4.12.

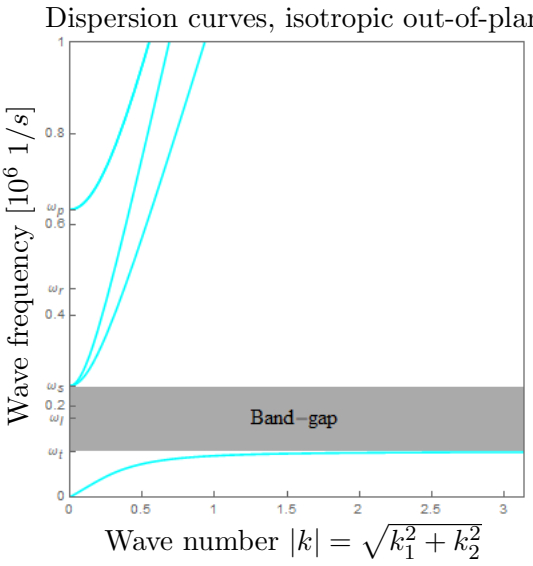

Figure 4.11

Figure 4.12: Dispersion diagrams for out-of-plane modes in the isotropic relaxed micromorphic continua. The material parameters used in these Figures are the ones given in Table 4.4.

Extra details are given in [65] and recalled in Appendix B4.4.

4.4 Reflective properties of a Cauchy/isotropic relaxed micromorphic interface

In this section, closely following what was done for the Cauchy case in section 4.2.1, we look for non-trivial solutions of the equations (4.75) imposing $\det A_1 = 0$ and $\det A_2 = 0$. Once again, we fix the second component k_2 (resp. $\widetilde{k}_2$) of the wave-vector and solve these equations with respect to k_1 (resp. $\widetilde{k}_1$).[18] The expressions for the solutions of these equations are quite complex and we do not present them explicitly here. As discussed before, we find five and four solutions for the two systems respectively[19]

$$\pm\, k_1^{(1)}(k_2,\omega),\ \pm k_1^{(2)}(k_2,\omega),\ \pm k_1^{(3)}(k_2,\omega),\ \pm k_1^{(4)}(k_2,\omega),\ \pm k_1^{(5)}(k_2,\omega), \tag{4.82}$$

[18] We will show later on that also in the case of an interface between a Cauchy and a relaxed micromorphic medium, the component k_2 of the wave-vector can be considered to be known when imposing the jump conditions holding at the interface

[19] Since, as already stated, in this case we cannot a priori distinguish which modes are longitudinal and which are shear, we slightly shift our notation and use numbers in parentheses instead of describing the nature of the mode.

for the in-plane problem and

$$\pm\,\widetilde{k}_1^{(1)}(\widetilde{k}_2,\omega),\ \pm\widetilde{k}_1^{(2)}(\widetilde{k}_2,\omega),\ \pm\widetilde{k}_1^{(3)}(\widetilde{k}_2,\omega),\ \pm\widetilde{k}_1^{(4)}(\widetilde{k}_2,\omega), \tag{4.83}$$

for the out-of-plane problem.

Such solutions for k_1 (resp. $\widetilde{k}_1$) depend on the second component k_2 (resp. $\widetilde{k}_2$) of the wave-vector and on the frequency, but of course also on the values of the material parameters of the relaxed micromorphic model. We plug these solutions of the characteristic polynomials into the matrix A_1 (resp. A_2) and calculate for each different k (resp. $\widetilde{k}$) the five (resp. four) nullspaces of the matrix. We find

$$\widehat{\phi}^{(1)},\widehat{\phi}^{(2)},\widehat{\phi}^{(3)},\widehat{\phi}^{(4)},\widehat{\phi}^{(5)}, \tag{4.84}$$

$$\widehat{\chi}^{(1)},\widehat{\chi}^{(2)},\widehat{\chi}^{(3)},\widehat{\chi}^{(4)}, \tag{4.85}$$

as solutions to the equations $A_1\cdot\widehat{\phi}=0$ and $A_2\cdot\widehat{\chi}=0$, respectively. We normalize these vectors, thus introducing the normal vectors

$$\phi^{(i)}=\frac{1}{|\widehat{\phi}^{(i)}|}\widehat{\phi}^{(i)},\quad \chi^{(j)}=\frac{1}{|\widehat{\chi}^{(j)}|}\widehat{\chi}^{(j)}, \tag{4.86}$$

$i=1,\dots 5$, $j=1,\dots 4$. Finally, we can write the solution to equations (3.34) as

$$v^1=\alpha_1\phi^{(1)}e^{i\left(\langle x,k^{(1)}\rangle-\omega t\right)}+\alpha_2\phi^{(2)}e^{i\left(\langle x,k^{(2)}\rangle-\omega t\right)}+\alpha_3\phi^{(3)}e^{i\left(\langle x,k^{(3)}\rangle-\omega t\right)}+\alpha_4\phi^{(4)}e^{i\left(\langle x,k^{(4)}\rangle-\omega t\right)}+\alpha_5\phi^{(5)}e^{i\left(\langle x,k^{(5)}\rangle-\omega t\right)}, \tag{4.87}$$

$$v^2=\beta_1\chi^{(1)}e^{i\left(\langle x,\widetilde{k}^{(1)}\rangle-\omega t\right)}+\beta_2\chi^{(2)}e^{i\left(\langle x,\widetilde{k}^{(2)}\rangle-\omega t\right)}+\beta_3\chi^{(3)}e^{i\left(\langle x,\widetilde{k}^{(3)}\rangle-\omega t\right)}+\beta_4\chi^{(4)}e^{i\left(\langle x,\widetilde{k}^{(4)}\rangle-\omega t\right)}, \tag{4.88}$$

where $\alpha_i,\beta_j\in\mathbb{C}$ for $i=1,\dots 5$, $j=1,\dots,4$ are the unknown amplitudes of the different modes of propagation.[20]

We explicitly remark that expressions (4.82) and (4.83) for the first component k_1 and $\widetilde{k}_1$ of the wave-vectors, can give rise, similarly to the Cauchy case, to different scenarios when varying the value of the frequency ω and the material parameters. As a matter of fact, we briefly remarked before that k_2 can be considered to be known when imposing jump conditions. Indeed, following analogous steps to those performed to obtain equation (4.35) for the interface between two Cauchy media, we can impose the continuity of displacements between a Cauchy and a relaxed micromorphic medium. Considering the first component of the vector equation for the continuity of displacement, in which the plane-wave ansatz has been used, one can find, when imposing a longitudinal incident wave on the Cauchy side[21]

$$\boxed{\begin{gathered}k_2^{L,\mathrm{i}}=k_2^{L,\mathrm{r}}=k_2^{SV,\mathrm{r}}=k_2^{(1),\mathrm{t}}=k_2^{(2),\mathrm{t}}=k_2^{(3),\mathrm{t}}=k_2^{(4),\mathrm{t}}=k_2^{(5),\mathrm{t}}.\\ \textbf{Generalized in-plane Snell's Law}\end{gathered}} \tag{4.89}$$

On the other hand, when imposing an out-of-plane shear incident wave, the continuity of displacement at the interface gives

$$\boxed{\begin{gathered}k_2^{SH,\mathrm{i}}=k_2^{SH,\mathrm{r}}=\widetilde{k}_2^{(1),\mathrm{t}}=\widetilde{k}_2^{(2),\mathrm{t}}=\widetilde{k}_2^{(3),\mathrm{t}}=\widetilde{k}_2^{(4),\mathrm{t}}.\\ \textbf{Generalized out-of-plane Snell's Law}\end{gathered}} \tag{4.90}$$

[20] We recall again that, once the eigenvalue problem is solved (i.e. once the wave-vector k (resp. $\widetilde{k}$ is known) and the eigenvectors ϕ (resp. χ) are computed, the only unknowns of the problem remain the five (resp. four) amplitudes α (resp β), which can be computed by imposing boundary conditions.

[21] When imposing a longitudinal incident wave on the Cauchy side, $k_2^{L,\mathrm{i}}$ is considered to be known. The same reasoning holds when imposing an incident SV wave; in this case, $k_2^{L,\mathrm{i}}$ must be replaced by $k_2^{SV,\mathrm{i}}$ in eq. (4.89).

Equations (4.89) and (4.90) tell us that, when fixing the incident wave in the Cauchy medium to be longitudinal ($k_2^{L,\mathrm{i}}$ known), in-plane shear ($k_2^{SV,\mathrm{i}}$ known) or out-of-plane shear ($k_2^{SH,\mathrm{i}}$ known), the second components of all the reflected and transmitted wave-vectors are known. They are the **generalized Snell's law** for the case of a Cauchy/relaxed micromorphic interface. As before, this traces two possible scenarios, given that the value of k_2 for the incident wave is always supposed to be real and positive (propagative wave)

1. both k_1 and k_2 (resp. $\widetilde{k}_1, \widetilde{k}_2$) are real (when computing k_1 or $\widetilde{k}_1$ via (4.82) or (4.83) respectively) so that one has propagative waves.

2. k_2 (resp. $\widetilde{k}_2$) is real and k_1 (resp. $\widetilde{k}_1$), when computed via (4.82) (resp. (4.83)) is imaginary, so that one has Stoneley waves propagating only along the interface and decaying away from it.

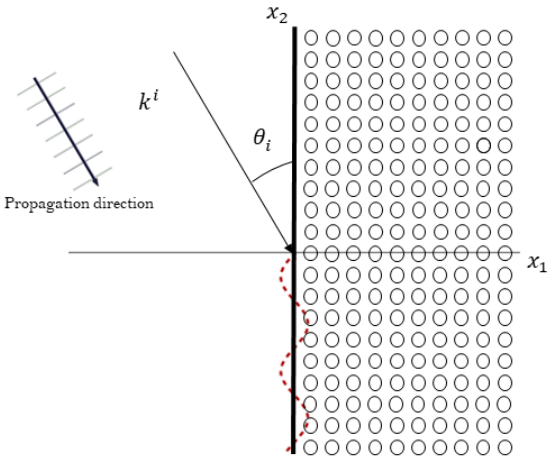

Figure 4.13: Simplified representation of the onset of an interface wave (in red) propagating along the interface between a homogeneous solid and a metamaterial. Depending on the relative stiffnesses of the two media, each of the existing low and high-frequency modes can either become Stoneley or remain propagative.

Depending on the values of the frequency, of the material parameters and of the angle of incidence, each of the five in-plane waves, or of the four out-of-plane waves, can be either propagative or Stoneley. Thus, Stoneley waves can appear at the considered homogeneous solid/metamaterial interface (see Fig. 4.13 for a simplified illustration), both for low and for high-frequency modes.

4.4.1 Determination of the reflection and transmission coefficients in the case of a relaxed micromorphic medium

As for the flux, the normal outward pointing vector to the surface (the x_2 axis) is $\nu = (-1, 0, 0)$. This means that in the expression (3.75) for the flux, we need only take into account the first component. According to our definition (3.75), we have

$$H_1 = -u_{i,t}\widetilde{\sigma}_{i1} - m_{ih}P_{ij,t}\varepsilon_{jh1}, \quad i,j,h \in \{1,2,3\}. \tag{4.91}$$

This equation for the flux must now be written with respect to the new variables v^1 and v^2. It is a tedious but easy calculation to see that the following holds

$$\widetilde{H} := H_1 = v^1_{,t} \cdot (H^{11} \cdot v^1_{,1} + H^{12} \cdot v^1_{,2} + H^{13} \cdot v^1), \tag{4.92}$$

for the in-plane problem and

$$\widetilde{H} := H_1 = v^2_{,t} \cdot (H^{21} \cdot v^2_{,1} + H^{22} \cdot v^2_{,2} + H^{23} \cdot v^2), \tag{4.93}$$

for the out-of plane problem, where H^{11}, H^{12}, H^{13}, and H^{21}, H^{22}, H^{23} are matrices of suitable dimensions (found in Appendix B4.6).

Having calculated the "transmitted" flux, we can now look at the reflection and transmission coefficients for the case of a Cauchy/relaxed micromorphic interface.

To that end, we again define

$$J^i = \frac{1}{T}\int_0^T H^i(x,t)dt, \quad J^r = \frac{1}{T}\int_0^T H^r(x,t)dt, \quad J^{\mathrm{t}} = \frac{1}{T}\int_0^T H^{\mathrm{t}}(x,t)dt, \tag{4.94}$$

where $H^{\mathrm{i}} = H^{L,\mathrm{i}}$, $H^{\mathrm{r}} = H^{L,\mathrm{r}} + H^{SV,\mathrm{r}}$ and $H^{\mathrm{t}} = \widetilde{H}$. Then the reflection and transmission coefficients are

$$\mathcal{R} = \frac{J^{\mathrm{r}}}{J^{\mathrm{i}}}, \quad \mathcal{T} = \frac{J^{\mathrm{t}}}{J^{\mathrm{i}}}. \tag{4.95}$$

In order to easily compute these coefficients, we again employ Lemma 1. Finally, once again we have that $\mathcal{R} + \mathcal{T} = 1$.

In the case of a Cauchy/relaxed micromorphic interface, the dependency of the fluxes on the frequency ω is maintained. This is due to the fact that the amplitudes needed to calculate the flux depend on ω (dispersive response), something which is not the case in the Cauchy/Cauchy interface, as was evident in the previous section.

4.5 Results

In this section we present our results concerning the reflective properties of an interface between a Cauchy medium and a relaxed micromorphic medium. We will show that, at low frequencies, the considered interface can be regarded as an interface between a Cauchy medium and a second Cauchy medium, equivalent to the relaxed micromorphic one and with macroscopic stiffnesses λ_{macro} and μ_{macro}, when suitable boundary conditions are imposed.

Moreover, we will be able to show that critical angles for the incident wave can be identified in the low-frequency regime, beyond which we can observe the onset of Stoneley waves. These angles are computed from the relations established in Table 4.1.

In order to present explicit numerical results for the reflective properties of the interface between a Cauchy and a relaxed micromorphic medium, we chose the values for the parameters of the relaxed micromorphic medium as shown in Table 4.4. We explicitly remark that other values of such parameters could be chosen, which would be more or less close to real metamaterials parameters ([29, 57, 58]). Nevertheless, the basic results which we want to show in the present chapter are not qualitatively affected by this choice since they only depend on the relative stiffness of the two media which are considered on the two sides and not on the absolute values of such stiffnesses.

ρ [kg/m^3]	η [kg/m]	μ_c [Pa]	μ_e [Pa]	μ_{micro} [Pa]	λ_{micro} [Pa]	λ_e [Pa]	L_c [m]
2000	10^{-2}	2×10^9	2×10^8	10^8	10^8	4×10^8	10^{-2}

Table 4.4: Numerical values of the constitutive parameters chosen for the relaxed micromorphic medium.

We can now use the homogenization formula (3.77) ([9, 29]), to compute the equivalent macroscopic coefficients of the Cauchy medium which is approximating the relaxed micromorphic medium at low frequencies. In this isotropic case, formula (3.77) particularizes to:

$$\mu_{\text{macro}} = \frac{\mu_e\, \mu_{\text{micro}}}{\mu_e + \mu_{\text{micro}}}, \qquad 2\mu_{\text{macro}} + 3\lambda_{\text{macro}} = \frac{(2\mu_e + 3\lambda_e)(2\mu_{\text{micro}} + 3\lambda_{\text{micro}})}{2(\mu_e + \mu_{\text{micro}}) + 3(\lambda_e + \lambda_{\text{micro}})}. \tag{4.96}$$

Note that the Cosserat couple modulus μ_c does not appear in the homogenization formulas (4.96).

Using formulas (4.96), we compute the stiffnesses λ_{macro} and μ_{macro} of the Cauchy medium which is equivalent to the relaxed micromorphic medium of Table 4.4 in the low-frequency regime, as in the following Table:

ρ [kg/m^3]	λ_{macro} [Pa]	μ_{macro} [Pa]
2000	8.25397×10^7	6.66667×10^7

Table 4.5: Macro parameters of the equivalent Cauchy medium corresponding to the relaxed medium of Table 4.4 at low frequencies.

At this point, we will consider the two cases in which the Cauchy medium on the "$-$" side (where the incident wave is traveling) is stiffer or softer than the equivalent Cauchy medium on the "$+$" side. We will show how, as expected, this difference in stiffness affects the onset of Stoneley waves at low frequencies and, as a consequence, the transmission patterns across the interface. Furthermore, we will show that the relaxed micromorphic model is able to predict the appearance of Stoneley waves at higher frequencies, which are substantially microstructure-related. Finally, we will show that the relaxed micromorphic model also allows for the description of wide frequency bounds, for which extraordinary reflection is observed. Such frequency bounds go beyond the band-gap region and are related to the presence of the interface, as well as the relative mechanical properties of the considered media. In some cases, high-frequency critical angles discriminating between total transmission and total reflection can also be identified.

4.5.1 Cauchy medium which is "stiffer" than the relaxed micromorphic one

We chose the material parameters of the left Cauchy medium to be those presented in Table 4.6 and we explicitly remark that these values are greater than those of Table 4.5, which are relative to the equivalent Cauchy medium corresponding to the considered relaxed micromorphic one.

For the chosen values of the constitutive parameters, the critical angles of the incident wave giving rise to low-frequency Stoneley waves can be calculated using Tables 4.1 and 4.2. They are found to be $\theta^{L,\text{r}}_{\text{crit}} = 33\pi/100$ and $\theta^{L,\text{t}}_{\text{crit}} = 17\pi/200$ for an incident SV wave. For this choice of parameters, no critical angles appear for incident L or SH waves.

Figure 4.14 shows the transmission coefficient for the considered Cauchy/relaxed micromorphic interface, as a function of the angle of incidence and of the frequency, when the microstructure is free to move at the interface (P is left arbitrary at the interface). The coloring of this plot

ρ [kg/m^3]	λ [Pa]	μ [Pa]
2000	4×10^8	2×10^8

Table 4.6: Lamé parameters and mass density of the Cauchy medium on the left side of the considered Cauchy/relaxed micromorphic interface.

(and of the subsequent ones) is such that the dark blue regions mean zero transmission, while the gradual change towards red is the increase in transmission (red being total transmission). Before commenting on the details of the behavior of the transmission coefficient, we recall that the case of free microstructure boundary condition is the only one which allows us to precisely obtain a Cauchy/equivalent Cauchy interface in the low-frequency regime, something which is not possible when imposing the fixed microstructure boundary condition ($P_{ij} = 0,\ i = 2, 3,\ j = 1, 2, 3$) at the interface. As a matter of fact, it is firmly established that a relaxed micromorphic continuum is equivalent to a Cauchy continuum with stiffnesses λ_{macro} and μ_{macro} when considering the low-frequency regime (see [79]), but this is proven only for the bulk medium. When considering an interface between a Cauchy and a relaxed micromorphic medium, the latter will behave exactly as an equivalent Cauchy medium at low frequencies only if the micro-distortion tensor P is left free at the interface. Indeed, this tensor will arrange its values at the interface in order to let the low-frequency reflective properties of the Cauchy/relaxed micromorphic interface be equivalent to those of a Cauchy/equivalent Cauchy interface. On the other hand, if we impose the fixed microstructure boundary conditions, the tangential components of the tensor P are forced to vanish at the interface, so that the effect of the microstructure is artificially introduced in the response of the material even for those low frequencies for which the bulk material would tend to behave as an equivalent Cauchy medium.

Having drawn such preliminary conclusions, we can now comment Figures 4.14 and 4.15 in detail. For the set of numerical values of the parameters given in Table 4.6 and 4.5, we established that Stoneley waves can appear in the low-frequency regime only when imposing the incident wave to be SV.

In particular, the onset of Stoneley waves in the low-frequency regime can be observed in this case only for longitudinal reflected and transmitted waves when the angles of incidence are beyond $\theta^{L,\text{r}}_{\text{crit}}$ and $\theta^{L,\text{t}}_{\text{crit}}$, respectively. This fact can be retrieved in Figure 4.14(b), in which an increase of the transmission coefficient can be observed in the low-frequency regime corresponding to $\theta^{L,\text{r}}_{\text{crit}}$ (Stoneley reflected waves are created, producing a decrease of the reflected normal flux and, due to energy conservation, a consequent increase of the transmitted normal flux). On the other hand, we can notice in the same figure a decrease of the transmitted energy in the low-frequency regime beyond the critical angle $\theta^{L,\text{t}}_{\text{crit}}$. This is sensible, given that beyond the value of $\theta^{L,\text{t}}_{\text{crit}}$, transmitted Stoneley waves are created, which do not contribute to propagative transmitted waves in the relaxed micromorphic continuum. We can also explicitly remark that such a decrease of transmitted energy beyond $\theta^{L,\text{t}}_{\text{crit}}$ in the low-frequency regime is much more pronounced than in the corresponding Figures 4.14(a) and 4.14(c).

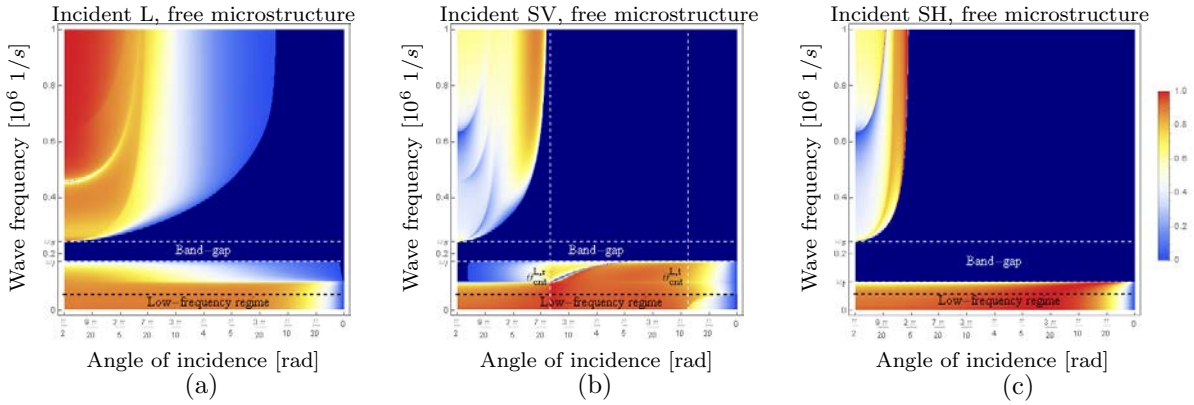

Figure 4.14: Transmission coefficients as a function of the angle of incidence θ_i and of the wave-frequency ω for L (a), SV (b) and SH (c) incident waves for the case of macro-clamp with free microstructure. The origin coincides with normal incidence ($\theta_i = \pi/2$), while the angle of incidence decreases towards the right until it reaches the value $\theta_i = 0$, which corresponds to the limit case where the incidence is parallel to the interface. The band-gap region is highlighted by two dashed horizontal lines, where, as expected, we observe no transmission. The low-frequency regime is highlighted by the bottom horizontal dashed line, while the critical angles for the onset of Stoneley waves are denoted by vertical dashed lines. The dark blue zone shows that no transmission takes place, while the gradual change from dark blue to red shows the increase of transmission, red being total transmission.

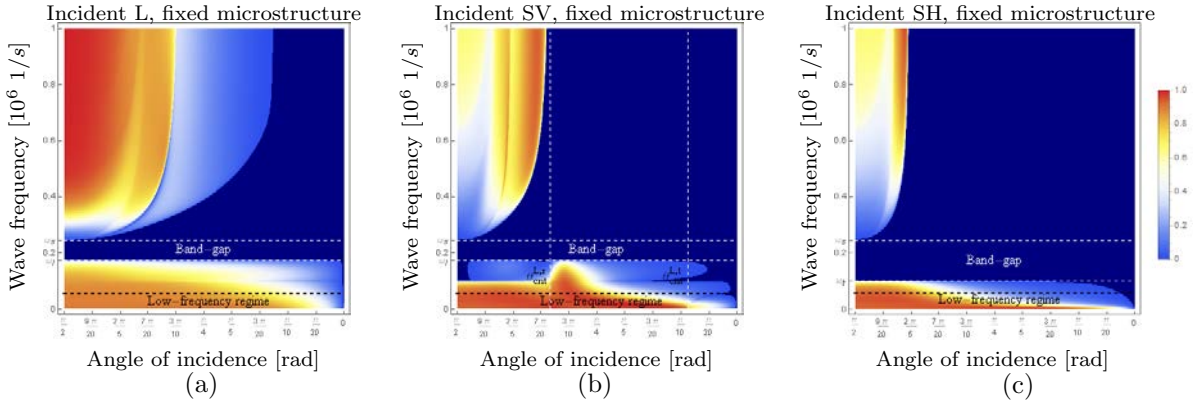

Figure 4.15: Transmission coefficients as a function of the angle of incidence θ_i and of the wave-frequency ω for L (a), SV (b) and SH (c) incident waves for the case of macro-clamp with fixed microstructure.

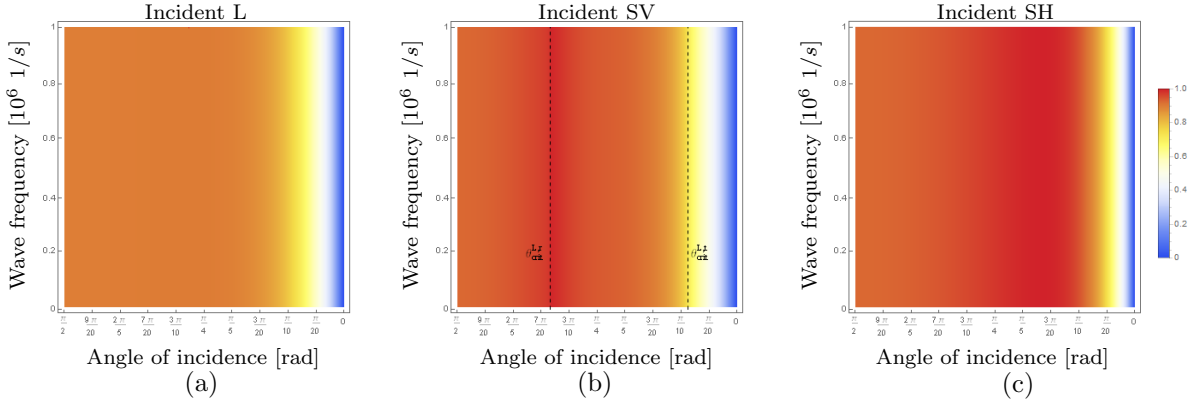

Figure 4.16: Transmission coefficients as a function of the angle of incidence θ_i and of the wave-frequency ω for L (a), SV (b) and SH (c) incident waves for the case of a Cauchy/Cauchy interface. The parameters of the left Cauchy continuum are given in Table 4.6, while the ones of the right Cauchy medium are given in Table 4.5.

This means that the creation of transmitted Stoneley waves contributes to a decrease of the transmitted energy in the low-frequency regime, but a decreasing trend for the transmission coefficient is observed also for the other cases, when considering angles which are far from normal incidence. This goes along the common feeling, according to which the more inclined the incident wave is with respect to the interface, the less transmission one can expect. The same behavior, even if qualitatively and quantitatively different, can be found in Figure 4.15(b), in which an increase of transmission can be observed after $\theta^{L,\mathrm{r}}_{\mathrm{crit}}$ and a decrease after $\theta^{L,\mathrm{t}}_{\mathrm{crit}}$, also for the case of fixed microstructure boundary conditions.

Direct comparison of Figures 4.14 and 4.15 allows us to identify the effect that the chosen type of boundary conditions has on the transmission properties of the interface. We already remarked that, at low frequencies, common trends can be identified which are related to critical angles determining the onset of Stoneley waves at the Cauchy/equivalent Cauchy interface. Nevertheless, some differences can also be remarked which are entirely related to the choice of boundary conditions. Surprisingly, the effect of boundary conditions intervenes already for low frequencies, meaning that imposing the value of P at the interface introduces a tangible effect of the interface microstructured properties on the overall behavior of the considered system. In particular, we can notice that forcing the tangential part of P to vanish at the interface globally reduces the low-frequency transmission for angles which are much closer to normal incidence, than for the case of free microstructure. This means that considering a microstructure which is not free to vibrate at the interface, allows for microstructure-related reflections, even if the frequency is relatively low. Such additional reduction of transmission takes place for incident waves which are very inclined with respect to the surface ($\theta_{\mathrm{i}} \leq \pi/4$).

For the sake of completeness and in order to immediately visualize the extent to which the relaxed micromorphic model generalizes the classical setting of linear elasticity, Figure 4.16 shows the analogous transmission coefficients for the case of a Cauchy/Cauchy interface. These coefficients are obtained for a Cauchy medium on the right, which is the low-frequency limit of the relaxed micromorphic continuum of Fig. 4.14. It is immediately evident that a reasonable agreement is observed only with the very low frequency regime of Figures 4.14 and 4.15. Given that in Cauchy elasticity the transmission coefficient does not depend on the frequency, all other effects at higher frequencies are lost, well before the band-gap region.

Up to now, we only discussed the transmittive properties of the considered Cauchy/relaxed micromorphic interface on the low-frequency regime. Some of the features that we discussed on Stoneley waves can be retrieved by observing Figures 4.17, 4.18 and 4.19 in which the plots of the imaginary part of the first component of the wave vector k_1 are given for each mode of the relaxed micromorphic medium, for L, SV and SH incident waves respectively.

The blue region denotes $\mathrm{Im}(k_1) = 0$ (which implies that k_1 is real), while $\mathrm{Im}(k_1)$ is not vanishing in the red regions. In other words, we can say that for each mode, the red color means that there are Stoneley waves associated to that mode. The first two modes in Figures 4.17 and 4.18 correspond to L and SV Cauchy-like modes, while the first mode in Figure 4.19 is the SH Cauchy-like mode in the low-frequency regime. Since we are considering a relaxed micromorphic medium, three additional modes with respect to the Cauchy case are present both for the in-plane (Figures 4.17 and 4.18) and for the out-of-plane problem (Fig. 4.19). For the Cauchy-like modes we can observe that at low frequencies they are always propagative, except in the case of an incident SV wave, for which Stoneley longitudinal waves appear beyond $\theta^{L,\mathrm{t}}_{\mathrm{crit}}$ (also Stoneley reflected waves can be observed in this case, but we do not present the plots of $\mathrm{Im}(k_1)$ for reflected waves to avoid overburdening). We can note by inspecting Figures 4.17, 4.18 and Fig. 4.19 that the presence of Stoneley waves at high frequencies is much more widespread

than at low frequencies for all 5 (resp. 4) modes.

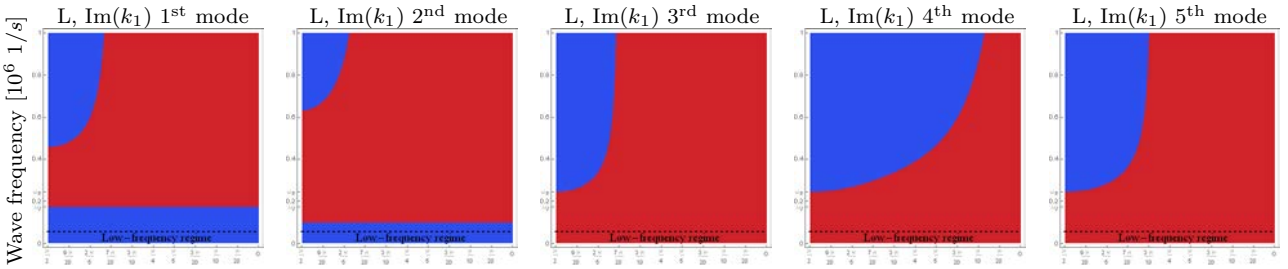

Figure 4.17: Values of $\mathrm{Im}(k_1)$ as a function of the angle of incidence θ_i and of the wave-frequency ω for the five modes of the relaxed micromorphic medium and for the case of an incident L wave. The origin coincides with normal incidence ($\theta_\mathrm{i} = \pi/2$), while the angle of incidence decreases towards the right until it reaches the value $\theta_\mathrm{i} = 0$, which corresponds to the limit case where the incidence is parallel to the interface. The first two modes (a) and (b) correspond to the L and SV modes for the equivalent Cauchy continuum at low frequencies. The red color in these plots means that the mode is Stoneley and does not propagate, while blue means that the mode is propagative.

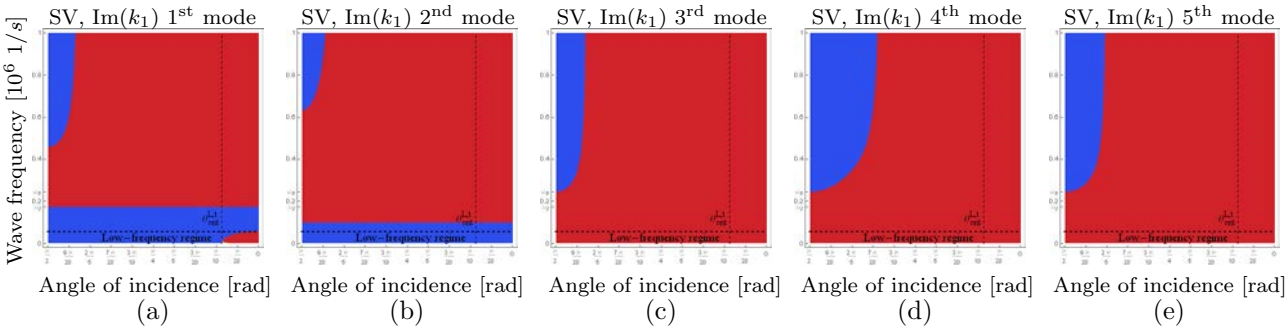

Figure 4.18: Values of $\mathrm{Im}(k_1)$ as a function of the angle of incidence θ_i and of the wave-frequency ω for the five modes of the relaxed micromorphic medium and for the case of an incident SV wave.

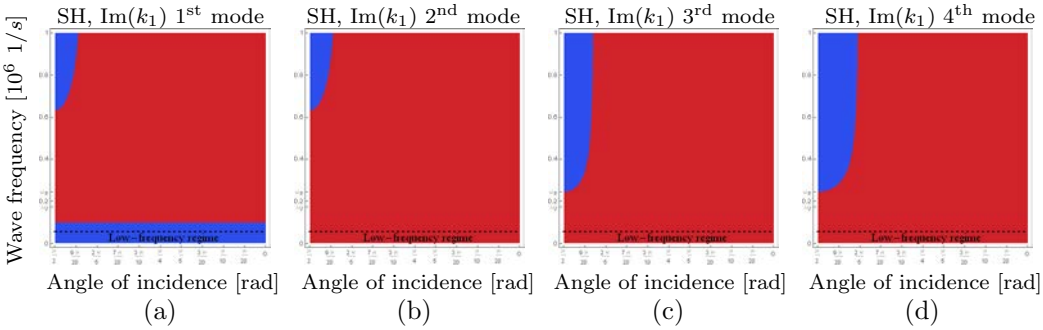

Figure 4.19: Values of $\mathrm{Im}(k_1)$ as a function of the angle of incidence θ_i and of the wave-frequency ω for the four modes of the relaxed micromorphic medium and for the case of an incident SH wave.

We can observe by direct observation of Figures 4.17, 4.18 and 4.19 that high-frequency critical angles exist for each mode corresponding to which a transition from Stoneley to propagative waves takes place. The value of such critical angles depends on the frequency for the medium-frequency regime and becomes constant for higher frequencies. The influence of the existence of such high-frequency critical angles can be directly observed on the patterns of the

transmission coefficient in Figures 4.14 and 4.15, in which high frequency transmission is observed for angles closer to normal incidence and no transmission is reported for smaller angles due to the simultaneous presence of Stoneley waves for all modes. We can call such zones in which transmission is equal to one "extraordinary transmission regions" (see e.g. [73]). Such extraordinary transmission can be used as a basis for the conception of innovative systems such as selective cloaking and non-destructive evaluation.

We can finally remark that the influence of the choice of boundary conditions on the high-frequency behavior of the transmission coefficient is still present, but does not determine drastic changes on the transmission patterns (see Figures 4.14 and 4.15).

4.5.2 Cauchy medium which is "softer" than the relaxed micromorphic one

In this section we present the reflective properties of a Cauchy/relaxed micromorphic interface for which we consider that the Cauchy medium on the left is "softer" than the relaxed micromorphic medium on the right in the same sense as in the previous section. To that end, we choose the material parameters of the left Cauchy medium to be those presented in Table 4.7 and we explicitly remark that these values are smaller than those of Table 4.5.

ρ [kg/m^3]	λ [Pa]	μ [Pa]
2000	2×10^7	0.7×10^7

Table 4.7: Lamé parameters of the "softer" Cauchy medium on the left side of the considered Cauchy/relaxed micromorphic interface.

With these new parameters we can compute again, following Tables 4.1 and 4.2, the critical angles for the appearance of Stoneley waves at low frequencies. They are found to be $\theta^{L,\mathrm{t}}_{\mathrm{crit}} = 37\pi/100$ and $\theta^{SV,\mathrm{t}}_{\mathrm{crit}} = 49\pi/200$ for an incident L wave (no reflected Stoneley mode), $\theta^{L,\mathrm{r}}_{\mathrm{crit}} = 7\pi/20$, $\theta^{L,\mathrm{t}}_{\mathrm{crit}} = 11\pi/25$ and $\theta^{SV,\mathrm{t}}_{\mathrm{crit}} = 39\pi/100$ for an incident SV wave and $\theta^{SH,\mathrm{t}}_{\mathrm{crit}} = 39\pi/100$ for an incident SH wave.

Figures 4.20 and 4.21 show the transmission coefficient for the softer Cauchy/relaxed micromorphic interface as a function of the angle of incidence and of frequency for both boundary conditions.

We see that when the incident wave travels in a soft medium and hits the interface separating this medium from a stiffer one, many critical angles exist which determine the onset of Stoneley waves for all types of incident waves at low frequencies. Since many more Stoneley waves are created with respect to the previous case of section 4.5.1, we would expect less transmission in the low-frequency regime than before. This is indeed the case if we inspect Figures 4.20 and 4.21: the presence of low-frequency Stoneley waves induces a wide zero-transmission zone in the low-frequency regime. We can also detect a certain role of boundary conditions in widening these zero-transmission zones when considering the fixed microstructure boundary condition (see Figure 4.21).

Also in this case of a left "softer" Cauchy medium, we plot in Fig. 4.22 the analogous transmission coefficient when the right side of the interface is occupied by a Cauchy medium. Again, this Cauchy medium on the right is the homogenized limit of the considered micromorphic material. By directly comparing to Fig. 4.20, we infer that a reasonable agreement can be observed only for very low frequencies. All other higher frequency effects are lost before the band-gap.

Figures 4.23, 4.24 and 4.25 once again show the imaginary part of the first component of the wave-vector k_1 for each mode of the relaxed micromorphic medium on the right. We see that Stoneley waves are observed almost everywhere both at low and high frequencies, with the exception of angles which are very close to normal incidence. Once again, the blue region denotes $\mathrm{Im}(k_1) = 0$ (which implies that k_1 is real), while $\mathrm{Im}(k_1)$ is not vanishing in the red regions, which means that for each mode, the red color denotes that there are Stoneley waves associated to that mode. The first two modes in Figures 4.23 and 4.24 correspond to L and SV Cauchy-like modes, while the first mode in Figure 4.25 is the SH Cauchy-like mode in the low-frequency regime.

Since we are considering a relaxed micromorphic medium, three additional modes with respect to the Cauchy case are present both for the in-plane (Figures 4.23 and 4.24) and for the out-of-plane problem. For this choice of parameters which make the left-side medium "softer" than the corresponding Cauchy medium on the right, we see that the Cauchy-like modes for all incident waves become Stoneley waves after a critical angle (clearly denoted on the plots with a vertical dashed line). Also Stoneley reflected waves can be observed in this case, but we do not present the plots of $\mathrm{Im}(k_1)$ for reflected waves to avoid overburdening.

We see that it is possible to create an almost perfect total screen, which completely reflects incident waves for almost all angles of incidence and wave frequencies. This extraordinary possibility can be obtained by simply tailoring the properties of the left Cauchy medium which has to be chosen to be suitably softer than the right equivalent Cauchy medium. Regions of extraordinary transmission for very wade ranges of incident angles and wave frequencies can be engineered, opening the door to exciting applications.

Before concluding the Results section, we point out a last interesting property of the transmission coefficient obtained by the relaxed micromorphic model. In both cases (see Figures 4.14, 4.15, 4.20, 4.21) the band-gap for SV incident waves is more extended than the band-gap for L incident waves for angles close to normal incidence. This phenomenon is due to the uncoupling of L and SV "activated" acoustic modes close to normal incidence outlined in Fig. 4.10. Close to normal incidence, only the green modes are activated by an incident SV wave, so that the band-gap is widened. This "uncoupling" effect can often be observed in real metamaterials. An analogous "mode uncoupling" at higher frequencies is responsible for the wider zero-transmission high-frequency region for SV incident waves compared to L incident waves.

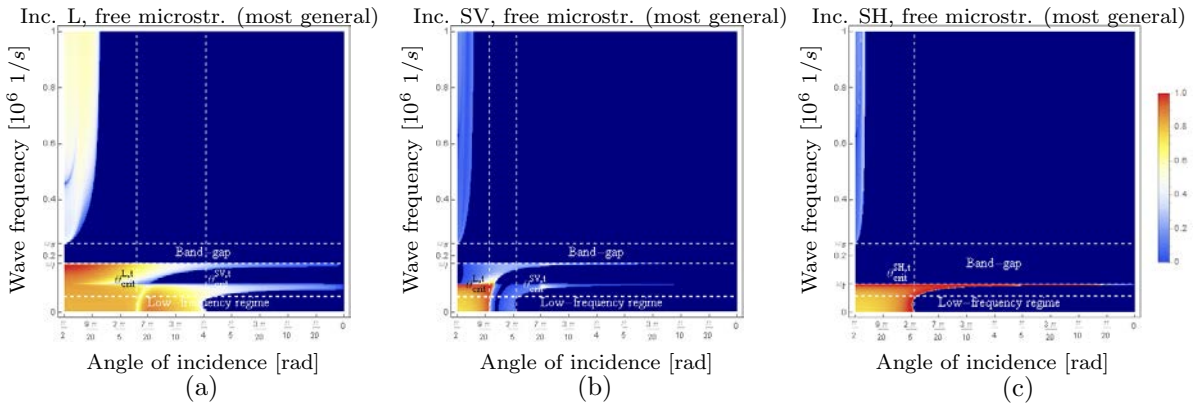

Figure 4.20: Transmission coefficients as a function of the angle of incidence θ_i and of the wave-frequency ω for L (a), SV (b) and SH (c) incident waves for the case of macro-clamp with free microstructure and for a "softer" Cauchy medium on the left.

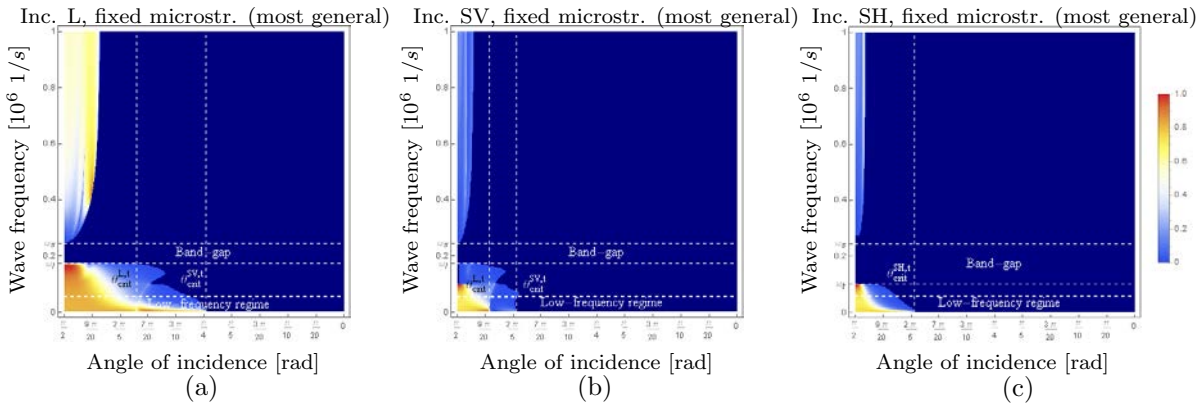

Figure 4.21: Transmission coefficients as a function of the angle of incidence θ_i and of the wave-frequency ω for L (a), SV (b) and SH (c) incident waves for the case of macro-clamp with fixed microstructure and for a "softer" Cauchy medium on the left.

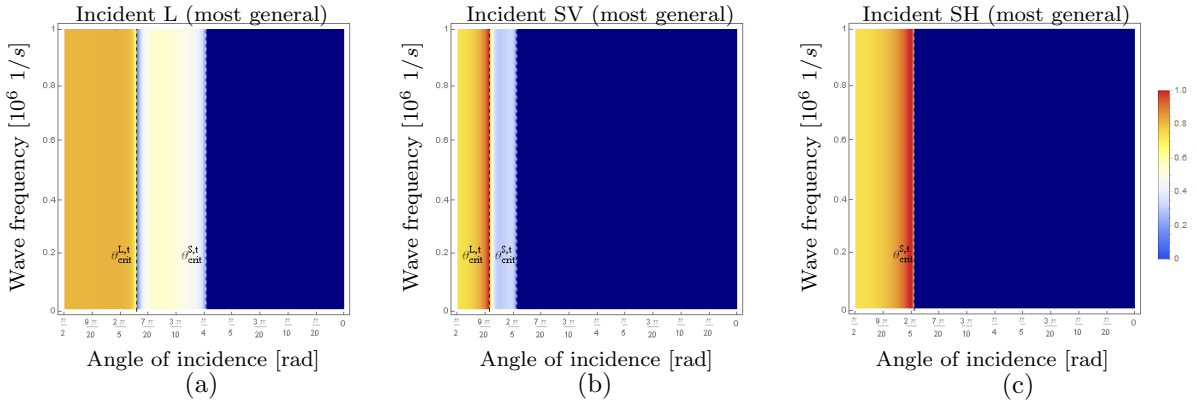

Figure 4.22: Transmission coefficients as a function of the angle of incidence θ_i and of the wave-frequency ω for L (a), SV (b) and SH (c) incident waves for the case of a Cauchy/Cauchy interface. The parameters of the left Cauchy continuum are given in Table 4.7, while the ones of the right Cauchy medium are given in Table 4.5.

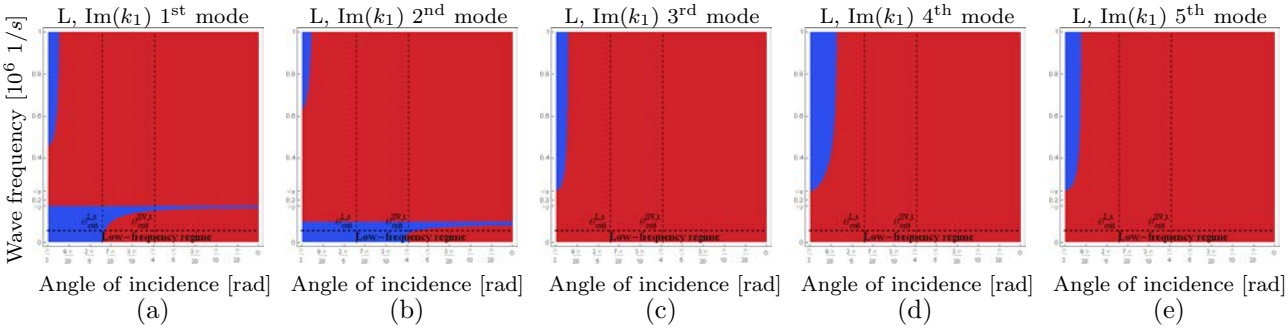

Figure 4.23: Values of $\mathrm{Im}(k_1)$ as a function of the angle of incidence θ_i and of the wave-frequency ω for the five modes of the relaxed micromorphic medium for the case of an incident L wave and a "softer" Cauchy medium on the left.

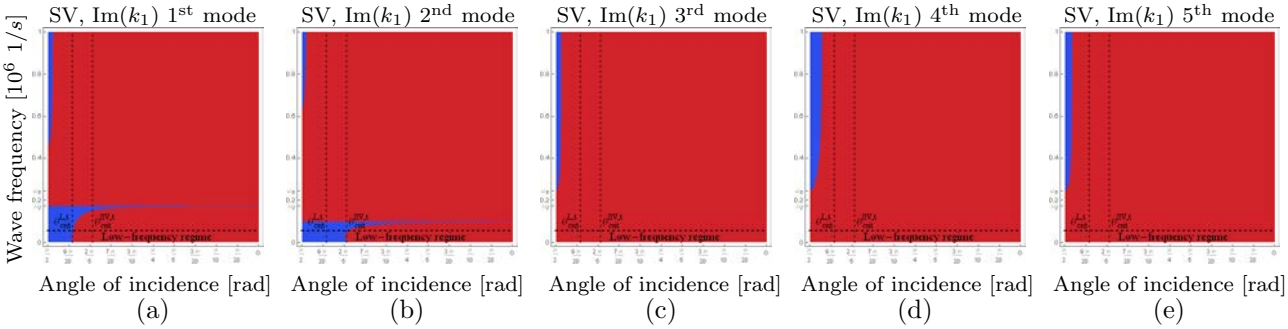

Figure 4.24: Values of $\mathrm{Im}(k_1)$ as a function of the angle of incidence θ_i and of the wave-frequency ω for the five modes of the relaxed micromorphic medium for the case of an incident SV wave and a "softer" Cauchy medium on the left.

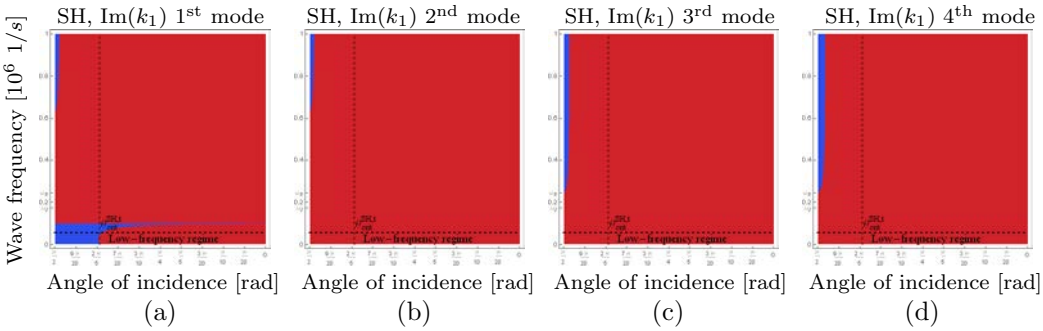

Figure 4.25: Values of $\mathrm{Im}(k_1)$ as a function of the angle of incidence θ_i and of the wave-frequency ω for the four modes of the relaxed micromorphic medium for the case of an incident SH wave and a "softer" Cauchy medium on the left.

4.6 Conclusions

In this chapter we presented the detailed study of the reflective and refractive properties of a two-dimensional interface separating a classical Cauchy medium from a relaxed micromorphic medium. Both media are assumed to be semi-infinite.

We show in great detail that critical angles of incidence exist, beyond which classical Stoneley waves appear at low frequencies. It is shown that these critical angles directly depend on the relative mechanical properties of the two media. Moreover, we unveil the existence of critical

angles which give rise to Stoneley waves at higher frequencies. These Stoneley waves are clearly related to the presence of an underlying microstructure in the metamaterial.

We show that, due to the onset of low and high-frequency Stoneley waves, wide frequency bounds where total reflection and/or total transmission occur can be engineered. This total reflection/transmission phenomenon is appealing for applications, in which total screens for elastic waves, such as cloaks or wave-filters, are desirable. It is clear that the ability of widening the frequency and incident angle intervals for which total reflection/transmission occur, would be of paramount importance for conceiving new devices which are more and more performant for wavefront manipulation.

We also clearly show that the simple fact of suitably tailoring the relative stiffnesses of the two media allows for the possibility of conceiving almost perfect total screens which do not transmit elastic waves for any kind of incident wave (longitudinal, in-plane and out-of-plane shear) and for almost all (low and high) frequencies and angles of incidence. Acting on such relative stiffnesses allows to achieve also the opposite situation, where total transmission occurs for large frequency bounds before a microstructure-related critical angle. This could be exploited for the conception of selective cloaks which make objects transparent to waves dependently on the angle of incidence.

The results presented in this chapter have been published in references [2] and [3].

Chapter 5

Relaxed micromorphic model of transient wave propagation in anisotropic band-gap metastructures

Forced (i.e. non-homogeneous) scalar (out-of-plane) and vector (in-plane) problems of linear elasticity in micro-structured unbounded domains have been studied extensively in the literature. The Green's function provides a formidable analytical tool to write down an integral representation of the solution which can be evaluated, via analytical or numerical tools, in different frequency regimes. Colquitt et al. [24] obtained the out-of-plane displacement field in square and triangular elastic lattices, with a particular emphasis on the resonances associated with dynamic anisotropy and *primitive waveforms* arising at saddle points in the dispersion diagram. These primitive waveforms have also been examined in the papers by Langley [49], Ruzzene et al. [89], Ayzenberg-Stepanenko and Slepyan [8], and Osharovich et al. [82], among others. We also mention the papers by Martin [67] and Movchan and Slepyan [74], which analyze the properties of the vector dynamic Green's functions for a square lattice in the pass and stop band, respectively. Nonetheless, the use of such analytical tools for continua with a complex microstructure can be challenging, especially in the transient regime. Therefore, transient and/or time-harmonic finite element solutions for such problems can be used.

One of the most widespread tools used to study the ability of periodic media to support or inhibit free wave propagation is the Bloch-Floquet analysis [14]. This technique allows to reduce the free wave propagation problem, posed in a periodic domain, to an eigenvalue problem in its period, referred to as unit-cell, with quasi-periodic boundary conditions at the boundaries of the unit-cell.

This chapter shows that the relaxed micromorphic model is rich enough to face exciting problems concerning the mechanical behavior of two-dimensional (2D) anisotropic micro-structured materials, which possess frequency band-gaps and non-trivial dispersive properties. More specifically, we compare the high-frequency dynamic response of a specific micro-structured material - subjected to space-concentrated and time-modulated loads - to the corresponding response issued by the relaxed micromorphic continuum. In particular, it is shown that the transient waveforms within the chosen metastructure are well-captured by the relaxed micromorphic continuum model, while the classical Cauchy continuum model is only accurate at lower frequencies.

We particularize our analysis to 2D plain-strain continua belonging to the tetragonal symmetry class. An outline of this chapter is given as follows: in section 5.2.1, we introduce the micro-structured material of interest, define its unit cell and perform Bloch-Floquet analysis. The dispersive properties of the periodic structure are shown, via dispersion curves along specified paths in the first Brillouin zone. In addition, we compare the Bloch-Floquet dispersion diagram with the dispersion diagram issued via the relaxed micromorphic continuum model,

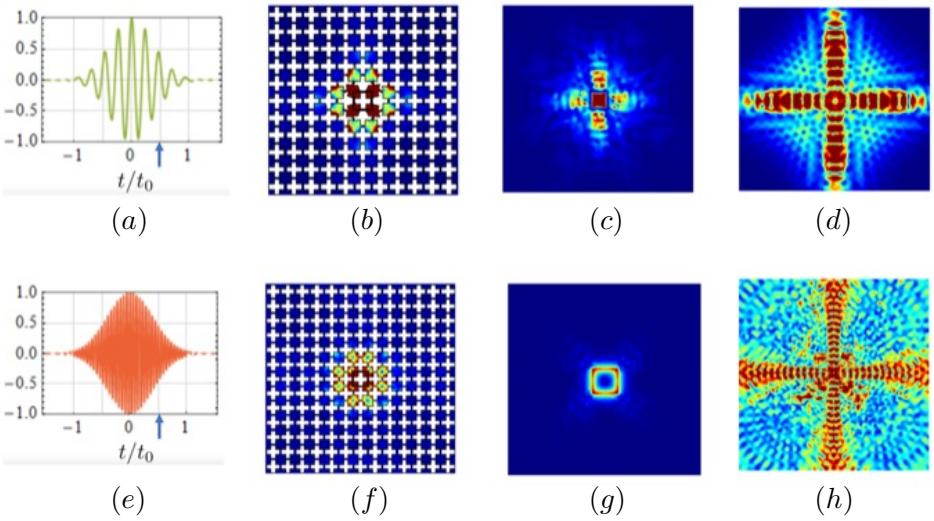

Figure 5.1: High-frequency waveforms in the transient regime for the considered tetragonal metastructure (panels (b) and (f)) agree with those obtained in a relaxed micromorphic continuum model (panels (c) and (g)). The aforementioned waveforms are generated by the application of space-concentrated pulses, whose time-dependence is shown in panels (a) and (e), respectively. The blue arrows in panels (a) and (e) indicate the time at which the waveforms on their right have been evaluated. Panels (d) and (h) report the transient waveform in an equivalent Cauchy continuum, showing propagation instead of localisation. We refer to section 5.4 for a detailed discussion.

enabling us to determine the constitutive parameters of our enriched model by a simple inverse approach. In section 5.3, we introduce a space-concentrated and time-modulated pulse to be applied to (i) a finite metastructure, (ii) a finite continuum governed by the relaxed micromorphic model and (iii) a finite continuum modeled by an equivalent Cauchy model. The time-dependence of the prescribed pulse is tailored in order to explore different frequency regions within the dispersion diagram of the corresponding periodic structure (see Fig. 5.1(a) and 5.1(e), for example). Section 5.4 is devoted to the discussion of the main results of this chapter: we show that a relaxed micromorphic continuum subjected to the aforementioned transient pulse, displays similar waveforms to those exhibited by the micro-structured domain, including localized waveforms corresponding to frequencies in the band-gap and optical branches. On the other hand, the Cauchy model is not descriptive outside the low frequency regime. An illustrative anticipation of the obtained results is shown in Fig. 5.1. In addition, we show that by using our enriched continuum model instead of the explicit calculation of all the details of the microstructure provides a true advantage in terms of computational time, especially when considering large metastructures.

5.1 The plane-strain tetragonal symmetry case

Contrary to our analysis in chapter 4, in this chapter we will focus only on the in-plane behavior of a metamaterial introducing the plane-strain assumption, which implies the following constraints:

- we consider only the in-plane degrees of freedom, i.e. u_3, P_{13}, P_{31}, P_{23}, P_{32} and P_{33} are

set to zero;

- we consider only the in-plane deformations i.e. all the derivatives on the out-of-plane direction are set to be zero.

These assumptions correspond to the following simplified form of the kinematical fields:

$$u(x_1,x_2,t)=\begin{pmatrix}u_1(x_1,x_2,t)\\ u_2(x_1,x_2,t)\\ 0\end{pmatrix},\qquad P(x_1,x_2,t)=\begin{pmatrix}P_{11}(x_1,x_2,t) & P_{12}(x_1,x_2,t) & 0\\ P_{21}(x_1,x_2,t) & P_{22}(x_1,x_2,t) & 0\\ 0 & 0 & 0\end{pmatrix}. \tag{5.1}$$

Moreover, since we are interested in studying the dynamic response of the metastructure generated by the unit cell given in Fig. 5.2, we consider that the corresponding relaxed micromorphic continuum must be particularized to the same symmetry class of the unit cell, i.e. the tetragonal symmetry.

Following [29], we denote the second order constitutive tensors in Voigt notation corresponding to the fourth order ones appearing in the kinetic and strain energy expressions (3.11) and (3.5) by a tilde, as done in chapter 3.4.[1] With the proposed assumptions, the constitutive tensors of the relaxed micromorphic model in the tetragonal symmetry case are given by (5.2) (see [9, 29])

$$\widetilde{\mathbb{C}}_e=\begin{pmatrix}2\,\mu_e+\lambda_e & \lambda_e & \star & 0 & 0 & 0\\ \lambda_e & 2\,\mu_e+\lambda_e & \star & 0 & 0 & 0\\ \star & \star & \star & 0 & 0 & 0\\ 0 & 0 & 0 & \star & 0 & 0\\ 0 & 0 & 0 & 0 & \star & 0\\ 0 & 0 & 0 & 0 & 0 & \mu_e^*\end{pmatrix},\quad \widetilde{\mathbb{C}}_c=\begin{pmatrix}\star & 0 & 0\\ 0 & \star & 0\\ 0 & 0 & 4\,\mu_c\end{pmatrix},$$

$$\widetilde{\mathbb{C}}_{\text{micro}}=\begin{pmatrix}2\,\mu_{\text{micro}}+\lambda_{\text{micro}} & \lambda_{\text{micro}} & \star & 0 & 0 & 0\\ \lambda_{\text{micro}} & 2\,\mu_{\text{micro}}+\lambda_{\text{micro}} & \star & 0 & 0 & 0\\ \star & \star & \star & 0 & 0 & 0\\ 0 & 0 & 0 & \star & 0 & 0\\ 0 & 0 & 0 & 0 & \star & 0\\ 0 & 0 & 0 & 0 & 0 & \mu_{\text{micro}}^*\end{pmatrix},$$

$$\widetilde{\mathbb{J}}_{\text{micro}}=\begin{pmatrix}2\,\eta_1+\eta_3 & \eta_3 & \star & 0 & 0 & 0\\ \eta_3 & 2\,\eta_1+\eta_3 & \star & 0 & 0 & 0\\ \star & \star & \star & 0 & 0 & 0\\ 0 & 0 & 0 & \star & 0 & 0\\ 0 & 0 & 0 & 0 & \star & 0\\ 0 & 0 & 0 & 0 & 0 & \eta_1^*\end{pmatrix},\qquad \widetilde{\mathbb{J}}_c=\begin{pmatrix}\star & 0 & 0\\ 0 & \star & 0\\ 0 & 0 & 4\,\eta_2\end{pmatrix},$$

[1] For example, the 4th order tensor $\mathbb{C}_e$ is written as $\widetilde{\mathbb{C}}_e$ in Voigt notation.

(5.2)

$$\widetilde{\mathbb{T}}_e = \begin{pmatrix} 2\,\bar{\eta}_1 + \bar{\eta}_3 & \bar{\eta}_3 & \star & 0 & 0 & 0 \\ \bar{\eta}_3 & 2\,\bar{\eta}_1 + \bar{\eta}_3 & \star & 0 & 0 & 0 \\ \star & \star & \star & 0 & 0 & 0 \\ 0 & 0 & 0 & \star & 0 & 0 \\ 0 & 0 & 0 & 0 & \star & 0 \\ 0 & 0 & 0 & 0 & 0 & \bar{\eta}_1^{\star} \end{pmatrix}, \qquad \widetilde{\mathbb{T}}_c = \begin{pmatrix} \star & 0 & 0 \\ 0 & \star & 0 \\ 0 & 0 & 4\,\bar{\eta}_2 \end{pmatrix},$$

where we denoted by a star those components, which work on out-of-plane macro- and micro-strains and do not play any role in the considered in plane (plane-strain) problem.

5.2 Dispersive properties of a band-gap metamaterial with tetragonal symmetry

In this section, we choose a specific two-dimensional (2D) metamaterial whose dispersive properties and frequency band-gaps have already been investigated in the literature (see [29] and section 5.2.3). The unit-cell of the considered metamaterial is represented in Fig. 5.2(a).

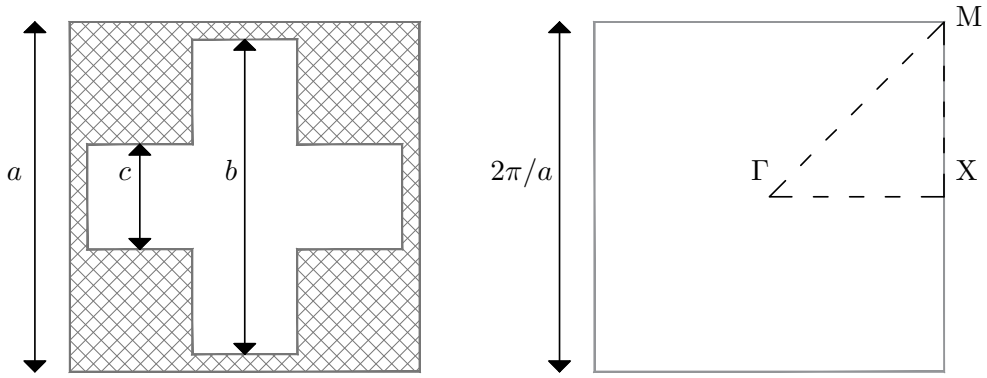

Figure 5.2: Panel (a) is a schematic representation of the unit-cell of the square lattice. In panel (b), the gray square represents the boundaries of the first Brillouin zone. The path connecting the high-symmetry points Γ, X and M, on which the dispersion surfaces will be projected is also shown (black dashed line).

In Fig. 5.2(a), the shaded areas represent aluminum while the white areas denote cross-shaped holes. In Table 5.1, we give the geometric parameters of the unit cell (left), as well as physical parameters for aluminum (right).

a	b	c	E	ν	μ	λ	ρ_{Al}
[mm]	[mm]	[mm]	[GPa]	–	[GPa]	[GPa]	$[\mathrm{Kg/m^3}]$
1	0.9	0.3	70	0.33	26.32	51.08	2700

Table 5.1: Geometric parameters of the unit-cell (see also Fig. 5.2(a)), elastic parameters and mass density ρ_{Al} of aluminum. For the reader's comfort we give both the values of Young's modulus and Poisson's ratio (E, ν), as well as the Lamé parameters (λ, μ).

In the following subsections, we will present the basis to analyze the dynamical behavior of the unit-cell by means of a Bloch-Floquet analysis (section 5.2.1), via the relaxed micromorphic model (section 5.2.2) and we will show the resulting dispersion curves in section 5.2.3.

5.2.1 Bloch-Floquet dispersion diagram

The 2D Bravais lattice with unit-cell in Fig. 5.2(a) has primitive vectors

$$a_1 = \begin{pmatrix} 1 \\ 0 \\ 0 \end{pmatrix} a, \quad \text{and} \quad a_2 = \begin{pmatrix} 0 \\ 1 \\ 0 \end{pmatrix} a, \tag{5.3}$$

and reciprocal lattice primitive vectors

$$G_1 = \frac{2\pi}{a} \begin{pmatrix} 1 \\ 0 \\ 0 \end{pmatrix}, \quad \text{and} \quad G_2 = \frac{2\pi}{a} \begin{pmatrix} 0 \\ 1 \\ 0 \end{pmatrix}. \tag{5.4}$$

The first Brillouin zone for the lattice coincides with the Wigner-Seitz unit cell of the reciprocal Bravais lattice and is represented in Fig. 5.2(b). We also mark the representative points in the first Brillouin zone

$$\Gamma = \frac{\pi}{a} \begin{pmatrix} 0 \\ 0 \\ 0 \end{pmatrix}, \quad \mathrm{X} = \frac{\pi}{a} \begin{pmatrix} 1 \\ 0 \\ 0 \end{pmatrix}, \quad \mathrm{M} = \frac{\pi}{a} \begin{pmatrix} 1 \\ 1 \\ 0 \end{pmatrix}, \tag{5.5}$$

which will be used for the representation and discussion of the dispersive properties of the periodic structure. Those properties are obtained by solving the PDE eigenfrequency problem governed by time-harmonic linear plain strain elasticity in the domain Ω_0 represented by the unit cell.

The Bloch-Floquet boundary conditions for the displacement field in the periodic structure are

$$u\left(x + l^{(n)}\right) = e^{i\langle k, l^{(n)} \rangle} u(x), \quad x \in \Omega_0, \tag{5.6}$$

where we have introduced the lattice nodal points

$$l^{(n)} = n_1 a_1 + n_2 a_2, \quad n = (n_1, n_2)^{\mathrm{T}} \in \mathbb{Z}^2, \tag{5.7}$$

and the Bloch-Floquet wave vector $k = (k_1, k_2, 0)^{\mathrm{T}}$, with

$$(k_1, k_2)^{\mathrm{T}} \in \left[-\frac{\pi}{a}, \frac{\pi}{a}\right] \times \left[-\frac{\pi}{a}, \frac{\pi}{a}\right]. \tag{5.8}$$

The right-hand-side in Eq (5.8) is the first Brillouin zone for the square lattice under consideration (see also Fig. 5.2(b) for a schematic representation). We assume that the cross-like holes in Fig 5.2(a) delimit vacuum. Therefore we assign traction-free boundary conditions in correspondence of the boundary of the cross-like hole in Fig 5.2(a). We use *Comsol Multiphysics*^{TM} to solve the Bloch-Floquet eigenvalue problem described above, with spectral parameter $\omega = \omega(k_1, k_2)$.

5.2.2 Relaxed micromorphic model: identification of the constitutive parameters and the plane wave ansatz

An explicit procedure for the a priori determination of the material parameters of a specific unit-cell has been proposed in [29]. Although the setup of this procedure is not the main objective of this chapter, it is, nevertheless, worthwhile to recap the determination procedure, as it is of crucial importance to understand the interest of using the relaxed micromorphic model with respect to other enriched continuum models available in the literature. In fact, the relaxed micromorphic model features a limited number of constitutive parameters, all with a clear physical meaning, which can be determined a-priori on the basis of simple static tests. More specifically, $\mathbb{C}_{\mathrm{macro}}$ represents the mechanical properties of a very large specimen of the considered metamaterial, $\mathbb{C}_{\mathrm{micro}}$ encloses the mechanical properties of smaller specimens, down to the unit cell scale, and $\mathbb{C}_e$ gives the transition between the two scales. As already anticipated, most of the parameters can be determined directly starting from a simulation of the unit-cell. Indeed,

- applying Periodic Boundary Conditions (PBCs) to the boundary of the unit-cell, the macroscopic tensor $\mathbb{C}_{\mathrm{M}}$ can be determined. This procedure is equivalent to running a standard mechanical test on a large specimen of the considered metamaterial to obtain its mechanical properties. It is also equivalent to classical homogenisation procedures;

- applying Kinematically Uniform (Dirichlet) Boundary Conditions (KUBCs) to the boundary of the unit-cell, the microscopic tensor $\mathbb{C}_{\mathrm{micro}}$ can be determined (see [29] for an extensive treatment and, in particular, for a motivation of the choice of KUBC rather than other possible boundary conditions); this procedure is equivalent to running mechanical tests on specimens of the metamaterial whose dimensions are comparable to those of the unit cell;

- $\mathbb{C}_e$ is directly computed inverting the harmonic tensor mean (3.77);

- from the cut-off frequencies (obtained via a Bloch-Floquet analysis, see section 5.2.3), we derive the micro-inertiae η_1, η_3 and η_1^* and an explicit relation between the Cosserat couple modulus μ_c and η_2. As a matter of fact, the cut-off frequencies are related to the parameters of the relaxed micromorphic model via the simple formulae

$$\omega_r = \sqrt{\frac{\mu_c}{\eta_2}}, \quad \omega_s = \sqrt{\frac{\mu_e + \mu_{\mathrm{micro}}}{\eta_1}}, \quad \omega_s^* = \sqrt{\frac{\mu_e^* + \mu_{\mathrm{micro}}^*}{\eta_1^*}}, \quad \omega_p = \sqrt{\frac{\mu_e + \mu_{\mathrm{micro}} + \lambda_e + \lambda_{\mathrm{micro}}}{\eta_1 + \eta_3}}. \tag{5.9}$$

Thus, the only parameters which are still free after the proposed identification procedure are the inertiae $\bar{\eta}_1$, $\bar{\eta}_1^*$ and $\bar{\eta}_3$ linked to $\nabla u_{,t}$ and η_2. Those parameters can be used to fine-tune the dispersion curves or some other specific behavior of the proposed metamaterial. In Table 6.1, we present the material parameters resulting from the systematic physically-grounded procedure described above (we refer the reader to [29] for an extensive discussion about this point), as well as the fine tuning of the dispersion curves. The characteristic length L_c is set to be 0. Nevertheless, a non-vanishing L_c is a crucial point for a description of the non-locality of metamaterials, but the task of its identification is postponed to forthcoming work.

λ_e	μ_e	μ_e^*	λ_e	μ_{micro}	μ^*_{micro}	μ_c	L_c	λ_{macro}	μ_{macro}	μ^*_{macro}
[GPa]	[GPa]	[GPa]	[GPa]	[GPa]	[GPa]	[GPa]	[m]	[GPa]	[GPa]	[GPa]
-0.77	17.34	0.67	5.98	8.93	8.33	$2.2 \cdot 10^{-2}$	0	1.74	5.89	0.62

ρ	η_1	η_2	η_3	η_1^*	$\overline{\eta}_1$	$\overline{\eta}_2$	$\overline{\eta}_3$	$\overline{\eta}_1^*$
$\left[\text{kg/m}^3\right]$	[kg/m]	[kg/m]	[kg/m]	[kg/m]	[kg/m]	[kg/m]	[kg/m]	[kg/m]
1485	$9.5 \cdot 10^{-5}$	$1 \cdot 10^{-7}$	$0.86 \cdot 10^{-5}$	$3.27 \cdot 10^{-5}$	$5 \cdot 10^{-5}$	$5 \cdot 10^{-5}$	$8 \cdot 10^{-5}$	0

Table 5.2: Summary of the numerical values for the elastic (top) and inertia (bottom) parameters of the tetragonal relaxed micromorphic model in 2D. The macroscopic parameters of the resulting homogenized Cauchy material are also provided.

The fitting performed in this chapter in order to capture the dispersive behavior of the tetragonal metamaterial with the relaxed micromorphic model is a preliminary one. Indeed, as we will see in chapter 6 where we will consider scattering problems in interfaces with this metamaterial, we will then have an additional tool which will help us fine-tune the material parameters.

As done for the case of isotropy in chapter 4, the fundamental analytical solutions of the PDEs system (3.28) are given by the plane waves

$$u(x,t) = \widehat{u}\, e^{i(\langle k,x\rangle - \omega t)}, \qquad P = \widehat{P}\, e^{i(\langle k,x\rangle - \omega t)}, \qquad k = (k_1, k_2, 0)^{\mathrm{T}}, \tag{5.10}$$

where $x = (x_1, x_2, 0)^{\mathrm{T}}$, and the plane strain assumption (see section 5.1) implies

$$\widehat{u} = \begin{pmatrix} \widehat{u}_1 \\ \widehat{u}_2 \\ 0 \end{pmatrix}, \qquad \widehat{P} = \begin{pmatrix} \widehat{P}_{11} & \widehat{P}_{12} & 0 \\ \widehat{P}_{21} & \widehat{P}_{22} & 0 \\ 0 & 0 & 0 \end{pmatrix}. \tag{5.11}$$

Substituting (5.10) in (3.28), the system of PDEs (3.28) turns into an algebraic problem:

$$\widehat{A}(k,\omega) \cdot v = 0, \tag{5.12}$$

where $\widehat{A}(k,\omega)$ is a 6×6 semi-positive definite matrix (see [79]), whose components are functions of the relaxed micromorphic constitutive parameters, of the wave vector k and of frequency ω and

$v = (\widehat{u}_1, \widehat{u}_2, \widehat{P}_{11}, \widehat{P}_{12}, \widehat{P}_{21}, \widehat{P}_{22})^{\mathrm{T}}$. The explicit expression of the matrix $\widehat{A}$ is algebraically involved, but easily tractable with standard numerical tools, such as *Mathematica*^{TM} or *Matlab*^{TM}. For the explicit expression of the matrix D, we refer to [29] and Appendix C1. The algebraic system (5.12) admits non-trivial solutions if and only if

$$\det \widehat{A}(k, \omega) = 0, \tag{5.13}$$

which is the dispersion equation for the micromorphic continuum. The solutions $\omega = \omega(k)$ of Eq. (5.13) provide the dispersion relations for plane wave propagation in the anisotropic micromorphic continuum.

We remark that, by choosing a wave vector k and thus a propagation direction, the frequencies $\omega = \omega(k)$ can be obtained as roots of Eq. (5.13). In the present thesis we choose to project the dispersion surfaces over the path v, by sampling such a path, and iteratively solving Eq. (5.13).

5.2.3 Dispersive properties of the metamaterial and of the equivalent continuum

Fig. 5.3 shows the dispersion diagrams over the path $k \in \mathrm{M\Gamma XM}$ in the first Brillouin zone of the considered periodic structure (see the dashed line in Fig. 5.2(b)). The dotted lines in Fig 5.3 are obtained by performing the Bloch-Floquet analysis outlined in section 5.2.1. The solid lines are the roots $\omega = \omega(k)$ of the relaxed micromorphic dispersion equation (5.13) for $k \in \mathrm{M\Gamma XM}$ (see section 5.2.2). For the considered microstructure, we obtain the cut-off frequencies shown in Table 5.3.

ω_r	ω_s	ω_s^*	ω_p
[rad/s]	[rad/s]	[rad/s]	[rad/s]
$0.4 \cdot 10^7$	$1.68 \cdot 10^7$	$1.68 \cdot 10^7$	$1.75 \cdot 10^7$

Table 5.3: Numerical values of the cut-offs for the considered metamaterial.

It is worthwhile pointing out that the notion of first Brillouin zone for a homogeneous continuum medium such as the relaxed micromorphic model, loses its sense, since a continuum is intrinsically macroscopic and a relation with specific unit cells can only be found a posteriori. On the other hand, dispersion diagrams in periodic media with microstructure are periodic in the reciprocal space identified by k, the period being the first Brillouin zone.

We explicitly remark that the relaxed micromorphic model is able to account for the overall dispersive properties of the metamaterial with unit cell in Fig. 5.2(a) (see Fig. 5.3). Some differences can be appreciated especially in the neighborhood of the boundaries of the first Brillouin zone, corresponding to large values of the Bloch vector. This means that the relaxed micromorphic continuum model is less accurate when considering small wavelengths which become comparable with the size of the unit cell. Even if a loss of precision for small wavelengths is expected when considering continuum models, further generalizations of the relaxed micromorphic model will allow a better precision also for such small wavelengths. Nevertheless, as we will show in the next section, the used homogenized model is precise enough for describing the propagation of pulses in metastructures, also at relatively high frequencies.

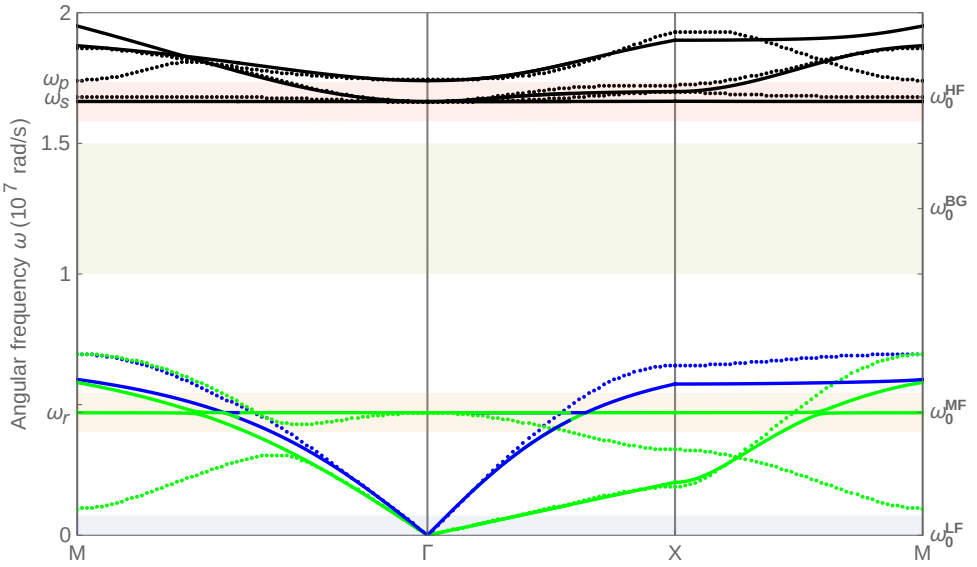

Figure 5.3: Comparison of dispersion curves obtained solving Eq. (5.13) for the relaxed micromorphic model (solid lines) and the Bloch-Floquet dispersion diagrams for the micro-structured domain (see section (5.2.1)) (dotted lines). We project the dispersion curves over the path MΓXM in the first Brillouin zone for the periodic structure (see Fig. 5.2(b)). With reference to Tab. 5.4, the blue shadow area has thickness $\Delta\omega^{\mathrm{LF}}/2$ (the negative part is omitted) and is delimited from below by $\omega_0^{\mathrm{LF}} = 0$. The vertical thicknesses of the remaining shadows, from bottom to top, correspond to the values of $\Delta\omega$ and are centred around ω_0^i, $i = \{\mathrm{MF},\mathrm{BG},\mathrm{HF}\}$, respectively (see Tab. 5.4). The blue curves refer to pressure dominated modes, while the green curves identify shear-dominated and rotation-dominated modes. Such identification cannot be done at high frequency, where the dispersion branches are represented in black.

5.3 Description of transient pulse propagation in metastructures via the relaxed micromorphic model

As pointed out in the introductory section, time-harmonic problems in discrete lattices and micro-structured continua have been extensively studied in the literature. For non-homogeneous elastic problems in infinite micro-structured domains, finite-element time-harmonic solutions heavily rely on the ability to model a perfectly absorbing frame in a finite computational domain. For lattice structures, it is often sufficient to introduce a damping term in the equations of motion for the masses belonging to an exterior computational frame [16, 24, 93, 94]. For continua with microstructure, this is not possible and the research is currently ongoing, even if several ad-hoc solutions, based on the perfectly matched layer method, have been already proposed [31].

To overcome this problem, we choose to apply a concentrated pulse in the middle of the considered metastructure. We show transient waveforms in the time-domain, before spurious reflections, stemming from the interaction with the boundaries of the computational domains, intervene. This method allows us to avoid the implementation of perfectly absorbing frames, but demands the precise definition of a *space-concentrated* and *time-modulated* prescribed displacement. The remainder of this section is devoted to such a definition.

5.3.1 Computational domains

The computational domains implemented in *Comsol Multiphysics*^{TM} are schematically represented in Fig. 5.4(a) and Fig. 5.4(b). These domains are squares each of which has side $A = 121\,a$ and is centered at the origin of the 2D Cartesian system of coordinates (x_1, x_2). Fig. 5.4(a) is textured with a microstructure, whose magnification is given in Fig. 5.4(c). Fig. 5.4(b) shows a continuous domain in which we solve the system of PDEs (3.28) for the relaxed micromorphic model and the system of PDEs (3.78) for the equivalent Cauchy continuum.

Fig. 5.4(d) is a magnification of Fig. 5.4(b). The solid red squares in Figs 5.4(c) and 5.4(d), here referred to as $\partial\Omega_0$, denote the boundaries on which the prescribed displacements are applied (see also the boundary conditions in equations (3.30), (3.31) and (3.78) for the boundary conditions pertaining the relaxed micromorphic and the equivalent Cauchy models, respectively). On the other hand, the micro-structured computational domain in Fig 5.4(a) is

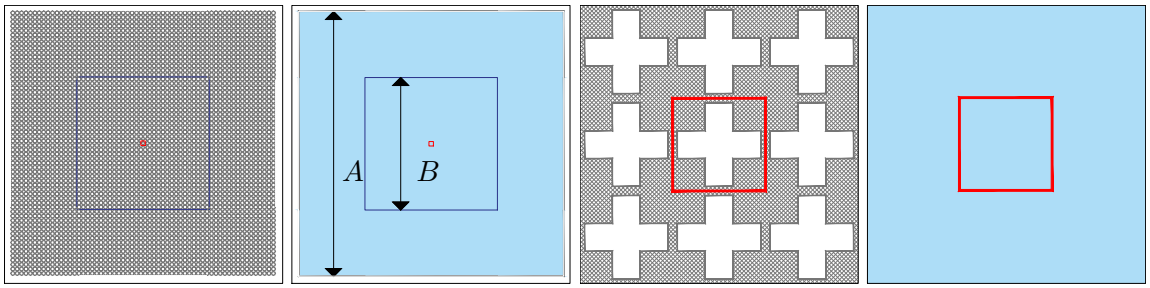

Figure 5.4: Schematic representations of the computational domains. Panel (a) is a micro-structured domain textured with cross-like holes. Panel (b) is a homogeneous domain modeled as a generalized continuum. The red inner square $\partial\Omega_0$, represents the boundary where the external prescribed displacement is applied. Panels (c) and (d) are magnifications of panels (a) and (b), respectively, comprising the square domain $\partial\Omega_0$. The dimension A is relative to the whole computational domain, while the squares of side B are the windows over which the results are reported (see Figs 5.7-5.15).

governed by the equations of classical linear elasticity

$$\begin{aligned} \rho_{\mathrm{Al}}\, u_{,tt} &= \mathrm{Div}\,[\mathbb{C}\ \mathrm{sym}\,\nabla u] && && \forall x \in \Omega, \\ f := (\mathbb{C}\ \mathrm{sym}\,\nabla u)\cdot n &= t^{\mathrm{ext}}(x,t) \qquad \text{or} \qquad u = \varphi(x,t), && && \forall x \in \partial\Omega_0, \end{aligned} \tag{5.14}$$

where $\mathbb{C}$ is the stiffness matrix for aluminum, with elastic parameters given in Tab. 5.1. In solving equation (5.14), traction-free boundary conditions are used at the cross-like holes and at the external boundary $\partial\Omega$[2]. In the following we define the time and space dependence of the external prescribed displacement φ, which appear in equations (3.30), (3.31) (3.78) and (5.14).

5.3.2 Definition of the concentrated and modulated pulse

The concentrated and modulated pulse is a prescribed displacement for the systems of PDEs governing the structures in Fig. 5.4. We assume that the frequency spectrum of the applied

[2]We explicitly remark that, for the micro-structured solid, the domain Ω which appears in equations (5.14) coincides with the gray area in Figs 5.4(a) and 5.4(c).

pulses is of the Gaussian-type. The Gaussian function describing the frequency content has a mean ω_0, corresponding to either the acoustic branches, the band-gap or the optical cut-offs of the dispersion diagram in Fig. 5.3 (see Table 5.3). The Gaussian function has a standard deviation proportional to $\Delta\omega$, whose values have been deliberately chosen to be much smaller than the highest cut-off frequency of the structure. The frequency content of the time-dependent part of the prescribed displacement can be represented as the following function

$$f(\omega) = \frac{2}{\Delta\omega} \exp\left[-2\left(\frac{\omega-\omega_0}{\Delta\omega}\right)^2\right], \qquad \text{with } \Delta\omega \ll \omega_p. \tag{5.15}$$

Since the problem is linear, the choice of a Fourier spectrum like in equation (5.15) guarantees that the structure will respond only to predefined frequency intervals which are $\Delta\omega$ wide and have ω_0 mean value.

The Fourier anti-transform of the function (5.15) is

$$\mathcal{I}(t) = \mathcal{F}^{-1}[f(\omega)] = \exp\left[-i\omega_0 t - \frac{1}{8}(\Delta\omega)^2 t^2\right]. \tag{5.16}$$

As mentioned earlier, a time-modulated pulse allows us to explore selected frequency regimes in the dispersion diagram. We denote these frequency regimes as low frequency regime (LF), medium frequency regime (MF), band-gap regime (BG) and high frequency (HF) regime. In each of these frequency regimes, the Fourier transform in equation (5.18) has to be considered with different values of ω_0 and $\Delta\omega$. Those values are listed in Tab. 5.4. The values of ω_0 are also marked along the $y-$axis of Fig. 5.3. In Fig. 5.5(a), we evaluate the functions (5.15), in each frequency regime, as a function of frequency: blue, orange, green and red curves correspond to the LF, MF, BG and HF regimes, respectively. Figs 5.5(b), 5.5(c), 5.5(d) and 5.5(e) represent the Fourier anti-transform (5.16) as a function of time, in the LF, MF, BG and HF regimes, respectively. With reference to Fig. 5.5, in panels (b), (c), (d) and (e) we have introduced a time scale t_0. We choose as initial and final time of the transient pulse the times $t = -t_0$ and $t = t_0$, respectively. The time scale t_0 is not arbitrary: with reference to equation (5.16), in order to have $\|\mathcal{I}(t)\|_{t=\pm t0} \ll 1$, i.e. a small pulse at the initial and final times, it follows that

$$|t_0| \gg 1/\Delta\omega. \tag{5.17}$$

This means that the values of t_0 have to be chosen according to the values of $\Delta\omega$, and thus depend on the frequency regime. The values we use for the time scale t_0 are reported in the third column of Tab. 5.4.

	ω_0 [10^7 rad/s]	$\Delta\omega$ [10^5rad/s]	t_0 [10^{-6} s]
LF	0	7.5	8.38
MF	0.47	7.5	7.02
BG	1.25	25	2.14
HF	1.66	7.5	6.72

Table 5.4: Parameters used to model the time dependence of the pulse.

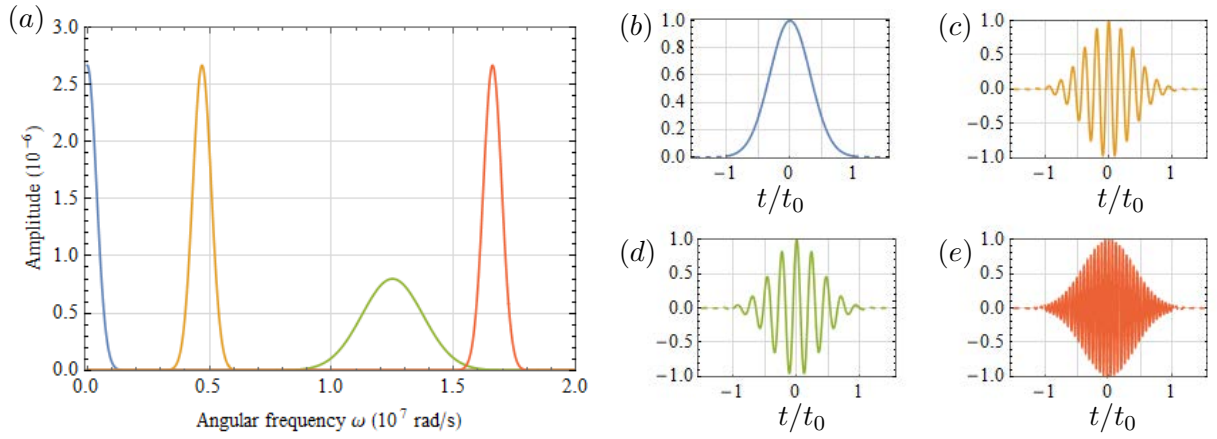

Figure 5.5: Frequency contents and time-dependence of four prescribed displacements. Panel (a) shows the time-Fourier transform of the pulses (see equation (5.15)). Blue, orange, green and red curves are the LF, MF, BG, HF regimes, respectively. Panel (b), (c), (d) and (e) are the real parts of the corresponding Fourier anti-transforms as a function of time (*i.e.* Re($\mathcal{I}(t)$), where $\mathcal{I}(t)$ is in equation (5.16)). The values of t_0 are given in Tab. 5.4 for each of the four frequency regimes.

The prescribed displacement has the space and time expression

$$\varphi_j\,(x,t) = \varphi_0\;\mathcal{I}\,(t)\;\; S_j(x),\;\; x \in \partial\Omega_0,\;\; j = \{p,s,\mathrm{r}\}, \tag{5.18}$$

where the function $\mathcal{I}\,(t)$ has been introduced in equation (5.16), the domain $\partial\Omega_0$ corresponds to the red squares in Fig. 5.2, and $\varphi_0 = 1.4 \times 10^{-4}$ m. The vector functions of the space variable in equation (5.18) are

$$S_p(x_1,x_2) = \begin{pmatrix} x_1/a \\ x_2/a \\ 0 \end{pmatrix},\;\; S_s(x_1,x_2) = \begin{pmatrix} x_2/a \\ x_1/a \\ 0 \end{pmatrix},\;\; S_r(x_1,x_2) = \begin{pmatrix} x_2/a \\ -x_1/a \\ 0 \end{pmatrix}, \tag{5.19}$$

where we recall that a is the side of the square unit-cell (see Fig. 5.2(a)). The functions of space (5.19) result in a pressure-like (p), shear-like (s) or rotation-like (r) deformation of the square $\partial\Omega_0$, respectively. A schematic representation of the deformations induced by the functions (5.19) is given in Fig. 5.6. The dashed red lines in Fig. 5.6 represent the undeformed squares $\partial\Omega_0$ and the solid lines represent, from left to right, pressure-like, shear-like and rotation-like deformations.

The advantage of the transient problem with a prescribed displacement as in equation (5.18) is that the anisotropic propagation or localization of the waveforms (both "fingerprints" of the non-trivial dispersion in metamaterials) can be studied over finite time intervals, short enough for the solution not to reach the boundary of the computational domain but long enough to allow the signal to develop.

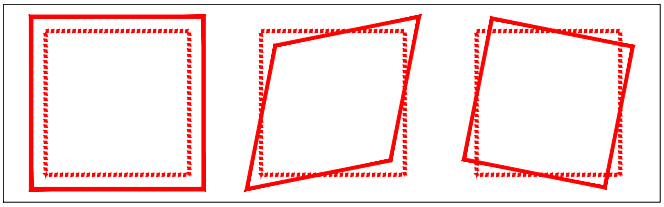

Figure 5.6: Schematic representations (from left to right) of pressure-like, shear-like and rotation-like prescribed displacement. The dotted red square represent the non-deformed square $\partial\Omega_0$ and the solid red contours represent its deformations as prescribed by equations (5.19). The figure is out of scale.

5.4 Results and discussion

In this section, we report transient finite element solutions for the following PDE models:

- a fully resolved micro-structured domain, with physical properties as in Table 5.1 and geometry depicted in Fig. 5.4(a); such medium is governed by the system of PDEs (5.14), with prescribed displacement as in equation (5.18);
- a relaxed micromorphic model, with physical properties as in Table 6.1 and the domain of Fig. 5.4(b); such enriched continuum is governed by the system of PDEs (3.28), with prescribed displacement as in equation (5.18);
- an equivalent macroscopic Cauchy continuum governed by $\mathbb{C}_{\text{macro}}$ (see equation (3.77) and Table 6.1), in the domain depicted in Fig. 5.4(b).

For the relaxed micromorphic model, rather than considering the strong form in equation (3.28), we implement the corresponding weak form, readily obtained imposing the first variation of the action functional to be zero

The variation is here intended with respect to the six independent kinematic fields entering the plane-strain assumption in equation (5.1).

In the following, transient solutions will be given at several times t, for the different models mentioned above and a prescribed displacement of the type in equation (5.18). We consider three different space dependencies (pressure-like, shear-like and rotation like) and the frequency regimes defined in section 5.3.2, i.e.:

1. low frequency (LF);
2. medium frequency (MF);
3. band-gap (BG);
4. high frequency (HF).

Each of the following subsections will be devoted to the analysis of the transient response of the metastructure in the aforementioned frequency regimes. The time domain is sampled with 10 time steps between the zeros of each signal in Figs 5.5(b) to 5.5(e). The results for the modulus of the displacement field are represented on a square frames of side $B = 30\ a$ (see Figs 5.4(a) and Figs 5.4(b)). The fully resolved finite element model solves for 250000 degrees-of-freedom at every time step, whereas only 100000 degrees of freedom are needed to obtain convergent results in the homogenized-Cauchy case and relaxed micromorphic case results. This reduction is due

to the fact that the relaxed micromorphic model is a continuous model, while the full resolution of the real system intrinsically reveals a discrete nature. Such intrinsic simplification related to the use of an enriched continuum modeling will result in a computational time-saving as it will be reported in the results section.

5.4.1 Low frequency regime

In this section, we consider a prescribed displacement as in equation (5.18) in the low frequency regime (see the nomenclature introduced in section 5.3). Specifically, the frequency content is centred around zero (see blue curve in Fig. 5.5(a)), which results in a Gaussian pulse in the time domain (see Fig. 5.5(b)).

The first case considered is the pressure-like prescribed displacement, obtained inserting the first of equations (5.19) in equation (5.18). In Fig. (5.7), we present snapshots of the resulting transient displacement for the micro-structured domain, the relaxed micromorphic continuum and a continuum governed by Cauchy elasticity, respectively. The directions of propagation are given by the properties of the micro-structure and, in particular, the wave propagates mainly on the directions of the beams in the micro-structure (0 and 90 degrees). As expected in the low frequency regime, the anisotropy is very well described by both the relaxed micromorphic model and the macroscopic Cauchy model. The columns correspond to different times, namely $t/t_0 = \{-1/2, 0, 1/2, 1\}$ (t_0 is the LF value in Tab. 5.4). The moduli of the displacements in each of the four different columns match very well. This proves that the propagation speed is very well described in the LF regime for pressure-like excitations.

Similar conclusions apply to Figures 5.8 and 5.9, where, shear-like and rotation-like pulse propagations are respectively shown. The direction of propagation is, once again, given by the micro-structure, leading to a relevant energy channeling at ± 45 degrees, in both cases. Furthermore, we observe that there is no substantial difference between the computations in Fig. 5.8 pertaining to a shear-like pulse and in Fig. 5.9 pertaining to a rotation-like pulse. In our opinion, the close similarity of the represented waveforms is due to the very low rotational stiffness of the unit cell leading to a shear-like propagation also for rotation-like pulses. The rotational mode, that is described by the skew-symmetric part of ∇u and P, has a very low stiffness also in the chosen material parameters of the relaxed micromorphic model ($\mu_c \simeq \mu_{\text{macro}}/200$). The substantial equivalence between shear-like and rotation-like excitation is preserved in all the frequency regimes. Therefore, we will refrain from showing the rotation-like excitations in the remainder of the chapter.

Overall, the presented results show that, in the low frequency regime, there is no significant difference between the three examined models. It also confirms a standard low frequency homogenisation result according to which the low frequency dispersion, and the corresponding PDEs, for a metamaterial with tetragonal symmetry are well captured by a macroscopic Cauchy continuum with the same symmetry. Moreover, in [9] it was proven that $\mathbb{C}_{\text{macro}}$ corresponds to a macroscopic limit case for the relaxed micromorphic model and, in [29], it has already been shown that the low frequency dispersion of the considered meta-structure is captured by the equations of classical linear elasticity with effective tensor $\mathbb{C}_{\text{macro}}$ in equation (3.77). More specifically, it is shown in [29] that, at low frequencies, the dispersion curves of the equivalent Cauchy continuum governed by $\mathbb{C}_{\text{macro}}$ provide an excellent approximation for the low frequency acoustic branches of the micromorphic continuum. By means of Fig. (5.7), (5.8) and (5.9), we provide a further illustration of this result in the context of low-frequency transient solutions of PDEs.

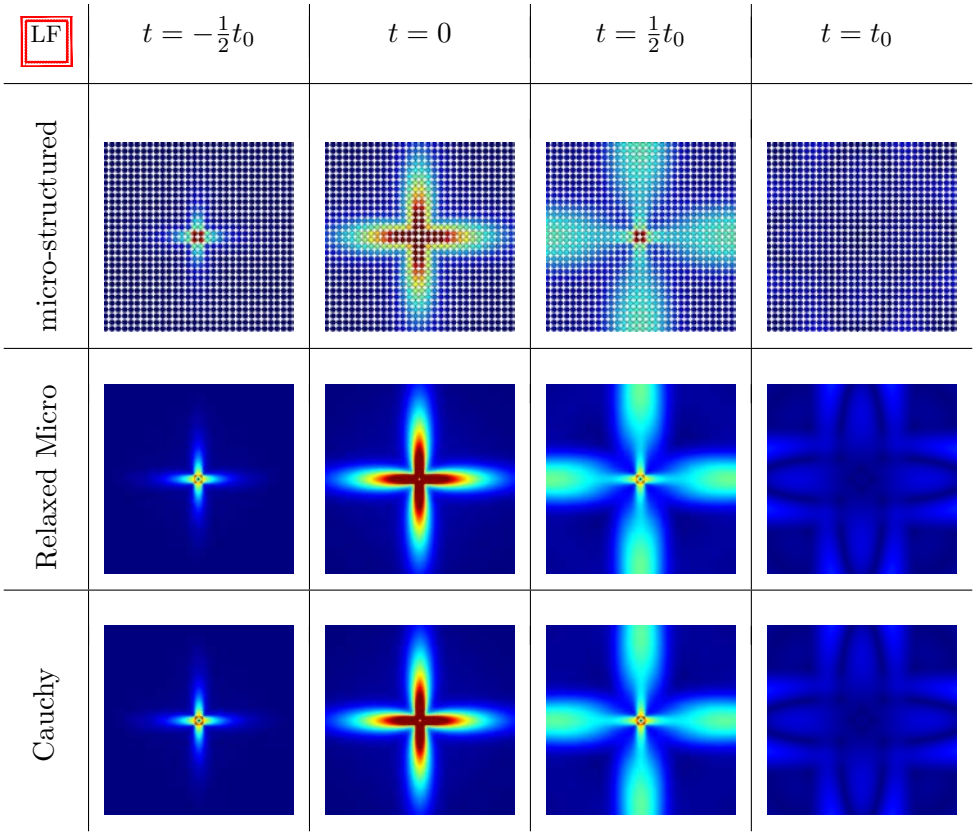

Figure 5.7: **Pressure-like** pulse propagation in the **low frequency** regime. The color map represents modulus of the displacement, with dark blue corresponding to zero displacement and dark red corresponding to the $|u_{\max}| = 3 \times 10^{-5}$ m. This color scale is adopted in the remainder of the chapter.

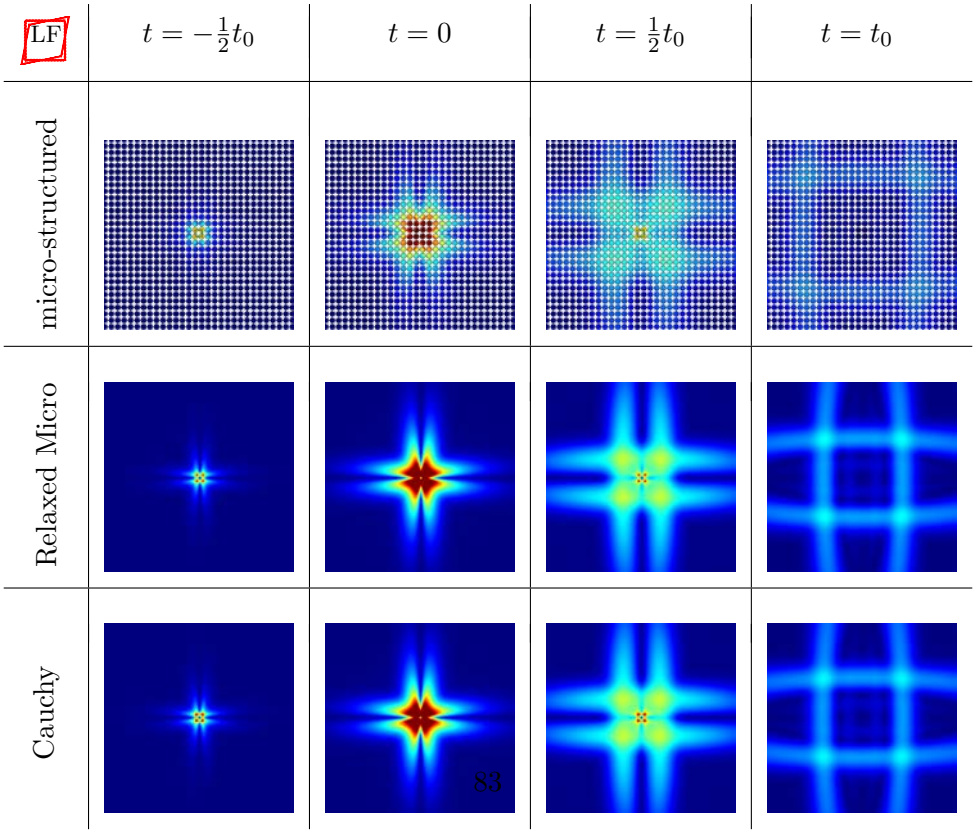

Figure 5.8: **Shear-like** pulse propagation in the **low frequency** regime.

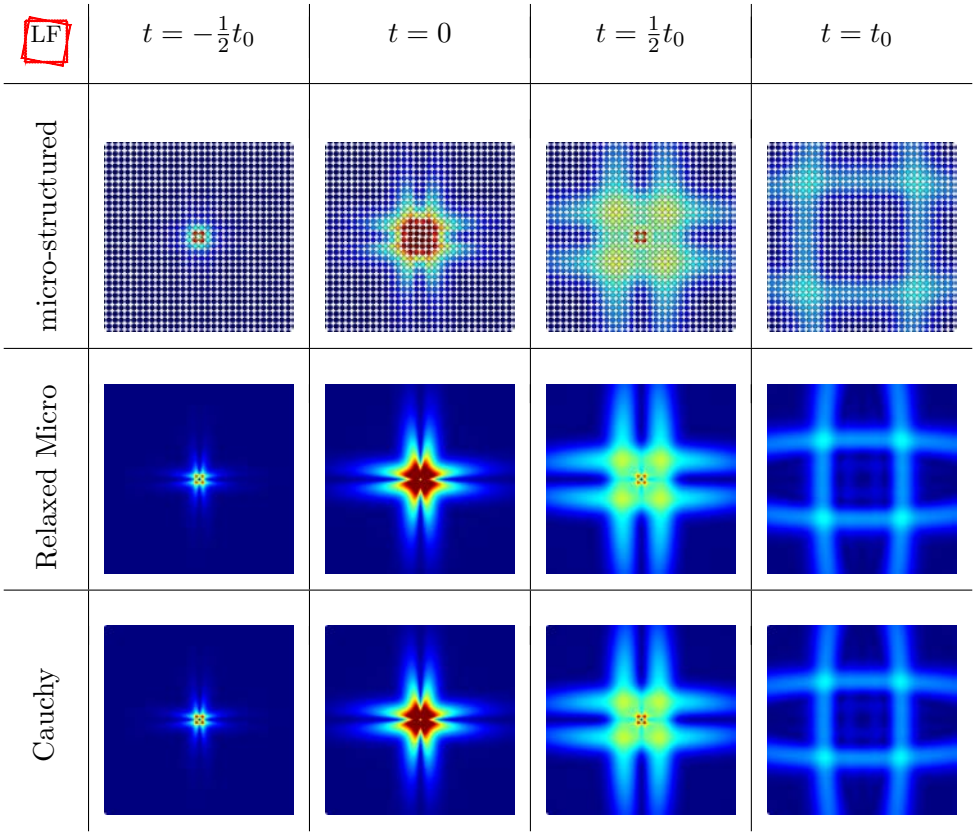

Figure 5.9: **Rotation-like** pulse propagation in the **low frequency** regime.

5.4.2 Medium frequency regime

In this section, we investigate the pulse propagation in the medium frequency regime. This is done by prescribing a displacement as in equation (5.19), with a time-dependence as in Fig. 5.5(c). The time-dependence has a spectral content as the orange curve in Fig. 5.5(a). The spectral width ($\Delta\omega_0^{\mathrm{MF}}$) and centre ($\omega_0^{\mathrm{MF}}$) of this signal is also shown in Fig. 5.3 by the orange shadow area (see MF-row in Tab. 5.4).

In Fig. 5.10, we report snapshots for the transient displacement as a result of a pressure-like displacement in equation (5.18) ($j = p$ in equation (5.19)), using the first of equations (5.19). The rows correspond to the micro-structured domain, relaxed micromorphic domain and Cauchy-elastic domain governed by $\mathbb{C}_{\mathrm{macro}}$, respectively. Different columns correspond to different times $t/t_0 = \{-1/2, 0, 1/2, 1\}$. With reference to Figs 5.10, we observe that the anisotropic transient waveforms in the micro-structured domain, are well captured by those pertaining to the relaxed micromorphic model. Moreover, the Cauchy continuum governed by $\mathbb{C}_{\mathrm{macro}}$ still represents an acceptable approximation for the waveforms in the micro-structured domain, as it can be appreciated by direct comparison of the first and the third rows of Figs 5.10. As shown in Fig. 5.3, the frequency mean value of the considered pulse (ω_0^{MF}) as well as its spectral width ($\Delta\omega_0^{\mathrm{MF}}$), are located in correspondence of the acoustic branches of the dispersion diagram, in a regime where such branches have a non-linear behavior as a function of the wave vector k. It is well known that, when the dispersion curves deviate from a linear behavior, the group velocity is not constant along the direction prescribed by k, thus depending on its modulus $|k| = 2\pi/\lambda_0$, with λ_0 being the wavelength. In this case the medium is said to be *dispersive*.

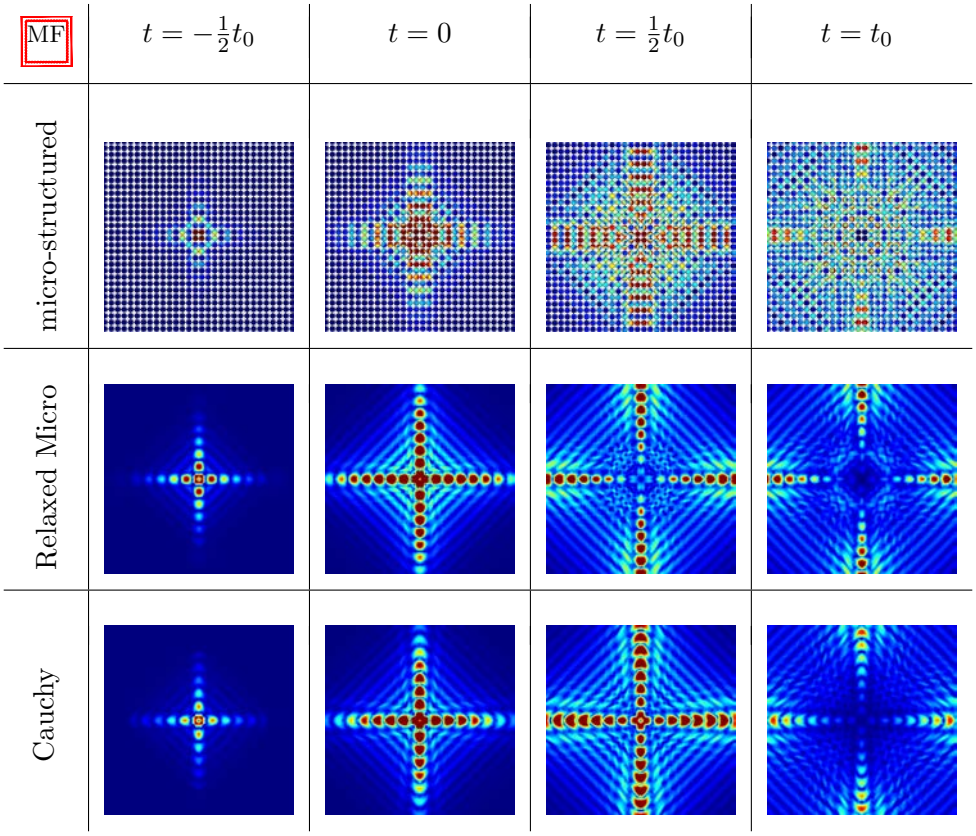

Figure 5.10: **Pressure-like** pulse propagation in the **medium frequency** regime.

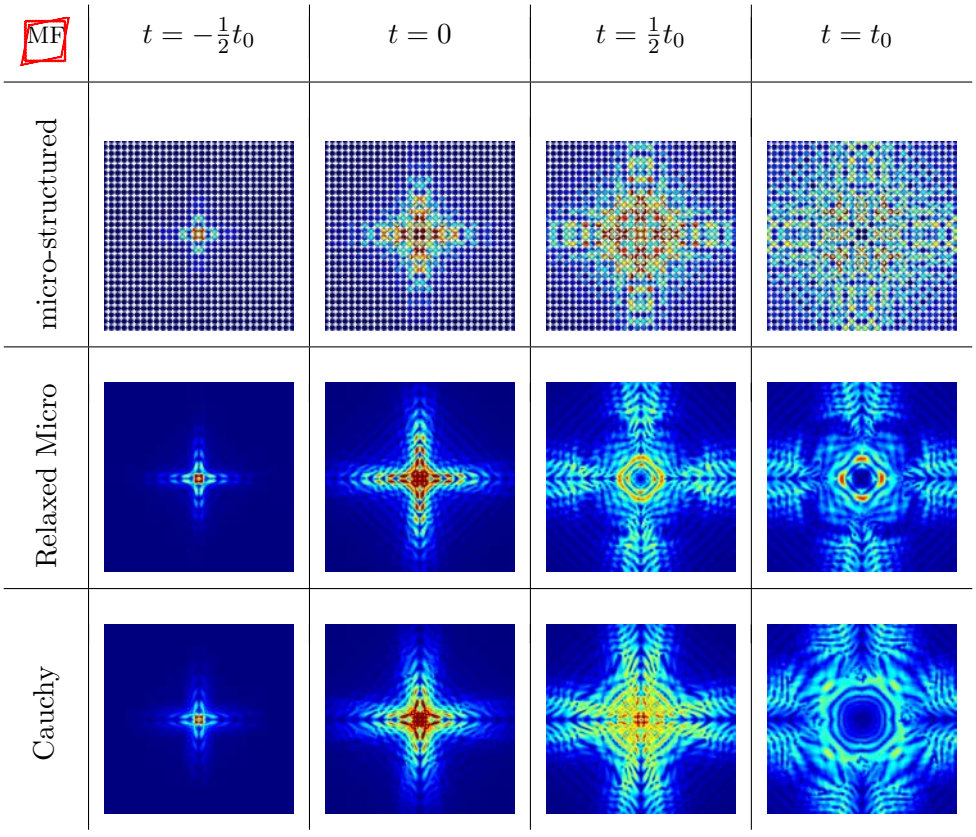

Figure 5.11: **Shear-like** pulse propagation in the **medium frequency** regime.

It is also very well known that the group velocity for a Cauchy infinite medium is constant along the direction prescribed by k, which translates into the fact that the dispersion curves as a function of $k = |k|\hat{k}$ - where $\hat{k}$ is a fixed unit direction - are simply straight lines. Hence, a Cauchy medium is referred to as *dispersionless*. Even if the relaxed micromorphic model is able to account for the aforementioned dispersion, we observe that this fact does not improve the descriptive power of the relaxed micromorphic model in the medium frequency regime with respect to the Cauchy one. At this stage, we would like to recall that a relaxed micromorphic model could be considered to be equivalent to a second gradient model for relatively low frequencies, where the dispersion diagram comprises acoustic branches only. On the other hand, second gradient models are not able to describe the behaviour of the metastructure at higher frequencies as instead the relaxed micromorphic can do. It is then doubtful how second gradient theories could give additional interesting information concerning wave propagation in real metastructures at frequencies higher than the Cauchy-like regime, and at least for the considered symmetry class.

5.4.3 Band-gap regime

The advantage of using the relaxed micromorphic model can be directly appreciated in the band-gap regime for the periodic structure (see Fig. 5.3). This section is devoted to such a frequency regime. To investigate the band-gap regime, we design a pulse with frequency content as represented by the green curve in Fig. (5.5)(a). The corresponding time dependence of the pulse is reported in Fig. 5.5(d) and it is used in equation (5.18) as a prescribed displacement over the square $\partial\Omega_0$.

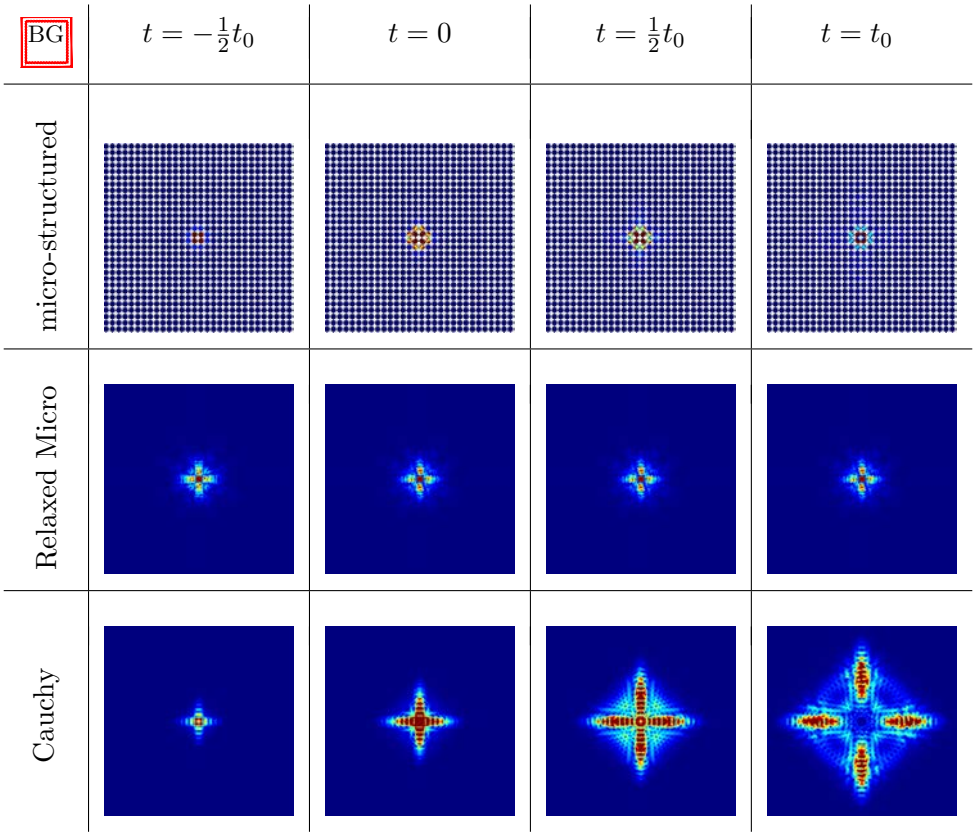

Figure 5.12: **Pressure-like** pulse propagation in the **band-gap** regime.

Fig. 5.12 shows the propagation of a pressure-like pulse ($j = p$ in equation (5.18)), in the first row a micro-structured domain, in the second row a continuous domain governed by the relaxed micromorphic model and in the last row a linear elastic continuous domain governed by $\mathbb{C}_{\text{macro}}$. We observe that the pulse is localised throughout all the considered times, in both the micro-structured medium (panels (a)) and in the relaxed micromorphic medium (panels (b)). This agrees with the fact that ω_0^{BG} is in the band gap for both the micro-structured medium and for the equivalent relaxed micromorphic continuum (see Fig. 5.3). This is not the case for the panels (c), where the same pulse can propagate in the computational domain. This is because a Cauchy medium, although able to capture anisotropy as shown earlier, is not able to reproduce band-gaps, leading to pulse propagation at every frequency. Fig. 5.13 shows the propagation of a shear-like pulse ($j = s$ in equation (5.18)). Similar considerations, already done for Fig. 5.12, apply for the shear-like pulse-localisation phenomena (Panels (a) and (b)) which are witnessed in Fig. (5.13).

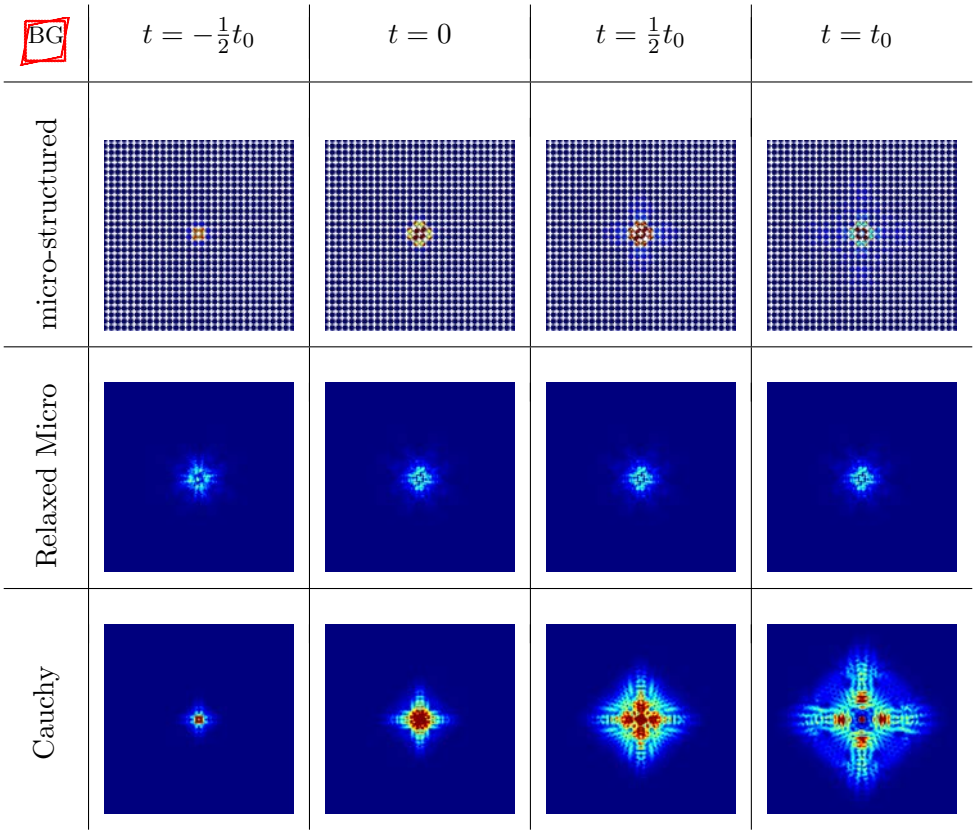

Figure 5.13: **Shear-like** pulse propagation in the **band-gap** regime.

5.4.4 High frequency regime

In this section, we conclude our analysis by presenting pulse propagation results in the high-frequency regime for the micro-structured domain and for the corresponding relaxed micromorphic continuum (see red shadow in Fig. 5.3). This is done by considering a frequency content for the pulse as the red curve in Fig. (5.5)(a). The corresponding time-dependence, shown in Fig. (5.5)(e), is assigned to the prescribed displacement in equation (5.18).

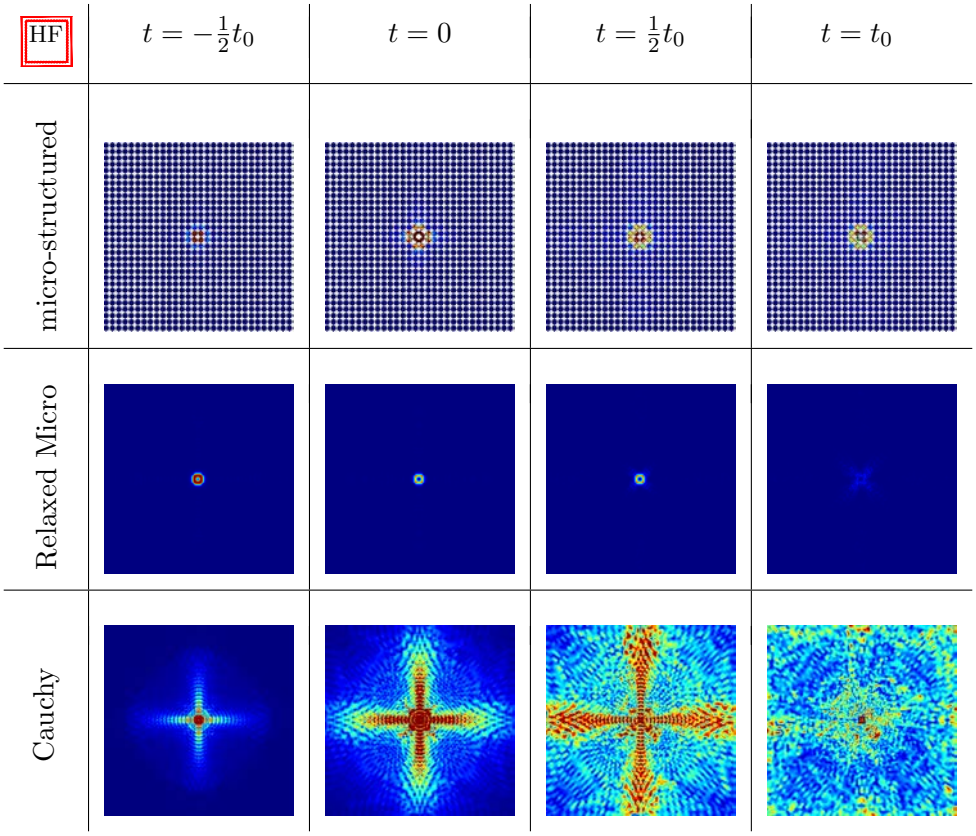

Figure 5.14: **Pressure-like** pulse propagation in the **high frequency** regime.

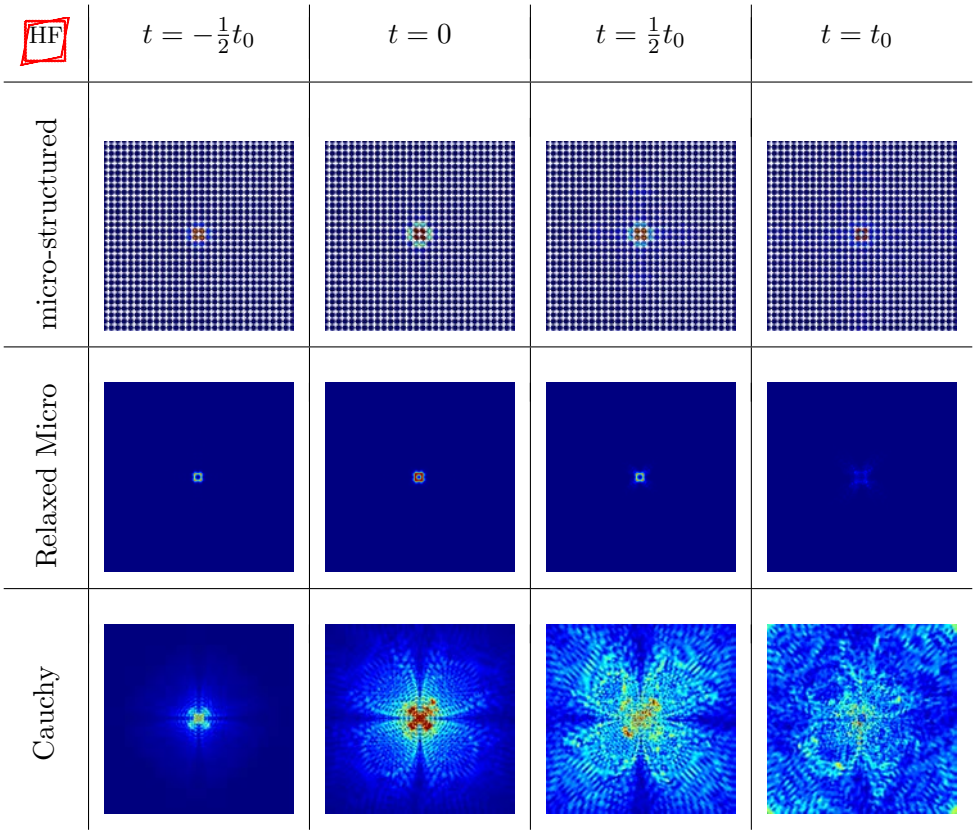

Figure 5.15: **Shear-like** pulse propagation in the **high frequency** regime.

Similarly to what we have done in the previous frequency regimes, we here focus on a pressure-like prescribed displacement (Fig. 5.14) and on a shear-like prescribed displacement (Fig. 5.15). As suggested by the zero group velocity in the dispersion diagram, we expect almost complete localization. The localization is observed for both the pressure-like and shear-like pulses, in both the micro-structured domain and in the relaxed micromorphic continuum. On the other hand, in the Cauchy continuum governed by $\mathbb{C}_{\text{macro}}$, the localization is completely lost since the dispersion is linear in all the investigated frequency regimes, and hence propagation of waves is always expected.

5.5 Conclusions

In this chapter we investigate the pertinence of using the relaxed micromorphic model to study wave propagation in band-gap anisotropic metastructures. To this aim, we compare transient waveforms corresponding to a pulse prescribed to the center of metastructures governed by several equations of motion. The considered equations of motion are (i) a micro-structured domain governed by linear elasticity; (ii) the relaxed micromorphic model; and (iii) an equivalent Cauchy continuum having the same macroscopic stiffness of the analogous relaxed micromorphic continuum. We show that the relaxed micromorphic model qualitatively captures the behavior of transient waveforms arising in metastructures, including localized waveforms in the band-gap and in the high frequency regime. The comparison has been performed using several types of prescribed displacements, namely pressure-like, shear-like and rotation-like deformations. We observe that the waveforms arising from rotation-like prescribed displacements - in every frequency regime - are identical to the waveforms obtained via the corresponding shear-like prescribed displacement. Such substantial equivalence between shear-like and rotation-like waveforms is remarked for the simple metastructure studied in the present chapter, and would deserve a deeper investigation to check if it is also possible in more complex situations.

We clearly show that the Cauchy equivalent continuum is able to describe the pulse propagation through the micro-structured domain only in the low frequency regime. The Cauchy equivalent continuum rapidly loses its predictive power when higher frequencies are considered. On the other hand, we show that the relaxed micromorphic model is able to account for the overall behavior of the metastructure for all the considered frequency regimes, including the band-gap and higher frequencies. This predictive ability is peculiar of the relaxed micromorphic model and is unrivaled by any other generalized continuum model. For example, for the considered metastructure, the so called "second gradient" models would not be able to add anything more to its description when compared to the equivalent Cauchy model. Second gradient models are based on a kinematical framework which is identical to Cauchy classical theory (only macroscopic displacements are provided) and the only difference with the latter consists in a modified constitutive law which also contains second gradients of displacement, instead of only first gradients. In the context of plane-wave propagation and dispersive properties of the generalized continuum, this means that only acoustic modes can be described by a second gradient medium and the only difference with Cauchy media would be the description of non-linear dispersion for high wavenumbers. Failure to capture optical branches and finite frequency band-gaps, represents an intrinsic limitation of second gradient models when applied to description of metamaterials with complex microstructure, even at relatively low frequencies.

The results presented in this chapter have been published in [10].

Chapter 6

Broadband scattering of finite-size anisotropic metastructures via the relaxed micromorphic model

We now turn back to the study of interface problems, but in this case we will be considering two reflection and transmission problems in **anisotropic** relaxed micromorphic media.

Very complex phenomena take place when an incident elastic wave hits a metamaterial's boundary, resulting in reflected and transmitted waves which can be propagative or evanescent depending on the frequency and angle of incidence of the incident wave itself. The primordial importance of evanescent (non-propagative) waves for the correct formulation of boundary value problems for metamaterials has been highlighted in [91, 107], where the need of infinite evanescent modes for obtaining continuity of displacement and of tractions at the considered metamaterial's boundary is pointed out.

We will show that we can describe, to a good extent, the overall behavior of the reflection coefficient (generated by a plane incident wave) of an interface between a homogeneous medium and a specific tetragonal band-gap metamaterial (both considered as semi-infinite in space), as a function of the frequency and of the angle of incidence of the incident wave. Moreover, given the auto-consistency of bulk PDEs and associated jump conditions, we are able to treat the more realistic case of a metamaterial slab of finite width treated as an inclusion between two semi-infinite homogeneous media. Also for the latter case, we are able to obtain the reflective properties of the slab as a function of the frequency and angle of incidence of the plane incident wave. To the authors' knowledge, a boundary value problem which describes the dynamical behavior of realistic finite-size metamaterial structures via the introduction of rigorous macroscopic boundary conditions, is presented here for the first time.

The results show very good agreement (for a wide range of frequencies extending from the low-frequency Cauchy limit to frequencies beyond the first band-gap and for all the possible angles of incidence) with the direct FEM numerical implementation of the considered system in *Comsol Multiphysics*^{TM}, where the detailed geometry of the unit cell has been implemented in the framework of classical linear elasticity. We observe a tremendous advantage in terms of the computational time needed to perform the numerical simulations (few hours for the relaxed micromorphic model against weeks for the direct FEM simulation).

We structure this chapter as follows: in Section 6.2 the plane-wave solutions for the Cauchy and relaxed micromorphic continua are obtained as solutions of the corresponding eigenvalue problems. In Section 6.1 we provide essential information concerning the correct boundary conditions which have to be imposed at the metamaterial's boundaries, in the relaxed micromorphic framework. In Sections 6.3 and 6.4 the problems of the scattering from a relaxed micromorphic single interface and relaxed micromorphic slab of finite size, respectively, are rigorously set

up and solved. Section 6.5 presents the detailed implementation of the microstructured metamaterial slab based on classical elasticity and implemented in the commercial Finite Element software *Comsol Multiphysics*^{TM}. Section 6.6 thoroughly presents our results by means of a detailed discussion. Section 6.7 is devoted to conclusions and perspectives.

Throughout this chapter, we again assume a tetragonal metamaterial under the plane-strain assumption, much as we did in chapter 5. Furthermore, from here on, we set again $L_c = 0$ for the remainder of this chapter. Indeed, it will be shown that even if non-locality is switched off ($L_c = 0$), the relaxed micromorphic model is able to capture the more relevant features of the considered problem. Taking the internal length into account provides small corrections to the overall behavior of the metamaterial.

6.1 Boundary Conditions

In this chapter we will study two types of interface problems: (i) a **single interface** separating a Cauchy and a relaxed micromorphic medium, both assumed to be semi-infinite (much like we did in chapter 4) and (ii) a **micromorphic slab** of finite size embedded between two semi-infinite Cauchy media. In the following, we will simply denote "single interface" and "micromorphic slab" the first and second problem, respectively.

In the single interface problem, two infinite half-spaces are occupied by two materials in perfect contact with each other, similarly to the case described in chapter 4. The material on the left of the interface is an isotropic classical Cauchy medium, while the material on the right is a microstructured tetragonal metamaterial modeled by the tetragonal relaxed micromorphic model (see Fig 6.1(a)).

In the micromorphic slab problem, two infinite half-spaces are separated by a micromorphic slab of finite width h. Three materials are thus in perfect contact with each other: the material on the left of the first interface is a classical linear elastic isotropic Cauchy medium, the material in the middle is an anisotropic relaxed micromorphic medium, while the material on the right of the second interface is again a classical isotropic Cauchy medium (see Fig. 6.1(b)).

6.1.1 Boundary conditions at an interface between a Cauchy continuum and a relaxed micromorphic continuum with vanishing characteristic length $L_c = 0$

In the particular case where $L_c = 0$, there are two sets of boundary conditions which have to be imposed: continuity of displacement and continuity of generalized traction (see [2, 3, 65] for more details).[1] For the displacement, we have:

$$[[u]] = 0 \Rightarrow u^- = u^+, \qquad \text{on} \quad x_1 = 0, \tag{6.1}$$

where u^- is the macroscopic displacement on the "minus" side (the $x_1 < 0$ half-plane, occupied by an isotropic Cauchy medium) and u^+ is the macroscopic displacement on the "plus" side (the $x_1 > 0$ half-plane, occupied by an anisotropic relaxed micromorphic medium). As for the jump of generalized traction we have:

$$t = \widetilde{t}, \tag{6.2}$$

where t is the Cauchy traction on the "minus" side and $\widetilde{t}$ is the generalized traction on the "plus" side. We recall that in a Cauchy medium, $t = \sigma \cdot \nu$, ν being the outward unit normal to

[1] On the other hand, if $L_c > 0$, one should also impose boundary conditions on the tangent part of the micro-distortion tensor P and of the double force, which was exactly the case in chapter 4 (see [2, 3, 65]).

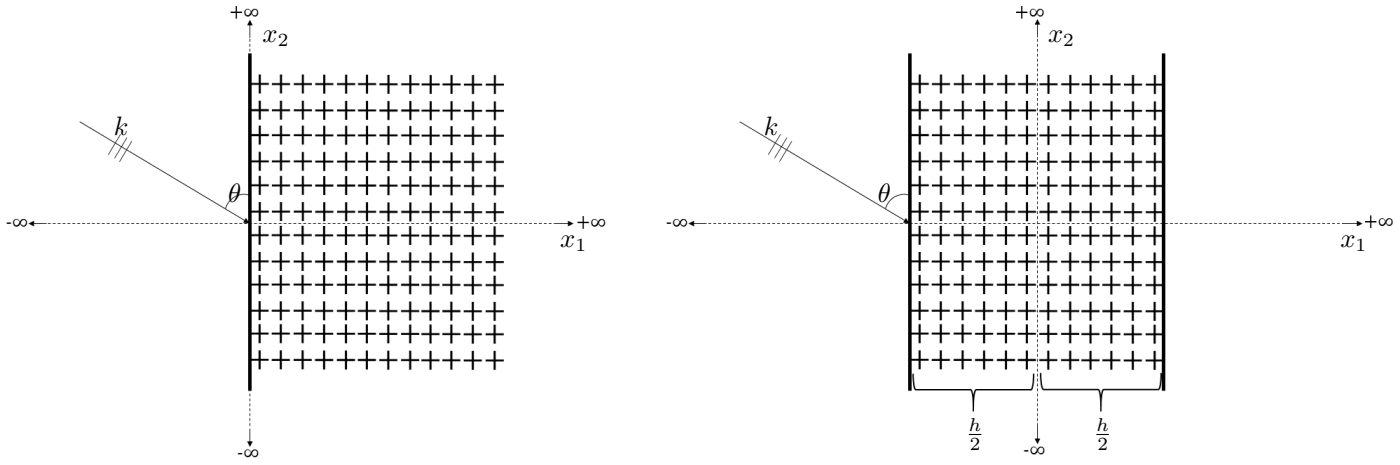

(a) (b)

Figure 6.1: Panel (a): single interface separating a Cauchy medium from a relaxed micromorphic medium (both semi-infinite in the x_1 direction). Panel (b): A micromorphic slab of width h between two semi-infinite elastic Cauchy media. Both configurations (a) and (b) are semi-infinite in the x_2 direction.

the surface and σ being the Cauchy stress tensor given by (2.5). The generalized traction for the relaxed micromorphic medium is given by

$$\widetilde{t} = (\widetilde{\sigma} + \widehat{\sigma}) \cdot \nu, \qquad \widetilde{t}_i = (\widetilde{\sigma}_{ij} + \widehat{\sigma}_{ij}) \cdot \nu_j, \qquad \text{on} \quad x_1 = 0, \tag{6.3}$$

where $\widetilde{\sigma}, \widehat{\sigma}$ are defined in (3.29).

Continuity of macroscopic displacement and of generalized traction implies conservation of energy at the interface

We have previously shown that conservation of energy for a bulk Cauchy and relaxed micromorphic medium is given by equation (2.10), where the energy flux is defined in (2.12) and (3.76), respectively. It is important to remark that the conservation of energy (2.10) has a "boundary counterpart". This establishes that the jump of the normal part of the flux must be vanishing, or, in other words, the normal part of the flux must be continuous at the considered interface (this comes from the bulk conservation law and the use of the Gauss divergence theorem). In symbols, when considering a surface Σ separating two continuous media, we have

$$[[H \cdot \nu]] = 0, \quad \text{on} \quad \Sigma. \tag{6.4}$$

We want to focus the reader's attention on the fact that, in the framework of a consistent theory in which the bulk equations and boundary conditions are simultaneously derived by means of a variational principle, the jump conditions imposed on Σ necessarily imply the surface conservation of energy (6.4), as far as a conservative system is considered. We explicitly show here that this is true for an interface Σ separating a Cauchy medium from a relaxed micromorphic one. The same arguments, however, hold for interfaces between two Cauchy or two relaxed micromorphic media.

To that end, considering for simplicity that the interface Σ is located at $x_1 = 0$ (so that its normal is $\nu = (1,0)^{\mathrm{T}}$) and assuming $L_c = 0$ we get from equation (3.76) that the normal flux computed on the "relaxed micromorphic" side is given by:

$$(H \cdot \nu)^+ := H_1^+ = -\nu^+ \cdot (\widetilde{\sigma} + \widehat{\sigma})^{\mathrm{T}} \cdot u_{,t}^+ \quad \text{at} \quad x_1 = 0. \tag{6.5}$$

By the same reasoning, the flux at the interface on the "Cauchy" side is computed from (2.12) and gives:

$$(H \cdot \nu)^- := H_1^- = -\nu^- \cdot \sigma \cdot u_{,t}^-. \tag{6.6}$$

Equation (6.4) can then be rewritten as:

$$-\nu^+ \cdot (\widetilde{\sigma} + \widehat{\sigma})^{\mathrm{T}} \cdot u_{,t}^+ = -\nu^- \cdot \sigma \cdot u_{,t}^-. \tag{6.7}$$

It is clear that, given the jump conditions (6.1) and (6.2), the latter relation is automatically verified.[2]

As we will show in the remainder of this chapter, when modeling a metamaterial's boundary via the relaxed micromorphic model, we only need a finite number of modes in order to exactly verify boundary conditions and, consequently, surface energy conservation. This provides the most powerful simplification of the relaxed micromorphic model with respect to classical homogenization methods, in which infinite modes are needed to satisfy conservation of stress and displacement at the metamaterial's boundary (see [105]). The first step towards the final goal of studying finite-sized complex metastructures, will be made in this chapter by studying the scattering properties of a finite-sized relaxed micromorphic slab.

6.1.2 Boundary conditions for a micromorphic slab embedded between two Cauchy media

Given the macroscopic nature of the boundary conditions presented in section 6.1.1, they can be used to solve more complex large-scale problems, in which multiple interfaces are present. In particular, the boundary conditions to be satisfied at the two interfaces separating the slab from the two Cauchy media in Fig. 6.1(b), are continuity of displacement and continuity of generalized traction. This means that we have four sets of boundary conditions, two on each interface. The finite slab has width h and we assume that the two interfaces are positioned at $x_1 = -h/2$ and $x_1 = h/2$, respectively. The continuity of displacement conditions to be satisfied at the two interfaces of the slab are:[3]

$$u^- = \widetilde{v}, \text{ on } x_1 = -\frac{h}{2}, \qquad \widetilde{v} = u^+, \text{ on } x_1 = \frac{h}{2}. \tag{6.8}$$

As for the continuity of generalized traction, we have:

$$t^- = \widetilde{t}, \text{ on } x_1 = -\frac{h}{2}, \qquad \widetilde{t} = t^+, \text{ on } x_1 = \frac{h}{2}, \tag{6.9}$$

where $t^{\pm} = \sigma^{\pm} \cdot \nu^{\pm}$ are classical Cauchy tractions and $\widetilde{t}$ is again given by (6.3).

[2] An analogous calculation can be done with $L_c > 0$, but in that case boundary conditions on the tangent part of P and of the double force need to be used in order to automatically verify the conservation of energy on the boundary.

[3] We denote by $\widetilde{v}$ the first two components of the micromorphic field v defined in equation (6.20).

6.2 Bulk wave propagation in Cauchy and relaxed micromorphic continua

6.2.1 Isotropic Cauchy continuum

We quickly repeat here the same procedure demonstrated in detail in chapter 4.

We make the plane-wave ansatz for the solution to (2.4):

$$u(x_1, x_2, t) = \widehat{\psi}\, e^{i(\langle k,x\rangle - \omega t)} = \widehat{\psi}\, e^{i(k_1 x_1 + k_2\, x_2 - \omega t)}, \quad \widehat{\psi} \in \mathbb{C}^2, \tag{6.10}$$

where $k = (k_1, k_2)^{\mathrm{T}}$ is the wave vector and ω is the angular frequency.[4] Plugging (6.10) into equation (2.4) we get a 2×2 algebraic system of the form

$$A \cdot \widehat{\psi} = 0, \tag{6.11}$$

where

$$A = \begin{pmatrix} \rho\,\omega^2 - (2\mu+\lambda)\,k_1^2 - \mu\,k_2^2 & -(\mu+\lambda)\;k_1\,k_2 \\ -(\mu+\lambda)\,k_1\,k_2 & \rho\,\omega^2 - (2\mu+\lambda)\,k_2^2 - \mu\,k_1^2 \end{pmatrix}. \tag{6.12}$$

The algebraic system (6.11) has a solution if and only if $\det A = 0$. This is a bi-quadratic polynomial equation which has the following four solutions:

$$k_1^{L,\mathrm{r}} = -\sqrt{\frac{\rho}{2\mu+\lambda}\omega^2 - k_2^2}, \quad k_1^{S,\mathrm{r}} = -\sqrt{\frac{\rho}{\mu}\omega^2 - k_2^2}, \quad k_1^{L,\mathrm{t}} = \sqrt{\frac{\rho}{2\mu+\lambda}\omega^2 - k_2^2}, \quad k_1^{S,\mathrm{t}} = \sqrt{\frac{\rho}{\mu}\omega^2 - k_2^2}, \tag{6.13}$$

where we denote by L and S the longitudinal and shear waves and by r and t whether they are "reflected" or "transmitted", respectively. In a semi-infinite medium, the sign of these solutions must be chosen according to the direction of propagation of the considered wave. We plug the solutions (6.13) into (6.11) to calculate the corresponding eigenvectors

$$\widehat{\psi}^{L,\mathrm{r}} = \begin{pmatrix} 1 \\ -\frac{k_2^{L,\mathrm{r}}}{k_1^{L,\mathrm{r}}} \end{pmatrix}, \widehat{\psi}^{S,\mathrm{r}} = \begin{pmatrix} 1 \\ \frac{k_1^{S,\mathrm{r}}}{k_2^{S,\mathrm{r}}} \end{pmatrix}, \quad \widehat{\psi}^{L,\mathrm{t}} = \begin{pmatrix} 1 \\ \frac{k_2^{L,\mathrm{t}}}{k_1^{L,\mathrm{t}}} \end{pmatrix}, \quad \widehat{\psi}^{S,\mathrm{t}} = \begin{pmatrix} 1 \\ -\frac{k_1^{S,\mathrm{t}}}{k_2^{S,\mathrm{t}}} \end{pmatrix}. \tag{6.14}$$

Normalizing these eigenvectors gives:

$$\psi^{L,\mathrm{r}} := \frac{1}{\left|\widehat{\psi}^{L,\mathrm{r}}\right|}\widehat{\psi}^{L,\mathrm{r}}, \quad \psi^{S,\mathrm{r}} := \frac{1}{\left|\widehat{\psi}^{S,\mathrm{r}}\right|}\widehat{\psi}^{S,\mathrm{r}}, \quad \psi^{L,\mathrm{t}} := \frac{1}{\left|\widehat{\psi}^{L,\mathrm{t}}\right|}\widehat{\psi}^{L,\mathrm{t}}, \quad \psi^{S,\mathrm{t}} := \frac{1}{\left|\widehat{\psi}^{S,\mathrm{t}}\right|}\widehat{\psi}^{S,\mathrm{t}}. \tag{6.15}$$

Then, the general solution to (2.4) can be written as:

$$\begin{aligned} u(x_1, x_2, t) = {} & a^{L,\mathrm{r}}\psi^{L,\mathrm{r}} e^{i\left(k_1^{L,\mathrm{r}} x_1 + k_2^{L,\mathrm{r}}\, x_2 - \omega t\right)} + a^{S,\mathrm{r}}\psi^{S,\mathrm{r}} e^{i\left(k_1^{S,\mathrm{r}} x_1 + k_2^{S,\mathrm{r}}\, x_2 - \omega t\right)} \\ & + a^{L,\mathrm{t}}\psi^{L,\mathrm{t}} e^{i\left(k_1^{L,\mathrm{t}} x_1 + k_2^{L,\mathrm{t}}\, x_2 - \omega t\right)} + a^{S,\mathrm{t}}\psi^{S,\mathrm{t}} e^{i\left(k_1^{S,\mathrm{t}} x_1 + k_2^{S,\mathrm{t}}\, x_2 - \omega t\right)}, \end{aligned} \tag{6.16}$$

where $a^{L,\mathrm{r}}, a^{S,\mathrm{r}}, a^{L,\mathrm{t}}, a^{S,\mathrm{t}} \in \mathbb{C}$ are constants to be determined from the boundary conditions, $k_1^{L,\mathrm{t}} = -k_1^{L,\mathrm{r}}$ and $k_1^{S,\mathrm{t}} = -k_1^{S,\mathrm{r}}$, according to (6.13). Depending on the specific problems which are considered (e.g. semi-infinite media), only some modes may propagate in specific directions.

[4] As we will show in the following, k_2, which is the second component of the wave-number, is always supposed to be known and is given by Snell's law when imposing boundary conditions on a given boundary.

In this case, some of the terms in the sum (6.16) have to be omitted. In particular, if we are considering waves propagating in the $x_1 < 0$ half-space, then the solution to (2.4) reduces to:[5]

$$u(x_1, x_2, t) = a^{L,\mathrm{r}}\psi^{L,\mathrm{r}} e^{i\left(k_1^{L,\mathrm{r}} x_1 + k_2^{L,\mathrm{r}} x_2 - \omega t\right)} + a^{S,\mathrm{r}}\psi^{S,\mathrm{r}} e^{i\left(k_1^{S,\mathrm{r}} x_1 + k_2^{S,\mathrm{r}} x_2 - \omega t\right)}, \tag{6.17}$$

while if we are considering the $x_1 > 0$ half-space, then the solution to (2.4) reduces to:

$$u(x_1, x_2, t) = a^{L,\mathrm{t}}\psi^{L,\mathrm{t}} e^{i\left(k_1^{L,\mathrm{t}} x_1 + k_2^{L,\mathrm{t}} x_2 - \omega t\right)} + a^{S,\mathrm{t}}\psi^{S,\mathrm{t}} e^{i\left(k_1^{S,\mathrm{t}} x_1 + k_2^{S,\mathrm{t}} x_2 - \omega t\right)}. \tag{6.18}$$

6.2.2 Relaxed micromorphic continuum

We start by collecting the unknown fields for the plane-strain case in a new variable:

$$v := (u_1, u_2, P_{11}, P_{12}, P_{21}, P_{22})^{\mathrm{T}}. \tag{6.19}$$

The plane-wave ansatz for this unknown field reads:

$$v = \widehat{\phi}\, e^{i(\langle k, x\rangle - \omega t)} = \widehat{\phi}\, e^{i(k_1 x_1 + k_2 x_2 - \omega\, t)}, \tag{6.20}$$

where $\widehat{\phi} \in \mathbb{C}^6$ is the vector of amplitudes, $k = (k_1, k_2)^{\mathrm{T}} \in \mathbb{C}^2$ is the wave-vector[6] and ω is the angular frequency. We plug this into (3.28) and get an algebraic system of the form

$$\widehat{A}(k_1, k_2, \omega) \cdot \widehat{\phi} = 0, \tag{6.21}$$

where $\widehat{A}(k_1, k_2, \omega) \in \mathbb{C}^{6\times 6}$ is a matrix depending on k_1, k_2, ω and all the material parameters of the plane-strain tetragonal relaxed micromorphic model (see Appendix C1 for an explicit presentation of this matrix). In order for this system to have a solution other than the trivial one, we impose $\det \widehat{A} = 0$.

The equation $\det \widehat{A} = 0$ is a polynomial of order 12 in ω and it involves only even powers of ω. This means that, plotting the roots $\omega = \omega(k)$ gives 6 dispersion curves in the $\omega - k$ plane (see Fig. 6.3). On the other hand, the same polynomial is of order 4 (and bi-quadratic), if regarded as a polynomial of k_1 (k_2 is supposed to be known when imposing boundary conditions) when setting $L_c = 0$. We can write the roots of the characteristic polynomial as:

$$k_1^{(1)}(k_2, \omega), \quad k_1^{(2)}(k_2, \omega), \quad k_1^{(3)}(k_2, \omega) = -k_1^{(1)}(k_2, \omega), \quad k_1^{(4)}(k_2, \omega) = -k_1^{(2)}(k_2, \omega). \tag{6.22}$$

We have verified that, plotting the two functions $k^{(1)}(\omega) := \sqrt{\left(k_1^{(1)}\right)^2 + \left(k_2^{(1)}\right)^2}$ and $k^{(2)}(\omega) := \sqrt{\left(k_1^{(2)}\right)^2 + \left(k_2^{(2)}\right)^2}$ gives the same diagrams as in Fig. 6.3. This means that each of the 2 modes $k^{(i)}$, $i = \{1, 2\}$ actually gives rise to 3 branches in the $k - \omega$ plane.

We plug the solutions (6.22) into (6.21) and calculate the eigenvectors of $\widehat{A}$, which we denote by: $\widehat{\phi}^{(1)}$, $\widehat{\phi}^{(2)}$, $\widehat{\phi}^{(3)}$, $\widehat{\phi}^{(4)}$. We normalize these eigenvectors, thus introducing the normal vectors

$$\phi^{(1)} := \frac{1}{|\widehat{\phi}^{(1)}|}\widehat{\phi}^{(1)}, \quad \phi^{(2)} := \frac{1}{|\widehat{\phi}^{(2)}|}\widehat{\phi}^{(2)}, \quad \phi^{(3)} := \frac{1}{|\widehat{\phi}^{(3)}|}\widehat{\phi}^{(3)}, \quad \phi^{(4)} := \frac{1}{|\widehat{\phi}^{(4)}|}\widehat{\phi}^{(4)}. \tag{6.23}$$

[5] This choice for the sign of k_1 always gives rise to a solution which verifies conservation of energy at the interface. We will show in the following, that this particular choice, which at a first instance is rather intuitive, is not always the correct one when dealing with a relaxed micromorphic medium.

[6] Here again, as in the case of a Cauchy medium, k_2 will be fixed and given by Snell's law when imposing boundary conditions.

Considering a micromorphic medium in which all waves travel simultaneously, the solution to (3.28) is:

$$v(x_1,x_2,t)=\sum_{j=1}^{4}\alpha_j\phi^{(j)}e^{i\left(k_1^{(j)}x_1+k_2^{(j)}\,x_2-\omega t\right)}, \tag{6.24}$$

where $\alpha_j\in\mathbb{C}$ are unknown constants which will be determined from the boundary conditions, $k_1^{(3)}=-k_1^{(1)}$ and $k_1^{(4)}=-k_1^{(3)}$. If, on the basis of the particular interface problem one wants to study only some waves traveling in the considered medium, then the extra waves must be omitted from the sum in (6.24). This means that if we are considering waves traveling in the $x_1>0$ direction, then the solution to (3.28) is given by

$$v(x_1,x_2,t)=\alpha_1\,\phi^{(1)}e^{i\left(k_1^{(1)}x_1+k_2^{(1)}\,x_2-\omega t\right)}+\alpha_2\,\phi^{(2)}e^{i\left(k_1^{(2)}x_1+k_2^{(2)}\,x_2-\omega t\right)}, \tag{6.25}$$

while if the wave is traveling in the $x_1<0$ direction, the solution to (3.28) is given by

$$v(x_1,x_2,t)=\alpha_3\,\phi^{(3)}e^{i\left(k_1^{(3)}x_1+k_2^{(3)}\,x_2-\omega t\right)}+\alpha_4\,\phi^{(4)}e^{i\left(k_1^{(4)}x_1+k_2^{(4)}\,x_2-\omega t\right)}. \tag{6.26}$$

6.3 Reflection and transmission at the single interface

In this section, we study the two-dimensional, plane-strain, time-harmonic scattering problem from an anisotropic micromorphic half-space (see equations (3.28)), occupying the region $x_1>0$ of Fig. 6.1(a). With reference to Fig. 6.1(a), the half-space $x_1<0$ is filled with a linear elastic Cauchy continuum, governed by equation (2.4). For simplicity, we assume that the incident wave hits the interface at the origin. Considering that reflected waves only travel in the $x_1<0$ Cauchy half-plane, only negative solutions for the k_1's must be kept in equation (4.18), so that the total solution in the left half-space is

$$\begin{aligned}u^-(x_1,x_2,t)&=a^{L/S,\mathrm{i}}\psi^{L/S,\mathrm{i}}e^{i\left(\langle x,k^{L/S,\mathrm{i}}\rangle-\omega t\right)}+a^{L,\mathrm{r}}\psi^{L,\mathrm{r}}e^{i\left(\langle x,k^{L,\mathrm{r}}\rangle-\omega t\right)}+a^{S,\mathrm{r}}\psi^{S,\mathrm{r}}e^{i\left(\langle x,k^{S,\mathrm{r}}\rangle-\omega t\right)}\\&=:u^{L/S,\mathrm{i}}+u^{L,\mathrm{r}}+u^{S,\mathrm{r}},\end{aligned} \tag{6.27}$$

where we write L or S in the incident wave depending on whether the wave is longitudinal or shear and i and r in the exponents stand for "incident" and "reflected". Analogously, the solution on the right half-space, which is occupied by a relaxed micromorphic medium, is[7]

$$v(x_1,x_2,t)=\alpha_1\,\phi^{(1)}e^{i\left(\langle x,k^{(1)}\rangle-\omega t\right)}+\alpha_2\,\phi^{(2)}e^{i\left(\langle x,k^{(2)}\rangle-\omega t\right)}, \tag{6.28}$$

where we have kept only terms with positive k_1's in the solution (6.22), since transmitted waves are supposed to propagate in the $x_1>0$ half-plane.

Since the incident wave is always propagative, the polarization and wave-vectors are given by:

$$\psi^{L,\mathrm{i}}=(\sin\theta^L,-\cos\theta^L)^{\mathrm{T}},\quad k^L=|k^L|(\sin\theta^L,-\cos\theta^L)^{\mathrm{T}}, \tag{6.29}$$

$$\psi^{S,\mathrm{i}}=(\cos\theta^S,\sin\theta^S)^{\mathrm{T}},\qquad k^S=|k^S|(\sin\theta^S,-\cos\theta^S)^{\mathrm{T}}, \tag{6.30}$$

where, according to (4.18), $|k^L|=\frac{\omega}{c_L}$ and $|k^S|=\frac{\omega}{c_S}$, with $c_L=\sqrt{(2\mu+\lambda)/\rho}$ and $c_S=\sqrt{\mu/\rho}$ the longitudinal and shear speeds of propagation and θ^L and θ^S the angles of incidence when the wave is longitudinal or shear, respectively (see Fig. 6.1 and [2] for a more detailed exposition).

[7] We suppose here that, for the transmitted wave we have to consider only the positive solutions of (6.22).

The continuity of displacement condition (6.1) provides us, as shown in detail in chapter 4 with the generalized Snell's law for the case of a Cauchy/relaxed micromorphic interface:

$$\boxed{\begin{array}{c} k_2^{L/S,\mathrm{i}} = k_2^{L,\mathrm{r}} = k_2^{S,\mathrm{r}} = k_2^{(1)} = k_2^{(2)}. \\ \textbf{Generalized Snell's Law} \end{array}} \tag{6.31}$$

As for the flux, the normal outward pointing vector to the surface (the x_2 axis) is $\nu = (-1, 0)$. This means that in expressions (2.12) and (3.76) for the fluxes, we need only take into account the first component. According to our definitions (2.12) and (3.76) (remembering that $L_c = 0$ and that we impose the plane-strain restriction), we have

$$H_1^- = -u_{i,t}\,\sigma_{i1}, \qquad H_1^+ = -v_{i,t}\,(\widetilde{\sigma}_{i1} + \widehat{\sigma}_{i1})\,, \quad i = 1, 2. \tag{6.32}$$

Having calculated the "transmitted" flux, we can now look at the reflection and transmission coefficients for the case of a Cauchy/relaxed micromorphic interface. We define[8]

$$J^{\mathrm{i}} = \frac{1}{T}\int_0^T H^{\mathrm{i}}(x,t)dt, \quad J^{\mathrm{r}} = \frac{1}{T}\int_0^T H^{\mathrm{r}}(x,t)dt, \quad J^{\mathrm{t}} = \frac{1}{T}\int_0^T H^{\mathrm{t}}(x,t)dt, \tag{6.33}$$

where T is the time period of the considered harmonic waves, $H^{\mathrm{i}} = H_1^-(u^{L/S,\mathrm{i}})$, $H^{\mathrm{r}} = H_1^-(u^{L,\mathrm{r}} + u^{S,\mathrm{r}})$ and $H^{\mathrm{t}} = H_1^+(v)$, with H_1^+ and H_1^- defined in (6.32). Then the reflection and transmission coefficients are

$$\mathcal{R} = \frac{J^{\mathrm{r}}}{J^{\mathrm{i}}}, \quad \mathcal{T} = \frac{J^{\mathrm{t}}}{J^{\mathrm{i}}}. \tag{6.34}$$

Since the system is conservative, we must have that $\mathcal{R} + \mathcal{T} = 1$.

6.4 Reflection and transmission at a relaxed micromorphic slab

As pointed out, in this case there are three media: the first Cauchy half-space, the anisotropic relaxed micromorphic slab and the second Cauchy half-space. The two Cauchy half-spaces are denoted by $-$ and $+$, while the quantities considered in the slab have their own notation.

The solution on the first Cauchy half space is given, as in the case of a single interface, by

$$u^-(x_1,x_2,t) = a^{L/S,\mathrm{i}}\psi^{L/S,\mathrm{i}}e^{i\left(\langle x,k^{L/S,\mathrm{i}}\rangle-\omega t\right)} + a^{L,\mathrm{r}}\psi^{L,,\mathrm{r}}e^{i\left(\langle x,k^{L,,\mathrm{r}}\rangle-\omega t\right)} + a^{S,\mathrm{r}}\psi^{S,\mathrm{r}}e^{i\left(\langle x,k^{S,\mathrm{r}}\rangle-\omega t\right)}. \tag{6.35}$$

In the case of a relaxed micromorphic slab, when solving the eigenvalue problem we must select and keep all the roots for k_1, as given in (6.22), both positive and negative. This is due to the fact that there are waves which transmit in the micromorphic part from the first interface ($x_1 = -h/2$), upon which the incident wave hits and waves which reflect on the second interface ($x_1 = h/2$). This means that the solution of the PDEs in the slab is

$$v(x_1,x_2,t) = \alpha_1\,\phi^{(1)}e^{i\left(\langle x,k^{(1)}\rangle-\omega t\right)} + \alpha_2\,\phi^{(2)}e^{i\left(\langle x,k^{(2)}\rangle-\omega t\right)} + \alpha_3\,\phi^{(3)}e^{i\left(\langle x,k^{(3)}\rangle-\omega t\right)} + \alpha_4\,\phi^{(4)}e^{i\left(\langle x,k^{(4)}\rangle-\omega t\right)}, \tag{6.36}$$

where $k_1^{(1)} = -k_1^{(3)}$ and $k_1^{(2)} = -k_1^{(4)}$ (see section 6.2.2). Finally, the solution on the right Cauchy half-space is

$$u^+(x_1,x_2,t) = a^{L,\mathrm{t}}\psi^{L,\mathrm{t}}e^{i\left(\langle x,k^{L,\mathrm{t}}\rangle-\omega t\right)} + a^{S,\mathrm{t}}\psi^{S,\mathrm{t}}e^{i\left(\langle x,k^{S,\mathrm{t}}\rangle-\omega t\right)}. \tag{6.37}$$

[8] In order to easily compute these coefficients in the numerical implementation of the code, we employ Lemma 1 given in Appendix B2

The continuity of displacement conditions (6.8) again imply a generalized form of Snell's law for the case of the micromorphic slab:

$$\boxed{k_2^{L/S,i} = k_2^{L,\mathrm{r}} = k_2^{S,\mathrm{r}} = k_2^{(1)} = k_2^{(2)} = k_2^{(3)} = k_2^{(4)} = k_2^{L,\mathrm{t}} = k_2^{S,\mathrm{t}}.} \quad (6.38)$$

Generalized Snell's Law in a micromorphic slab

In order to define the reflection and transmission coefficients in the case of the anisotropic slab, we follow the same reasoning as for the single interface. However, in this case, the transmitted flux is defined as the flux on the right of the second interface, which is occupied by an isotropic Cauchy medium.

In this case, the reflected flux is evaluated at $x_1 = -h/2$ and the transmitted flux at $x_1 = h/2$. Both the reflected and the transmitted fields propagate in isotropic Cauchy media, so that the quantities $J^{\mathrm{i}}, J^{\mathrm{r}}, J^{\mathrm{t}}$ defined in (6.33) are given by (see [2])

$$J^{\mathrm{i}}_{\mathrm{slab}} = \frac{1}{2}\mathrm{Re}\left(\left[(2\mu^- + \lambda^-)\left|\psi_1^{j,\mathrm{i}}\right|^2 k_1^{j,\mathrm{i}} + \lambda^-\left(\psi_1^{j,\mathrm{i}}\right)^* \psi_2^{j,\mathrm{i}} k_2^{j,\mathrm{i}} + \mu^-\left(\psi_1^{\mathrm{i}}\left(\psi_2^{j,\mathrm{i}}\right)^* k_2^{j,\mathrm{i}} + \left|\psi_2^{j,\mathrm{i}}\right|^2 k_1^{j,\mathrm{i}}\right)\right]\left|a^{j,\mathrm{i}}\right|^2 \omega\right), \quad (6.39)$$

$$J^{\mathrm{r}}_{\mathrm{slab}} = \sum_{j\in\mathcal{J}} \frac{1}{2}\mathrm{Re}\left(\left[(2\mu^- + \lambda^-)\left|\psi_1^{j,\mathrm{r}}\right|^2 k_1^{j,\mathrm{r}} + \lambda^-\left(\psi_1^{j,\mathrm{r}}\right)^* \psi_2^{j,\mathrm{r}} k_2^{j,\mathrm{i}} + \mu^-\left(\psi_1^{j,\mathrm{r}}\left(\psi_2^{j,(2)}\right)^* k_2^{j,\mathrm{i}}\left|\psi_2^{j,\mathrm{r}}\right|^2 k_1^{j,\mathrm{r}}\right)\right]\left|a^{j,\mathrm{r}}\right|^2 \omega\right), \quad (6.40)$$

$$J^{\mathrm{t}}_{\mathrm{slab}} = \sum_{j\in\mathcal{J}} \frac{1}{2}\mathrm{Re}\left(\left[(2\mu^+ + \lambda^+)\left|\psi_1^{j,\mathrm{t}}\right|^2 k_1^{j,\mathrm{t}} + \lambda^+\left(\psi_1^{j,\mathrm{t}}\right)^* \psi_2^{j,\mathrm{t}} k_2^{j,\mathrm{i}} + \mu^+\left(\psi_1^{j,\mathrm{t}}\left(\psi_2^{j,\mathrm{t}}\right)^* k_2^{j,\mathrm{i}} + \left|\psi_2^{j,\mathrm{t}}\right|^2 k_1^{j,\mathrm{t}}\right)\right]\left|a^{j,\mathrm{t}}\right|^2 \omega\right), \quad (6.41)$$

where, $\mathcal{J} \in \{L, S\}$, $a^{j,\mathrm{i}}, a^{j,\mathrm{r}}, a^{j,\mathrm{t}} \in \mathbb{C}$ and $\psi^{j,\mathrm{i}}, \psi^{j,(2)}, \psi^{j,\mathrm{t}} \in \mathbb{C}^2$ with $\mathcal{J} \in \{L, S\}$, are the amplitudes and polarization vectors for incident, reflected and transmitted waves, respectively (see also equation (6.15)), μ^-, λ^- and μ^+, λ^+ are the Lamé parameters of the left and right Cauchy half-spaces, respectively.

So, the reflection and transmission coefficients for the slab are

$$\mathcal{R}_{\mathrm{slab}} = \frac{J^{\mathrm{r}}_{\mathrm{slab}}}{J^{\mathrm{i}}_{\mathrm{slab}}}, \quad \mathcal{T}_{\mathrm{slab}} = \frac{J^{\mathrm{t}}_{\mathrm{slab}}}{J^{\mathrm{i}}_{\mathrm{slab}}}. \quad (6.42)$$

Since the system is conservative, we must have $\mathcal{R}_{\mathrm{slab}} + \mathcal{T}_{\mathrm{slab}} = 1$.

6.5 Reflective properties of a micro-structured slab

Here, we consider the scattering of in-plane elastic waves from a slab containing cross like holes drilled in an isotropic elastic material (see Fig. 6.2(a)). The holes in the micro-structured slab are arranged according to a truncated square lattice, i.e. a finite number N of cells in the x_1 direction and an infinite number of cells in the x_2 direction.

We consider an incident time-harmonic plane wave

$$u^{j,\mathrm{i}}(x,t) = \bar{u}^{j,\mathrm{i}}(x)e^{-i\omega t} = d^j\, e^{i\langle k^j, x\rangle - i\omega t}, \quad (6.43)$$

where the index $j \in \{L, S\}$ denotes longitudinal and shear waves, respectively. Accordingly, $k^j = \omega/c_j(\sin\theta, -\cos\theta, 0)^{\mathrm{T}}$, with $j \in \{L, S\}$ and θ the angle of incidence, $c_L = \sqrt{(\lambda_{\mathrm{Al}} + 2\mu_{\mathrm{Al}})/\rho_{\mathrm{Al}}}$ and $c_S = \sqrt{\mu_{\mathrm{Al}}/\rho_{\mathrm{Al}}}$ are the longitudinal and shear wave speeds for aluminum. The Lamé parameters of aluminum are $\lambda_{\mathrm{Al}} = 5.11 \times 10^{10}$ Pa and $\mu_{\mathrm{Al}} = 2.63 \times 10^{10}$ Pa, and the density of

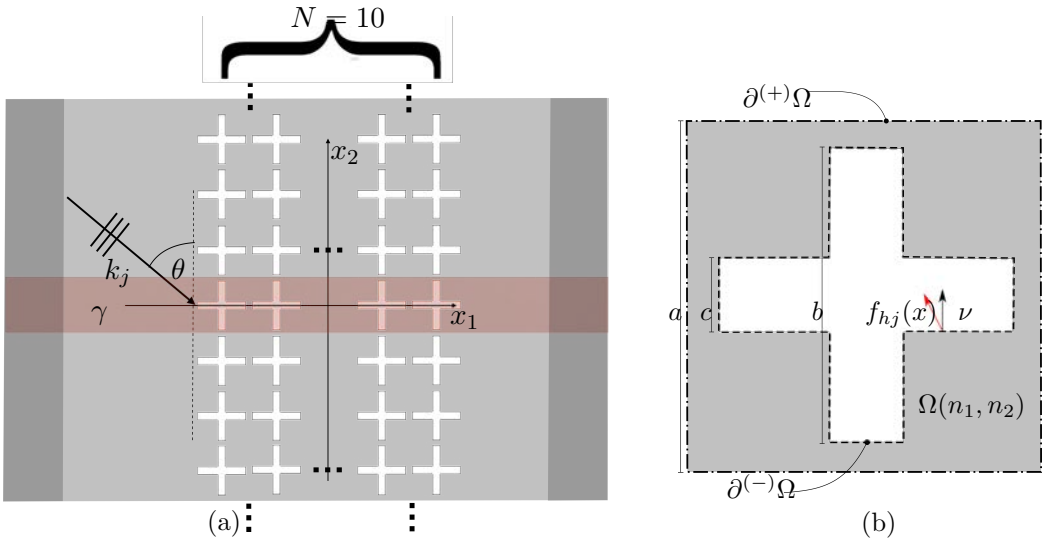

Figure 6.2: Panel (a) is a schematic representation of a slab of cross like-holes which is finite in the x_1-direction ($N = 10$ number of unit cells) and periodic in the x_2-direction. The red shadows represent the finite element domain γ where the scattering problem is set up and solved. The domain γ contains two perfectly matched layers (darker red regions at the sides of the rectangular domain γ). Panel (b) is a schematic representation of a unit cell $\Omega(n_1, n_2)$, for a generic pair of integers (n_1, n_2). The inner boundary $\partial^{(-)}\Omega(n_1, n_2)$ (dashed black line), the outer boundary $\partial^{(+)}\Omega(n_1, n_2)$ (dot-dashed black line), and the normal and traction vectors along $\partial^{(-)}\Omega(n_1, n_2)$ (black and red arrow lines, respectively) are also shown.

aluminum is $\rho_{\text{Al}} = 2700\ \text{Kg/m}^3$. The Lamé parameters define uniquely the fourth order stiffness tensor $\mathbb{C}_{\text{Al}}$, whose Voigt representation is

$$\tilde{\mathbb{C}}_{\text{Al}} = \begin{pmatrix} 2\mu_{\text{Al}} + \lambda_{\text{Al}} & \lambda_{\text{Al}} & \star & 0 & 0 & 0 \\ \lambda_{\text{Al}} & 2\mu_{\text{Al}} + \lambda_{\text{Al}} & \star & 0 & 0 & 0 \\ \star & \star & \star & 0 & 0 & 0 \\ 0 & 0 & 0 & \star & 0 & 0 \\ 0 & 0 & 0 & 0 & \star & 0 \\ 0 & 0 & 0 & 0 & 0 & \mu_{\text{Al}} \end{pmatrix}, \tag{6.44}$$

where the stars denote the components which do not intervene in the plane-strain case. In equation (6.43) we have introduced the polarization vectors d^j, $j \in \{L, S\}$ of amplitude d_0 for longitudinal and shear waves, defined as $d^L = d_0(\sin\theta, -\cos\theta, 0)^{\text{T}}$ and $d^S = d_0(\cos\theta, \sin\theta, 0)^{\text{T}}$, respectively. The scattering problem in terms of the elastic plane-strain field $u^j \equiv u^j(x, t)$, $j \in \{L, S\}$, in the micro-structured material, according to linear elasticity, can be written as

$$\begin{cases} \rho_{\text{Al}}\ u^j_{,tt} = \ \text{Div}\left(\mathbb{C}_{\text{Al}}\ \text{sym}\ \nabla u^j\right), \quad x \in\ \Omega_0(n_1, n_2) \\ \\ f(u^j) = 0, \quad x \in \partial^{(-)}\Omega(n_1, n_2), \quad \forall n_1 \in \{1, \cdots, N\} \quad \text{and} \quad \forall n_2 \in \mathbb{Z}, \end{cases} \tag{6.45}$$

where we have introduced the traction vectors

$$f(u^j) = (\mathbb{C}_{\text{Al}} \text{ sym } \nabla u^j) \cdot \nu, \quad j \in \{L, S\}, \tag{6.46}$$

ν being the normal unit vector (see black arrow line in Fig. 6.2(b)) to the cross-like holes boundaries $\partial^{(-)}\Omega(n_1, n_2)$ and where we denote by Ω_0 the part of the domain Ω, which is non-empty (occupied by aluminum). The elastic field in (6.45) can be written according to the scattering time-harmonic ansatz

$$u^j(x,t) = \left(\bar{u}^{j,\text{i}}(x) + \bar{u}^{j,\text{sc}}(x)\right) e^{-i\omega t}, \quad j \in \{L, S\}, \tag{6.47}$$

where $\bar{u}^{j,\text{i}}$ has been introduced in equation (6.43) and $\bar{u}^{j,\text{sc}}$ is the so-called scattered solution. By linearity of the traction vector (6.46), and using equation (6.47), we obtain

$$f(u^j(x,t)) = \left[f(\bar{u}^{j,\text{i}}(x)) + f(\bar{u}^{j,\text{sc}}(x))\right] e^{-i\omega t} = 0, \quad j \in \{L, S\}. \tag{6.48}$$

Using the fact that $u^{j,\text{i}}(x,t)$ is a solution of the PDE in equation (6.45), together with equation (6.48), the PDEs system (6.45) can be rewritten in a time-harmonic form with respect to the field $u^{j,\text{sc}}(x)$, as:

$$\begin{cases} -\omega^2 \rho_{\text{Al}}\, \bar{u}^{j,\text{sc}} = \text{ Div}\left(\mathbb{C}_{\text{Al}} \text{ sym } \nabla \bar{u}^{j,\text{sc}}\right), \quad x \in \ \Omega_0 \\ \\ f(\bar{u}^{j,\text{sc}}) \equiv (\mathbb{C}_{\text{Al}} \text{ sym } \nabla \bar{u}^{j,\text{sc}}) \cdot \nu = -f(\bar{u}^{j,\text{i}}), \quad x \in \partial^{(-)}\Omega(n_1, n_2), \quad \forall n_1 \in \{1, \cdots, N\} \quad \text{and} \quad \forall n_2 \in \mathbb{Z}, \end{cases} \tag{6.49}$$

with $j \in \{L, S\}$ and where we have canceled out time-harmonic factors. The analytical expressions for the boundary conditions for the scattered field (see right-hand side of the boundary conditions in equation (6.49)) are given component-wise as:

$$\begin{aligned} f(\bar{u}^{j,\text{i}}) \cdot e_1 &:= f^j_{\text{v}}(x) = (\mathbb{C}_{\text{Al}} \text{ sym } \nabla \bar{u}^{j,\text{i}}) \cdot e_1 \\ &= \frac{i\omega\rho}{c_j} \left\{ \left[c_L^2 \sin\theta\, d_1^{j,\text{i}} - (c_L^2 - 2c_S^2)\cos\theta\, d_2^{j,\text{i}} \right] e_1 + c_S^2 \left[-\cos\theta\, d_1^{j,\text{i}} + \sin\theta\, d_2^{j,\text{i}} \right] e_2 \right\} e^{i\langle k^{j,\text{i}}, x\rangle}, \end{aligned} \tag{6.50}$$

with $j \in \{L, S\}$ for vertical boundaries of $\partial^{(-)}\Omega(n_1, n_2)$ with normal vector parallel to e_1 (see Fig. 6.2(b)). Similarly, for vertical boundaries with normal vector anti-parallel to e_1 we have $f(\bar{u}^{j,\text{i}}) = -f^j_{\text{v}}(x)$. In addition, for horizontal boundaries in $\partial^{(-)}\Omega(n_1, n_2)$ whose normal vector is parallel to e_2 we have:

$$\begin{aligned} f(\bar{u}^{j,\text{i}}) \cdot e_2 &:= f^j_{\text{h}}(x) = (\mathbb{C}_{\text{Al}} \text{ sym } \nabla \bar{u}^{j,\text{i}}) \cdot e_2 \\ &= \frac{i\omega\rho}{c_j} \left\{ \left[(c_L^2 - 2c_S^2) \sin\theta\, d_1^{j,\text{i}} - c_L^2 \cos\theta\, d_2^{j,\text{i}} \right] e_2 + c_S^2 \left[-\cos\theta\, d_1^{j,\text{i}} + \sin\theta\, d_2^{j,\text{i}} \right] e_1 \right\} e^{i\langle k^{j,\text{i}}, x\rangle}, \end{aligned} \tag{6.51}$$

with $j \in \{L, S\}$. Similarly, for vertical boundaries with normal vector anti-parallel to e_2 we have $f(\bar{u}^{j,\text{i}}) = -f^j_{\text{h}}(x)$.

6.5.1 Bloch-Floquet conditions

We recall that the primitive vectors of a square lattice are defined as:

$$a_1 = a\, e_1, \quad \text{and} \quad a_2 = a\, e_2, \tag{6.52}$$

where a is the side of the unit-cell (see Fig. 6.2(b)). Since the scatterers (i.e. the cross-like holes) are periodic in the x_2-direction, the displacement field in equation (6.47) satisfies Bloch-Floquet boundary conditions

$$\bar{u}^{j,\mathrm{sc}}(x + n_2\ a_2) = e^{in_2k_2a}\,\bar{u}^{j,\mathrm{sc}}(x), \quad \text{for} \quad x \in \gamma, \quad \text{and} \quad n_2 \in \mathbb{Z}, \tag{6.53}$$

where k_2 is the component along the x_2-direction of the wave vector k. The value of k_2 is known and should be equal, given the considered geometry represented in Fig. 6.2(a), to the second component of the wave vector of the incident wave. This requirement is essential in order to construct a solution which satisfies the prescribed boundary conditions within a micro-structured medium which is periodic in one dimension, i.e. in a layered micro-structured medium (see e.g. [86]). This, of course, is the well known Snell's law governing the refraction of waves at the interface between two half-spaces with different material parameters which we derived in (4.35) (see the book by Leckner [50] for a mathematical introduction encompassing several physical scenarios). As it is customary in Floquet theory of PDEs with periodic coefficients, we can obtain the solution of the PDEs system (6.49), by solving the problem in its period (i.e. the red strip in Fig. 6.2(a) here denoted as γ) provided that the Bloch-Floquet condition (6.53) on the scattered field is satisfied.

Although the x_1 extension of the domain γ is infinite in our model problem, in the finite-element implementation of the boundary value problem we are of course restricted to finite computational domains. In order to annihilate the reflection from the sides of γ with constant x_1, we use perfectly matched layers [11] away from the microstructure.

6.5.2 Reflectance

The time-averaged Poynting vector associated with a 2D time-harmonic displacement field $u(x,t) = \bar{u}(x)\,e^{-i\omega t}$ is defined as [2, 6]

$$F = -\frac{\omega}{2}\,\mathrm{Re}\,(i\sigma \cdot u^*)\,, \tag{6.54}$$

where "$*$" denotes complex conjugation and $\sigma = \mathbb{C}_{\mathrm{Al}}\,\mathrm{sym}\,\nabla u$ is the Cauchy stress tensor associated with the elastic field u. From equation (6.54), and using equation (6.43), it follows that the energy flux associated with the incident displacement field (6.43) is

$$F^{j,\mathrm{i}} = \frac{1}{2}\rho\, c_j |d^{j,\mathrm{i}}|^2 \frac{k^{j,\mathrm{i}}}{|k^{j,\mathrm{i}}|}, \quad j \in \{L, S\}. \tag{6.55}$$

Similarly, we define the flux $F^{j,\mathrm{sc}}$ of the scattered field to be as in equation (6.54) with $u(x,t) = \bar{u}^{j,\mathrm{sc}}(x)e^{-i\omega t}$, where $\bar{u}^{j,\mathrm{sc}}$ is the solution of the PDEs system (6.49)). The reflectance, i.e. the ratio of reflected energy and incident energy passing through a vertical line of length a, is

$$\begin{aligned}\mathcal{R}^j &= \frac{1}{\langle F^{j,\mathrm{i}}, e_1\rangle}\frac{1}{a}\int_{-a/2}^{a/2}\langle F^{j,\mathrm{sc}}\big|_{x_1 \ll -aN/2}, e_1\rangle\,\mathrm{d}x_2, \\ &= \frac{2}{\rho\, c_j |d^{j,\mathrm{i}}|^2 \sin(\theta)}\frac{1}{a}\int_{-a/2}^{a/2}\langle F^{j,\mathrm{sc}}\big|_{x_1 \ll -aN/2}, e_1\rangle\,\mathrm{d}x_2, \quad j \in \{L, S\}.\end{aligned} \tag{6.56}$$

The reflectance associated with incident shear waves ($\mathcal{R}^S$) differs from that associated with incident longitudinal waves ($\mathcal{R}^L$). The Poynting vector is evaluated at a given $x_1 \ll -aN/2$ away

from the slab to avoid the contribution from the near elastic field close to the microstructure. Provided the condition $x_1 \ll -aN/2$ is satisfied, we have verified that the reflectance (6.56) does not depend on the exact value of x_1.

6.6 Results and discussion

In this section we present the comparison between the refractive behavior of the finite metamaterial's slab, as modeled in *Comsol Multiphysics*^{TM} (see Fig.6.2) and the relaxed micromorphic model (see Fig. 6.1). We also provide the results concerning the relaxed micromorphic single interface, which will be seen as an average behavior with respect to the micromorphic slab of finite size. To this end, we chose the material parameters of the relaxed micromorphic model as in Table 6.1.

λ_e	μ_e	μ_e^*	λ_{micro}	μ_{micro}	μ^*_{micro}	μ_c	L_c	λ_{macro}	μ_{macro}	μ^*_{macro}
[GPa]	[GPa]	[GPa]	[GPa]	[GPa]	[GPa]	[GPa]	[m]	[GPa]	[GPa]	[GPa]
2.33	10.93	0.67	5.27	10.28	8.33	$2.26 \cdot 10^{-3}$	0	1.74	5.89	0.62

ρ	η_1	η_2	η_3	η_1^*	$\overline{\eta}_1$	$\overline{\eta}_2$	$\overline{\eta}_3$	$\overline{\eta}_1^*$
$\left[\text{kg/m}^3\right]$	[kg/m]	[kg/m]	[kg/m]	[kg/m]	[kg/m]	[kg/m]	[kg/m]	[kg/m]
1485	$8.6 \cdot 10^{-5}$	$1 \cdot 10^{-7}$	$0.86 \cdot 10^{-5}$	$3.27 \cdot 10^{-5}$	10^{-5}	$2 \cdot 10^{-4}$	$2.5 \cdot 10^{-8}$	$2.85 \cdot 10^{-5}$

Table 6.1: Summary of the numerical values for the elastic (top) and inertia (bottom) parameters of the tetragonal relaxed micromorphic model in the 2D plane-strain case. The macroscopic parameters of the resulting homogenized Cauchy material (see [2, 29]) are also provided (top right).

The choice of the metamaterial parameters is made according to the procedure presented in [29], which allows to determine the parameters of the relaxed micromorphic model on a specific metamaterial by an inverse approach. This fitting procedure is based on the determination of the elastic parameters of the relaxed micromorphic model via numerical static tests on the unit cell and of the remaining inertia parameters via a simple inverse fitting of the dispersion curves on the analogous dispersion patterns as obtained by Bloch-Floquet analysis (see [29] for details). The fitting of the bulk dispersion curves for the periodic metamaterial, whose unit cell is shown in Fig. 6.2(b), is presented in Fig. 6.3.

The choice of parameters presented in Table 6.1 differs from Table 5.2. This is mainly due to the fact that when we performed the fitting procedure for the following results, we had an additional fine-tuning tool: the reflection coefficient. Given the reflection coefficient provided by direct discrete numerical simulations, we were able to calibrate the parameters of the relaxed micromorphic model in such a way as to (almost) perfectly capture the behavior of this new curve. An additional difference from the fitting performed in the previous chapter, is the range of frequency, where we present our results. It became clear that the discrete numerical simulations performed in *Comsol Multiphysics*^{TM} were unable to provide convergent results for the reflection coefficient at very high frequencies ($\omega \geq 1.74$ rad/sec). We thus chose to neglect the mode which

has a cut-off frequency higher than this limit. A possible way out of this issue is to introduce additional degrees of freedom in the energy densities, which will generate one Shear-like mode in higher frequencies and will more accurately fit the dispersion diagram. This is still an open question for forthcoming works, which is being worked upon and, as such, we limit our discussion on frequencies lower than 1.74 rad/sec.

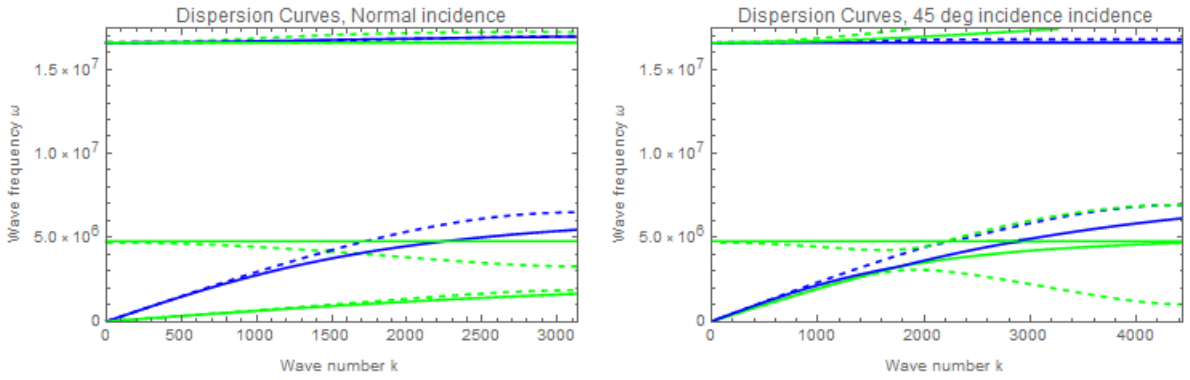

(a) (b)

Figure 6.3: Dispersion diagrams for normal (a) and 45 degrees (b) incidence. The solid curves are obtained via the tetragonal anisotropic relaxed micromorphic model, while the dashed curves are issued by Bloch-Floquet analysis. In panel (a), green color stands for modes which are mostly activated by a shear incident wave, while blue color indicates modes which are mostly activated by a longitudinal incident wave. This uncoupling between L and S activated modes at normal incidence is analytically checked in the relaxed micromorphic model and only approximate for Bloch-Floquet modes. In panel (b), we keep the same coloring, but all curves are coupled together, which means that L and S incident waves may simultaneously activate all modes.

We checked that a sort of distinction between modes which are activated by an L or S incident wave can be made for an incident wave which is orthogonal to the interface. This is exactly true for the relaxed micromorphic model, but an analogous trend can be found for Bloch-Floquet modes at least for the lower frequency modes (before the band-gap). The uncoupling between L and S activated modes is present only for $\theta = 0$ (and, by symmetry, $\theta = \pi/2$), but is lost for any other direction of propagation. In general, for any given frequency, all modes which are pertinent at that frequency may be simultaneously activated by an L or S incident wave (excluding the particular case of normal incidence). Nevertheless, we will show that this uncoupling hypothesis can be retained with little error for angles of incidence which are close to normal incidence.

Once the bulk properties of the considered metamaterial, as modeled by the relaxed micromorphic model, have been established, they can be used to study the scattering problems presented before.

6.6.1 Scattering at a relaxed micromorphic slab

We start by presenting the reflection coefficient of the relaxed micromorphic slab as a function of the frequency for two fixed directions of propagation of the incident wave ($\theta = \frac{\pi}{2}$ and $\theta = \frac{\pi}{4}$) and for both longitudinal and shear incident waves.

Figure 6.4 shows the behavior of the reflection coefficient for the considered microstructured slab in the case of a longitudinal incident wave and for normal incidence (Fig. 6.4(a)) as well as for incidence at 45° (Fig. 6.4(b)). The black dashed line is the solution issued via the

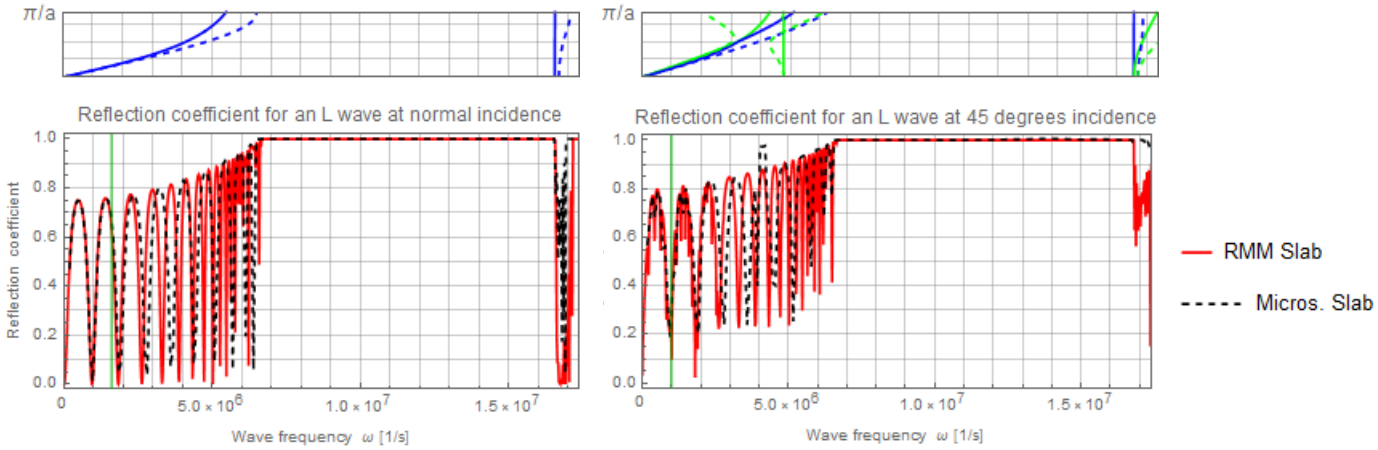

(a) (b)

Figure 6.4: Reflection coefficient at the relaxed micromorphic slab for an incident L wave and for two directions of propagation $\theta = \pi/2$ (normal incidence) (a) and $\theta = \pi/4$ (b). The red curve is generated by the analytical tetragonal relaxed micromorphic model and the black dashed line indicates the microstructured model. The green vertical lines denote the long-wave limit, below which the relaxed micromorphic model is equivalent to a homogenized Cauchy model. The dispersion diagrams for $\theta = \pi/2$ and $\theta = \pi/4$, given in Fig. 6.3 are also rotated and displayed on the top of each picture to allow for a better interpretation of results.

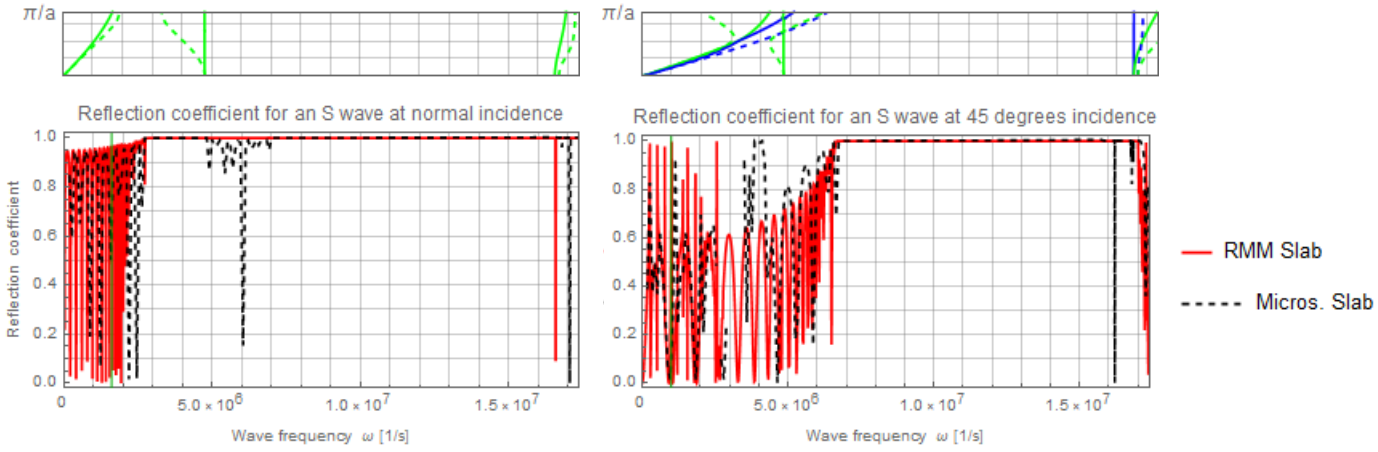

(a) (b)

Figure 6.5: Reflection coefficient at the relaxed micromorphic slab for an incident S wave and for two directions of propagation $\theta = \pi/2$ (normal incidence) (a) and $\theta = \pi/4$ (b).

microstructured model obtained by coding all the details of the unit cell presented in section 6.5. The red continuous line is obtained by solving the relaxed micromorphic problem presented in section 6.4, using the software Mathematica.

It is immediately evident that the relaxed micromorphic model is able to capture the overall behavior of the reflection coefficient for a very wide range of frequencies. More particularly, for lower frequencies and up to the band-gap region, oscillations of the reflection coefficient due to the finite size of the slab are observed in both models. The band-gap region is also correctly described and corresponds to the frequency interval for which complete reflection ($\mathcal{R} = 1$) is

observed.

After the band-gap region, a characteristic frequency can be identified corresponding to which almost complete transmission occurs. This phenomenon is related to internal resonances at the level of the microstructure. It is easy to see that the relaxed micromorphic model is able to correctly describe also the internal resonance phenomenon. The internal resonance is clearly visible in both the discrete and the relaxed micromorphic model at normal incidence. It is, however, lost in the discrete simulation at 45° notwithstanding the presence of a zero group velocity mode in both models. Similar arguments can be carried out for an S incident wave with reference to Fig. 6.5.

In addition to the comments carried out for an L incident wave, we remark in Fig. 6.5(a) the presence of a spurious internal resonance in the lower part of the band-gap for the relaxed micromorphic model. This spurious resonance can be eliminated by activating the non-locality of the model by setting $L_c > 0$. In this case, the moderate transmission present in Fig. 6.5(a) before the band-gap can be reproduced. More details about non-localities will be given in forthcoming papers. This moderate transmission observed in the microstructured simulations are due to the imperfect uncoupling of the S (green) modes from the L (blue) acoustic mode in the Bloch-Floquet dispersion diagram. Thus, there exist some small frequency ranges, for which the L acoustic mode can be activated also by an S incident wave. The associated transmission remains very small.

At this point, in order to fully present the potentialities of the relaxed micromorphic model, we depict in Figures 6.6 and 6.7 the transmission coefficient ($\mathcal{T} = 1 - \mathcal{R}$) as a function of both the angle and frequency of the longitudinal incident wave for both the relaxed micromorphic and the microstructured models.

Figure 6.6 shows the broadband transmission coefficient's behavior for an L incident wave as a function of the frequency and angle of incidence. We observe an excellent agreement between the continuous and discrete simulation for frequencies lower than the band-gap. Transmission is principally allowed by the blue acoustic mode for all directions of propagation. Even if there exists some coupling at non-orthogonal incidence with the other lower frequency modes, the blue acoustic mode is the one which is predominantly activated by an L incident wave and it is, to a big extent, responsible for the transmission across the metamaterial slab. The band-gap region is also correctly described. The validation of the fitting performed on higher frequencies was impossible due to the difficulty of establishing the convergence of the microstructured simulations with the semi-analytical results of relaxed micromorphic model. This issue deserves deeper investigation and will be addressed in forthcoming works.

Figure 6.7 depicts the analogous results for an S incident wave. For frequencies lower than the band-gap, we observe once again an excellent agreement between the discrete and continuous simulations for all angles of incidence.

We also remark additional interesting phenomena. Firstly, for smaller angles of incidence, we see that the band-gap region extends to lower frequencies. This is related to the previously discussed acoustic mode uncoupling, which is observed for angles close to normal incidence. A shear incident wave mostly activates the green acoustic mode (see Fig. 6.3) which is almost entirely responsible for the propagation pattern. Since the blue acoustic mode is not activated for angles close to normal incidence, the bottom band-gap limit is consequently lower compared to the case of an L incident wave.

A first threshold value of the angle of incidence exists (around $5\pi/24$), for which the two acoustic modes start to couple and energy starts being transmitted. More remarkably, a second threshold value of the incident angle exists (around $\pi/3$), for which the amount of transmission

suddenly increases, approaching a total transmission pattern. This is due to a stronger coupling between the two acoustic modes which are activated by an S incident wave for incident angles beyond the second threshold. This impressive pattern is clearly associated to the tetragonal symmetry of the metamaterial: the need for introducing "generalized classes of symmetry" in an enriched continuum environment is now evident. The investigations for higher frequencies will be discussed in forthcoming works.

We deduce that the agreement is very satisfactory for all the considered angles (going from normal incidence to incidence almost parallel to interface) and for the considered range of frequencies. This fact corroborates the hypothesis, which has been made according to Neumann's principle and which states that the class of symmetry of the metamaterial at the macroscopic scale is the same as the symmetry of the unit cell (tetragonal symmetry in this case).

We conclude this section by pointing out that the simulations performed to obtain Figures 6.6 and 6.7 took less than 1 hour for the relaxed micromorphic model and 3 weeks for the discrete model. Both computations were made with 200 points in the frequency range and for 90 angles. This tremendous gain in computational time underlines the usefulness of an enriched continuum model versus a discrete one for the description of the mechanical behavior of finite-size metamaterials structures. Metamaterial characterization through the relaxed micromorphic model opens the way to effective FEM implementation of other morphologically complex metastructures.

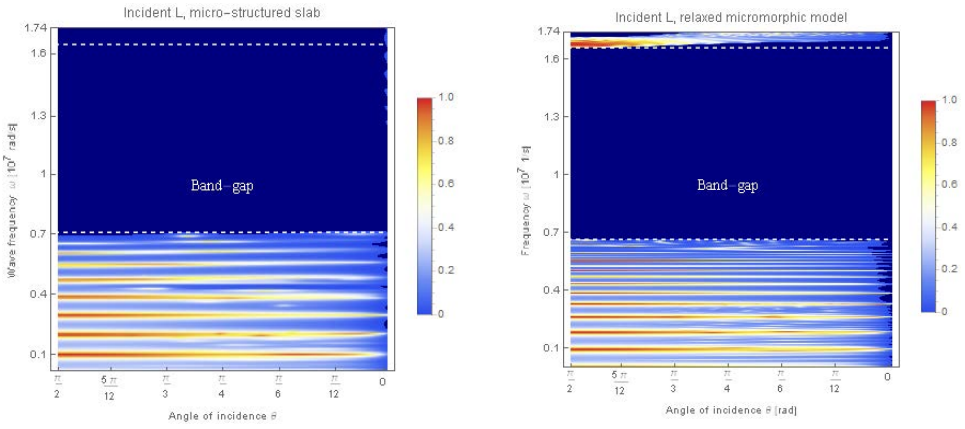

(a) (b)

Figure 6.6: Transmission coefficient of the metamaterial slab as a function of the angle of incidence θ and of the wave-frequency ω for an incident L wave. Panel (a) depicts the microstructured simulations, while panel (b) the analytical relaxed micromorphic model. The origin coincides with normal incidence ($\theta = \pi/2$), while the angle of incidence decreases towards the right until it reaches the value $\theta = 0$, which corresponds to the limit case where the incidence is parallel to the interface. The band-gap region is highlighted by two dashed horizontal lines, where, as expected, we observe no transmission. The dark blue zone shows that no transmission takes place, while the gradual change from dark blue to red shows the increase of transmission, red being total transmission.

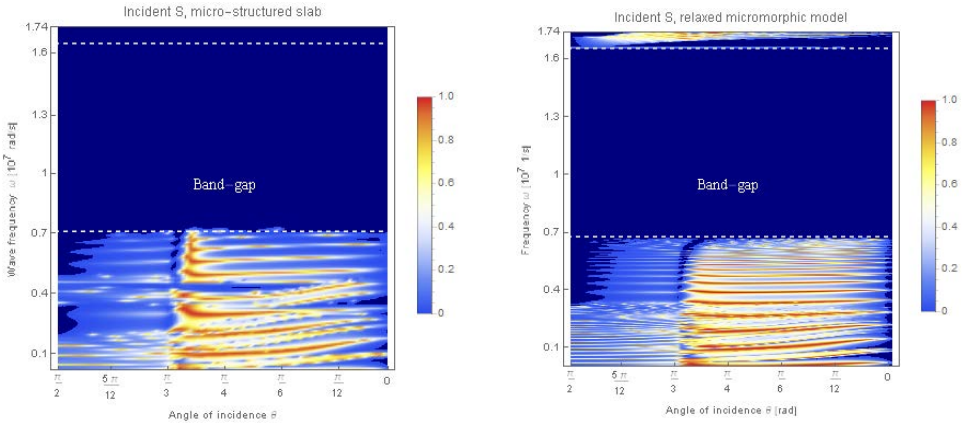

(a) (b)

Figure 6.7: Transmission coefficient of the metamaterial slab as a function of the angle of incidence θ and of the wave-frequency ω for an incident S wave.

6.6.2 Scattering at a single relaxed micromorphic interface

In this subsection we show the results for the reflection coefficient obtained by using the single interface boundary conditions for the relaxed micromorphic continuum as described in section 6.1.1.

Figure 6.8 shows the reflection coefficient as a function of the frequency for two different angles of incidence ($\theta = \pi/2$ and $\theta = \pi/4$), when considering an L incident wave for the "single interface" boundary conditions. Figure 6.9 shows the analogous results for an incident S wave. As expected, the solution obtained using the "single interface" boundary conditions, provides a sort of average behavior for the oscillation at lower frequencies. This is sensible, since when considering a semi-infinite metamaterial, multiple reflections on the two boundaries of the slab are not accounted for. The difference between "single" and "double interface" boundary conditions in the relaxed micromorphic model becomes less pronounced for higher frequencies, since the wavelength of the considered waves is expected to be much lower than the characteristic-size of the slab.

We conclude this subsection by showing the transmission coefficients at the "single interface", as a function of the frequency and the angle of incidence for L and S incident waves (Fig. 6.10(a) and 6.10(b), respectively). Comparing Fig. 6.6(b) to 6.10(a) and 6.7(b) to 6.10(b), we can visualize the extent to which the single interface can be considered to represent a metastructure of finite size. Although some basic averaged information is contained in Figures 6.10(a) and 6.10(b) (band-gap, critical angles), the detailed scattering behavior of the finite slab cannot be inferred from it. This provides additional evidence for the real need to propose a framework in which macroscopic boundary conditions can be introduced in a simplified way. Semi-infinite problems for metamaterials are solved in the context of homogenization methods in [91, 104], but to the author's knowledge, the rigorous solution of scattering problems for metamaterials of finite size is not available in the literature.

6.7 Conclusions

In this chapter we presented for the first time the scattering solution of a metamaterial slab of finite size, modeled via a rigorous boundary value problem describing its homogenized behavior.

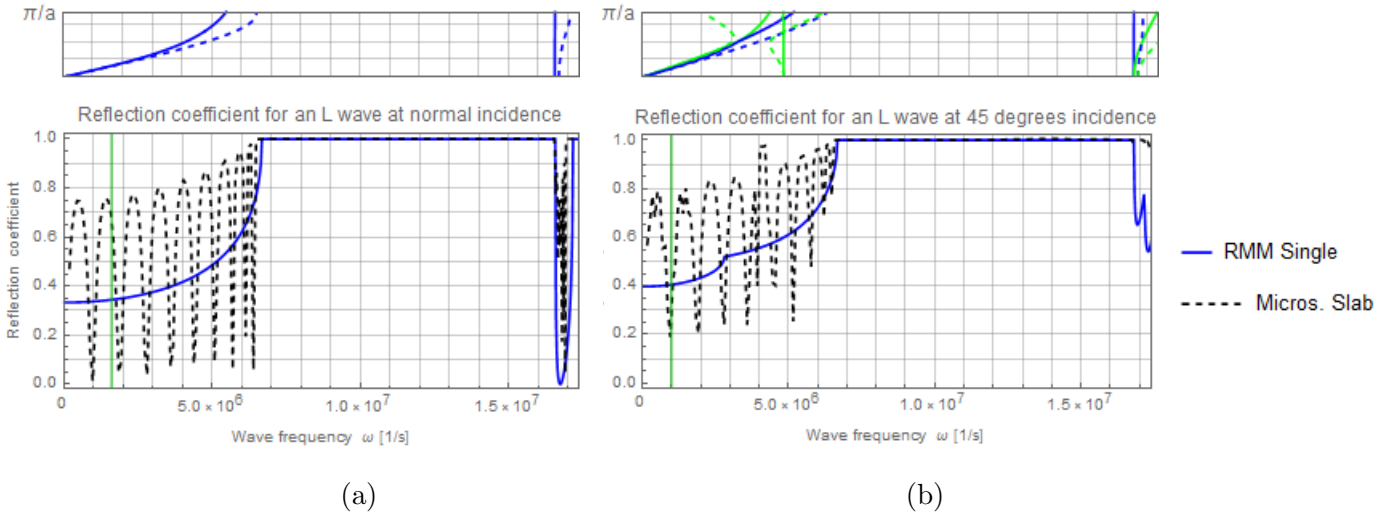

(a) (b)

Figure 6.8: Reflection coefficient at the single interface for an incident L wave and for two directions of propagation $\theta = \pi/2$ (normal incidence) (a) and $\theta = \pi/4$ (b). The blue curve is generated by the tetragonal relaxed micromorphic model and the black dashed line indicates the microstructured model. The green vertical lines denote the long-wave limit, below which the relaxed micromorphic model is equivalent to a homogenized Cauchy model.The dispersion diagrams for $\theta = \pi/2$ and $\theta = \pi/4$, given in Fig. 6.3 are also rotated and displayed on the top of each picture to allow for a better interpretation of results.

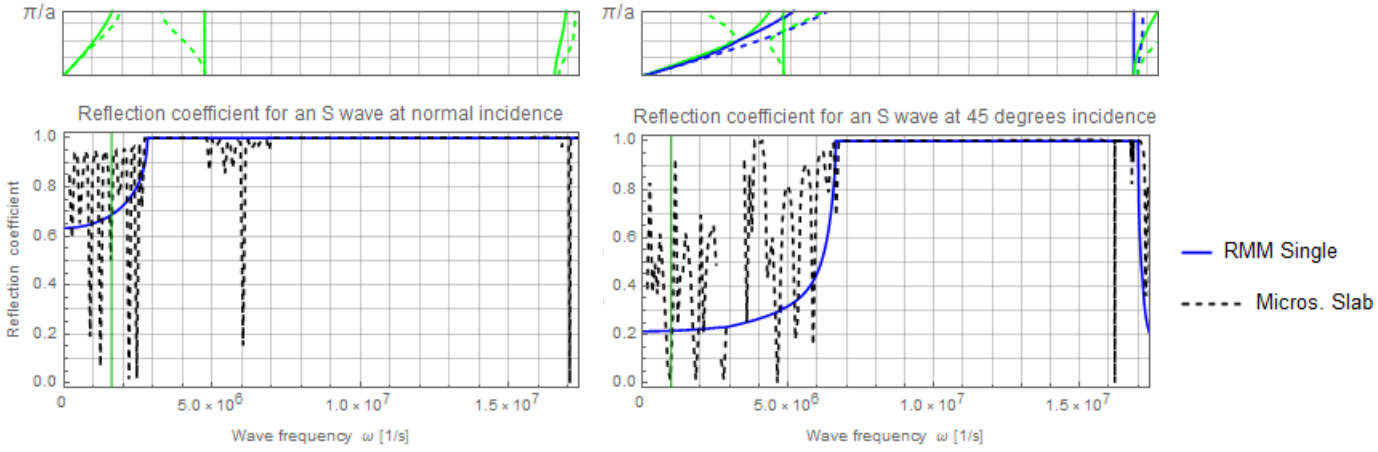

(a) (b)

Figure 6.9: Reflection coefficient at the single interface for an incident S wave and for two directions of propagation $\theta = \pi/2$ (normal incidence) (a) and $\theta = \pi/4$ (b).

The correct macroscopic boundary conditions (continuity of macroscopic displacement and of generalized tractions) are presented and are intrinsically compatible with the used macroscopic bulk PDEs. The scattering properties of the considered finite-size metastructures, as obtained via the relaxed micromorphic model, are compared to a direct microstructured simulation. This simulation is obtained by assuming that the metamaterial's unit cell is periodic and linear-elastic. Excellent agreement is found for all angles of incidence and for frequencies going from the long-wave limit to the first band-gap and beyond. Further work will be devoted to better understanding the high-frequency behavior of the considered metamaterials so as to provide a

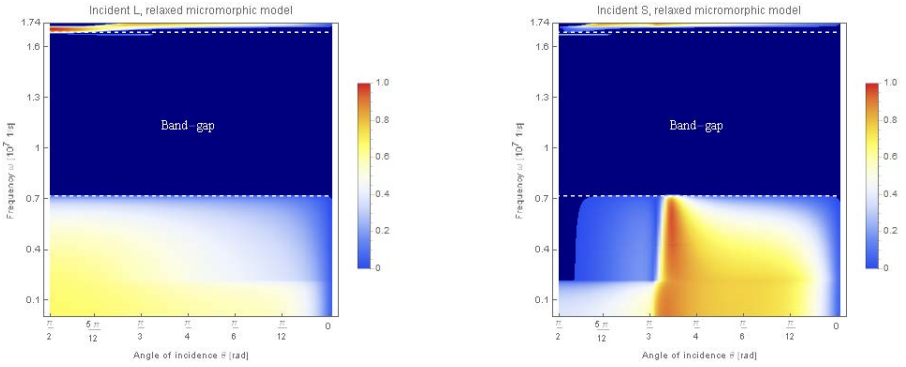

(a) (b)

Figure 6.10: Transmission coefficient of the single interface as a function of the angle of incidence θ and of the wave-frequency ω. Panel (a) depicts the case of an incident L wave, while panel (b) the case of an incident S wave. The origin coincides with normal incidence ($\theta = \pi/2$), while the angle of incidence decreases towards the right until it reaches the value $\theta = 0$, which corresponds to the limit case where the incidence is parallel to the interface. The band-gap region is highlighted by two dashed horizontal lines, where, as expected, we observe no transmission. The dark blue zone shows that no transmission takes place, while the gradual change from dark blue to red shows the increase of transmission, red being total transmission.

final validation of the relaxed micromorphic model also for such higher frequencies.

The results presented in this chapter open the way to the future study of the scattering properties of more complex 2D or 3D finite-sized metastructures in a simplified macroscopic environment.

The results presented in this chapter can be found in [4].

Chapter 7

Conclusions and further perspectives

Using a continuum relaxed micromorphic model could be an incredibly powerful tool for the design of complex metastructures which are constituted by metamaterials with already known mechanical properties. Indeed, the fact of dealing with few macroscopic elastic coefficients makes the finite element implementation of the model rather easy, so allowing for the possibility of designing complex structures with a relatively contained computational effort. Once the material parameters of the considered metamaterials have been estimated by inverse approach, standard finite element codes could be used in order to design structures with extended sizes and complex geometries.

The results presented in this thesis strongly encourage the promotion of the relaxed micromorphic model to engineering science. Indeed, the following challenges can be identified and will be treated in forthcoming works:

- The entire metamaterial's characterization in the framework of the relaxed micromorphic model presented in this thesis must be generalized to 3D metamaterials in order to enable the conception of **metastructures**, which will have a true impact on our everyday life.
- Study of the behavior of more "geometrically complex" metastructures (e.g. morphologically complex 2D or simplified 3D); this will allow to demonstrate impressive time savings in computations considering that, even for the relatively simple metastructure presented here, we obtain a considerable reduction in computational time, from 53 minutes in the micro-structured case down to 18 minutes for the relaxed micromorphic case.
- Study of the effect of the characteristic length scale L_c on description of the dynamic response of metastructures. We will show in a forthcoming paper that the characteristic length plays a non-negligible role when considering diffractive phenomena at an interface embedded in a relaxed micromorphic model. Some non-negligible effects of L_c are also expected for very high frequency and will be investigated in further works. The way to that goal includes introducing additional degrees of freedom which will account for a Shear-like mode in the very high frequency regime.
- Study of transient wave propagation in metastructures whose unit cell belongs to different symmetry classes; this will demonstrate the unprecedented advantage of using the relaxed micromorphic model rather than other enriched continua. In fact, due to its simplicity compared to existing generalized continua - the relaxed micromorphic model features 4th order tensors rather than 6th order tensors, as in the second gradient model - the relaxed micromorphic model is able to add tangible improvements to the classical and (infinitely simpler) Cauchy description.

- Extend the present results to more general classes of symmetry of anisotropic media and study refection/transmission properties at such interfaces.
- Study of the reflection and transmission properties at interfaces between finite media.

Appendix A

Appendix for chapter 3.

A1 Variation of the strain energy

Using expression (3.5), we have:

$$\begin{aligned}\delta\int_0^T\int_\Omega W(\nabla u,P,\operatorname{Curl}P)dx\,dt = &\underbrace{\delta\int_0^T\int_\Omega \frac{1}{2}\langle\mathbb{C}_e\operatorname{sym}(\nabla u-P),\operatorname{sym}(\nabla u-P)\rangle\,dx\,dt}_{P_1}\\ &+\underbrace{\delta\int_0^T\int_\Omega \frac{1}{2}\langle\mathbb{C}_{\text{micro}}\operatorname{sym}P,\operatorname{sym}P\rangle\,dx\,dt}_{P_2}\\ &+\underbrace{\delta\int_0^T\int_\Omega \frac{1}{2}\langle\mathbb{C}_c\operatorname{skew}(\nabla u-P),\operatorname{skew}(\nabla u-P)\rangle\,dx\,dt}_{P_3}\\ &+\underbrace{\delta\int_0^T\int_\Omega \frac{L_c^2}{2}\langle\mathbb{L}_e\operatorname{sym}\operatorname{Curl}P,\operatorname{sym}\operatorname{Curl}P\rangle\,dx\,dt}_{P_4}\\ &+\underbrace{\delta\int_0^T\int_\Omega \langle\mathbb{L}_c\operatorname{skew}\operatorname{Curl}P,\operatorname{skew}\operatorname{Curl}P\rangle\,dx\,dt}_{P_5}.\end{aligned}$$

We consider each term P_1, P_2, P_3, P_4, P_5 separately.

For the term P_1, we have:

$$\begin{aligned}P_1 &= \frac{1}{2}\int_0^T\int_\Omega \langle\mathbb{C}_e\operatorname{sym}(\nabla\delta u-\delta P),\operatorname{sym}(\nabla u-P)\rangle+\langle\mathbb{C}_e\operatorname{sym}(\nabla u-P),\operatorname{sym}(\nabla\delta u-\delta P)\rangle\,dx\,dt\\ &= \int_0^T\int_\Omega \langle\mathbb{C}_e\operatorname{sym}(\nabla u-P),\operatorname{sym}(\nabla\delta u-\delta P)\rangle\,dx\,dt = \int_0^T\int_\Omega \langle\mathbb{C}_e\operatorname{sym}(\nabla u-P),\nabla\delta u-\delta P\rangle\,dx\,dt\\ &= \int_0^T\int_\Omega \langle\mathbb{C}_e\operatorname{sym}(\nabla u-P),\nabla\delta u\rangle\,dx\,dt-\int_0^T\int_\Omega \langle\mathbb{C}_e\operatorname{sym}(\nabla u-P),\delta P\rangle\,dx\,dt\\ &= \int_0^T\int_\Omega \langle\operatorname{div}(\mathbb{C}_e\operatorname{sym}(\nabla u-P)\cdot\delta u)dx\,dt-\int_0^T\int_\Omega \langle\operatorname{Div}(\mathbb{C}_e\operatorname{sym}(\nabla u-P)),\delta u\rangle\,dx\,dt\\ &\quad-\int_0^T\int_\Omega \langle\mathbb{C}_e\operatorname{sym}(\nabla u-P),\delta P\rangle\,dx\,dt\\ &= \int_0^T\int_{\partial\Omega}\langle(\mathbb{C}_e\operatorname{sym}(\nabla u-P))\cdot\nu,\delta u\rangle-\int_0^T\int_\Omega \langle\operatorname{Div}(\mathbb{C}_e\operatorname{sym}(\nabla u-P)),\delta u\rangle\,dx\,dt\end{aligned}$$

$$- \int_0^T \int_\Omega \langle \mathbb{C}_e \operatorname{sym}(\nabla u - P), \delta P \rangle \, dx \, dt$$

For the term P_2, we have:

$$P_2 = \frac{1}{2} \int_0^T \int_\Omega \langle \mathbb{C}_{\text{micro}} \operatorname{sym} \delta P, \operatorname{sym} P \rangle + \langle \mathbb{C}_{\text{micro}} \operatorname{sym} P, \operatorname{sym} \delta P \rangle dx \, dt = \int_0^T \int_\Omega \langle \mathbb{C}_{\text{micro}} \operatorname{sym} P, \operatorname{sym} \delta P \rangle \, dx \, dt$$
$$= \int_0^T \int_\Omega \mathbb{C}_{\text{micro}} \operatorname{sym} P, \delta P \rangle \, dx \, dt$$

For the term P_3, we have:

$$\begin{aligned}
P_3 &= \frac{1}{2} \int_0^T \int_\Omega \langle \mathbb{C}_c \operatorname{skew}(\nabla \delta u - \delta P), \operatorname{skew}(\nabla u - P) \rangle + \langle \mathbb{C}_c \operatorname{skew}(\nabla u - P), \operatorname{skew}(\nabla \delta u - \delta P) \rangle \, dx \, dt \\
&= \int_0^T \int_\Omega \langle \mathbb{C}_c \operatorname{skew}(\nabla u - P), \operatorname{skew}(\nabla \delta u - \delta P) \rangle \, dx \, dt = \int_0^T \int_\Omega \langle \mathbb{C}_c \operatorname{skew}(\nabla u - P), \nabla \delta u - \delta P \rangle \, dx \, dt \\
&= \int_0^T \int_\Omega \langle \mathbb{C}_c \operatorname{skew}(\nabla u - P), \nabla \delta u \rangle \, dx \, dt - \int_0^T \int_\Omega \langle \mathbb{C}_c \operatorname{skew}(\nabla u - P), \delta P \rangle \, dx \, dt \\
&= \int_0^T \int_\Omega \langle \operatorname{div}(\mathbb{C}_c \operatorname{skew}(\nabla u - P) \cdot \delta u) dx \, dt - \int_0^T \int_\Omega \langle \operatorname{Div}(\mathbb{C}_c \operatorname{skew}(\nabla u - P)), \delta u \rangle \, dx \, dt \\
&\quad - \int_0^T \int_\Omega \langle \mathbb{C}_c \operatorname{skew}(\nabla u - P), \delta P \rangle \, dx \, dt \\
&= \int_0^T \int_{\partial\Omega} \langle (\mathbb{C}_c \operatorname{skew}(\nabla u - P)) \cdot \nu, \delta u \rangle - \int_0^T \int_\Omega \langle \operatorname{Div}(\mathbb{C}_c \operatorname{skew}(\nabla u - P)), \delta u \rangle \, dx \, dt \\
&\quad - \int_0^T \int_\Omega \langle \mathbb{C}_c \operatorname{skew}(\nabla u - P), \delta P \rangle \, dx \, dt
\end{aligned}$$

For the term P_4, we have:

$$\begin{aligned}
P_4 &= \frac{L_c^2}{2} \delta \int_0^T \int_\Omega \langle \mathbb{L}_e \operatorname{sym} \operatorname{Curl} P, \operatorname{sym} \operatorname{Curl} P \rangle \, dx \, dt = L_c^2 \int_0^T \int_\Omega \langle \mathbb{L}_e \operatorname{sym} \operatorname{Curl} P, \operatorname{sym} \operatorname{Curl} \delta P \rangle \, dx \, dt \\
&= L_c^2 \int_0^T \int_\Omega \langle \mathbb{L}_e \operatorname{sym} \operatorname{Curl} P, \operatorname{Curl} \delta P \rangle \, dx \, dt \\
&= L_c^2 \int_0^T \int_\Omega \sum_{i=1}^3 \langle (\mathbb{L}_e \operatorname{sym} \operatorname{Curl} P)_i, (\operatorname{Curl} \delta P)_i \rangle_{\mathbb{R}^3} \, dx \, dt \\
&= L_c^2 \int_0^T \int_\Omega \sum_{i=1}^3 \langle (\mathbb{L}_e \operatorname{sym} \operatorname{Curl} P)_i, \operatorname{curl} (\delta P)_i \rangle_{\mathbb{R}^3} \, dx \, dt \\
&= L_c^2 \int_0^T \int_\Omega \sum_{i=1}^3 \left(\operatorname{div} \left((\mathbb{L}_e \operatorname{sym} \operatorname{Curl} P)_i \times \operatorname{curl} (\delta P)_i \right) + \langle \operatorname{curl} (\mathbb{L}_e \operatorname{sym} \operatorname{Curl} P)_i, (\delta P)_i \rangle_{\mathbb{R}^3} \right) \\
&= L_c^2 \sum_{i=1}^3 \int_0^T \int_{\partial\Omega} \langle \left((\mathbb{L}_e \operatorname{sym} \operatorname{Curl} P)_i \times \operatorname{curl} (\delta P)_i \right), \nu \rangle \, dx \, dt \\
&\quad + L_c^2 \int_0^T \int_\Omega \langle \operatorname{Curl} \left(\mathbb{L}_e \operatorname{sym} \operatorname{Curl} P \right), \delta P \rangle_{\mathbb{R}^3 \times \mathbb{R}^3} \, dx \, dt
\end{aligned}$$

Finally, for the term P_5, we have:

$$P_5 = \frac{L_c^2}{2} \delta \int_0^T \int_\Omega \langle \mathbb{L}_c \operatorname{skew} \operatorname{Curl} P, \operatorname{skew} \operatorname{Curl} P \rangle \, dx \, dt = L_c^2 \int_0^T \int_\Omega \langle \mathbb{L}_c \operatorname{skew} \operatorname{Curl} P, \operatorname{skew} \operatorname{Curl} \delta P \rangle \, dx \, dt$$

$$
\begin{aligned}
&= L_c^2 \int_0^T \int_\Omega \langle \mathbb{L}_c \operatorname{skew} \operatorname{Curl} P, \operatorname{Curl} \delta P \rangle \, dx \, dt \\
&= L_c^2 \int_0^T \int_\Omega \sum_{i=1}^3 \langle (\mathbb{L}_c \operatorname{skew} \operatorname{Curl} P)_i, (\operatorname{Curl} \delta P)_i \rangle_{\mathbb{R}^3} \, dx \, dt \\
&= L_c^2 \int_0^T \int_\Omega \sum_{i=1}^3 \langle (\mathbb{L}_c \operatorname{skew} \operatorname{Curl} P)_i, \operatorname{curl} (\delta P)_i \rangle_{\mathbb{R}^3} \, dx \, dt \\
&= L_c^2 \int_0^T \int_\Omega \sum_{i=1}^3 \left(\operatorname{div} \left((\mathbb{L}_c \operatorname{skew} \operatorname{Curl} P)_i \times \operatorname{curl} (\delta P)_i \right) + \langle \operatorname{curl} (\mathbb{L}_c \operatorname{skew} \operatorname{Curl} P)_i, (\delta P)_i \rangle_{\mathbb{R}^3} \right) \\
&= L_c^2 \sum_{i=1}^3 \int_0^T \int_{\partial\Omega} \langle \left((\mathbb{L}_c \operatorname{skew} \operatorname{Curl} P)_i \times \operatorname{curl} (\delta P)_i \right), \nu \rangle \, dx \, dt \\
&\quad + L_c^2 \int_0^T \int_\Omega \langle \operatorname{Curl} \left(\mathbb{L}_c \operatorname{skew} \operatorname{Curl} P \right), \delta P \rangle_{\mathbb{R}^3 \times \mathbb{R}^3} \, dx \, dt
\end{aligned}
$$

A2 Variation of the kinetic energy

Using expression (3.11), we have:

$$
\begin{aligned}
\delta \int_0^T \int_\Omega J(u_{,t}, \nabla u_{,t}, P_{,t}) dx \, dt = \frac{1}{2} \, \delta \int_0^T \int_\Omega \rho \, \|u_{,t}\|^2 + \langle \mathbb{J}_{\text{micro}} \operatorname{sym} P_{,t}, \operatorname{sym} P_{,t} \rangle + \langle \mathbb{J}_c \operatorname{skew} P_{,t}, \operatorname{skew} P_{,t} \rangle \\
+ \langle \mathbb{T}_e \operatorname{sym} \nabla u_{,t}, \operatorname{sym} \nabla u_{,t} \rangle + \langle \mathbb{T}_c \operatorname{skew} \nabla u_{,t}, \operatorname{skew} \nabla u_{,t} \rangle \, dx \, dt \\
= \underbrace{\rho \int_0^T \int_\Omega \langle u_{,t}, \delta u_{,t} \rangle \, dx \, dt}_{K_1} + \underbrace{\int_0^T \int_\Omega \langle \mathbb{J}_{\text{micro}} \operatorname{sym} P_{,t}, \operatorname{sym} \delta P_{,t} \rangle dx \, dt}_{K_2} \\
+ \underbrace{\int_0^T \int_\Omega \langle \mathbb{J}_c \operatorname{skew} P_{,t}, \operatorname{skew} \delta P_{,t} \rangle \, dx \, dt}_{K_3} + \underbrace{\int_0^T \int_\Omega \langle \mathbb{T}_e \operatorname{sym} \nabla u_{,t}, \operatorname{sym} \nabla \delta u_{,t} \rangle \, dx \, dt}_{K_4} \\
+ \underbrace{\int_0^T \int_\Omega \langle \mathbb{T}_c \operatorname{skew} \nabla u_{,t}, \operatorname{skew} \nabla \delta u_{,t} \rangle \, dx \, dt}_{K_5} .
\end{aligned}
$$

Once again, we consider each term K_1, K_2, K_3, K_4, K_5 separately and apply integration by parts to each of these terms.

For the term K_1, we have:

$$
\begin{aligned}
K_1 &= \rho \int_0^T \int_\Omega \frac{d}{dt} \langle u_{,t}, \delta u \rangle \, dx \, dt - \rho \int_0^T \int_\Omega \langle u_{,tt}, \delta u \rangle \, dx \, dt \\
&= \rho \int_0^T \frac{d}{dt} \left(\int_\Omega \langle u_{,t}, \delta u \rangle \, dx \right) dt - \rho \int_0^T \int_\Omega \langle u_{,tt}, \delta u \rangle \, dx \, dt \\
&= \int_{\Omega \times \{T\}} \langle u_{,t}(x,T), \delta u(x,T) \rangle \, dx - \int_{\Omega \times \{0\}} \langle u_{,t}(x,0), \delta u(x,0) \rangle \, dx - \rho \int_0^T \int_\Omega \langle u_{,tt}, \delta u \rangle \, dx \, dt.
\end{aligned}
$$

For the term K_2, we have:

$$
\begin{aligned}
K_2 &= \int_0^T \int_\Omega \frac{d}{dt} \langle \mathbb{J}_{\text{micro}} \operatorname{sym} P_{,t}, \operatorname{sym} \delta P \rangle dx \, dt - \int_0^T \int_\Omega \langle \mathbb{J}_{\text{micro}} \operatorname{sym} P_{,tt}, \operatorname{sym} \delta P \rangle dx \, dt \\
&= \int_0^T \frac{d}{dt} \left(\int_\Omega \langle \mathbb{J}_{\text{micro}} \operatorname{sym} P_{,t}, \delta P \rangle dx \right) dt - \int_0^T \int_\Omega \langle \mathbb{J}_{\text{micro}} \operatorname{sym} P_{,tt}, \operatorname{sym} \delta P \rangle dx \, dt
\end{aligned}
$$

$$= \int_{\Omega\times\{T\}} \langle \mathbb{J}_{\text{micro}} \operatorname{sym} P_{,t}(x,T), \delta P(x,T)\rangle dx - \int_{\Omega\times\{0\}} \langle \mathbb{J}_{\text{micro}} \operatorname{sym} P_{,t}(x,0), \delta P(x,0)\rangle dx$$
$$- \int_0^T \int_\Omega \langle \mathbb{J}_{\text{micro}} \operatorname{sym} P_{,tt}, \delta P\rangle dx\, dt$$

For the term K_3, we have:

$$K_3 = \int_0^T \int_\Omega \frac{d}{dt}\langle \mathbb{J}_c \operatorname{skew} P_{,t}, \operatorname{skew} \delta P\rangle dx\, dt - \int_0^T \int_\Omega \langle \mathbb{J}_c \operatorname{skew} P_{,tt}, \operatorname{skew} \delta P\rangle dx\, dt$$
$$= \int_0^T \frac{d}{dt}\left(\int_\Omega \langle \mathbb{J}_c \operatorname{skew} P_{,t}, \delta P\rangle dx\right) dt - \int_0^T \int_\Omega \langle \mathbb{J}_c \operatorname{skew} P_{,tt}, \operatorname{skew} \delta P\rangle dx\, dt$$
$$= \int_{\Omega\times\{T\}} \langle \mathbb{J}_c \operatorname{skew} P_{,t}(x,T), \delta P(x,T)\rangle dx - \int_{\Omega\times\{0\}} \langle \mathbb{J}_c \operatorname{skew} P_{,t}(x,0), \delta P(x,0)\rangle dx$$
$$- \int_0^T \int_\Omega \langle \mathbb{J}_c \operatorname{skew} P_{,tt}, \delta P\rangle dx\, dt$$

For the term K_4, we have:

$$K_4 = \int_0^T \int_\Omega \langle \mathbb{T}_e \operatorname{sym} \nabla u_{,t}, \nabla \delta u_{,t}\rangle\, dx\, dt$$
$$= \int_0^T \int_{\partial\Omega} \langle (\mathbb{T}_e \operatorname{sym} \nabla u_{,t})\cdot \nu, \delta u_{,t}\rangle\, dx\, dt - \int_0^T \int_\Omega \langle \operatorname{Div}(\mathbb{T}_e \operatorname{sym} \nabla u_{,t}), \delta u_{,t}\rangle\, dx\, dt$$
$$= \int_{\partial\Omega\times\{T\}} \langle (\mathbb{T}_e \operatorname{sym} \nabla u_{,t}(x,T))\cdot \nu, \delta u_{,t}(x,T)\rangle\, dx - \int_{\partial\Omega\times\{0\}} \langle (\mathbb{T}_e \operatorname{sym} \nabla u_{,t}(x,0))\cdot \nu, \delta u_{,t}(x,0)\rangle\, dx$$
$$- \int_0^T \int_{\partial\Omega} \langle (\mathbb{T}_e \operatorname{sym} \nabla u_{,tt})\cdot \nu, \delta u\rangle\, dx\, dt$$
$$- \left(\int_0^T \int_\Omega \frac{d}{dt}\langle \operatorname{Div}(\mathbb{T}_e \operatorname{sym} \nabla u_{,t}), \delta u\rangle\, dx\, dt - \int_0^T \int_\Omega \langle \operatorname{Div}(\mathbb{T}_e \operatorname{sym} \nabla u_{,tt}, \delta u\rangle\, dx\, dt\right)$$

Finally, for the term K_5, we have:

$$K_5 = \int_0^T \int_\Omega \langle \mathbb{T}_c \operatorname{skew} \nabla u_{,t}, \nabla \delta u_{,t}\rangle\, dx\, dt$$
$$= \int_0^T \int_{\partial\Omega} \langle (\mathbb{T}_c \operatorname{skew} \nabla u_{,t})\cdot \nu, \delta u_{,t}\rangle\, dx\, dt - \int_0^T \int_\Omega \langle \operatorname{Div}(\mathbb{T}_c \operatorname{skew} \nabla u_{,t}), \delta u_{,t}\rangle\, dx\, dt$$
$$= \int_{\partial\Omega\times\{T\}} \langle (\mathbb{T}_c \operatorname{skew} \nabla u_{,t}(x,T))\cdot \nu, \delta u_{,t}(x,T)\rangle\, dx - \int_{\partial\Omega\times\{0\}} \langle (\mathbb{T}_c \operatorname{skew} \nabla u_{,t}(x,0))\cdot \nu, \delta u_{,t}(x,0)\rangle\, dx$$
$$- \int_0^T \int_{\partial\Omega} \langle (\mathbb{T}_c \operatorname{skew} \nabla u_{,tt})\cdot \nu, \delta u\rangle\, dx\, dt$$
$$- \left(\int_0^T \int_\Omega \frac{d}{dt}\langle \operatorname{Div}(\mathbb{T}_c \operatorname{skew} \nabla u_{,t}), \delta u\rangle\, dx\, dt - \int_0^T \int_\Omega \langle \operatorname{Div}(\mathbb{T}_c \operatorname{skew} \nabla u_{,tt}, \delta u\rangle\, dx\, dt\right)$$

A3 Energy flux for the anisotropic relaxed micromorphic model

A3.1 Derivation of expression (3.76)

The total energy is given by:

$$E = J(u_{,t}, \nabla u_{,t}, P_{,t}) + W(\nabla u, P, \operatorname{Curl} P), \tag{A.1}$$

where $J(u_{,t}, \nabla u_{,t}, P_{,t})$ and $W(\nabla u, P, \operatorname{Curl} P)$ are defined in (3.11) and (3.5). Differentiating (A.1) with respect to time[1] we have:

$$\begin{aligned} E_{,t} = &\langle u_{,t}, \rho u_{,tt}\rangle + \langle \operatorname{sym} P_{,t}, \mathbb{J}_{\text{micro}} \operatorname{sym} P_{,tt}\rangle + \langle \operatorname{skew} P_{,t}, \mathbb{J}_c \operatorname{skew} P_{,tt}\rangle + \langle \operatorname{sym} \nabla u_{,t}, \mathbb{T}_e \operatorname{sym} \nabla u_{,tt}\rangle \\ &+ \langle \operatorname{skew} \nabla u_{,t}, \mathbb{T}_c \operatorname{skew} \nabla u_{,tt}\rangle + \langle \mathbb{C}_e \operatorname{sym}(\nabla u - P), \operatorname{sym}(\nabla u - P)_{,t}\rangle + \langle \mathbb{C}_c \operatorname{skew}(\nabla u - P), \operatorname{skew}(\nabla u - P)_{,t}\rangle \\ &+ \langle \mathbb{C}_{\text{micro}} \operatorname{sym} P, \operatorname{sym} P_{,t}\rangle + L_c^2 \left(\langle \mathbb{L}_e \operatorname{sym} \operatorname{Curl} P, \operatorname{sym} \operatorname{Curl} P_{,t}\rangle + \langle \mathbb{L}_c \operatorname{skew} \operatorname{Curl} P, \operatorname{skew} \operatorname{Curl} P_{,t}\rangle\right). \end{aligned} \tag{A.5}$$

Using the governing equations (3.28), definitions (3.33) for $\widetilde{\sigma}, \widehat{\sigma}, s, m$ and (A.2), (A.3), (A.4) we have:

$$\begin{aligned} \langle u_{.t}, \rho\, u_{,tt}\rangle &= \langle u_{,t}, \operatorname{Div}(\mathbb{T}_e \operatorname{sym} \nabla u_{,tt} + \mathbb{T}_c \operatorname{skew} \nabla u_{,tt}) + \operatorname{Div} \widetilde{\sigma}\rangle \\ &= \langle u_{,t}, \operatorname{Div} \widetilde{\sigma}\rangle + \langle u_{,t}, \operatorname{Div}(\underbrace{\mathbb{T}_e \operatorname{sym} \nabla u_{,tt} + \mathbb{T}_c \operatorname{skew} \nabla u_{,tt}}_{:=\widehat{\sigma}})\rangle \\ &= \langle u_{,t}, \operatorname{Div} \widetilde{\sigma}\rangle + \langle u_{,t}, \operatorname{Div} \widehat{\sigma}\rangle, \end{aligned}$$

$$\begin{aligned} &\langle \operatorname{sym} P_{,t}, \mathbb{J}_{\text{micro}} \operatorname{sym} P_{,tt}\rangle + \langle \operatorname{skew} P_{,t}, \mathbb{J}_c \operatorname{skew} P_{,tt}\rangle \\ &\quad= \langle \operatorname{sym} P_{,t} + \operatorname{skew} P_{,t}, \mathbb{J}_{\text{micro}} \operatorname{sym} P_{,tt}\rangle + \langle \operatorname{sym} P_{,t} + \operatorname{skew} P_{,t}, \mathbb{J}_c \operatorname{skew} P_{,tt}\rangle \\ &\quad= \langle P_{,t}, \mathbb{J}_{\text{micro}} \operatorname{sym} P_{,tt} + \mathbb{J}_c \operatorname{skew} P_{,tt}\rangle = \langle P_{,t}, \widetilde{\sigma}_e - s - \operatorname{sym} \operatorname{Curl} m + \widetilde{\sigma}_c - \operatorname{skew} \operatorname{Curl} m\rangle \\ &\quad= \langle P_{,t}, \widetilde{\sigma} - s - \operatorname{Curl} m\rangle = \langle P_{,t}, \widetilde{\sigma}\rangle - \langle P_{,t}, s\rangle - \langle P_{,t}, \operatorname{Curl} m\rangle, \end{aligned}$$

$$\begin{aligned} &\langle \operatorname{sym} \nabla u_{,t}, \mathbb{T}_e \operatorname{sym} \nabla u_{,tt}\rangle + \langle \operatorname{skew} \nabla u_{,t}, \mathbb{T}_c \operatorname{skew} \nabla u_{,tt}\rangle \\ &\quad= \langle \operatorname{sym} \nabla u_{,t} + \operatorname{skew} \nabla u_{,t}, \mathbb{T}_e \operatorname{sym} \nabla u_{,tt}\rangle + \langle \operatorname{sym} \nabla u_{,t} + \operatorname{skew} \nabla u_{,t}, \mathbb{T}_c \operatorname{skew} \nabla u_{,tt}\rangle \\ &\quad= \langle \nabla u_{,t}, \underbrace{\mathbb{T}_e \operatorname{sym} \nabla u_{,tt} + \mathbb{T}_c \operatorname{skew} \nabla u_{,tt}}_{=\widehat{\sigma}}\rangle = \langle \nabla u_{,t}, \widehat{\sigma}\rangle = \operatorname{Div}(u_{,t} \cdot \widehat{\sigma}) - \langle u_{,t}, \operatorname{Div} \widehat{\sigma}\rangle, \end{aligned}$$

$$\begin{aligned} &\langle \mathbb{C}_e \operatorname{sym}(\nabla u - P), \operatorname{sym}(\nabla u - P)_{,t}\rangle + \langle \mathbb{C}_c \operatorname{skew}(\nabla u - P), \operatorname{skew}(\nabla u - P)_{,t}\rangle \\ &\quad= \langle \mathbb{C}_e \operatorname{sym}(\nabla u - P), \operatorname{sym}(\nabla u - P)_{,t} + \operatorname{skew}(\nabla u - P)_{,t}\rangle \\ &\quad\quad+ \langle \mathbb{C}_c \operatorname{skew}(\nabla u - P), \operatorname{sym}(\nabla u - P)_{,t} + \operatorname{skew}(\nabla u - P)_{,t}\rangle \\ &\quad= \langle \mathbb{C}_e \operatorname{sym}(\nabla u - P) + \mathbb{C}_c \operatorname{skew}(\nabla u - P), (\nabla u - P)_{,t}\rangle = \langle \widetilde{\sigma}, (\nabla u - P)_{,t}\rangle \\ &\quad= \langle \widetilde{\sigma}, \nabla u_{,t}\rangle - \langle \widetilde{\sigma}, P_t\rangle = \operatorname{Div}(u_{,t} \cdot \widetilde{\sigma}) - \langle u_{,t}, \operatorname{Div} \widetilde{\sigma}\rangle - \langle \widetilde{\sigma}, P_t\rangle, \end{aligned}$$

$$\langle \mathbb{C}_{\text{micro}} \operatorname{sym} P, \operatorname{sym} P_{,t}\rangle = \langle \mathbb{C}_{\text{micro}} \operatorname{sym} P, \operatorname{sym} P_{,t} + \operatorname{skew} P_{,t}\rangle = \langle \mathbb{C}_{\text{micro}} \operatorname{sym} P, P_{,t}\rangle = \langle s, P_{,t}\rangle,$$

[1] We repeat again some identities from differential calculus. Let ψ be a vector field and A a second order tensor field. Then

$$\langle \nabla \psi, A\rangle = \operatorname{Div}(\psi \cdot A) - \langle \psi, \operatorname{Div} A\rangle. \tag{A.2}$$

Taking $\psi = u_{,t}$ and $A = \widetilde{\sigma}$ we have

$$\langle \nabla u_{,t}, \widetilde{\sigma}\rangle = \operatorname{Div}(u_{,t} \cdot \widetilde{\sigma}) - \langle u_{,t}, \operatorname{Div} \widetilde{\sigma}\rangle. \tag{A.3}$$

Furthermore, we have the following identity

$$\langle m, \operatorname{Curl} P_{,t}\rangle = \operatorname{Div}\left((m^{\mathrm{T}} \cdot P_{,t}) : \epsilon\right) + \langle \operatorname{Curl} m, P_{,t}\rangle, \tag{A.4}$$

which follows from the identity $\operatorname{div}(v \times w) = w \cdot \operatorname{curl} v - v \cdot \operatorname{curl} w$, where v, w are suitable vector fields, $\times$ is the usual vector product and : is the double contraction between tensors.

$$
\begin{aligned}
&L_c^2 \left(\langle \mathbb{L}_e \operatorname{sym} \operatorname{Curl} P, \operatorname{sym} \operatorname{Curl} P_{,t} \rangle + \langle \mathbb{L}_c \operatorname{skew} \operatorname{Curl} P, \operatorname{skew} \operatorname{Curl} P_{,t} \rangle \right) \\
&= L_c^2 \left(\langle \mathbb{L}_e \operatorname{sym} \operatorname{Curl} P, \operatorname{sym} \operatorname{Curl} P_{,t} + \operatorname{skew} \operatorname{Curl} P_{,t} \rangle + \langle \mathbb{L}_c \operatorname{skew} \operatorname{Curl} P, \operatorname{sym} \operatorname{Curl} P_{,t} + \operatorname{skew} \operatorname{Curl} P_{,t} \rangle \right) \\
&= \langle L_c^2 (\mathbb{L}_e \operatorname{sym} \operatorname{Curl} P + \mathbb{L}_c \operatorname{skew} \operatorname{Curl} P), \operatorname{Curl} P_{,t} \rangle = \langle m, \operatorname{Curl} P_{,t} \rangle = \operatorname{Div} \left((m^{\mathrm{T}} \cdot P_{,t}) : \epsilon \right) - \langle \operatorname{Curl} m, P_t \rangle .
\end{aligned}
$$

So, by adding all the above and simplifying, (A.5) becomes:

$$
E_{,t} = \operatorname{Div} \left[(\widetilde{\sigma} + \widehat{\sigma})^{\mathrm{T}} \cdot u_{,t} + \left(m^{\mathrm{T}} \cdot P_{,t} \right) : \epsilon \right], \tag{A.6}
$$

from which we can define the energy flux for the general anisotropic relaxed micromorphic model:

$$
H = - (\widetilde{\sigma} + \widehat{\sigma})^{\mathrm{T}} \cdot u_{,t} - \left(m^{\mathrm{T}} \cdot P_{,t} \right) : \epsilon. \tag{A.7}
$$

Appendix B

Appendix for chapter 4

B1 Calculation of the determinant of A

We demonstrate the explicit calculation of the determinant of the matrix

$$A = \begin{pmatrix} \omega^2 - c_l^2 k_1^2 - c_s^2 k_2^2 & -c_V^2 k_1 k_2 \\ -c_V^2 k_1 k_2 & \omega^2 - c_l^2 k_2^2 - c_s^2 k_1^2 \end{pmatrix}. \tag{B.1}$$

We have

$$\begin{aligned}
\det A &= (\omega^2 - c_l^2 k_1^2 - c_s^2 k_2^2)(\omega^2 - c_l^2 k_2^2 - c_s^2 k_1^2) - c_V^4 k_1^2 k_2^2 \\
&= \omega^4 - \omega^2 c_l^2 (k_1^2 + k_2^2) - \omega^2 c_s^2 (k_1^2 + k_2^2) + c_l^2 c_s^2 (k_1^4 + k_2^4) + (c_l^4 + c_s^4) k_1^2 k_2^2 - c_V^4 k_1^2 k_2^2 \qquad \text{(B.2)} \\
&= \omega^4 - \omega^2 (k_1^2 + k_2^2)(c_l^2 + c_s^2) + c_l^2 c_s^2 (k_1^4 + k_2^4) + (c_l^4 + c_s^4) k_1^2 k_2^2 - c_V^2 k_1^2 k 2^2 \\
&= \omega^4 - \omega^2 (k_1^2 + k_2^2) \frac{2\mu + \lambda + \mu}{\rho} + \frac{(2\mu + \lambda)\mu}{\rho^2} (k_1^4 + k_2^4) + \frac{(2\mu + \lambda)^2 + \mu^2}{\rho^2} k_1^2 k_2^2 - \frac{(\mu + \lambda)^2}{\rho^2} k_1^2 k_2^2 \\
&= \frac{1}{\rho^2} \left[\rho^2 \omega^4 - \rho \omega^2 \left((2\mu + \lambda) k_1^2 + (2\mu + \lambda) k_2^2 + \mu k_1^2 + \mu k_2^2 \right) + \mu (2\mu + \lambda) k_1^4 + \mu (2\mu + \lambda) k_2^4 + 2\mu (2\mu + \lambda) k_1^2 k_2^2 \right] \\
&= \frac{1}{\rho^2} \left[\rho^2 \omega^4 - \rho \omega^2 (2\mu + \lambda)(k_1^2 + k_2^2) - \rho \omega^2 \mu (k_1^2 + k_2^2) + (2\mu + \lambda)(k_1^2 + k_2^2) \mu (k_1^2 + k_2^2) \right] \\
&= \frac{1}{\rho^2} \left[(\mu (k_1^2 + k_2^2) - \rho \omega^2)(2\mu + \lambda)(k_1^2 + k_2^2) - \rho \omega^2 (2\mu + \lambda)(k_1^2 + k_2^2) + \rho^2 \omega^4 \right] \\
&= \frac{1}{\rho^2} \left((2\mu + \lambda)(k_1^2 + k_2^2) - \rho \omega^2 \right) \left(\mu (k_1^2 + k_2^2) - \rho \omega^2 \right). \qquad \text{(B.3)}
\end{aligned}$$

B2 Lemma 1

We have the following well-known result.

Lemma 1. Let

$$u(x,t) = A(x) e^{i(\langle k, x \rangle - \omega t)}, \quad \sigma(x,t) = B(x) e^{i(\langle k, x \rangle - \omega t)}$$

be two functions with $A, B : \mathbb{R}^3 \to \mathbb{C}$. Then the following holds

$$\frac{1}{T} \int_0^T \mathrm{Re}\{u(x,t)\} \mathrm{Re}\{\sigma(x,t)\} dt = \frac{1}{2} \mathrm{Re}(u(x,t) \sigma^*(x,t)), \tag{B.4}$$

where $T = \frac{2\pi}{\omega}$ is the period of the functions u, σ, $*$ denotes the complex conjugate, $x = (x_1, x_2)^{\mathrm{T}}$ and $k = (k_1, k_2)^{\mathrm{T}}$.

Proof. We have:

$$\begin{aligned}
\frac{1}{T}\int_0^T \mathrm{Re}\{u(x,t)\}\mathrm{Re}\{\sigma(x,t)\}dt =& \frac{1}{T}\int_0^T \mathrm{Re}\left(Ae^{i(\langle k,x\rangle-\omega t)}\right)\mathrm{Re}\left(Be^{i(\langle k,x\rangle-\omega t)}\right)dt \\
=& \frac{1}{T}\int_0^T \frac{Ae^{i(\langle k,x\rangle-\omega t)}+A^*e^{-i(\langle k,x\rangle-\omega t)}}{2}\frac{Be^{i(\langle k,x\rangle-\omega t)}+B^*e^{-i(\langle k,x\rangle-\omega t)}}{2}dt \\
=& \frac{1}{4T}\int_0^T AB e^{i2\langle k,x\rangle}\underbrace{e^{-i2\omega t}}_{\text{periodic}}+AB^*+A^*B+A^*B^*e^{-i2\langle k,x\rangle}\underbrace{e^{i2\omega t}}_{\text{periodic}}\,dt \\
=& \frac{1}{4T}\int_0^T AB^*+A^*Bdt \\
=& \frac{1}{2}\mathrm{Re}\left(AB^*\right) \\
=& \frac{1}{2}\mathrm{Re}\left(u(x,t)\sigma^*(x,t)\right), \qquad \text{(B.5)}
\end{aligned}$$

since

$$\frac{1}{2}\mathrm{Re}\left(u(x,t)\sigma^*(x,t)\right)=\frac{1}{2}\mathrm{Re}\left(Ae^{i(\langle k,x\rangle-\omega t)}B^*e^{-i(\langle k,x\rangle-\omega t)}\right)=\frac{1}{2}\mathrm{Re}\left(AB^*\right)$$

where we used the facts that the integral of the periodic function $e^{2i\omega t}$ over its period is zero and that for any complex number $z\in\mathbb{C}$: $\mathrm{Re}(z)=\frac{z+z^*}{2}$. ■

Remark. In our case, when we use the above result to compute the fluxes in equations (4.54) and (4.56), the coefficients A and B of the previous lemma are combinations of the wave-vector components k_1 and k_2, the frequency ω, the amplitudes and the Lamé parameters of the material.

The reflected and transmitted fluxes are the sum of the flux of each mode, i.e. $H_1^r=H_1^{L,r}+H_1^{SV,r}$ and
$H_1^t=H_1^{L,t}+H_1^{SV,t}$ and since all operations involved (derivation, complex conjugation and the real part of a complex quantity) are linear, Lemma B.4 is applied to each of the summands. This is the reason why in the proof above we used the same k in both functions u and σ. Furthermore, this reasoning allows us to deduce that the reflection and transmission coefficients as defined in (4.53) and (4.95) do not depend either on x_1 or x_2.

B3 Conditions for the appearance of Stoneley waves

We explicitly demonstrate all calculations carried out in order to produce Tables 4.1 and 4.2.

Incident L, transmitted waves

In this case, $k_2=-|k|\cos\theta=-\frac{\omega}{c_L^-}\cos\theta$.

- L-mode:

$$\left(\frac{\omega}{c_L^+}\right)^2-k_2^2<0\Rightarrow\left(\frac{\omega}{c_L^+}\right)^2<k_2^2\Rightarrow\left(\frac{\omega}{c_L^+}\right)^2<\left(\frac{\omega}{c_L^-}\right)^2\cos^2\theta\Rightarrow\cos^2\theta>\left(\frac{c_L^-}{c_L^+}\right)^2=\frac{\rho^+(2\mu^-+\lambda^-)}{\rho^-(2\mu^++\lambda^+)}. \qquad \text{(B.6)}$$

- SV-mode:

$$\left(\frac{\omega}{c_S^+}\right)^2-k_2^2<0\Rightarrow\left(\frac{\omega}{c_S^+}\right)^2<k_2^2\Rightarrow\left(\frac{\omega}{c_S^+}\right)^2<\left(\frac{\omega}{c_L^-}\right)^2\cos^2\theta\Rightarrow\cos^2\theta>\left(\frac{c_L^-}{c_S^+}\right)^2=\frac{\rho^+(2\mu^-+\lambda^-)}{\rho^-\mu^+}. \qquad \text{(B.7)}$$

Incident SV, transmitted waves

In this case, $k_2 = -|k|\cos\theta = -\frac{\omega}{c_S^-}\cos\theta$.

- L-mode:

$$\left(\frac{\omega}{c_L^+}\right)^2 - k_2^2 < 0 \Rightarrow \left(\frac{\omega}{c_L^+}\right)^2 < k_2^2 \Rightarrow \left(\frac{\omega}{c_L^+}\right)^2 < \left(\frac{\omega}{c_S^-}\right)^2 \cos^2\theta \Rightarrow \cos^2\theta > \left(\frac{c_S^-}{c_L^+}\right)^2 = \frac{\rho^+\mu^-}{\rho^-(2\mu^+ + \lambda^+)}. \tag{B.8}$$

- SV-mode:

$$\left(\frac{\omega}{c_S^+}\right)^2 - k_2^2 < 0 \Rightarrow \left(\frac{\omega}{c_S^+}\right)^2 < k_2^2 \Rightarrow \left(\frac{\omega}{c_S^+}\right)^2 < \left(\frac{\omega}{c_S^-}\right)^2 \cos^2\theta \Rightarrow \cos^2\theta > \left(\frac{c_S^-}{c_S^+}\right)^2 = \frac{\rho^+\mu^-}{\rho^-\mu^+}. \tag{B.9}$$

Incident SH, transmitted waves

In this case, $k_2 = -|k|\cos\theta = -\frac{\omega}{c_S^-}\cos\theta$.

- SH-mode:

$$\left(\frac{\omega}{c_S^+}\right)^2 - k_2^2 < 0 \Rightarrow \left(\frac{\omega}{c_S^+}\right)^2 < k_2^2 \Rightarrow \left(\frac{\omega}{c_S^+}\right)^2 < \left(\frac{\omega}{c_S^-}\right)^2 \cos^2\theta \Rightarrow \cos^2\theta > \left(\frac{c_S^-}{c_S^+}\right)^2 = \frac{\rho^+\mu^-}{\rho^-\mu^+}. \tag{B.10}$$

Incident Longitudinal, reflected waves

In this case, $k_2 = -|k|\cos\theta = -\frac{\omega}{c_L^-}\cos\theta$.

- L-mode:

$$\left(\frac{\omega}{c_L^-}\right)^2 - k_2^2 < 0 \Rightarrow \left(\frac{\omega}{c_L^-}\right)^2 < k_2^2 \Rightarrow \left(\frac{\omega}{c_L^-}\right)^2 < \left(\frac{\omega}{c_L^-}\right)^2 \cos^2\theta \Rightarrow \cos^2\theta > \left(\frac{c_L^-}{c_L^-}\right)^2 = 1, \tag{B.11}$$

  which renders the L mode becoming Stoneley in the case of an incident Longitudinal wave, impossible.

- SV-mode:

$$\left(\frac{\omega}{c_S^-}\right)^2 - k_2^2 < 0 \Rightarrow \left(\frac{\omega}{c_S^-}\right)^2 < k_2^2 \Rightarrow \left(\frac{\omega}{c_S^-}\right)^2 < \left(\frac{\omega}{c_L^-}\right)^2 \cos^2\theta \Rightarrow \cos^2\theta > \left(\frac{c_L^-}{c_S^-}\right)^2 > 1, \tag{B.12}$$

which renders the SV mode becoming Stoneley in the case of an incident Longitudinal wave, impossible, since $c_L > c_S$ by definition.

Incident SV, reflected waves

In this case, $k_2 = -|k|\cos\theta = -\frac{\omega}{c_S^-}\cos\theta$.

- L-mode:

$$\left(\frac{\omega}{c_L^-}\right)^2 - k_2^2 < 0 \Rightarrow \left(\frac{\omega}{c_L^-}\right)^2 < k_2^2 \Rightarrow \left(\frac{\omega}{c_L^-}\right)^2 < \left(\frac{\omega}{c_S^-}\right)^2 \cos^2\theta \Rightarrow \cos^2\theta > \left(\frac{c_S^-}{c_L^-}\right)^2 = \frac{\mu^-}{(2\mu^- + \lambda^-)}. \tag{B.13}$$

- SV-mode:

$$\left(\frac{\omega}{c_S^-}\right)^2 - k_2^2 < 0 \Rightarrow \left(\frac{\omega}{c_S^-}\right)^2 < k_2^2 \Rightarrow \left(\frac{\omega}{c_S^-}\right)^2 < \left(\frac{\omega}{c_S^-}\right)^2 \cos^2\theta \Rightarrow \cos^2\theta > \left(\frac{c_S^-}{c_S^-}\right)^2 = 1, \tag{B.14}$$

  which renders the SV mode becoming Stoneley in the case of an incident SV wave, impossible.

Incident SH, reflected waves

In this case, $k_2 = -|k|\cos\theta = -\frac{\omega}{c_S^-}\cos\theta$.

- SH-mode:

$$\left(\frac{\omega}{c_S^-}\right)^2 - k_2^2 < 0 \Rightarrow \left(\frac{\omega}{c_S^-}\right)^2 < k_2^2 \Rightarrow \left(\frac{\omega}{c_S^-}\right)^2 < \left(\frac{\omega}{c_S^-}\right)^2 \cos^2\theta \Rightarrow \cos^2\theta > \left(\frac{c_S^-}{c_S^-}\right)^2 = 1, \quad \text{(B.15)}$$

  which shows that there can be no reflected Stoneley waves in the case of an incident SH wave.

B4 Appendix for the relaxed micromorphic model

B4.1 Governing equations in component-wise notation

$$\begin{aligned}
u_{1,tt} &= \frac{\lambda_e+2\mu_e}{\rho}u_{1,11} + \frac{\mu_e+\mu_c}{\rho}u_{1,22} + \frac{\mu_e-\mu_c+\lambda_e}{\rho}u_{2,12} - \frac{2\mu_e}{\rho}P_{11,1} - \frac{\lambda_e}{\rho}(P_{11,1}+P_{22,1}+P_{33,1}) \\
&\quad - \frac{(\mu_e+\mu_c)}{\rho}P_{12,2} - \frac{(\mu_e-\mu_c)}{\rho}P_{21,2}, \\
u_{2,tt} &= \frac{(\lambda_e+2\mu_e)}{\rho}u_{2,22} + \frac{\mu_c+\mu_e}{\rho}u_{2,11} + \frac{\mu_e-\mu_c+\lambda_e}{\rho}u_{1,12} - \frac{2\mu_e}{\rho}P_{22,2} - \frac{\lambda_e}{\rho}(P_{11,2}+P_{22,2}+P_{33,2}) \\
&\quad - \frac{\mu_e+\mu_c}{\rho}P_{21,1} - \frac{\mu_e-\mu_c}{\rho}P_{12,1}, \\
u_{3,tt} &= \frac{\mu_e+\mu_c}{\rho}(u_{3,11}+u_{3,22}) - \frac{\mu_e-\mu_c}{\rho}(P_{13,1}+P_{23,2}) - \frac{\mu_e+\mu_c}{\rho}(P_{31,1}+P_{32,2}), \\
P_{11,tt} &= \frac{2\mu_e+\lambda_e}{\eta}u_{1,1} + \frac{\lambda_e}{\eta}u_{2,2} - 2\frac{\mu_e+\mu_{\text{micro}}}{\eta}P_{11} - \frac{\lambda_e+\lambda_{\text{micro}}}{\eta}(P_{11}+P_{22}+P_{33}) + \frac{\mu_e L_c^2}{\eta}(P_{11,22}-P_{12,12}), \\
P_{12,tt} &= \frac{\mu_e+\mu_c}{\eta}u_{1,2} + \frac{\mu_e-\mu_c}{\eta}u_{2,1} - \frac{\mu_e+\mu_c+\mu_{\text{micro}}}{\eta}P_{12} - \frac{\mu_e-\mu_c+\mu_{\text{micro}}}{\eta}P_{21} + \frac{\mu_e L_c^2}{\eta}(P_{12,11}-P_{11,12}), \\
P_{13,tt} &= \frac{\mu_e-\mu_c}{\eta}u_{3,1} - \frac{\mu_e+\mu_c+\mu_{\text{micro}}}{\eta}P_{13} - \frac{\mu_e-\mu_c+\mu_{\text{micro}}}{\eta}P_{31} + \frac{\mu_e L_c^2}{\eta}(P_{13,22}+P_{13,11}), \\
P_{21,tt} &= \frac{\mu_e-\mu_c}{\eta}u_{1,2} + \frac{\mu_e+\mu_c}{\eta}u_{2,1} - \frac{\mu_e-\mu_c+\mu_{\text{micro}}}{\eta}P_{12} - \frac{\mu_e+\mu_c+\mu_{\text{micro}}}{\eta}P_{21} + \frac{\mu_e L_c^2}{\eta}(P_{21,22}-P_{22,12}), \\
P_{22,tt} &= \frac{2\mu_e+\lambda_e}{\eta}u_{2,2} + \frac{\lambda_e}{\eta}u_{1,1} - 2\frac{\mu_e+\mu_{\text{micro}}}{\eta}P_{22} - \frac{\lambda_e+\lambda_{\text{micro}}}{\eta}(P_{11}+P_{22}+P_{33}) + \frac{\mu_e L_c^2}{\eta}(P_{22,11}-P_{21,12}), \\
P_{23,tt} &= \frac{\mu_e-\mu_c}{\eta}u_{3,2} - \frac{\mu_e+\mu_c+\mu_{\text{micro}}}{\eta}P_{23} - \frac{\mu_e-\mu_c+\mu_{\text{micro}}}{\eta}P_{32} + \frac{\mu_e L_c^2}{\eta}(P_{23,22}+P_{23,11}), \\
P_{31,tt} &= \frac{\mu_e+\mu_c}{\eta}u_{3,1} - \frac{\mu_e-\mu_c+\mu_{\text{micro}}}{\eta}P_{13} - \frac{\mu_c+\mu_e+\mu_{\text{micro}}}{\eta}P_{31} + \frac{\mu_e L_c^2}{\eta}(P_{31,22}-P_{32,12}), \\
P_{32,tt} &= \frac{\mu_e+\mu_c}{\eta}u_{3,2} - \frac{\mu_e-\mu_c+\mu_{\text{micro}}}{\eta}P_{23} - \frac{\mu_e+\mu_c+\mu_{\text{micro}}}{\eta}P_{32} + \frac{\mu_e L_c^2}{\eta}(P_{32,11}-P_{31,12}), \\
P_{33,tt} &= \frac{\lambda_e}{\eta}(u_{1,1}+u_{2,2}) - 2\frac{\mu_e+\mu_{\text{micro}}}{\eta}P_{33} - \frac{\lambda_e+\lambda_{\text{micro}}}{\eta}(P_{11}+P_{22}+P_{33}) + \frac{\mu_e L_c^2}{\eta}(P_{33,22}+P_{313,11}).
\end{aligned}$$

B4.2 Governing equations with new variables

Define the new variables[1]

$$P^S = \frac{1}{3}(P_{11}+P_{22}+P_{33}), \quad P^D_1 = P_{11}-P^S, \quad P^D_2 = P_{22}-P^S, \quad P_{(1\gamma)} = \frac{1}{2}(P_{1\gamma}+P_{\gamma 1}),$$
$$P_{[1\gamma]} = \frac{1}{2}(P_{1\gamma}-P_{\gamma 1}), \quad P_{(23)} = \frac{1}{2}(P_{23}+P_{32}), \quad P_{[23]} = \frac{1}{2}(P_{12}-P_{21}),$$

with $\gamma = 2,3$ and rewrite the equations with respect to these new variables:

$$\begin{aligned}
u_{1,tt} &= \frac{2\mu_e+\lambda_e}{\rho}u_{1,11} + \frac{\mu_e+\mu_c}{\rho}u_{1,22} + \frac{\mu_e-\mu_c+\lambda_e}{\rho}u_{2,12} - 2\frac{\mu_e}{\rho}P^D_{1,1} - \frac{3\lambda_e+2\mu_e}{\rho}P^S_{,1} - 2\frac{\mu_e}{\rho}P_{(12),2} - 2\frac{\mu_c}{\rho}P_{[12],2},\\
u_{2,tt} &= \frac{\mu_e-\mu_c+\lambda_e}{\rho}u_{1,12} + \frac{\mu_e+\mu_c}{\rho}u_{2,11} + \frac{2\mu_e+\lambda_e}{\rho}u_{2,22} - 2\frac{\mu_e}{\rho}P^D_{2,2} - \frac{3\lambda_e+2\mu_e}{\rho}P^S_{,2} - 2\frac{\mu_e}{\rho}P_{(12),1} + 2\frac{\mu_c}{\rho}P_{[12],1},\\
P^D_{1,tt} &= \frac{4}{3}\frac{\mu_e}{\eta}u_{1,1} - \frac{2}{3}\frac{\mu_e}{\eta}u_{2,2} - 2\frac{\mu_e+\mu_{\text{micro}}}{\eta}P^D_1 + \frac{\mu_e L_c^2}{3\eta}P^D_{1,11} + \frac{\mu_e L_c^2}{\eta}P^D_{1,22} + \frac{\mu_e L_c^2}{3\eta}P^D_{2,22} - \frac{2}{3}\frac{\mu_e L_c^2}{\eta}P^S_{,11} + \frac{\mu_e L_c^2}{3\eta}P^S_{,22}\\
&\quad - \frac{\mu_e Lc}{3\eta}P_{(12),12} - \frac{\mu_e L_c^2}{\eta}P_{[12],12},\\
P^D_{2,tt} &= -\frac{2}{3}\frac{\mu_e}{\eta}u_{1,1} + \frac{4}{3}\frac{\mu_e}{\eta}u_{2,2} + \frac{\mu_e L_c^2}{3\eta}P^D_{1,11} - 2\frac{\mu_e+\mu_{\text{micro}}}{\eta}P^D_2 + \frac{\mu_e L_c^2}{\eta}P^D_{2,11} + \frac{\mu_e L_c^2}{3\eta}P^D_{2,22} + \frac{\mu_e L_c^2}{3\eta}P^S_{,11} - \frac{2}{3}\frac{\mu_e L_c^2}{\eta}P^S_{,22}\\
&\quad - \frac{\mu_e L_c^2}{3\eta}P_{(12),12} + \frac{\mu_e L_c^2}{\eta}P_{[12],12},\\
P^S_{,tt} &= \frac{2\mu_e+3\lambda_e}{3\eta}u_{1,1} + \frac{2\mu_e+3\lambda_e}{3\eta}u_{2,2} - \frac{\mu_e L_c^2}{3\eta}P^D_{1,11} - \frac{\mu_e L_c^2}{3\eta}P^D_{2,22} - \frac{(2\mu_e+3\lambda_e)+(2\mu_{\text{micro}}+3\lambda_{\text{micro}})}{\eta}P^S + \frac{2}{3}\frac{\mu_e L_c^2}{\eta}P^S_{,11}\\
&\quad + \frac{2}{3}\frac{\mu_e L_c^2}{\eta}P^S_{,22} - \frac{2}{3}\frac{\mu_e L_c^2}{\eta}P_{(12),12},\\
P_{(12),tt} &= \frac{\mu_e}{\eta}u_{1,2} + \frac{\mu_e}{\eta}u_{2,1} - \frac{1}{2}\frac{\mu_c L_c^2}{\eta}P^D_{1,12} - \frac{1}{2}\frac{\mu_c L_c^2}{\eta}P^D_{2,12} - \frac{\mu_c L_c^2}{\eta}P^S_{,12} - 2\frac{\mu_e+\mu_{\text{micro}}}{\eta}P_{(12)} + \frac{1}{2}\frac{\mu_c L_c^2}{\eta}P_{(12),11} + \frac{1}{2}\frac{\mu_c L_c^2}{\eta}P_{(12),22}\\
&\quad + \frac{1}{2}\frac{\mu_c L_c^2}{\eta}P_{[12],11} - \frac{1}{2}\frac{\mu_c L_c^2}{\eta}P_{[12],22},\\
P_{[12],tt} &= \frac{\mu_c}{\eta}u_{1,2} - \frac{\mu_c}{\eta}u_{2,1} - \frac{1}{2}\frac{\mu_e L_c^2}{\eta}P^D_{1,12} + \frac{1}{2}\frac{\mu_e L_c^2}{\eta}P^D_{2,12} + \frac{1}{2}\frac{\mu_e L_c^2}{\eta}P_{(12),11} - \frac{1}{2}\frac{\mu_e L_c^2}{\eta}P_{(12),22} - 2\frac{\mu_c}{\eta}P_{[12]} + \frac{1}{2}\frac{\mu_e L_c^2}{\eta}P_{[12],11}\\
&\quad + \frac{1}{2}\frac{\mu_e L_c^2}{\eta}P_{[12],22},\\
u_{3,tt} &= \frac{\mu_e+\mu_c}{\rho}(u_{3,11}+u_{3,22}) - 2\frac{\mu_e}{\rho}P_{(13),1} + 2\frac{\mu_c}{\rho}P_{[13],1} - 2\frac{\mu_e}{\rho}P_{(23),2} + 2\frac{\mu_c}{\rho}P_{[23],2},\\
P_{(13),tt} &= \frac{\mu_e}{\eta}u_{3,1} - 2\frac{\mu_e+\mu_{\text{micro}}}{\eta}P_{(13)} + \frac{1}{2}\frac{\mu_e L_c^2}{\eta}P_{(13),11} + \frac{\mu_e L_c^2}{\eta}P_{(13),22} + \frac{1}{2}\frac{\mu_e L_c^2}{\eta}P_{[13],11} - \frac{1}{2}\frac{\mu_e L_c^2}{\eta}P_{(23),12} + \frac{1}{2}\frac{\mu_e L_c^2}{\eta}P_{[23],12},\\
P_{[13],tt} &= -\frac{\mu_c}{\eta}u_{3,1} + \frac{1}{2}\frac{\mu_e L_c^2}{\eta}P_{(13),11} - 2\frac{\mu_c}{\eta}P_{[13]} + \frac{1}{2}\frac{\mu_e L_c^2}{\eta}P_{[13],11} + \frac{\mu_e L_c^2}{\eta}P_{[13],22} + \frac{1}{2}\frac{\mu_e L_c^2}{\eta}P_{(23),12} - \frac{1}{2}\frac{\mu_e L_c^2}{\eta}P_{[23],12},\\
P_{(23),tt} &= \frac{\mu_e}{\eta}u_{3,2} - \frac{1}{2}\frac{\mu_e L_c^2}{\eta}P_{(13),12} + \frac{1}{2}\frac{\mu_e L_c^2}{\eta}P_{[13],12} - 2\frac{\mu_e+\mu_{\text{micro}}}{\eta}P_{(23)} + \frac{\mu_e L_c^2}{\eta}P_{(23),11} + \frac{1}{2}\frac{\mu_e L_c^2}{\eta}P_{(23),22} + \frac{1}{2}\frac{\mu_e L_c^2}{\eta}P_{[23],22},\\
P_{[23],tt} &= -\frac{\mu_c}{\eta}u_{3,2} + \frac{1}{2}\frac{\mu_e L_c^2}{\eta}P_{(13),12} - \frac{1}{2}\frac{\mu_e L_c^2}{\eta}P_{[13],12} + \frac{1}{2}\frac{\mu_e L_c^2}{\eta}P_{(23),22} - 2\frac{\mu_c}{\eta}P_{[23]} + \frac{\mu_e L_c^2}{\eta}P_{[23],11} + \frac{1}{2}\frac{\mu_e L_c^2}{\eta}P_{[23],22}.
\end{aligned}$$

Collect the new variables as

$$v^1 = \left(u_1, u_2, P^D_1, P^D_2, P^S, P_{(12)}, P_{[12]}\right)^{\mathrm{T}}, \tag{B.16}$$
$$v^2 = \left(u_3, P_{(13)}, P_{[13]}, P_{(23)}, P_{[23]}\right)^{\mathrm{T}}. \tag{B.17}$$

[1]The definitions are motivated by the Cartan-Lie decomposition of the tensor P.

B4.3 The matrices A_1 and A_2

The form of the matrices being too complicated to fit in one page, we present both A_1 and A_2 in a column-wise sense.

$$A_{11} = \begin{pmatrix} \left(k_1^2 \frac{2\mu_e+\lambda_e}{\rho} + k_2^2 \frac{\mu_e+\mu_c}{\rho}\right) - \omega^2 \\ k_1 k_2 \frac{\mu_e-\mu_c+\lambda_e}{\rho} \\ -2ik_1 \frac{\mu_e}{\rho} \\ 0 \\ -ik_1 \frac{3\lambda_e+2\mu_e}{\rho} \\ -2ik_2 \frac{\mu_e}{\rho} \\ 2ik_2 \frac{\mu_e}{\rho} \end{pmatrix}^{\mathrm{T}}, \quad A_{12} = \begin{pmatrix} k_1 k_2 \frac{\mu_e-\mu_c+\lambda_e}{\rho} \\ \left(k_1^2 \frac{\mu_e+\mu_c}{\rho} + k_2^2 \frac{2\mu_e+\lambda_e}{\rho}\right) - \omega^2 \\ 0 \\ -2ik_2 \frac{\mu_e}{\rho} \\ -ik_2 \frac{3\lambda_e+2\mu_e}{\rho} \\ -2ik_1 \frac{\mu_e}{\rho} \\ 2ik_1 \frac{\mu_e}{\rho} \end{pmatrix}^{\mathrm{T}}, \tag{B.18}$$

$$A_{13} = \begin{pmatrix} \frac{4}{3}ik_1 \frac{\mu_e}{\eta} \\ -\frac{2}{3}ik_2 \frac{\mu_e}{\eta} \\ \left(k_1^2 \frac{\mu_e Lc}{3\eta} + k_2^2 \frac{\mu_e L_c^2}{\eta}\right) + 2\frac{\mu_e+\mu_{\mathrm{micro}}}{\eta} - \omega^2 \\ k_2^2 \frac{\mu_e L_c^2}{3\eta} \\ \left(k_2^2 \frac{\mu_e L_c^2}{3\eta} - k_1^2 \frac{\mu_e L_c^2}{\eta}\right) \\ -k_1 k_2 \frac{\mu_e L_c^2}{3\eta} \\ -k_1 k_2 \frac{\mu_e L_c^2}{\eta} \end{pmatrix}^{\mathrm{T}}, \quad A_{14} = \begin{pmatrix} -\frac{2}{3}ik_1 \frac{\mu_e}{\eta} \\ +\frac{4}{3}ik_2 \frac{\mu_e}{\eta} \\ k_1^2 \frac{\mu_e L_c^2}{3\eta} \\ \left(k_1^2 \frac{\mu_e L_c^2}{\eta} + k_2^2 \frac{\mu_e L_c^2}{3\eta}\right) + 2\frac{\mu_e+\mu_{\mathrm{micro}}}{\eta} - \omega^2 \\ \left(k_1^2 \frac{\mu_e L_c^2}{3\eta} - \frac{2}{3}k_2^2 \frac{\mu_e L_c^2}{\eta}\right) \\ -k_1 k_2 \frac{\mu_e L_c^2}{3\eta} \\ k_1 k_2 \frac{\mu_e L_c^2}{\eta} \end{pmatrix}^{\mathrm{T}},$$

$$A_{15} = \begin{pmatrix} ik_1 \frac{2\mu_e+3\lambda_e}{3\eta} \\ ik_2 \frac{2\mu_e+3\lambda_e}{3\eta} \\ -k_1^2 \frac{\mu_e L_c^2}{3\eta} \\ -k_2^2 \frac{\mu_e L_c^2}{3\eta} \\ \frac{2}{3}(k_1^2+k_2^2)\frac{\mu_e L_c^2}{\eta} + \frac{(2\mu_e+3\lambda_e)+(2\mu_{\mathrm{micro}}+3\lambda_{\mathrm{micro}})}{\eta} - \omega^2 \\ -\frac{2}{3}k_1 k_2 \frac{\mu_e L_c^2}{\eta} \\ 0 \end{pmatrix}^{\mathrm{T}}, \quad A_{16} = \begin{pmatrix} ik_2 \frac{\mu_e}{\eta} \\ ik_1 \frac{\mu_e}{\eta} \\ -\frac{1}{2}k_1 k_2 \frac{\mu_e L_c^2}{\eta} \\ -\frac{1}{2}k_1 k_2 \frac{\mu_e L_c^2}{\eta} \\ -k_1 k_2 \frac{\mu_e L_c^2}{\eta} \\ \frac{1}{2}(k_1^2+k_2^2)\frac{\mu_e L_c^2}{\eta} + 2\frac{\mu_e+\mu_{\mathrm{micro}}}{\eta} - \omega^2 \\ \frac{1}{2}(k_1^2-k_2^2)\frac{\mu_e L_c^2}{\eta} \end{pmatrix}^{\mathrm{T}}, \tag{B.19}$$

$$A_{17} = \begin{pmatrix} ik_2 \frac{\mu_c}{\eta} \\ -ik_1 \frac{\mu_c}{\eta} \\ -\frac{1}{2}k_1 k_2 \frac{\mu_e L_c^2}{\eta} \\ \frac{1}{2}k_1 k_2 \frac{\mu_e L_c^2}{\eta} \\ 0 \\ \frac{1}{2}(k_1^2-k_2^2)\frac{\mu_e L_c^2}{\eta} \\ \frac{1}{2}(k_1^2+k_2^2)\frac{\mu_e L_c^2}{\eta} + 2\frac{\mu_c}{\eta} - \omega^2 \end{pmatrix}^{\mathrm{T}}. \tag{B.20}$$

Then, the matrix A_1 is

$$A_1 = (A_{11}, A_{12}, A_{13}, A_{14}, A_{15}, A_{16}, A_{17})^{\mathrm{T}}. \tag{B.21}$$

As for A_2 we have:

$$A_{21} = \begin{pmatrix} (k_1^2+k_2^2)\frac{\mu_e+\mu_c}{\rho} - \omega^2 \\ 2ik_1\frac{\mu_e}{\rho} \\ -2ik_1\frac{\mu_c}{\rho} \\ 2ik_2\frac{\mu_e}{\rho} \\ -2ik_2\frac{\mu_c}{\rho} \end{pmatrix}^{\mathrm{T}} \quad A_{22} = \begin{pmatrix} -ik_1\frac{\mu_e}{\eta} \\ \left(k_1^2\frac{\mu_e L_c^2}{2\eta} + k_2^2\frac{\mu_e L_c^2}{\eta}\right) + 2\frac{\mu_e+\mu_{\mathrm{micro}}}{\eta} - \omega^2 \\ k_1^2\frac{\mu_e L_c^2}{2\eta} \\ -k_1k_2\frac{\mu_e L_c^2}{2\eta} \\ k_1k_2\frac{\mu_e L_c^2}{2\eta} \end{pmatrix}^{\mathrm{T}}$$

$$A_{23} = \begin{pmatrix} ik_1\frac{\mu_c}{\eta} \\ k_1^2\frac{\mu_e L_c^2}{2\eta} \\ \left(k_1^2\frac{\mu_e L_c^2}{2\eta} + k_2^2\frac{\mu_e L_c^2}{\eta}\right) + 2\frac{\mu_c}{\eta} - \omega^2 \\ k_1k_2\frac{\mu_e L_c^2}{2\eta} \\ -k_1k_2\frac{\mu_e L_c^2}{2\eta} \end{pmatrix}^{\mathrm{T}} \quad A_{24} = \begin{pmatrix} -ik_2\frac{\mu_e}{\eta} \\ -k_1k_2\frac{\mu_e L_c^2}{2\eta} \\ k_1k_2\frac{\mu_e L_c^2}{2\eta} \\ \left(k_1^2\frac{\mu_e L_c^2}{\eta} + k_2^2\frac{\mu_e L_c^2}{2\eta}\right) + 2\frac{\mu_e+\mu_{\mathrm{micro}}}{\eta} - \omega^2 \\ k_2^2\frac{\mu_e L_c^2}{2\eta} \end{pmatrix}^{\mathrm{T}} \tag{B.22}$$

$$A_{25} = \begin{pmatrix} ik_2\frac{\mu_c}{\eta} \\ k_1k_2\frac{\mu_e L_c^2}{2\eta} \\ -k_1k_2\frac{\mu_e L_c^2}{2\eta} \\ k_2^2\frac{\mu_e L_c^2}{2\eta} \\ \left(k_1^2\frac{\mu_e L_c^2}{\eta} + k_2^2\frac{\mu_e L_c^2}{2\eta}\right) + 2\frac{\mu_c}{\eta} - \omega^2 \end{pmatrix}^{\mathrm{T}}. \tag{B.23}$$

Then, the matrix A_2 is

$$A_2 = (A_{21}, A_{22}, A_{23}, A_{24}, A_{25})^{\mathrm{T}}. \tag{B.24}$$

B4.4 Dispersion curves analysis of the relaxed micromorphic model

In-plane variables

First, observe that after replacing the wave form (4.76) in (3.34), A_1 can be written as (see Appendix B4.5 for a demonstration of these matrices):

$$A_1 = |k|^2 A_1^R - \omega^2 \mathbb{1} - i|k|B_1^R - C_1^R. \tag{B.25}$$

We now investigate the behaviour of the polynomial $\det A_1$ for the two limiting cases $|k| \to 0$ and $|k| \to \infty$, the final goal being to be able to determine the cut-off frequencies and asymptotes of the dispersion curves.

Letting $|k| \to 0$ and using (B.25), the equation $A_1 \cdot v^1 = 0$ becomes

$$(\omega^2 \mathbb{1} + C_1^R) \cdot v^1 = 0. \tag{B.26}$$

Using expression (B.45) for C_1^R, we get

$$\begin{pmatrix} \omega^2 & 0 & 0 & 0 & 0 & 0 & 0 \\ 0 & \omega^2 & 0 & 0 & 0 & 0 & 0 \\ 0 & 0 & \omega^2-\omega_s^2 & 0 & 0 & 0 & 0 \\ 0 & 0 & 0 & \omega^2-\omega_s^2 & 0 & 0 & 0 \\ 0 & 0 & 0 & 0 & \omega^2-\omega_p^2 & 0 & 0 \\ 0 & 0 & 0 & 0 & 0 & \omega^2-\omega_s^2 & 0 \\ 0 & 0 & 0 & 0 & 0 & 0 & \omega^2-\omega_r^2 \end{pmatrix} \cdot v^1 = 0. \tag{B.27}$$

This allows us to deduce that for small values of $|k|$, the cut-off frequencies of the dispersion curves are $\omega = 0$, $\omega = \omega_s$, $\omega = \omega_r$, $\omega = \omega_p$ as shown in Figure 4.10.

As for when $|k| \to \infty$, we consider the case where the ratio $|k|/\omega$ remains finite and so instead of studying the whole system we can simply regard the reduced system

$$\left(|k|^2 A_1^R - \omega^2 \mathbb{1}\right) \cdot v^1 = 0. \tag{B.28}$$

The determinant of $|k|^2 A_1^R - \omega^2 \mathbb{1}$ is

$$\det\left(|k|^2 A_1^R - \omega^2 \mathbb{1}\right) = \omega^4 (|k|^2 c_m^2 - \omega^2)^3 (|k|^2 c_f^2 - \omega^2)(|k|^2 c_p^2 - \omega^2). \tag{B.29}$$

If we solve the equation $\det\left(|k|^2 A_1^R - \omega^2 \mathbb{1}\right) = 0$, we find the solution $\omega = 0$, which has to be excluded since it violates the requirement $|k|/\omega$ finite for $|k| \to \infty$. The other solutions are $\omega = c_m|k|$, $\omega = c_f|k|$, $\omega = c_p|k|$; these are the asymptotes to the dispersion curves.

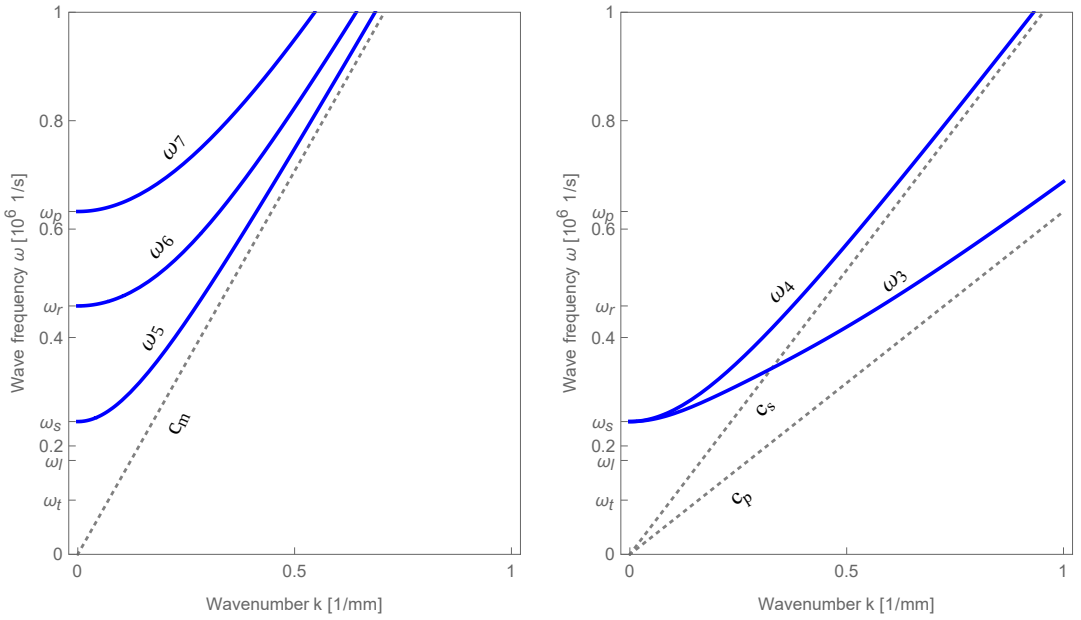

(a) (b)

Figure B.1: (a) Three distinct modes have distinct cut-off frequencies but a common asymptote with slope c_m, (b) Two distinct modes have the same cut-off frequencies but asymptotes with different slopes c_f and c_p.

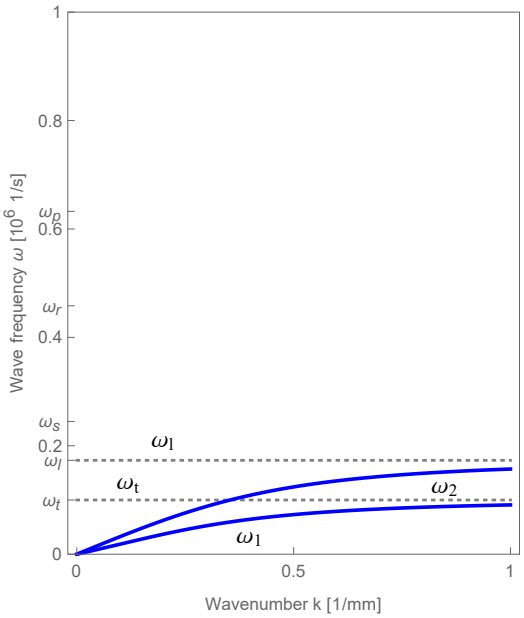

Figure B.2: Two modes with horizontal asymptotes ω_l and ω_t.

Finally, the two horizontal asymptotes are $\omega = \omega_l$ and $\omega = \omega_t$ (see Section B4.4 for the analytical method of how to find them).

The first, second and fifth modes all have the same asymptote $\omega = c_m|k|$ (Figure B.1 (a)). Unfortunately, due to the very complicated expressions for $\omega_2(|k|)$ and $\omega_3(|k|)$, this cannot be analytically reaffirmed; numerically, however, we find:

$$\lim_{|k|\to\infty} |\omega_i(|k|) - c_m|k|| = 0,$$

for $i = 1, 2, 5$.

Figure 4.10 summarizes the main characteristics of the dispersion curves that we find for an isotropic relaxed micromorphic medium (cut-off frequencies, horizontal and oblique asymptotes). Figures B.1 (a), (b) and B.2 show in more detail the oblique and horizontal asymptotes for the different modes.

Out-of-plane variables

Similarly to the in-plane case, we can again write

$$A_2 = |\widetilde{k}|^2 A_2^R - \omega^2 \mathbb{1} - i|\widetilde{k}| B_2^R - C_2^R. \tag{B.30}$$

We now investigate the behavior of the polynomial $\det A_2$ for the two limiting cases $|\widetilde{k}| \to 0$ and $|\widetilde{k}| \to \infty$.

Letting $|\widetilde{k}| \to 0$, equation $A_2 \cdot v^2 = 0$ becomes

$$\begin{pmatrix} \omega^2 & 0 & 0 & 0 & 0 \\ 0 & \omega^2 - \omega_s^2 & 0 & 0 & 0 \\ 0 & 0 & \omega^2 - \omega_r^2 & 0 & 0 \\ 0 & 0 & 0 & \omega^2 - \omega_s^2 & 0 \\ 0 & 0 & 0 & 0 & \omega^2 - \omega_r^2 \end{pmatrix} \cdot v^2 = 0. \tag{B.31}$$

This allows us to deduce that for small values of $|\widetilde{k}|$, the cut-off frequencies of the dispersion curves are $\omega = 0$, $\omega = \omega_s$, $\omega = \omega_r$ as shown in Figure 4.12.

We now let $|\widetilde{k}| \to \infty$ and we once again assume that the ratio $|\widetilde{k}|/\omega$ remains finite. Then, the system reduces to

$$E_2 \cdot v^2 := (|\widetilde{k}|^2 A_2^R - \omega^2 \mathbb{1}) \cdot v^2 = 0, \tag{B.32}$$

where[2]

$$E_2 = \begin{pmatrix} |\widetilde{k}|^2 c_f^2 - \omega^2 & 0 & 0 & 0 & 0 \\ 0 & |\widetilde{k}|^2 c_m^2 \left(\frac{1}{2}\xi_1^2 + \xi_2^2\right) - \omega^2 & \frac{1}{2}|\widetilde{k}|^2 c_m^2 \xi_1^2 & -\frac{1}{2}|\widetilde{k}|^2 c_m^2 \xi_1 \xi_2 & \frac{1}{2}|\widetilde{k}|^2 c_m^2 \xi_1 \xi_2 \\ 0 & \frac{1}{2}|\widetilde{k}|^2 c_m^2 \xi_1^2 & |\widetilde{k}|^2 c_m^2 \left(\frac{1}{2}\xi_1^2 + \xi_2^2\right) - \omega^2 & \frac{1}{2}|\widetilde{k}|^2 c_m^2 \xi_1 \xi_2 & -\frac{1}{2}|\widetilde{k}|^2 c_m^2 \xi_1 \xi_2 \\ 0 & -\frac{1}{2}|\widetilde{k}|^2 c_m^2 \xi_1 \xi_2 & \frac{1}{2}|\widetilde{k}|^2 c_m^2 \xi_1 \xi_2 & |\widetilde{k}|^2 c_m^2 (\xi_1^2 + \frac{1}{2}\xi_2^2) - \omega^2 & \frac{1}{2}\xi |\widetilde{k}|^2 c_m^2 2^2 \\ 0 & \frac{1}{2}|\widetilde{k}|^2 c_m^2 \xi_1 \xi_2 & -\frac{1}{2}|\widetilde{k}|^2 c_m^2 \xi_1 \xi_2 & \frac{1}{2}|\widetilde{k}|^2 c_m^2 \xi_2^2 & |\widetilde{k}|^2 c_m^2 (\xi_1^2 + \frac{1}{2}\xi_2^2) - \omega^2 \end{pmatrix} \tag{B.33}$$

The determinant of E_2 is

$$\det E_2 = -\omega^2 (|\widetilde{k}|^2 c_m^2 - \omega^2)^3 (|\widetilde{k}|^2 c_f^2 - \omega^2). \tag{B.34}$$

The solutions of $\det E_2 = 0$ obviously are $\omega = 0, \omega = c_m, \omega = c_f$. We have to exclude the first since it violates the condition that k/ω is finite for $|\widetilde{k}| \to \infty$ and so we conclude that the two non-horizontal asymptotes are the two remaining solutions. Finally, the only horizontal asymptote is $\omega = \omega_t$ (see Section B4.4).

In this case, we have that as $|\widetilde{k}| \to \infty$, the two modes $\widetilde{\omega}_2$ and $\widetilde{\omega}_3$ overlap. Indeed, it can be checked (numerically) that

$$\lim_{|\widetilde{k}| \to \infty} |\widetilde{\omega}_2(|\widetilde{k}|) - \widetilde{\omega}_3(|\widetilde{k}|)| = 0.$$

Furthermore, we again see that the first, second and third modes have the same asymptote $\omega = c_m |\widetilde{k}|$, a fact which cannot be analytically shown due to the complicated expressions involved; however, numerically we find that

$$\lim_{|\widetilde{k}| \to \infty} |\widetilde{\omega}_i(|\widetilde{k}|) - c_m |\widetilde{k}|| = 0,$$

for $i = 1, 2, 3$.

Figures B.3 and B.4 show in more detail the oblique and horizontal asymptotes for different curves.

[2] We present the form such a matrix takes for the out-of-plane variables in the main text since it has a more transparent form, being of smaller dimension.

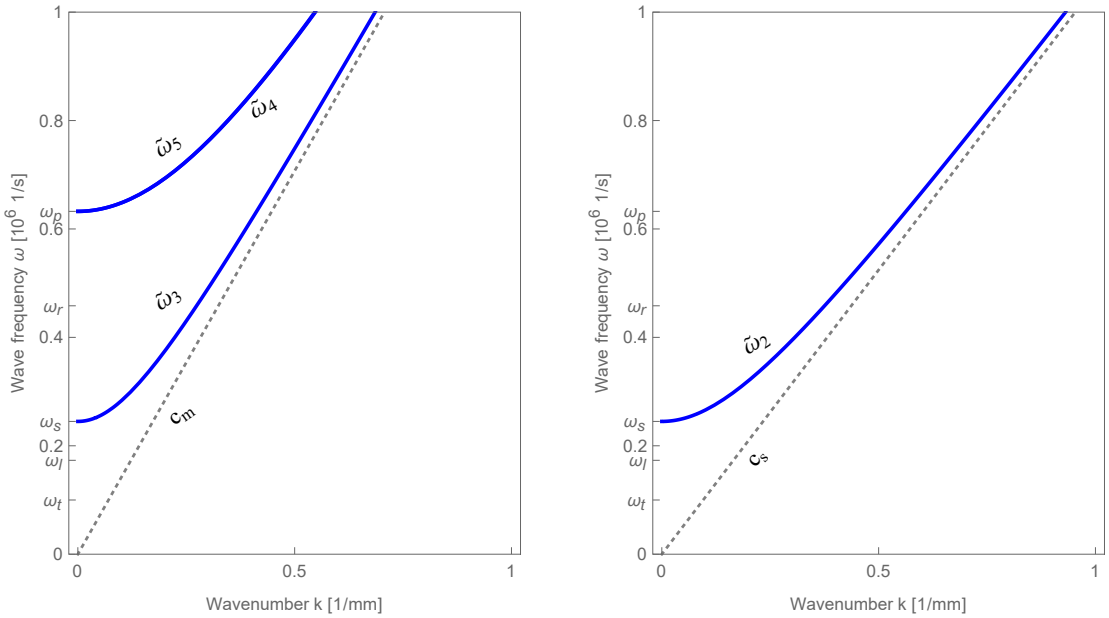

(a) (b)

Figure B.3: (a) First mode with cut-off frequency ω_p and second and third modes which overlap for large values of $|\widetilde{k}|$, all have the same asymptote c_m, (b) The fourth mode has an asymptote with slope c_f.

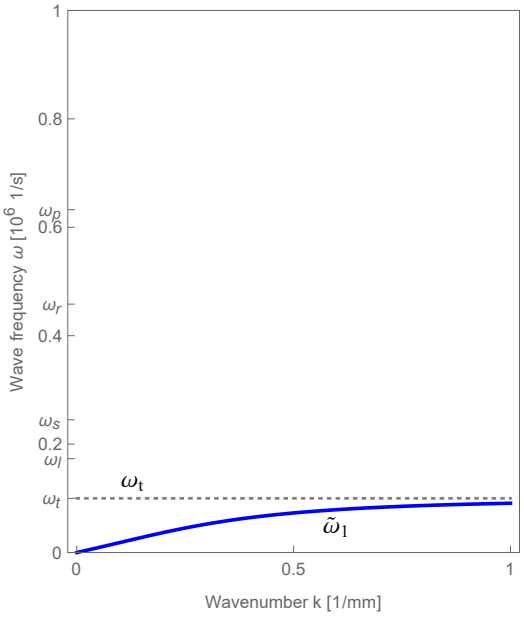

Figure B.4: The fourth mode has the horizontal asymptote ω_t.

How to find the horizontal asymptotes

In order to be sure that the horizontal asymptotes, computed before by splitting the whole problem of the relaxed model in two uncoupled problems, are ω_t and ω_l, we follow what was done in [30].

We begin by constructing the following matrix:

$$A_0 = \begin{pmatrix} & & & & & & & 0 & 0 & 0 & 0 & 0 \\ & & & & & & & 0 & 0 & 0 & 0 & 0 \\ & & & & & & & 0 & 0 & 0 & 0 & 0 \\ & & & & A_1 & & & 0 & 0 & 0 & 0 & 0 \\ & & & & & & & 0 & 0 & 0 & 0 & 0 \\ & & & & & & & 0 & 0 & 0 & 0 & 0 \\ & & & & & & & 0 & 0 & 0 & 0 & 0 \\ 0 & 0 & 0 & 0 & 0 & 0 & 0 & & & & & \\ 0 & 0 & 0 & 0 & 0 & 0 & 0 & & & & & \\ 0 & 0 & 0 & 0 & 0 & 0 & 0 & & & A_2 & & \\ 0 & 0 & 0 & 0 & 0 & 0 & 0 & & & & & \\ 0 & 0 & 0 & 0 & 0 & 0 & 0 & & & & & \end{pmatrix}, \tag{B.35}$$

which is the full matrix of coefficients of the governing equations (3.34) after making the plane-wave ansatz. Furthermore, we define the two auxiliary matrices

$$\widehat{A}_1 = \begin{pmatrix} A_1 & 0 \\ 0 & \mathbb{1}_5 \end{pmatrix}, \quad \widehat{A}_2 = \begin{pmatrix} \mathbb{1}_7 & 0 \\ 0 & A_2 \end{pmatrix}. \tag{B.36}$$

We immediately see that

$$A_0 = \widehat{A}_1 \widehat{A}_2, \tag{B.37}$$

which implies that

$$\det A_0 = \det \widehat{A}_1 \det \widehat{A}_2 = \det A_1 \det A_2. \tag{B.38}$$

Now, the polynomial $p(|k|, \omega) = \det A_0$ is of degree 18 in $|k|$ and only involves even powers of $|k|$. We can write it as

$$p(|k|, \omega) = \sum_{h=0}^{9} c_{2h}(\omega^2)|k|^{2h}. \tag{B.39}$$

Following the same proof as found in [30], we find again the necessary condition a horizontal asymptote has to satisfy is $c_{18}(\omega_*^2) = 0$.[3] This gives us the two solutions

$$\omega = \omega_t, \quad \omega = \omega_l. \tag{B.40}$$

B4.5 Decompositions of A_1 and A_2

We recall that

$$A_1 = |k|^2 A_1^R - \omega^2 \mathbb{1} - i|k| B_1^R - C_1^R, \tag{B.41}$$

$$A_2 = |k|^2 A_2^R - \omega^2 \mathbb{1} - i|k| B_2^R - C_2^R. \tag{B.42}$$

[3] This result follows if we divide by $|k|^{18}$ and let $|k| \to \infty$.

The matrices $A_1^R, B_1^R, C_1^R, A_2^R, B_2^R, C_2^R$, are presented here.

$$A_1^R = \begin{pmatrix} \xi_1^2\frac{\lambda_e+2\mu_e}{\rho}+\xi_2^2\frac{\mu_c+\mu_e}{\rho} & \xi_1\xi_2\frac{\mu_e-\mu_c+\lambda_e}{\rho} & 0 & 0 & 0 & 0 & 0 \\ -\xi_1\xi_2\frac{\mu_e-\mu_c+\lambda_e}{\rho} & \xi_1^2\frac{\mu_c+\mu_e}{\rho}+\xi_2^2\frac{\lambda_e+2\mu_e}{\rho} & 0 & 0 & 0 & 0 & 0 \\ 0 & 0 & (\xi_1^2+3\xi_2^2)\frac{\mu_e L_c^2}{3\eta} & \xi_2^2\frac{\mu_e L_c^2}{3\eta} & (-2\xi_1^2+\xi_2^2)\frac{\mu_e L_c^2}{3\eta} & -\xi_1\xi_2\frac{\mu_e L_c^2}{3\eta} & -\xi_1\xi_2\frac{\mu_e L_c^2}{\eta_2} \\ 0 & 0 & \xi_1^2\frac{\mu_e L_c^2}{3\eta} & (\xi_1^2-+\xi_2^2)\frac{\mu_e L_c^2}{3\eta} & (\xi_1^2-\xi_2^2)\frac{2\mu_e L_c^2}{3\eta} & -\xi_1\xi_2\frac{\mu_e L_c^2}{3\eta} & \xi_1\xi_2\frac{\mu_e L_c^2}{\eta} \\ 0 & 0 & -\xi_1^2\frac{\mu_e L_c^2}{3\eta} & -\xi_2^2\frac{\mu_e L_c^2}{3\eta} & \frac{2\mu_e L_c^2}{3\eta} & -\xi_1\xi_2\frac{2\mu_e L_c^2}{3\eta} & 0 \\ 0 & 0 & -\xi_1\xi_2\frac{\mu_e L_c^2}{2\eta} & -\xi_1\xi_2\frac{\mu_e L_c^2}{2\eta} & -\xi_1\xi_2\frac{\mu_e L_c^2}{\eta} & \frac{\mu_e L_c^2}{2\eta} & (\xi_1^2-\xi_2^2)\frac{\mu_e L_c^2}{2\eta} \\ 0 & 0 & -\xi_1\xi_2\frac{\mu_e L_c^2}{2\eta} & \xi_1\xi_2\frac{\mu_e L_c^2}{2\eta} & 0 & (\xi_1^2-\xi_2^2)\frac{\mu_e L_c^2}{2\eta} & \frac{\mu_e L_c^2}{2\eta} \end{pmatrix}, \tag{B.43}$$

$$B_1^R = \begin{pmatrix} 0 & 0 & -\xi_1\frac{2\mu_e}{\rho} & 0 & -\xi_1\frac{3\lambda_e+2\mu_e}{\rho} & -\xi_2\frac{2\mu_e}{\rho} & -\xi_2\frac{2\mu_e}{\rho} \\ 0 & 0 & 0 & -\xi_2\frac{2\mu_e}{\rho} & -\xi_2\frac{3\lambda_e+2\mu_e}{\rho} & -\xi_1\frac{2\mu_e}{\rho} & \xi_1\frac{2\mu_e}{\rho} \\ \xi_1\frac{4\mu_e}{3\eta} & -\xi_2\frac{2\mu_e}{3\eta} & 0 & 0 & 0 & 0 & 0 \\ -\xi_1\frac{2\mu_e}{3\eta} & \xi_2\frac{4\mu_e}{3\eta} & 0 & 0 & 0 & 0 & 0 \\ \xi_1\frac{3\lambda_e+2\mu_e}{3\eta} & \xi_2\frac{3\lambda_e+2\mu_e}{3\eta} & 0 & 0 & 0 & 0 & 0 \\ \xi_2\frac{\mu_e}{\eta} & \xi_1\frac{\mu_e}{\eta} & 0 & 0 & 0 & 0 & 0 \\ \xi_2\frac{\mu_c}{\eta} & -\xi_1\frac{\mu_c}{\eta} & 0 & 0 & 0 & 0 & 0 \end{pmatrix}, \tag{B.44}$$

$$C_1^R = \begin{pmatrix} 0 & 0 & 0 & 0 & 0 & 0 & 0 \\ 0 & 0 & 0 & 0 & 0 & 0 & 0 \\ 0 & 0 & -\frac{2(\mu_e+\mu_{\text{micro}})}{\eta} & 0 & 0 & 0 & 0 \\ 0 & 0 & 0 & -\frac{2(\mu_e+\mu_{\text{micro}})}{\eta} & 0 & 0 & 0 \\ 0 & 0 & 0 & 0 & -\frac{(2\mu_e+3\lambda_e)+(2\mu_{\text{micro}}+3\lambda_{\text{micro}})}{\eta} & 0 & 0 \\ 0 & 0 & 0 & 0 & 0 & -\frac{2(\mu_e+\mu_{\text{micro}})}{\eta} & 0 \\ 0 & 0 & 0 & 0 & 0 & 0 & -\frac{2\mu_c}{\eta} \end{pmatrix}. \tag{B.45}$$

Finally, we have that

$$A_1 = |k|^2 A_1^R - \omega^2 \mathbb{1} - i|k| B_1^R - C_1^R. \tag{B.46}$$

As for A_2, it can be written in a similar fashion. We have

$$A_2^R = \begin{pmatrix} \frac{\mu_c+\mu_e}{\rho} & 0 & 0 & 0 & 0 \\ 0 & \frac{\mu_e L_c^2}{\eta}(\frac{1}{2}\xi_1^2+\xi_2^2) & \frac{\mu_e L_c^2}{2\eta}\xi_1^2 & -\frac{\mu_e L_c^2}{2\eta}\xi_1\xi_2 & \frac{\mu_e L_c^2}{2\eta}\xi_1\xi_2 \\ 0 & \frac{\mu_e L_c^2}{2\eta}\xi_1^2 & \frac{\mu_e L_c^2}{\eta}(\frac{1}{2}\xi_1^2+\xi_2^2) & \frac{\mu_e L_c^2}{2\eta}\xi_1\xi_2 & -\frac{\mu_e L_c^2}{2\eta}\xi_1\xi_2 \\ 0 & -\frac{\mu_e L_c^2}{2\eta}\xi_1\xi_2 & \frac{\mu_e L_c^2}{2\eta}\xi_1\xi_2 & \frac{\mu_e L_c^2}{\eta}(\xi_1^2+\frac{1}{2}\xi_2^2) & \frac{\mu_e L_c^2}{2\eta}\xi_2^2 \\ 0 & \frac{\mu_e L_c^2}{2\eta}\xi_1\xi_2 & -\frac{\mu_e L_c^2}{2\eta}\xi_1\xi_2 & \frac{\mu_e L_c^2}{2\eta}\xi_2^2 & \frac{\mu_e L_c^2}{\eta}(\xi_1^2+\frac{1}{2}\xi_2^2) \end{pmatrix}, \tag{B.47}$$

$$B_2^R = \begin{pmatrix} 0 & -\frac{2\mu_e}{\rho}\xi_1 & \frac{2\mu_c}{\rho}\xi_1 & -\frac{2\mu_e}{\rho}\xi_2 & \frac{2\mu_c}{\rho}\xi_2 \\ \frac{\mu_e}{\eta}\xi_1 & 0 & 0 & 0 & 0 \\ -\frac{\mu_c}{\eta}\xi_1 & 0 & 0 & 0 & 0 \\ \frac{\mu_e}{\eta}\xi_2 & 0 & 0 & 0 & 0 \\ -\frac{\mu_c}{\eta}\xi_2 & 0 & 0 & 0 & 0 \end{pmatrix}, \quad C_2^R = \begin{pmatrix} 0 & 0 & 0 & 0 & 0 \\ 0 & -\frac{2(\mu_e+\mu_{\text{micro}})}{\eta} & 0 & 0 & 0 \\ 0 & 0 & -\frac{2\mu_c}{\eta} & 0 & 0 \\ 0 & 0 & 0 & -\frac{2(\mu_e+\mu_{\text{micro}})}{\eta} & 0 \\ 0 & 0 & 0 & 0 & -\frac{2\mu_c}{\eta} \end{pmatrix}. \tag{B.48}$$

And then, we can write A_2 as

$$A_2 = |k|^2 A_2^R - \omega^2 \mathbb{1} - i|k| B_2^R - C_2^R. \tag{B.49}$$

B4.6 Energy flux matrices

The expression for the energy flux in the relaxed micromorphic model for the case of in-plane motion is given by

$$H_1 = v^1_{,t} \cdot (H^{11} \cdot v^1_{,1} + H^{12} \cdot v^1_{,2} + H^{13} \cdot v^1),$$

where

$$H^{11} = \begin{pmatrix} -2\mu_e - \lambda_e & 0 & 0 & 0 & 0 & 0 & 0 \\ 0 & -\mu_e - \mu_c & 0 & 0 & 0 & 0 & 0 \\ 0 & 0 & -L_c^2\mu_e & -L_c^2\mu_e & L_c^2\mu_e & 0 & 0 \\ 0 & 0 & -L_c^2\mu_e & -2L_c^2\mu_e & 0 & 0 & 0 \\ 0 & 0 & L_c^2\mu_e & 0 & -2L_c^2\mu_e & 0 & 0 \\ 0 & 0 & 0 & 0 & 0 & -L_c^2\mu_e & -L_c^2\mu_e \\ 0 & 0 & 0 & 0 & 0 & -L_c^2\mu_e & -L_c^2\mu_e \end{pmatrix}, \tag{B.50}$$

$$H^{12} = \begin{pmatrix} 0 & -\lambda_e & 0 & 0 & 0 & 0 & 0 \\ \mu_c - \mu_e & 0 & 0 & 0 & 0 & 0 & 0 \\ 0 & 0 & 0 & 0 & 0 & 0 & 0 \\ 0 & 0 & 0 & 0 & 0 & L_c^2\mu_e & -L_c^2\mu_e \\ 0 & 0 & 0 & 0 & 0 & L_c^2\mu_e & -L_c^2\mu_e \\ 0 & 0 & L_c^2\mu_e & 0 & L_c^2\mu_e & 0 & 0 \\ 0 & 0 & L_c^2\mu_e & 0 & L_c^2\mu_e & 0 & 0 \end{pmatrix}, \quad H^{13} = \begin{pmatrix} 0 & 0 & 2\mu_e & 0 & 2\mu_e + 3\lambda_e & 0 & 0 \\ 0 & 0 & 0 & 0 & 0 & 2\mu_e & -2\mu_c \\ 0 & 0 & 0 & 0 & 0 & 0 & 0 \\ 0 & 0 & 0 & 0 & 0 & 0 & 0 \\ 0 & 0 & 0 & 0 & 0 & 0 & 0 \\ 0 & 0 & 0 & 0 & 0 & 0 & 0 \\ 0 & 0 & 0 & 0 & 0 & 0 & 0 \end{pmatrix}. \tag{B.51}$$

In the case of out-of-plane motion, the expression for the energy flux in the relaxed micromorphic model is given by

$$H_1 = v^2_{,t} \cdot (H^{21} \cdot v^2_{,1} + H^{22} \cdot v^2_{,2} + H^{23} \cdot v^2),$$

where

$$H^{21} = \begin{pmatrix} -\mu_c - \mu_e & 0 & 0 & 0 & 0 \\ 0 & 0 & 0 & 0 & 0 \\ 0 & 0 & 0 & 0 & 0 \\ 0 & 0 & 0 & 0 & 0 \\ 0 & 0 & 0 & -L_c^2\mu_e & L_c^2\mu_e \\ 0 & 0 & 0 & L_c^2\mu_e & -L_c^2\mu_e \end{pmatrix}, \quad H^{22} = \begin{pmatrix} 0 & 0 & 0 & 0 & 0 \\ 0 & 0 & 0 & 0 & 0 \\ 0 & 0 & 0 & 0 & 0 \\ 0 & 0 & 0 & 0 & 0 \\ 0 & L_c^2\mu_e & -L_c^2\mu_e & 0 & 0 \\ 0 & -L_c^2\mu_e & L_c^2\mu_e & 0 & 0 \end{pmatrix}, \tag{B.52}$$

$$H^{23} = \begin{pmatrix} 0 & 2\mu_e & -2\mu_c & 0 & 0 \\ 0 & 0 & 0 & 0 & 0 \\ 0 & 0 & 0 & 0 & 0 \\ 0 & 0 & 0 & 0 & 0 \\ 0 & 0 & 0 & 0 & 0 \\ 0 & 0 & 0 & 0 & 0 \end{pmatrix}. \tag{B.53}$$

Appendix C

Appendix for chapter 6

C1 The matrix $\widehat{A}$

We present the matrix row-wise. We have

$$\widehat{A}_1 = \begin{pmatrix} -\left(\rho + k_1^2(2\bar{\eta}_1 + \bar{\eta}_3) + k_2^2\left(\frac{1}{4}\bar{\eta}_2 + \bar{\eta}_1^*\right)\right)\omega^2 + k_1^2(\lambda_e + 2\mu_e) + k_2^2\left(\mu_c + \mu_e^*\right) \\ k_1k_2\left(\frac{1}{4}\bar{\eta}_2 - \bar{\eta}_3 + \bar{\eta}_1^*\right)\omega^2 + k_1k_2(\lambda_e - \mu_c + \mu_e^*) \\ i\,k_1(\lambda_e + 2\mu_e) \\ i\,k_2(\mu_c + \mu_e^*) \\ i\,k_2(-\mu_c + \mu_e^*) \\ i\,k_1\lambda_e \end{pmatrix}^{\mathrm{T}},$$

$$\widehat{A}_2 = \begin{pmatrix} k_1k_2\left(\frac{1}{4}\bar{\eta}_2 - \bar{\eta}_3 - \bar{\eta}_1^*\right)\omega^2 + k_1k_2\left(\lambda_e - \mu_c + \mu_e^*\right) \\ -\left(\rho + k_2^2(2\bar{\eta}_1 + \bar{\eta}_3) + k_1^2\left(\frac{1}{4}\bar{\eta}_2 + \bar{\eta}_1^*\right)\right)\omega^2 + k_2^2(\lambda_e + 2\mu_e) + k_1^2\left(\mu_c + \mu_e^*\right) \\ i\,k_2\lambda_e \\ -i\,k_1(\mu_c - \mu_e^*) \\ i\,k_1(\mu_e + \mu_e^*) \\ i\,k_2(\lambda_e + 2\mu_e) \end{pmatrix}^{\mathrm{T}},$$

$$\widehat{A}_3 = \begin{pmatrix} -i\,k_1(\lambda_e + 2\mu_e) \\ -i\,k_2\lambda_e \\ -(2\eta_1 + \eta_3)\,\omega^2 + \lambda_e + \lambda_{\text{micro}} + 2(\mu_e + \mu_{\text{micro}}) + k_2^2 L_c^2 \\ -k_1 k_2 L_c^2 \\ 0 \\ -\eta_3\,\omega^2 + \lambda_e + \lambda_{\text{micro}} \end{pmatrix}^{\text{T}},$$

$$\widehat{A}_4 = \begin{pmatrix} -i\,k_2(\mu_c + \mu_e^*) \\ i\,k_1(\mu_c - \mu_e^*) \\ -k_1 k_2 L_c^2 \\ -(\eta_2 + \eta_1^*)\,\omega^2 + \mu_c + \mu_e^* + \mu_{\text{micro}}^* + k_1^2 L_c^2 \\ (\eta_2 - \eta_1^*)\,\omega^2 - \mu_c + \mu_e^* + \mu_{\text{micro}}^* \\ 0 \end{pmatrix}^{\text{T}},$$

$$\widehat{A}_5 = \begin{pmatrix} i\,k_2(\mu_c - \mu_e^*) \\ -i\,k_1(\mu_c + \mu_e^*) \\ 0 \\ (\eta_2 - \eta_1^*)\,\omega^2 - \mu_c + \mu_e^* + \mu_{\text{micro}}^* \\ -(\eta_2 + \eta_1^*)\,\omega^2 + \mu_c + \mu_e^* + \mu_{\text{micro}}^* + k_2^2 L_c^2 \\ -k_1 k_2 L_c^2 \end{pmatrix}^{\text{T}},$$

$$\widehat{A}_6 = \begin{pmatrix} -i\,k_1\lambda_e \\ -i\,k_2(\lambda_e + 2\mu_e) \\ -\eta_3\,\omega^2 + \lambda_e + \lambda_{\text{micro}} \\ 0 \\ -k_1 k_2 L_c^2 \\ -(2\eta_1 + \eta_3)\,\omega^2 + \lambda_e + \lambda_{\text{micro}} + 2(\mu_e + \mu_{\text{micro}}) + k_1^2 L_c^2 \end{pmatrix}^{\text{T}},$$

Then, the matrix $\widehat{A}$ is

$$\widehat{A} = \left(\widehat{A}_1, \widehat{A}_2, \widehat{A}_3, \widehat{A}_4, \widehat{A}_5, \widehat{A}_6\right)^{\text{T}} \tag{C.1}$$

C2 Analytical expression of the flux for the relaxed micromorphic model when $L_c = 0$

The flux H of the relaxed micromorphic model when $L_c = 0$ can be written as (using Lemma 1)

$$H = \frac{1}{2}\text{Re}\left[\left(\alpha_1\omega(-2\omega^2\mathcal{A} + \mathcal{B}) + \alpha_2\omega(-2\omega^2\mathcal{C} + \mathcal{D})\right)\mathcal{E}^\star + \left(\alpha_1\omega\left(\mathcal{F} + \omega\,\mathcal{G} + \omega^2\mathcal{H}\right) + \alpha_2\omega(\mathcal{I} + \omega\,\mathcal{J} + \omega^2\mathcal{K})\right)\mathcal{L}^\star\right], \tag{C.2}$$

with

$$
\begin{aligned}
\mathcal{A} &= k_1^{(1)}\phi_1^{(1)}\left(\overline{\eta}_1 + \frac{1}{2}\overline{\eta}_3\right) + k_0\,\phi_2^{(1)}\overline{\eta}_3,\\
\mathcal{B} &= (\lambda_e + 2\mu_e)\left(k_1^{(1)}\phi_1^{(1)} - \phi_3^{(1)}\omega\right) + \lambda_e\left(k_0\,\phi_2^{(1)} - \phi_6^{(1)}\omega\right),\\
\mathcal{C} &= k_1^{(2)}\phi_1^{(2)}\left(\overline{\eta}_1 + \frac{1}{2}\overline{\eta}_3\right) + k_0\,\phi_2^{(2)}\overline{\eta}_3,\\
\mathcal{D} &= (\lambda_e + 2\mu_e)\left(k_1^{(2)}\phi_1^{(2)} - \phi_3^{(2)}\omega\right) + \lambda_e\left(k_0\,\phi_2^{(2)} - \phi_6^{(2)}\omega\right),\\
\mathcal{E} &= \alpha_1\phi_1^{(1)} + \alpha_2\phi_1^{(2)},\\
\mathcal{F} &= k_0\,\left(\mu_e^* - \mu_c\right)\phi_1^{(1)} + k_1^{(1)}\left(\mu_e^* + \mu_c\right)\phi_2^{(1)},\\
\mathcal{G} &= -\left(\mu_e^* - \mu_c\right)\phi_4^{(1)} - \left(\mu_e^* + \mu_c\right)\phi_5^{(1)},\\
\mathcal{H} &= k_0\,\phi_1^{(1)}\left(\frac{1}{4}\overline{\eta}_2 - \overline{\eta}^*\right) - k_1^{(1)}\phi_2^{(1)}\left(\frac{1}{4}\overline{\eta}_2 + \overline{\eta}^*\right),\\
\mathcal{I} &= k_0\,\left(\mu_e^* - \mu_c\right)\phi_1^{(2)} + k_1^{(2)}\left(\mu_e^* + \mu_c\right)\phi_2^{(2)},\\
\mathcal{J} &= -\left(\mu_e^* - \mu_c\right)\phi_4^{(2)} - \left(\mu_e^* + \mu_c\right)\phi_5^{(2)},\\
\mathcal{K} &= k_0\,\phi_1^{(2)}\left(\frac{1}{4}\overline{\eta}_2 - \overline{\eta}^*\right) - k_1^{(2)}\phi_2^{(1)}\left(\frac{1}{4}\overline{\eta}_2 + \overline{\eta}^*\right),\\
\mathcal{L} &= \alpha_1\phi_2^{(1)} + \alpha_2\phi_2^{(2)}.
\end{aligned}
\tag{C.3}
$$

Bibliography

[1] Jan D. Achenbach. *Wave propagation in elastic solids*. North-Holland Publishing Company, Amsterdam, The Netherlands, 1973.

[2] Alexios Aivaliotis, Ali Daouadji, Gabriele Barbagallo, Domenico Tallarico, Patrizio Neff, and Angela Madeo. Low-and high-frequency stoneley waves, reflection and transmission at a cauchy/relaxed micromorphic interface. *arXiv preprint arXiv:1810.12578*, 2018.

[3] Alexios Aivaliotis, Ali Daouadji, Gabriele Barbagallo, Domenico Tallarico, Patrizio Neff, and Angela Madeo. Microstructure-related stoneley waves and their effect on the scattering properties of a 2d cauchy/relaxed-micromorphic interface. *Wave Motion*, 2019.

[4] Alexios Aivaliotis, Domenico Tallarico, Ali Daouadji, Patrizio Neff, and Angela Madeo. Broadband scattering properties of finite-size anisotropic metastructures via the relaxed micromorphic model. *arXiv preprint*, 2019.

[5] Nicolas Auffray. On the algebraic structure of isotropic generalized elasticity theories. *Mathematics and Mechanics of Solids*, 20(5):565–581, 2015.

[6] Bertram A. Auld. *Acoustic Fields and Waves in Solids, Vol. I.* Wiley-Interscience Publication, 1973.

[7] Bertram A. Auld. *Acoustic Fields and Waves in Solids, Vol. II.* Wiley-Interscience Publication, 1973.

[8] Mark V. Ayzenberg-Stepanenko and Leonid I. Slepyan. Resonant-frequency primitive waveforms and star waves in lattices. *J. Sound Vibration*, 313:812–821, 2008.

[9] Gabriele Barbagallo, Angela Madeo, Marco Valerio d'Agostino, Rafael Abreu, Ionel-Dumitrel Ghiba, and Patrizio Neff. Transparent anisotropy for the relaxed micromorphic model: macroscopic consistency conditions and long wave length asymptotics. *International Journal of Solids and Structures*, 120:7–30, 2017.

[10] Gabriele Barbagallo, Domenico Tallarico, Marco Valerio d'Agostino, Alexios Aivaliotis, Patrizio Neff, and Angela Madeo. Relaxed micromorphic model of transient wave propagation in anisotropic band-gap metastructures. *International Journal of Solids and Structures*, 2018.

[11] Ushnish Basu and Anil K. Chopra. Perfectly matched layers for time-harmonic elastodynamics of unbounded domains: theory and finite-element implementation. *Computer methods in applied mechanics and engineering*, 192(11-12):1337–1375, 2003.

[12] Cédric Bellis and Bruno Lombard. Simulating transient wave phenomena in acoustic metamaterials using auxiliary fields. *Wave Motion*, 86:175–194, 2019.

[13] Felix Bloch. Über die Quantenmechanik der Elektronen in Kristallgittern. *Zeitschrift für Physik*, 52(7-8):555–600, 1929.

[14] Leon Brillouin. *Wave propagation in periodic structures: electric filters and crystal lattices*. Courier Corporation, 2003.

[15] Tiemo Bückmann, Muamer Kadic, Robert Schittny, and Martin Wegener. Mechanical cloak design by direct lattice transformation. *Proceedings of the National Academy of Sciences*, 112(6):4930–4934, 2015.

[16] Giorgio Carta, Michele Brun, Alexander B. Movchan, Natalia V. Movchan, and Ian S. Jones. Dispersion properties of vortex-type monatomic lattices. *International Journal of Solids and Structures*, 51(11-12):2213–2225, 2014.

[17] Augustin-Louis Cauchy. Sur les équations qui expriment les conditions d'équilibre, ou les lois du mouvement intérieur d'un corps solide, élastique ou non élastique (1828). In *Œuvres complétes*, volume 2(8) of *Cambridge Library Collection - Mathematics*, pages 195–226. Cambridge University Press, Cambridge, 2009.

[18] Peter Chadwick, Maurizio Vianello, and Stephen C. Cowin. A new proof that the number of linear elastic symmetries is eight. *Journal of the Mechanics and Physics of Solids*, 49(11):2471–2492, 2001.

[19] GJ Chaplain, MP Makwana, and RV Craster. Rayleigh–bloch, topological edge and interface waves for structured elastic plates. *Wave Motion*, 86:162–174, 2019.

[20] Huanyang Chen and C. T. Chan. Acoustic cloaking in three dimensions using acoustic metamaterials . *Applied Physics Letters*, 91, 2007.

[21] Huanyang Chen and Che Ting Chan. Acoustic cloaking and transformation acoustics. *Journal of Physics D: Applied Physics*, 43(11):113001, 2010.

[22] Philippe G. Ciarlet. *Mathematical elasticity - Volume I: Three-Dimensional elasticity*, volume 1 of *Studies in Mathematics*. North-Holland Publishing Company, Amsterdam, The Netherlands, 1988.

[23] William D. Claus Jr. and Ahmed Cemal Eringen. Dislocation dispersion of elastic waves. *International Journal of Engineering Science*, 9(7):605–610, 1971.

[24] Daniel J. Colquitt, Ian S. Jones, Natalia V. Movchan, Alexander B. Movchan, and Ross C. McPhedran. Dynamic anisotropy and localization in elastic lattice systems. *Waves Random Complex Media*, 22(2):143–159, 2012.

[25] Eugène Cosserat and François Cosserat. *Théorie des corps déformables (engl. translation by D. Delphenich 2007, pdf available at http://www.uni-due.de/%7ehm0014/Cosserat_files/Cosserat09_eng.pdf)*. A. Hermann et Fils, Paris, 1909.

[26] Richard V. Craster and Sébastien Guenneau. *Acoustic metamaterials: Negative refraction, imaging, lensing and cloaking*, volume 166. Springer Science & Business Media, 2012.

[27] Richard V. Craster, Julius Kaplunov, and Aleksey V. Pichugin. High-frequency homogenization for periodic media. *Proceedings of the Royal Society A: Mathematical, Physical and Engineering Sciences*, 466(2120):2341–2362, 2010.

[28] Steven A. Cummer, Johan Christensen, and Andrea Alú. Controlling sound with acoustic metamaterials. *Nature Reviews Materials*, 113(3), 2014.

[29] Marco Valerio d'Agostino, Gabriele Barbagallo, Ionel-Dumitrel Ghiba, Bernhard Eidel, Patrizio Neff, and Angela Madeo. Effective description of anisotropic wave dispersion in mechanical band-gap metamaterials via the relaxed micromorphic model. *Submitted, Arxiv Preprint*, 1709.07054, 2018.

[30] Marco Valerio d'Agostino, Gabriele Barbagallo, Ionel-Dumitrel Ghiba, Angela Madeo, and Patrizio Neff. A panorama of dispersion curves for the weighted isotropic relaxed micromorphic model. *Zeitschrift für Angewandte Mathematik und Mechanik*, 97(11):1436—-1481, 2017.

[31] Andre Diatta, Muamer Kadic, Martin Wegener, and Sebastien Guenneau. Scattering problems in elastodynamics. *Physical Review B*, 94(10):100105, 2016.

[32] Pierre Duhem. *Introduction à la mécanique chimique*. G. Carré, 1893.

[33] Nader Engheta and Richard W Ziolkowski. *Metamaterials: physics and engineering explorations*. John Wiley & Sons, 2006.

[34] Ahmed Cemal Eringen. Mechanics of micromorphic materials. In *Applied Mechanics*, pages 131–138. Springer Berlin Heidelberg, Berlin, Heidelberg, 1966.

[35] Ahmed Cemal Eringen. Theory of thermo-microstretch elastic solids. *International Journal of Engineering Science*, 28(12):1291–1301, 1990.

[36] Ahmed Cemal Eringen. *Microcontinuum field theories*. Springer-Verlag, New York, 1999.

[37] Ahmed Cemal Eringen and William D. Claus Jr. A micromorphic approach to dislocation theory and its relation to several existing theories. In *Fundamental aspects of dislocation theory, Volume II. National Bureau of Standards Special. 317(2)*, pages 1023–1040. 1969.

[38] Ahmed Cemal Eringen and Erdogan S. Suhubi. Nonlinear theory of simple micro-elastic solids – I. *International Journal of Engineering Science*, 2(2):189–203, 1964.

[39] Gaston Floquet. Sur les equations differentielles lineaires. *Ann. ENS [2]*, 12(1883):47–88, 1883.

[40] Marc G.D. Geers, Varvara G. Kouznetsova, and W.A.M. Brekelmans. Multi-scale computational homogenization: Trends and challenges. *Journal of computational and applied mathematics*, 234(7):2175–2182, 2010.

[41] Paul Germain. The method of virtual power in continuum mechanics. Part 2: Microstructure. *SIAM Journal on Applied Mathematics*, 25(3):556–575, 1973.

[42] Ionel-Dumitrel Ghiba, Patrizio Neff, Angela Madeo, Luca Placidi, and Giuseppe Rosi. The relaxed linear micromorphic continuum: Existence, uniqueness and continuous dependence in dynamics. *Mathematics and Mechanics of Solids*, 20(10):1171–1197, 2015.

[43] Karl F. Graff. *Wave Motion in Elastic Solids*. Dover Publications, Inc., New York, 1975.

[44] A.E. Green and Ronald S. Rivlin. Multipolar continuum mechanics. *Archive for Rational Mechanics and Analysis*, 17(2):113–147, 1964.

[45] Sébastien Guenneau, Alexander Movchan, Gunnar Pétursson, and S. Anantha Ramakrishna. Acoustic metamaterials for sound focusing and confinement. *New Journal of Physics*, 9(399), 2007.

[46] Muamer Kadic, Tiemo Bückmann, Robert Schittny, and Martin Wegener. Metamaterials beyond electromagnetism. *Reports on Progress in Physics*, 76(12):126501, 2013.

[47] Nadége Kaina, Alexandre Causier, Yoan Bourlier, Mathias Fink, Thomas Berthelot, and Geoffroy Lerosey. Slow waves in locally resonant metamaterials line defect waveguides. *Scientific Reports*, 7(1), 2014.

[48] Anastasiia O. Krushynska, Varvara G. Kouznetsova, and Marc G.D. Geers. Towards optimal design of locally resonant acoustic metamaterials. *Journal of the Mechanics and Physics of Solids*, 71:179–196, 2014.

[49] Robin S. Langley. The response of two-dimensional periodic structures to point harmonic forcing. *Journal of Sound and Vibration*, 197(4):447–469, 1996.

[50] John Leckner. *Theory of Reflection: Reflection and Transmission of Electromagnetic, Particle and Acoustic Waves*. New York., John Wiley & Sons, 1973.

[51] Sam Hyeon Lee, Choon Mahn Park, Yong Mun Seo, Zhi Guo Wang, and Chul Koo Kim. Negative effective density in an acoustic metamaterial. *arXiv preprint arXiv:0812.2954*, 2008.

[52] Sam Hyeon Lee, Choon Mahn Park, Yong Mun Seo, Zhi Guo Wang, and Chul Koo Kim. Acoustic metamaterial with negative modulus. *Journal of Physics: Condensed Matter*, 21(17):175704, 2009.

[53] Yong Li and Badreddine M. Assouar. Acoustic metasurface-based perfect absorber with deep subwavelength thickness . *Applied Physics Letters*, 108(6), 2016.

[54] Ben Lieang, Jian-chun Chang, and Cheng-Wei Qiu. Wavefront manipulation by acoustic metasurfaces: from physics and applications. *Nanophotonics*, 7(6):1191–1205, 2018.

[55] J.-L. Lions and G. Papanicolaou. *Asymptotic Analysis for Periodic Structures*. AMS Chelsea Publishing, 1978.

[56] Zhengyou Liu, Xixiang Zhang, Yiwei Mao, Yirong Zhu, Zhiyu Yang, Che Ting Chan, and Ping Sheng. Locally resonant sonic materials. *Science*, 289(5485):1734–1736, 2000.

[57] Angela Madeo, Gabriele Barbagallo, Manuel Collet, Marco Valerio d'Agostino, Marco Miniaci, and Patrizio Neff. Relaxed micromorphic modeling of the interface between a homogeneous solid and a band-gap metamaterial: New perspectives towards metastructural design. *Mathematics and Mechanics of Solids*, Preprint, 2017.

[58] Angela Madeo, Gabriele Barbagallo, Marco Valerio d'Agostino, Luca Placidi, and Patrizio Neff. First evidence of non-locality in real band-gap metamaterials: determining parameters in the relaxed micromorphic model. *Proceedings of the Royal Society A: Mathematical, Physical and Engineering Sciences*, 472(2190):20160169, 2016.

[59] Angela Madeo, Manuel Collet, Marco Miniaci, Kévin Billon, Morvan Ouisse, and Patrizio Neff. Modeling phononic crystals via the weighted relaxed micromorphic model with free and gradient micro-inertia. *Journal of Elasticity*, 130(1):59–83, 2018.

[60] Angela Madeo, Patrizio Neff, Elias C. Aifantis, Gabriele Barbagallo, and Marco Valerio d'Agostino. On the role of micro-inertia in enriched continuum mechanics. *Proceedings of the Royal Society A: Mathematical, Physical and Engineering Science*, 473(2198):20160722, 2017.

[61] Angela Madeo, Patrizio Neff, Gabriele Barbagallo, Marco Valerio d'Agostino, and Ionel-Dumitrel Ghiba. A review on wave propagation modeling in band-gap metamaterials via enriched continuum models. In Francesco dell'Isola, Mircea Sofonea, and David J. Steigmann, editors, *Mathematical Modelling in Solid Mechanics*, Advanced Structured Materials, pages 89–105. Springer, Singapore, 2017.

[62] Angela Madeo, Patrizio Neff, Marco Valerio d'Agostino, and Gabriele Barbagallo. Complete band gaps including non-local effects occur only in the relaxed micromorphic model. *Comptes Rendus Mécanique*, 344(11-12):784–796, 2016.

[63] Angela Madeo, Patrizio Neff, Ionel-Dumitrel Ghiba, Luca Placidi, and Giuseppe Rosi. Band gaps in the relaxed linear micromorphic continuum. *Zeitschrift für Angewandte Mathematik und Mechanik*, 95(9):880–887, 2014.

[64] Angela Madeo, Patrizio Neff, Ionel-Dumitrel Ghiba, Luca Placidi, and Giuseppe Rosi. Wave propagation in relaxed micromorphic continua: modeling metamaterials with frequency band-gaps. *Continuum Mechanics and Thermodynamics*, 27(4-5):551–570, 2015.

[65] Angela Madeo, Patrizio Neff, Ionel-Dumitrel Ghiba, and Giuseppe Rosi. Reflection and transmission of elastic waves in non-local band-gap metamaterials: a comprehensive study via the relaxed micromorphic model. *Journal of the Mechanics and Physics of Solids*, 95:441–479, 2016.

[66] Jean Mandel. Plastic waves in an infinite three dimensional medium. *Journal de Mécanique*, 1:3–30, 1962.

[67] Paul A. Martin. Discrete scattering theory: Green's function for a square lattice. *Wave Motion*, 43(7):619 – 629, 2006.

[68] Gérard A. Maugin. *Non-Classical Continuum Mechanics*, volume 51. Springer, 2016.

[69] Graeme W Milton and Andrej V Cherkaev. Which elasticity tensors are realizable? *Journal of engineering materials and technology*, 117(4):483–493, 1995.

[70] Raymond David Mindlin. Microstructure in linear elasticity. Technical report, Office of Naval Research, 1963.

[71] Raymond David Mindlin. Micro-structure in linear elasticity. *Archive for Rational Mechanics and Analysis*, 16(1):51–78, 1964.

[72] Raymond David Mindlin and N. N. Eshel. On first strain-gradient theories in linear elasticity. *International Journal of Solids and Structures*, 4(1):109–124, 1968.

[73] Diego Misseroni, Daniel J. Colquitt, Alexander B. Movchan, Natasha V. Movchan, and Ian Samuel Jones. Cymatics for the cloaking of flexural vibrations in a structured plate. *Scientific Reports*, 6(23929), 2016.

[74] Alexander B. Movchan and Leonid I. Slepyan. Band gap green's function and localised oscillations. *Proceedings of the Royal Society of Science A*, 463:2709–2727, 2009.

[75] Ingo Münch and Patrizio Neff. Rotational invariance conditions in elasticity, gradient elasticity and its connection to isotropy. *Mathematics and Mechanics of Solids*, Preprint, 2016.

[76] Patrizio Neff. The Cosserat couple modulus for continuous solids is zero viz the linearized Cauchy-stress tensor is symmetric. *Zeitschrift für Angewandte Mathematik und Mechanik*, 86(11):892–912, 2006.

[77] Patrizio Neff, Ionel-Dumitrel Ghiba, Markus Lazar, and Angela Madeo. The relaxed linear micromorphic continuum: well-posedness of the static problem and relations to the gauge theory of dislocations. *The Quarterly Journal of Mechanics and Applied Mathematics*, 68(1):53–84, 2015.

[78] Patrizio Neff, Ionel-Dumitrel Ghiba, Angela Madeo, Luca Placidi, and Giuseppe Rosi. A unifying perspective: the relaxed linear micromorphic continuum. *Continuum Mechanics and Thermodynamics*, 26(5):639–681, 2014.

[79] Patrizio Neff, Angela Madeo, Gabriele Barbagallo, Marco Valerio d'Agostino, Rafael Abreu, and Ionel-Dumitrel Ghiba. Real wave propagation in the isotropic-relaxed micromorphic model. *Proceedings of the Royal Society A: Mathematical, Physical and Engineering Sciences*, 473(2197):20160790, 2017.

[80] Zachary G Nicolaou and Adilson E Motter. Mechanical metamaterials with negative compressibility transitions. *Nature materials*, 11(7):608, 2012.

[81] Andrew N. Norris. Acoustic cloacking. *Acoustics Today*, 11(1):38, 46.

[82] Grigory Osharovich, Mark V. Ayzenberg-Stepanenko, and Olga Tsareva. Wave propagation in elastic lattices subjected to a local harmonic loading ii. two-dimensional problems. *Continuum Mech.Therm.*, 22:599–616, 2010.

[83] Sebastian Owczarek, Ionel-Dumitrel Ghiba, Marco-Valerio d'Agostino, and Patrizio Neff. Nonstandard micro-inertia terms in the relaxed micromorphic model: well-posedness for dynamics. *to appear in Mathematics and Mechanics of Solids*, 2018.

[84] John Page. Metamaterials: Neither solid nor liquid. *Nature materials*, 10(8):565, 2011.

[85] Gabrio Piola. Intorno alle equazioni fondamentali del movimento di corpi qualsivogliono, considerati secondo la naturale loro forma e costituzione (1846). In Francesco Dell'Isola, Ugo Andreaus, Luca Placidi, and Daria Scerrato, editors, *The complete works of Gabrio Piola*, volume I of *Advanced Structured Materials*, pages 1–370. Springer International Publishing, 2014.

[86] Steven B. Platts, Natalia V. Movchan, Ross C. McPhedran, and Alexander B. Movchan. Two-dimensional phononic crystals and scattering of elastic waves by an array of voids. 458(2026):2327–2347, 2002.

[87] Lord John William Strutt Rayleigh. On waves propagated along the plane surface of an elastic solid. *Proceedings of the London Mathematical Society*, 17:4–11, 1885.

[88] Giovanni Romano, Raffaele Barretta, and Marina Diaco. Micromorphic continua: non-redundant formulations. *Continuum Mechanics and Thermodynamics*, 28(6):1659–1670, 2016.

[89] Massimo Ruzzene, Fabrizio Scarpa, and Francesco Soranna. Wave beaming effects in two-dimensional cellular structures. *Smart Mater. Struct.*, 12:363–372, 2003.

[90] Ashwin Sridhar, Varvara G. Kouznetsova, and Marc G. D. Geers. A general multiscale framework for the emergent effective elastodynamics of metamaterials. *Journal of the Mechanics and Physics of Solids*, 111:414–433, 2018.

[91] Ankit Srivastava and John R. Willis. Evanescent wave boundary layers in metamaterials and sidestepping them through a variational approach. *Proc. R. Soc. A*, 473(2200):20160765, 2017.

[92] Robert Stoneley. Elastic waves at the surface of separation of two solids. *Proceedings of the Royal Society A: Mathematical, Physical and Engineering Sciences*, 106(738):416–428, 1924.

[93] Domenico Tallarico, Natalia V. Movchan, Alexander B. Movchan, and Daniel J. Colquitt. Tilted resonators in a triangular elastic lattice: Chirality, Bloch waves and negative refraction. *Journal of the Mechanics and Physics of Solids*, 103:236–256, 2017.

[94] Domenico Tallarico, Alessio Trevisan, Natalia V. Movchan, and Alexander B. Movchan. Edge waves and localization in lattices containing tilted resonators. *Frontiers in Materials*, 4(June):1–13, 2017.

[95] Richard A. Toupin. Theories of elasticity with couple-stress. *Archive for Rational Mechanics and Analysis*, 17(2):85–112, 1964.

[96] Clifford Truesdell and Richard A. Toupin. The classical field theories. In Siegfried Flügge, editor, *Principles of Classical Mechanics and Field Theory / Prinzipien der Klassischen Mechanik und Feldtheorie*, pages 226–858. Springer, Berlin, Heidelberg, 1960.

[97] Jason Valentine, Jensen Li, Thomas Zentgraf, Guy Bartal, and Xiang Zhang. An optical cloak made of dielectrics. *Nature Materials*, 8(7):568–571, 2009.

[98] VG Veselago. Electrodynamics of substances with simultaneously negative electrical and magnetic permeabilities. *Physics-Uspekhi*, 10(4):504–509, 1968.

[99] Woldemar Voigt. *Theoretische studien über die Elasticitätsverhältnisse der Krystalle*. Königliche Gesellschaft der Wissenschaften zu Göttingen, 1887.

[100] Woldemar Voigt. Ueber die Beziehung zwischen den beiden Elasticitätskonstanten isotroper Körper. *Annalen der Physik*, 274(12):573–587, 1889.

[101] Woldemar Voigt. *Lehrbuch der Kristallphysik*. Vieweg+Teubner Verlag, Wiesbaden, 1966 edition, 1909.

[102] Pai Wang, Filippo Casadei, Sicong Shan, James C. Weaver, and Katia Bertoldi. Harnessing buckling to design tunable locally resonant acoustic metamaterials. *Physical Review Letters*, 113, 2014.

[103] John R. Willis. Dynamics of composites. In *Continuum micromechanics*, pages 265–290. Springer, 1997.

[104] John R. Willis. Exact effective relations for dynamics of a laminated body. *Mechanics of Materials*, 41(4):385–393, 2009.

[105] John R. Willis. Effective constitutive relations for waves in composites and metamaterials. In *Proceedings of the Royal Society of London A: Mathematical, Physical and Engineering Sciences*, volume 467, pages 1865–1879. The Royal Society, 2011.

[106] John R. Willis. The construction of effective relations for waves in a composite. *Comptes Rendus Mécanique*, 340(4-5):181–192, 2012.

[107] John R. Willis. Negative refraction in a laminate. *Journal of the Mechanics and Physics of Solids*, 97:10–18, 2016.

[108] Yong Xiao, Jihong Wen, and Xisen Wen. Longitudinal wave band gaps in metamaterial-based elastic rods containing multi-degree-of-freedom resonators. *New Journal of Physics*, 14, 2011.

[109] Yangbo Xie, Wenqi Wang, Huanyang Chen, Adam Konneker, Bogdan-Ioan Popa, and Steven A. Cummer. Wavefront modulation and subwavelength diffractive acoustics with an acoustic metasurface. *Nature Communications*, 5(1):1191–1205, 2014.

[110] R. Zhu, X. N. Liu, and G. L. Huang. Study of anomalous wave propagation and reflection in semi-infinite elastic metamaterials. *Wave Motion*, 55:73–83, 2015.

[111] Saïd Zouhdi, Ari Sihvola, and Alexey P Vinogradov. *Metamaterials and plasmonics: fundamentals, modelling, applications*. Springer Science & Business Media, 2008.